TECHNISCHE
UNIVERSITÄT
DARMSTADT

ULB

Sediments of two Gondwana glaciations in Ethiopia: Provenance of the Enticho Sandstone and the Edaga Arbi Glacials

Lewin, Anna

(2020)

Sediments of two Gondwana glaciations in Ethiopia: Provenance of the Enticho Sandstone and the Edaga Arbi Glacials

TECHNISCHE UNIVERSITÄT DARMSTADT

Fachbereich Material- und Geowissenschaften der Technischen Universität Darmstadt

Dissertation
zur Erlangung des akademischen Grades
Doctor rerum naturalium (Dr.rer.nat.)

Von Anna Lewin

Erstgutachter: Prof. Dr. Matthias Hinderer
Zweitgutachter: PD Dr. Guido Meinhold

Darmstadt, 2020

Anna Lewin
geboren am 09.09.1988 in Marl

Prof. Dr. Matthias Hinderer
Fachgebiet Sedimentgeologie
Institut für Angewandte Geowissenschaften
Technische Universität Darmstadt
Schnittspahnstraße 9
64287 Darmstadt

Ich erkläre hiermit, die vorliegende Dissertation ohne Hilfe Dritter und nur mit den angegebenen Quellen und Hilfsmitteln angefertigt zu haben. Alle Stellen, die aus Quellen übernommen wurden, sind als solche kenntlich gemacht worden. Diese Arbeit hat in dieser oder ähnlicher Form noch keiner Prüfungsbehörde vorgelegen. Die schriftliche Fassung stimmt mit der elektronischen Fassung überein.

I hereby certify that the complete work to this PhD thesis was done by myself and only with the use of the referenced literature and the described methods.

Darmstadt, den

Anna Lewin

Acknowledgements

Table of contents

List of abbreviations and symbols

ANS	Arabian–Nubian Shield
ATi	Apatite-tourmaline index
CIA	Chemical index of alteration
clr	centred-log ratio
EAO	East African Orogen
GTi	Garnet-tourmaline index
ICP-MS	Inductively coupled plasma mass spectrometry
LA-ICP-MS	Laser ablation inductively coupled plasma mass spectrometry
LPIA	Late Palaeozoic Ice Age
PCA	Principal component analysis
PC	Principal component
REE	Rare earth elements (HREE/LREE – Heavy/light rare earth elements)
RZi	Rutile-zircon index
SMC	Saharan Metacraton
STi	Staurolite-tourmaline index
UCC	Upper continental crust
XRF	X-ray fluorescence spectroscopy
ZTR	Zircon-tourmaline-rutile

Preface

The work presented in this thesis is part of the DFG project "Palaeozoic source to sink relationship around the northern Trans-Gondwana Mountain Belt (East Africa, Arabia)" in which Palaeozoic sandstones in Saudi Arabia and Ethiopia were studied using different provenance techniques. This PhD thesis covers the Ethiopia part of the project. The cumulative thesis includes three published articles on the provenance of two Palaeozoic glaciation-related sandstone formations in Ethiopia – the Ordovician–Silurian Enticho Sandstone and the Carboniferous–Permian Edaga Arbi Glacials. A multi-method provenance analysis has been conducted on samples of these two formations. The articles cover different methodological approaches to sandstone provenance. In the following, a brief overview over the structure of the thesis is given.

Chapter 1 is an introductory chapter into the overall topic of the thesis. A brief general literature review about the two ice ages, which are recorded in the studied formations, provenance studies on correlative sandstone formations in the region and previous studies on the Ethiopian Palaeozoic succession is given. Afterwards, the aims and objectives of this thesis are presented and an overview of the methodological strategy is given.

Chapter 2 (first article):
Lewin, A., Meinhold, G., Hinderer, M., Dawit, E.L., Bussert, R., 2018. Provenance of sandstones in Ethiopia during Late Ordovician and Carboniferous–Permian Gondwana glaciations: Petrography and geochemistry of the Enticho Sandstone and the Edaga Arbi Glacials. Sedimentary Geology 375, 188-202.
This article covers methods applied to the bulk samples: petrographic analysis of thin sections and analysis of the bulk chemical composition of the sandstone. By this, the questions of proximal vs. distal provenance and climate and weathering conditions that led to the petrographic and geochemical characteristics are discussed. The results are set in context with published models on extent and configuration of glaciers and ice sheets during the two glacial periods, during which the studied formations formed.

Chapter 3 (second article):
Lewin, A., Meinhold, G., Hinderer, M., Dawit, E.L., Bussert, R., Berndt, J., 2020. Provenance of Ordovician–Silurian and Carboniferous–Permian glaciogenic successions in Ethiopia revealed by detrital zircon U–Pb geochronology. Journal of the Geological Society London 177, 141-152.
In this article, results of radiometric dating of detrital zircons from the two studied formations are presented. The age populations of zircons are compared to ages of potential source rocks on the super-continent Gondwana. Furthermore, a statistical comparison with published zircon ages in stratigraphically equivalent and older sandstone formations of northern Gondwana is performed, discussing regional homogenisation of the sediment and the possibility of sedimentary recycling.

Chapter 4 (third article):
Lewin, A., Meinhold, G., Hinderer, M., Dawit, E.L., Bussert, R., Lünsdorf, N.K., 2020. Heavy minerals as provenance indicator in glaciogenic successions: An example from the Palaeozoic of Ethiopia. Journal of African Earth Sciences 165, 103813.
This article covers the study of the heavy mineral assemblages in the studied samples, complemented with chemical analyses of rutile and garnet minerals. The ideas of the previous two articles are further developed and the provenance and the issue of sediment recycling are further constrained.

Chapter 5 is a synthesis of the results and conclusions of the three articles. Here, the methodological strategy is revised and conclusions about the methods used and their helpfulness in answering the research questions are drawn. An integrated discussion of the new insights into the provenance of the two studied formations is presented with implications for the evolution of the regional sediment transport system.

In this PhD project, furthermore, a contribution was made to the article *Detrital zircon provenance of north Gondwana Palaeozoic sandstones from Saudi Arabia* (G. Meinhold, A. Bassis, M. Hinderer, A. Lewin and J. Berndt), which is in revision for publication in the Geological Magazine. The contribution included part of the zircon U–Pb analysis using LA-ICP-MS and assistance during preparation of the manuscript.

Summary

The Gondwana supercontinent was completely assembled in the Late Neoproterozoic by closure of the Mozambique Ocean and formation of the extensive East African Orogen at the suture of East and West Gondwana. A peneplain formed on the northern margin of the supercontinent, on which a vast blanket of Palaeozoic sediment was deposited. Major amounts of sediment are assumed to have been eroded and transported from the East African Orogen to the continental margin via large sediment fans (Gondwana super-fan system).

The Palaeozoic sedimentary succession of northern Ethiopia evidences two Gondwana glaciations, which are recorded in the Upper Ordovician–Lower Silurian Enticho Sandstone and the Upper Carboniferous–Lower Permian Edaga Arbi Glacials. These formations have been studied sedimentologically and palynologically, but their provenance remained unclear. This thesis presents a multi-method provenance study on samples of these two formations. Thin section petrography provides the basis; then the bulk sandstone samples were analysed for their major and trace element geochemistry. Heavy minerals were separated from the samples and their assemblage was determined. Mineral chemical analyses were conducted on rutile and garnet grains from both formations. Finally, detrital zircon ages were determined. The study followed the objective to fill a data gap in correlation of provenance patterns across Palaeozoic sedimentary rocks of northern Gondwana, providing further insights into the Palaeozoic sediment dispersal system and the influence of the two glaciations on sediment provenance.

The Enticho Sandstone is composed of tillite at the base followed by glaciogenic sandstone, probably representing meltwater deposits. At the top of the formation, better sorting and distinct cross stratification show shallow marine reworking and evidence the post-glacial transgression. The Edaga Arbi Glacials comprise tillite and finely laminated sand- and siltstone with dropstones, interrupted by sandy layers.

The two formations differ strongly in their mineralogical maturity. The Enticho Sandstone is highly mature and unusually quartzose for glaciogenic sandstone. The marine sub-unit shows even higher quartz contents. The geochemical composition underlines this high maturity and yields a high chemical index of alteration (85), pointing to intense chemical weathering and reworking of the material. It is likely that the alteration has taken place before the glaciation. The Edaga Arbi Glacials feature lower maturity with higher amounts of feldspar and rock fragments and a chemical index of alteration of 62. Trace and rare earth elements indicate a higher influence of juvenile source material than for the Enticho Sandstone. Juvenile crustal rocks are abundant in the underlying Nubian Shield. Comparison of the geochemical data with age-equivalent formations in Saudi Arabia shows similar patterns for the Ordovician–Silurian, but major differences in the Carboniferous–Permian, supporting previous assumptions of a large, uniform sedimentary system during the Late Ordovician glaciation and more localised sediment transport during the Carboniferous–Permian.

Detrital zircon chronology resulted in main age populations of Pan-African (700–550 Ma), Tonian (900–700 Ma), Stenian–Tonian (1200–900 Ma) and minor Palaeoproterozoic and Archaean zircons for both formations. The relation of the Tonian and Stenian–Tonian populations, however, differs strongly between the two formations. The Enticho Sandstone is characterised by a prominent Stenian–Tonian population, which can be used to trace the Gondwana super-fan system. Correlation with Upper Ordovician (glaciogenic) and Cambrian–Ordovician sandstones in northern Africa and the Middle East yields high similarity with those in Israel, Jordan and Libya, which are assumed to represent a super-fan. It further shows that no change in zircon age patterns occurs with the onset of the glaciation. It is

thus likely that the Enticho Sandstone contains recycled super-fan material. The Edaga Arbi Glacials have a characteristic Tonian population. Such ages are omnipresent in the southern Nubian Shield and represent its earliest formation stage, supporting the assumption of a rather proximal provenance. No regional or stratigraphic trends could be observed within one of the studied formations.

The heavy mineral assemblages of both formations are highly different as well. The Enticho Sandstone is characterised by a large proportion of the ultra-stable heavy minerals zircon, tourmaline and rutile (ZTR). In the lower, glaciogenic sub-unit, significant amounts of garnet are also present. In the Edaga Arbi Glacials, on the other hand, apatite and garnet make up most of the heavy mineral assemblage. No stratigraphic trends were identified within the Edaga Arbi Glacials. Neither could regional trends be observed in one of the studied formations. These patterns underline the differences in mineralogical maturity revealed by petrography and geochemistry. Very little chemical alteration must have affected the Edaga Arbi Glacials, whereas the material forming the Enticho Sandstone is strongly altered. In the well sorted and permeable marine subunit of the Enticho Sandstone it is likely that diagenetic modification by corrosive pore fluids took place and reinforced the high mineralogical maturity. Rutile and garnet chemical analyses point to a combination of magmatic and metamorphic source rocks with metamorphic temperatures of mainly amphibolite-, but also granulite-facies grade for both formations. For the Enticho Sandstone, the heavy mineral analysis confirms the assumption that it contains recycled super-fan material, which was strongly weathered before on the North Gondwana peneplain. The garnet is thought to have been delivered by varying erosion of the basement of the Saharan Metacraton (and maybe also the Nubian Shield) by the glaciers. The proximal provenance of the Edaga Arbi Glacials is confirmed again by the high amounts of unstable heavy minerals. Since the directly underlying basement does not contain high-grade metamorphic rocks, a provenance from the southern hinterland is likely, where the Nubian Shield merges the Mozambique Belt and higher metamorphic grades were reached.

Combining all methods and their outcome with information from the literature, the following provenance models can be inferred for the two studied formations. The Enticho Sandstone was formed during the Late Ordovician (Hirnantian) glaciation, when a large ice sheet covered much of northern Africa with a spreading centre in North-West Africa. The ice reached as far south-east as the study area. Ice and meltwater transported sediments to the study area; sediments, which were spread before via the Gondwana super-fan system and strongly weathered on the North Gondwana peneplain during the Cambrian and pre-glacial Ordovician. The original provenance of this super-fan material remains unclear. Material of the Saharan Metacraton basement was eroded by glaciers and admixed to variable amounts. During the post-glacial transgression in the Early Silurian, the upper part of the sedimentary succession was reworked by seawater without adding new detritus. In contrast, the Edaga Arbi Glacials are sourced from the southern hinterland of the Nubian Shield at the transition to the Mozambique Belt. In the Late Palaeozoic, a complex regional topography led to mountain glaciers that eroded the uplifted basement and transported material to nearby depressions, in which proglacial lakes formed. A period of non-deposition between the two formations may have been caused by a consecutive combination of isostatic-rebound after the Late Ordovician glaciation, eustatic sea-level fall in the late Silurian–early Devonian and up-doming prior to Neo-Tethys rifting. No recycling of the Enticho Sandstone by the Edaga Arbi Glacials took place on a grand scale. This was either because the deposition of the former was limited to northern Ethiopia and the source area for the latter was to the south or because the Enticho Sandstone was eroded in the source area of the Edaga Arbi Glacials before the Carboniferous–Permian glaciation.

Zusammenfassung

Der endgültige Zusammenschluss des Superkontinents Gondwana ereignete sich im späten Neoproterozoikum, mit Schließung des Mozambique Ozeans und der Bildung des ausgedehnten Ostafrikanischen Orogens entlang der Verbindung von Ost- und Westgondwana. Am nördlichen Rand des Kontinents entstand eine weitläufige Ebene, die durch paläozoische Sedimente überdeckt wurde. Ein Großteil dieser Sedimente wurde vermutlich vom Ostafrikanischen Orogen abgetragen und über große Sedimentfächer (Gondwana super fan-System) transportiert.

Die paläozoische Sedimentabfolge in Nordäthiopien entstand im Zuge zweier Gondwana-Vereisungen und setzt sich zusammen aus dem Enticho Sandstone (Oberes Ordovizium–Unteres Silur) und den Edaga Arbi Glacials (Oberes Karbon–Unteres Perm). An beiden Formationen haben bereits sedimentologische und palynologische Untersuchungen stattgefunden, deren Provenienz blieb jedoch unklar. Im Rahmen dieser Doktorarbeit wurde eine multi-proxy Provenienzanalyse an Proben beider Formationen durchgeführt. Die Basis bilden Dünnschliffanalysen, gefolgt von Haupt- und Spurenelementanalysen der Gesamtgesteinsproben. Die Schwerminerale wurden von den Gesamtgesteinsproben abgetrennt und ihre jeweiligen Anteile bestimmt. Mineralchemische Analysen wurden an Rutil und Granat aus beiden Formationen durchgeführt. Auch detritische Zirkone wurden datiert. Die Arbeit verfolgte das Ziel, eine Datenlücke in der Korrelation von Provenienzmustern paläozoischer Sandsteine Nordgondwanas zu schließen, um den Wissensstand über Sedimenttransportsysteme in Nordgondwana und den Einfluss der beiden Vereisungen auf die Sedimentprovenienz zu erweitern.

An der Basis des Enticho Sandstone befindet sich Tillit, gefolgt von glaziogenem Sandstein, vermutlich Schmelzwasserablagerungen. Am Top zeugen eine bessere Sortierung und eine charakteristische Schrägschichtung von mariner Aufarbeitung und weisen auf die post-glaziale Transgression hin. Die Edaga Arbi Glacials setzen sich aus Tillit und feinlaminierten Sand- und Siltsteinen zusammen, unterbrochen von Sandlagen.

Die beiden Formationen unterscheiden sich stark in ihrer mineralogischen Reife. Der Enticho Sandstone ist sehr reif und für glaziogenen Sandstein ungewöhnlich quarzhaltig. In der marinen Untereinheit sind sogar noch höhere Quarzgehalte zu finden. Die geochemische Zusammensetzung unterstreicht diese hohe Reife. Ein hoher Chemical Index of Alteration (CIA) von 85 lässt eine intensive chemische Verwitterung und Aufarbeitung des Materials vermuten. Diese hat wahrscheinlich schon vor Beginn der Eiszeit stattgefunden. Die Edaga Arbi Glacials zeichnen sich durch eine geringere Reife mit höheren Anteilen von Feldspat und Gesteinsfragmenten und einem CIA von 62 aus. Spurenelemente und seltene Erden deuten auf einen höheren Einfluss von juvenilem Ausgangsgestein hin, als beim Enticho Sandstone. Juvenile Krustengesteine finden sich im unterlagernden Nubischen Schild. Ein Vergleich der Geochemiedaten mit solchen von äquivalenten Formationen in Saudi-Arabien zeigt ähnliche Elementverteilungen für das Ordovizium–Silur, aber deutliche Unterschiede im Karbon–Perm. Dies stützt Hypothesen eines großen, homogenen Sedimentsystems während der spätordovizischen Vereisung und lokalem Sedimenttransport im Karbon–Perm.

Die Datierung detritischer Zirkone in beiden Formationen zeigt Hauptpopulationen pan-afrikanischen (700–550 Ma), tonischen (900–700 Ma), stenisch–tonischen (1200–900 Ma) und untergeordnet paläoproterozoischen und archaischen Alters. Das Verhältnis tonischer und stenisch–tonischer Zirkone unterscheidet sich zwischen den Formationen stark. Im Enticho Sandstone überwiegt eine prominente stenisch–tonische Population, welche charakteristisch für Sedimente des Gondwana super fan-Systems ist. Ein Vergleich mit anderen glazigenen Sandsteinen aus dem Oberordovizium und Sandsteinen aus

dem Kambrium bis Mittelordovizium in Nordafrika und dem Mittleren Osten ergab starke Ähnlichkeiten mit Sandsteinen in Israel, Jordanien und Libyen, die vermutlich einen super fan bildeten. Weiterhin fällt auf, dass mit Beginn der Vergletscherung keine Änderung in den Zirkonaltersspektren erfolgt. Es ist also wahrscheinlich, dass der Enticho Sandstone rezykliertes super fan-Material enthält. Die Edaga Arbi Glacials zeichnen sich durch eine charakteristische tonische Population aus. Diese Alter treten häufig in Gesteinen des südlichen Nubischen Schildes auf und repräsentieren dessen frühe Bildungsphase. Die Vermutung einer eher proximalen Provenienz der Edaga Arbi Glacials wird hierdurch bestätigt. Innerhalb der beiden Formationen konnten keine regionalen oder stratigraphischen Trends identifiziert werden.

Die Schwermineralzusammensetzungen der beiden untersuchten Formationen unterscheiden sich ebenfalls stark. Der Enticho Sandstone weist einen hohen Anteil der ultrastabilen Schwerminerale Zirkon, Turmalin und Rutil (ZTR) auf, was die zuvor attestierte hohe mineralogische Reife bestätigt. In der unteren, glazigenen Einheit sind auch höhere Anteile Granat enthalten. Im oberen, marinen Teil wurden wahrscheinlich Minerale durch korrosive Porenwässer diagenetisch gelöst, wodurch die hohe Reife verstärkt wurde. In den Edaga Arbi Glacials ist die Schwermineralfraktion von Apatit und Granat geprägt. Hier konnten keine stratigraphischen Trends beobachtet werden. Die Sedimente müssen extrem wenig chemische Verwitterung erfahren haben. Regionale Trends konnten in keiner der Formationen festgestellt werden. Rutil- und Granatchemie in beiden Formationen deuten auf eine Kombination von magmatischen und metamorphen Ausgangsgesteinen hin, wobei metamorphe Temperaturen im amphibolitfaziellen bis teilweise granulitfaziellen Bereich erreicht wurden. Für den Enticho Sandstone wird durch die Schwermineralanalyse die Vermutung bestätigt, dass er rezykliertes super fan-Material enthält, welches zuvor stark verwittert wurde. Der Granat wurde wahrscheinlich aus dem Basement des Sahara-Metakraton (eventuell auch des Nubischen Schildes) beigemengt. Die Hypothese eines proximalen Liefergebiets für die Edaga Arbi Glacials wird durch die hohen Anteile weniger stabiler Schwerminerale bestätigt. Da das direkt unterlagernde Basement jedoch nur geringmetamorphe Gesteine aufweist, ist ein Liefergebiet im südlichen Hinterland wahrscheinlich, wo das Nubische Schild in den Mozambique Belt übergeht und höhere Metamorphosegrade erreicht wurden.

Führt man die Ergebnisse aller durchgeführten Untersuchungen und Informationen aus der Literatur zusammen, lassen sich folgende Provenienzmodelle für die beiden untersuchten Formationen ableiten. Der Enticho Sandstone wurde während der Hirnantischen Vereisung im späten Ordovizium und der nachfolgenden Transgression gebildet. Ein Eisschild bedeckte große Teile Nordafrikas, wobei das Zentrum in Nord-Westafrika lag. Das Eis reichte bis ins Untersuchungsgebiet. Eis und Schmelzwasser transportierten Sedimente in Richtung des heutigen Äthiopiens. Diese Sedimente wurden zuvor im Gondwana super fan-System transportiert und auf der Tiefebene im Norden Gondwanas abgelagert, wo sie während des Kambriums und prä-glazialen Ordoviziums stark verwitterten. Die ursprüngliche Provenienz des super-fan Materials bleibt unklar. Material aus dem Sahara-Metakraton wurde teilweise von Gletschern erodiert und dem Sediment beigemengt. Während der Transgression im frühen Silur wurde der obere Teil der glazigenen Sedimentablagerungen vom Meerwasser aufgearbeitet, ohne dass neues Material dazu kam. Die Edaga Arbi Glacials hingegen wurden vom südlichen Hinterland des Nubischen Schildes am Übergang zum Mozambique Belt gespeist. Im späten Paläozoikum entstand eine komplexe regionale Topographie und führte zur Bildung von Eiskappen in ausreichender Höhenlage. Diese erodierten exponiertes Basementmaterial und transportierten es in nahegelegene Vertiefungen, wo sich proglaziale Seen bildeten. Zwischen dem Enticho Sandstone und den Edaga Arbi Glacials sind keine Ablagerungen erhalten. Gründe dafür könnten ein Aufeinanderfolgen von isostatischem Rebound nach der spätordovizischen Vereisung, eustatischem Meeresspiegelabfall im späten Silur–frühen Devon und Aufdomen vor der Öffnung der Neo-Tethys sein. Interessant ist zudem, dass kein bedeutendes Recycling des Enticho Sandstone durch die Edaga Arbi Glacials stattgefunden hat. Dies ist

wahrscheinlich so, weil die Ablagerung des Enticho Sandstone auf Nordäthiopien beschränkt war, während das Liefergebiet für die Edaga Arbi Glacials im Süden lag oder weil der Enticho Sandstone im Süden erodiert wurde.

1. Introduction

Reconstructing sedimentary systems of the past delivers valuable information about palaeo-environments, climate and tectonics and their evolution. This, in turn, can be of use for assessing future developments. Furthermore, understanding the sedimentary system is an important aspect of exploration of groundwater and hydrocarbon reservoirs or sedimentary mineral deposits. Sedimentary provenance analysis aims to reconstruct and to interpret the history of sediment from the erosion of parent rocks to deposition and burial based on its mineralogical and chemical composition (Weltje and von Eynatten, 2004).

In this thesis, a combination of different sedimentary provenance methods is applied to two Palaeozoic sandstone formations in Ethiopia. It provides a piece of the puzzle disentangling the provenance and sedimentary history of a large blanket of Palaeozoic sandstone deposited along the northern part of the supercontinent Gondwana after its assembly in the Late Neoproterozoic.

Core Gondwana comprised the modern continents of South America, Africa, Antarctica and Australia, as well as Madagascar and the Indian Subcontinent (Torsvik and Cocks, 2013). Gondwana was built of several Precambrian cratons "welded together" by Neoproterozoic orogenic belts. These formed during the Pan-African Orogeny and the largely contemporaneous Brasiliano and Pampean orogenies in South America, the Cadomian Orogeny in southern Europe and North Africa and the Kuungan Orogeny between India and East Antarctica (Torsvik and Cocks, 2013). The Pan-African Orogeny formed the East African Orogen (EAO), one of the largest accretionary orogens in the Earth's history (Stern, 1994; Collins and Pisarevsky, 2005; Squire et al., 2006; Figure 1-1). Products of weathering and erosion of this extensive mountain range and the other Neoproterozoic orogens extended over large parts of Gondwana and covered millions of square kilometres (Garfunkel, 2002; Avigad et al., 2005). Outcrops of sandstones deposited in this time occur nowadays in many places in northern and north-eastern Africa and across the Arabian Peninsula (Avigad et al., 2005). Two glaciations affected the sedimentary systems of Gondwana, the Hirnantian glaciation in the Late Ordovician and the Late Palaeozoic Ice Age (LPIA) in the Carboniferous–Permian.
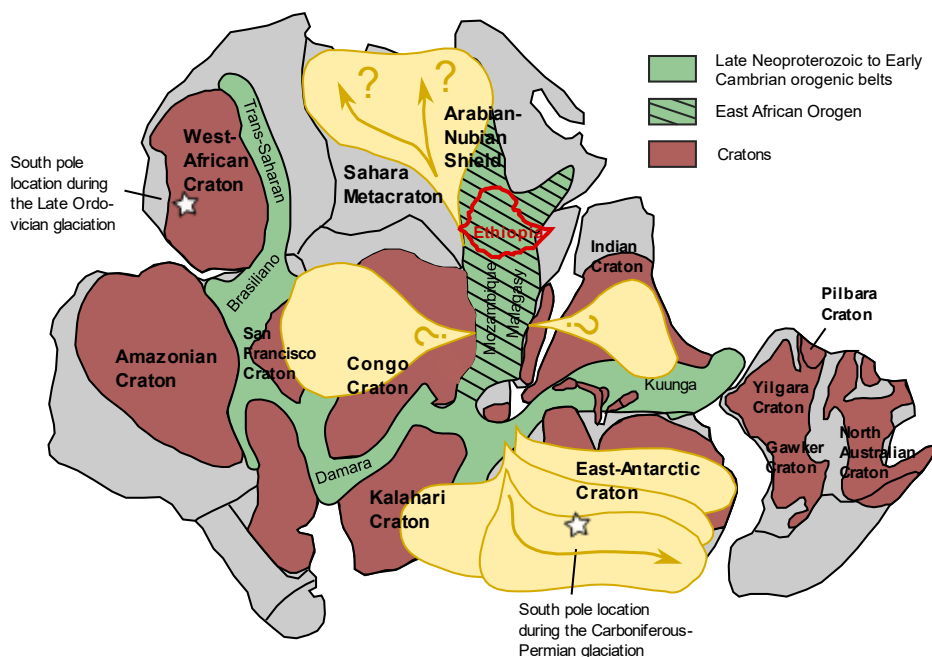
Figure 1-1: Configuration of Gondwana in the Palaeozoic with its cratons and orogenic belts after Torsvik and Cocks (2013) and Avigad et al. (2017) and super-fan model for the East African Orogen proposed by Squire et al. (2006).

1.1. Gondwana glaciations

Late Ordovician (Hirnantian) glaciation
During the Late Ordovician, the South Pole was in the region of north-western Africa (Eyles, 1993; Torsvik and Cocks, 2013). A large polar ice sheet evolved – similar in size to the modern Antarctic ice sheet – that spanned over much of northern Africa and Arabia (Eyles, 1993 and references therein; Figure 1-2). Ghienne (2003) assumes a minimum configuration with a large ice sheet in North-West Africa and smaller ice sheets in the area of the Arabian–Nubian Shield (ANS), in South Africa and the centre of South America. Ghienne et al. (2007) suggest a small and a large scenario: in the small scenario, an ice sheet covered whole northern Africa and the Arabian Peninsula with satellite ice sheets in South Africa and the centre of South America; in the large scenario, these three ice sheets are connected. This large scenario was also drawn by Vaslet (1990). Le Heron and Craig (2008) assume a continuous ice cover of northern Africa from Mauritania to Egypt with a northern ice margin following the margin of the modern African continent and an undefined ice extent to the south.

Uplift related to the Taconic orogeny along the West African plate margin in combination with high palaeolatitudes may have triggered the glaciation (Eyles, 1993). Late Ordovician climate was probably also affected by changes in the eccentricity of the Earth's orbit (Sutcliffe et al., 2000). The Hirnantian glaciation was short. Villas et al. (2006) suggest a time span of less than a million years. Brenchley et al. (1994) infer a time span of 0.5–1 million years from changes in oxygen isotopes of brachiopod samples. Two phases of the Late Ordovician mass extinction can be correlated with changes in oxygen and carbon isotopes indicating onset and ending of the Hirnantian glaciation (Brenchley et al., 2003).

The age of glacially related deposits is well constrained across northern Africa by microfossil assemblages in the strata and those below (Le Heron and Craig, 2008). Within the Hirnantian strata of North Gondwana, two first-order cycles of ice sheet advance and retreat can be recognized with a major mid-Hirnantian deglaciation event between them (Ghienne et al., 2007). Each cycle included 2–3 glacial phases separated by ice front retreats of several hundreds of kilometres (Ghienne et al., 2007). At the basal glacial unconformity, large palaeo-valleys are present, which can be traced over 50 km in West Africa and are of similar scale in the central Sahara and Saudi Arabia (Eyles, 1993). Their location and extent may be controlled by faults and lineaments in the underlying basement (Eyles, 1993). These tunnel valleys are created by ice-streams, corridors of fast-flowing ice (Ghienne et al., 2007; Le Heron and Craig, 2008). Such ice streams are areas of preferential glacial erosion and sediment deposition during glacier retreat (Ghienne et al., 2007). They define an ice stream network flowing outward from the central or southern Sahara region (Le Heron and Craig, 2008). The large amount of sediment that accumulated on the North Gondwana platform is striking assuming a polar ice sheet – the modern Antarctic ice sheet is characterised by cold-based glaciers and releases very little meltwater into the oceans (Eyles, 1993). Eyles (1993), therefore, suggest that the extensive sedimentary volume of the North Gondwana platform records the final decay phase of the ice sheet when climate was more temperate. Based on sediment structures, Le Heron (2004; 2005) and Keller et al. (2011) propose a model of a polythermal regime with an oscillating ice front and alternating cold-based and warm-based phases, followed by a late glacial surge and deglaciation for Libya and Saudi Arabia, respectively.

Carboniferous–Permian glaciation/Late Palaeozoic Ice Age (LPIA)
The Late Palaeozoic Ice Age lasted for about 100 Ma (ca. 350–250 Ma) and hence was the longest period of glaciation in the Phanerozoic (Eyles, 1993). However, the glaciation was not characterized by one single large ice sheet, but rather by several smaller ice masses that waxed and waned across the supercontinent (Crowell, 1983; Eyles, 1993; Figure 1-2). Fielding et al. (2008) suggest a series of glacial events of ca. 1-8 Ma duration with periods of warmer climate in between. In general, the glacial record

is oldest in the west and youngest in the east of Gondwana (Eyles, 1993). The ice age began with localized glacial events in South America in the latest Devonian and early Carboniferous and then spread further over South America, South Africa and Australia (Fielding et al., 2008). In the late Carboniferous (Middle to Late Pennsylvanian), a warmer period with a eustatic sea-level rise is inferred from the landward progradation of marine sedimentary systems, marine fauna and coal deposits on land (Montañez and Poulsen, 2013). The acme of the LPIA was reached in the early Permian when glaciation affected South America, South Africa, Antarctica, Australia, the Arabian Peninsula, India and the South Asian crustal blocks (Fielding et al., 2008; Montañez and Poulsen, 2013). Glacial deposits in Siberia point to a bipolar glaciation at that time (Fielding et al., 2008). The extensive occurrence of glaciomarine deposits indicate that glaciers reached sea-level, which requires widespread cooling (Isbell et al., 2012). The decline of the LPIA is recorded in marine transgressive deposits and the loss of ice-contact deposits across Gondwana (Montañez and Poulsen, 2013).
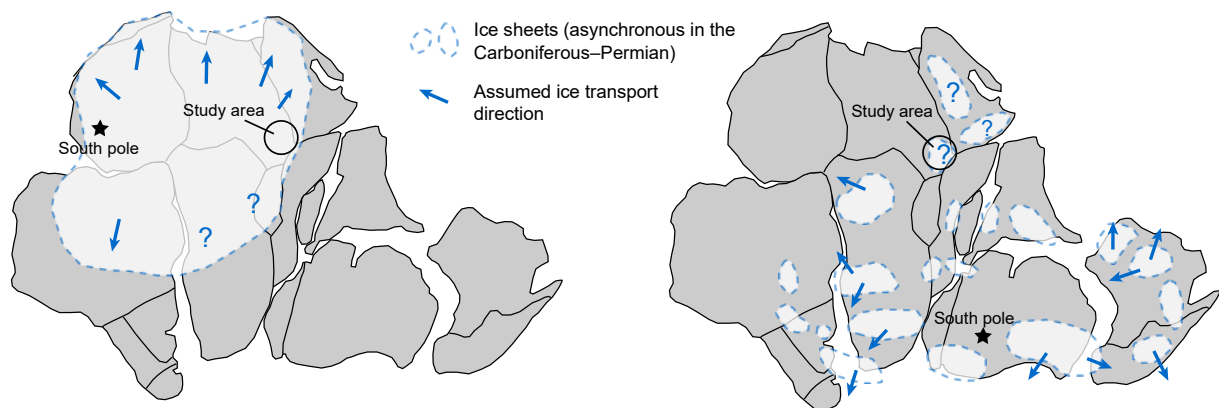
Figure 1-2: Ice configurations during the two Gondwana glaciations. Gondwana palaeogeography and South Pole positions from Torsvik and Cocks (2013). Ice sheet locations and transport directions for the Late Ordovician after Ghienne et al. (2007), Le Heron and Craig (2008) and Torsvik and Cocks (2013), for the Carboniferous–Permian after Bussert and Schrank (2007), Fielding et al. (2008) and Isbell et al. (2012). In the Carboniferous–Permian, ice cover was diachronous.

The triggers for the LPIA were probably a combination of several factors. Powell and Veevers (1987) suggest that the main control was the closure of the Palaeotethys ocean joining Gondwana and Laurussia and orogenic uplift was a second-order control. Atmospheric pCO_2 fluctuations probably have played a fundamental role (Eyles, 1993; Fielding et al., 2008). During the Carboniferous–Permian, the lowest pCO_2 values of the whole Phanerozoic prevailed, similar to the modern icehouse (Prokoph et al., 2008). A major factor causing this drop in pCO_2 was the spread of vascular plants to upland areas in the Devonian, which, due to deep rooting and good drainage affected the chemical weathering of silicate rocks (Berner, 1998). Roots and root symbionts remove nutrients from silicates and enhance chemical weathering, which, in turn, removes CO_2 from the atmosphere (Beerling and Berner, 2005). Another factor is the increased burial of plant-derived organic matter, as evidenced by the formation of vast coal deposits in the Mississippian and Permian (Berner, 1998; Beerling and Berner, 2005). Increased organic burial is also indicated by elevated $\delta^{13}C$ in marine carbonates, while a decrease in seawater temperature is marked by an increase in $\delta^{18}O$ (Veizer et al., 1999; Prokoph et al., 2008). The diachronous development of ice sheets and glaciers across different regions of Gondwana was probably caused by the migration of the continent across the south pole (Eyles, 1993; Fielding et al., 2008; López-Gamundí and Buatois, 2010). However, since there is little immediate correlation between the apparent polar wander path for the Carboniferous and the patterns of glacial growth, an additional, yet unknown, control may have been involved (Fielding et al., 2008).

North-East Africa and Arabia were not in polar position during the late Palaeozoic, but in mid-latitudes (50–60° south after Torsvik and Cocks, 2013). Glaciation most probably was of plateau or mountain type (Bussert and Schrank, 2007). A prominent upland in the Horn of Africa may have existed (Bussert and Schrank, 2007, and references therein). According to Eyles (1993), the glaciogenic deposits in Yemen, Saudi Arabia and Oman are placed on top of an unconformity surface recording Hercynian uplift. The tectonic-stratigraphic setting may be that of intracratonic subsidence accompanying and immediately postdating Hercynican uplift (Eyles, 1993; Sharland et al., 2001). The setting is directly comparable to upper Palaeozoic strata of the Parana (South America) and Karoo (South Africa) basins (Eyles, 1993).

1.2. Provenance studies on North Gondwana sandstones

Cambrian to Ordovician sandstones in Israel and Jordan have been studied intensively. They show an exceptionally high maturity, especially in the Middle Cambrian to Ordovician (Weissbrod and Nachmais, 1986; Amireh, 1991; Avigad et al., 2003; Avigad et al., 2005). Avigad et al. (2003; 2005) suggest that these sediments are first-cycle sediments and largely derived from the Arabian–Nubian Shield (ANS), the northern part of the EAO (Figure 1-1). They explain their high maturity by strong chemical weathering due to a corrosive Cambrian–Ordovician atmosphere and warm, humid climate. Kolodner et al. (2006) propose the ANS as main source area for the lower Palaeozoic sandstone as well but inferred a progressive influence of source areas further south as stratigraphic ages get younger from a change in detrital zircon age spectra. Morag et al. (2011) confirmed a significant contribution from source areas outside the ANS by Hf isotopic analyses of detrital zircons, which do not fit the signature of the ANS. They suggest that a significant proportion of the sediment is sourced from areas in the centre of Gondwana, which would mean that the ANS has been levelled by the middle of the Cambrian. Ben Dor et al. (2018) came to the same conclusion by using Sr, Nd and Pb isotopes of feldspars and clays in Cambrian–Ordovician sandstones in Israel. An early levelling of orogenic topography is also suggested by Avigad et al. (2017) from detrital rutile cooling ages in lower Palaeozoic sandstones of Israel and Jordan combined with zircon chronology. They inferred rapid cooling and exhumation of the source area and no direct linkage of the lower Palaeozoic sediments with active tectonics.

In Saudi Arabia, a Palaeozoic sandstone succession from the Cambrian to the Permian can be found. Knox et al. (2007) studied heavy minerals in the whole succession and identified provenance changes in the course of the Cambrian–Ordovician. They describe a sharp boundary towards the deposits of the Hirnantian glaciation, but with the same heavy mineral composition as in the deposits below. Another change in heavy mineral composition could be identified in the Devonian–Carboniferous. The deposits of the Late Palaeozoic Ice Age (LPIA) show a great variability in heavy minerals ascribed to a combination of different sources. Further studies on the Palaeozoic sedimentary succession of Saudi Arabia were performed by Bassis et al. (2016a; 2016b): they found an overall high mineralogical maturity, but assumed the Cambrian–Ordovician sandstones to be first-cycle sediments, likely derived from the underlying basement of the ANS. As proposed by Avigad et al. (2005) they assume that the ANS has been exposed to intense chemical weathering. For the Hirnantian deposits they suggest recycling of these first-cycle sediments. A higher influence of fresh basement material in the Late Palaeozoic, inferred from unstable heavy minerals, is associated with increasing tectonic activity at the northern margin of Gondwana during that time (Bassis et al., 2016a). This activity is attributed to crustal updoming and rifting prior to opening of the Neotethys ocean (Sharland et al., 2001). Detrital zircon chronology on sandstones of the Saudi Arabian Palaeozoic succession points to a main provenance from igneous rocks in the ANS with significant contribution of material of the Gondwana super-fan system described below and Palaeoproterozoic and Archaean zircons of uncertain provenance (Meinhold et al., in revision).

Palaeozoic sandstones in northern Africa are preserved from Egypt to Morocco and especially the Hirnantian glaciogenic sandstones are well studied and allow reconstructions of the palaeo-ice sheet (Ghienne et al., 2007; Le Heron and Craig, 2008) that is further described in Section 1.1. Lower Palaeozoic sandstones in Egypt are sub-mature to mature and based on bulk geochemistry, their provenance is assumed to be mainly the felsic plutons in the northern ANS (Akarish and El-Gohary, 2008; Tawfik et al., 2017).

In Libya, sandstones of the whole Palaeozoic are preserved and well studied: Three major provenance changes are identified from heavy mineral analysis. Thea are ascribed to 1) the final pulse of the Late Ordovician (Hirnantian) glaciation and the subsequent transgression, 2) eustatic sea-level fall in late Silurian/Early Devonian that led to a change in river systems and 3) the Late Palaeozoic Ice Age (LPIA) in the Carboniferous–Permian (Morton et al., 2011). The main source for the Libyan Palaeozoic sandstones is assumed to be the underlying Sahara Metacraton (Meinhold et al., 2011; Morton et al., 2012; Altumi et al., 2013). Altumi et al. (2013) suggested also Neoproterozoic orogenic belts to the west and the West African Craton based on detrital zircon ages. For late Mesoproterozoic zircons, Meinhold et al. (2011) and Morton et al. (2012) propose source areas in the Congo and Tanzania cratons, implying a long transport distance, or Mesoproterozoic igneous rocks in eastern Chad.

Cambrian–Ordovician sandstones in Algeria are studied petrographically and geochemically by Sabaou et al. (2009). They describe high mineralogical maturity and infer deeply weathered cratonic landmasses or recycled sediments as source rocks. Linnemann et al. (2011) studied detrital zircons of these sandstones and found ages consistent with a provenance in the Trans-Sahara or Brasiliano belts and the West African or Amazonian cratons of West Gondwana (Figure 1-1). They exclude source areas in the ANS or the EAO. A separation of two major provenance zones in northern Africa is evident based on detrital zircon age spectra with the boundary between Algeria and Libya (Linnemann et al., 2011; Stephan et al., 2019), named by Stephan et al. (2019) the "West African zircon province" and "East African–Arabian zircon province".

Avigad et al. (2012) studied Cambrian sandstones in Morocco regarding the U-Pb-Hf isotopes of detrital zircons. They found the lower Cambrian units to have values reflecting the local Anti-Atlas crustal evolution. In the upper and mineralogically more mature Cambrian sandstones, they found a higher influence of a source area dominated by crustal reworking and ascribed it to a more distal source, possibly the Tuareg Shield to the west of the Sahara Metacraton.

In summary, lower Palaeozoic sedimentary rocks of North Gondwana are well studied in many places. They are generally highly mature, probably due to intense chemical weathering or recycling of earlier sediments (the latter especially assumed for sediments of the Hirnantian glaciation, e.g. Bassis et al., 2016a). In most studies, a provenance from the underlying basement combined with variable contribution of further distal sources in central Gondwana is assumed. An extremely distal provenance is suggested by Rösel et al. (2014) for the Hirnantian glaciogenic Lederschiefer in Germany (Saxo-Thuringia, which lay to the north of Gondwana during that time): based on a characteristic population of Stenian–Tonian zircons, they speculate that part of the material is derived from the Rayner Complex–Eastern Ghats regions of Antarctica and India and has been transported several thousands of kilometres, either in a single or multiple sedimentary cycles.

"Mass production" of Cambrian–Ordovician sediment and large-scale homogenisation of the distally sourced material that spread over the Gondwana peneplain after the Pan-African orogenies is likely (Garfunkel, 2002; Avigad et al., 2005). For the EAO, Squire et al. (2006) proposed a model of large sediment fans ("super-fans") that transported detritus towards the continental margins (Figure 1-1). They

based their model on similar zircon age spectra in lower Palaeozoic sandstones from India, Israel, Africa, Australia, New Zealand, South America and Antarctica. For north-eastern Africa and the Arabian Peninsula, however, the model is very speculative. Meinhold et al. (2013) constrained the super-fan model for this area by correlating detrital zircon ages from Morocco, Algeria, Libya, Israel and Jordan (Figure 1-1). They assumed that there was a fan system in this area that reached Libya and the north-western Arabian Peninsula, but not Algeria and Morocco. Stephan et al. (2019) statistically analysed an extensive dataset of zircon ages from northern Gondwana and the peri-Gondwana terranes and found three zircon provinces, one of which, namely the East African–Arabian zircon province, is in accordance with the assumed super-fan in this area. Lately, a detrital zircon study of Palaeozoic sandstones in Saudi Arabia could confirm that the super-fan reached Saudi Arabia (Meinhold et al., in revision).

The upper Palaeozoic sandstones of North Gondwana are less intensively studied. Investigations show a lower mineralogical maturity, more variable composition and also higher variations between the different study areas (e.g. Knox et al., 2007; Morton et al., 2011; Bassis et al., 2016a). The late Palaeozoic topography of North Gondwana was more complex and regionally variable than it was in the early Palaeozoic and was influenced by Hercynian tectonism and Neotethys rifting (Sharland et al., 2001; Laboun, 2010; Torsvik and Cocks, 2011).

1.3. Palaeozoic sandstones in Ethiopia

The peculiarity of the Palaeozoic sedimentary succession in Ethiopia is that it consists mainly of two formations that were deposited during and directly after the two major Gondwana glaciations in the Late Ordovician (Hirnantian glaciation) and Carboniferous–Permian (Late Palaeozoic Ice Age, LPIA): the Upper Ordovician–lower Silurian **Enticho Sandstone** and the upper Carboniferous–lower Permian **Edaga Arbi Glacials**. Their spatial extent in outcrops is limited: they occur mainly in the northern Ethiopian province Tigray and to a very minor extent in the west of the country. Dow et al. (1971) presented the first evidence for Palaeozoic glaciogenic rocks in northern Ethiopia. They described two facies, tillite facies and sandstone facies, and ascribed both to one single glaciation, either the Late Ordovician or the Carboniferous–Permian. Beyth (1972a; 1972b) confirmed the occurrence of these sandstones in other localities in northern Ethiopia and provided facies descriptions. Saxena and Assefa (1983) found *Discophyllum*, a fossil hydrozoa, in glaciomarine sandstone near the town of Enticho and concluded an Ordovician age. Based on trace fossils, Kumpulainen et al. (2006) assumed an Ordovician age for equivalent deposits to the Edaga Arbi Glacials in Eritrea. Bussert and Schrank (2007), however, were able to refute this assumption: palynological analyses of the Edaga Arbi Glacials in northern Ethiopia prove a Carboniferous–Permian age. They suggest that the Enticho Sandstone, which was assumed to be a lateral equivalent of the Edaga Arbi Glacials, as well as the rocks described by Kumpulainen et al. (2006) in Eritrea represent older sedimentary units. The sedimentary record of two different Palaeozoic glaciations in northern Ethiopia was confirmed by Bussert and Dawit (2009) and complemented with detailed sedimentological descriptions, trace fossil and palynological observations. The Carboniferous–Permian Edaga Arbi Glacials were further studied regarding their glaciogenic landforms and depositional environments by Bussert (2010; 2014). A summary of the sedimentological descriptions of both formations, complemented with own observations and field photographs is given in Section 2.2.

The provenance of the two Palaeozoic glaciogenic formations in Ethiopia has not been studied so far and data on geochemistry, heavy minerals or zircon chronology are not yet available. Such analyses are provided by work presented in this thesis.

1.4. Aims and objectives

By the work presented in this thesis, the data gap of specific provenance-relevant data for the Palaeozoic sandstones of Ethiopia is filled. Such data comprise geochemical composition, heavy mineral spectra, mineral chemical analyses and detrital zircon ages. They are published for many Palaeozoic successions in North-East Africa and the Arabian Peninsula (see Section 1.2), but are not yet provided for the Ethiopian sandstones. By complementing existing data on sedimentology, biostratigraphy and facies analyses (see Section 1.3) with provenance-specific data, further insights into the configuration of the sedimentary systems during the two time slices recorded in the Enticho Sandstone and the Edaga Arbi Glacials are possible. The fact that two major Palaeozoic Gondwana glaciations are recorded in the Ethiopian succession makes it possible to study aspects of ice sheet extent and glacier dynamics in comparison with existing models (e.g. Ghienne et al., 2007; Fielding et al., 2008; Le Heron and Craig, 2008; Bussert, 2010; Isbell et al., 2012; Section 1.1). In southern Libya (Morton et al., 2011) and Saudi Arabia (Knox et al., 2007; Bassis et al., 2016a) changing heavy mineral spectra in the Carboniferous suggest a re-organisation of the sediment dispersal system in the late Palaeozoic (Section 1.2). These changes may also be visible in the Ethiopian Palaeozoic formations. The super-fan model described in Section 1.2 (Squire et al., 2006; Meinhold et al., 2013; Stephan et al., 2019) is based on detrital zircon chronology and is still not well constrained for northern Gondwana nor confirmed with other methods. Ethiopia lies more proximal on the assumed sediment pathway of the super-fans and is thus highly interesting to test the model.

In summary, the objectives of this thesis are the following:
- provide provenance-specific data for the Ordovician–Silurian Enticho Sandstone and the Carboniferous–Permian Edaga Arbi Glacials to enable comparison and correlation with corresponding successions across north-eastern Gondwana,
- test the Gondwana super-fan model at a more proximal location,
- contribute to research on ice sheet extent and glacier dynamics during the Hirnantian glaciation and the Late Palaeozoic Ice Age (LPIA) by identifying source regions.

By this, a better understanding of the Palaeozoic sediment dispersal system of northern Gondwana and the influence of the two glaciations is possible.

1.5. Methodological strategy

1.5.1. Sampling

Samples for this thesis were mainly collected during a two weeks field trip in the province Tigray in northern Ethiopia in October 2015 (Figure 1-3). A second field trip has taken place to the Blue Nile region in western Ethiopia in April 2017 but in that area the sandstone formations of interest are hardly present. Therefore, the focus of this thesis is on samples from Tigray. Some samples were provided by Robert Bussert (TU Berlin), who collected them during previous field work. Two samples from the Blue Nile region (sample Hu-1 and Hu-2) were provided by him as well. Sampling in the field was based on previous stratigraphic and sedimentological work of Robert Bussert and Dawit Enkurie Lebenie (University of Mekele at that time, now University of Gondar, Ethiopia). They studied many sections in the region, provided facies analyses and stratigraphic classification through palynology, trace fossils and facies correlations (Bussert and Schrank, 2007; Bussert and Dawit, 2009; Bussert, 2014; Brocke et al., 2015). Sandstone samples were taken from surface outcrops at sections that were studied by the two colleagues before with priority to sections that are biostratigraphically constrained. Moreover, we made sure that the sampling locations covered a large geographical spread. In long sections, several samples were taken to capture stratigraphic variations. However, in many places, especially in the lower part of

the Enticho Sandstone, the sediments are rather massive, suggesting that they have been deposited in relatively short time and little stratigraphic variations can be expected.

During sampling, homogeneous areas in the outcrops were picked and samples with the grain size of fine sand were taken, where possible. Approximately 1–2 kg sandstone was taken per sample. Additionally, some samples were taken from granitoids, metasediments and metabasites from the local basement. Furthermore, boulders of granitoid, basalt and gneiss incorporated in tillites of the Edaga Arbi Glacials were sampled at two locations. In total, 16 samples were taken from the Enticho Sandstone (additional 11 samples were provided by R. Bussert), 15 samples from the Edaga Arbi Glacials (plus two additional from R. Bussert), 16 from the basement and 11 from boulders in tillite of the Edaga Arbi Glacials. A list of all taken samples with sampling location and short lithological classification can be found in the appendix (Table A 1). Prepared for analyses were 19 samples from the Enticho Sandstone, 13 from the Edaga Arbi Glacials, 7 samples from basement and all boulder samples. The selection of samples for analyses was made by giving priority to samples that are biostratigraphically constrained for the sandstones, to cover a large geographic and stratigraphic spread and by the quality of the samples (little weathering, uniform grain size). An overview of the selected samples for analyses and the applied methods is given in the appendix (Table A 2). Sections 2, 3 and 4 contain lists of the samples used in the respective study as well as maps with the sample locations. All samples are stored at the Institute of Applied Geosciences, Technical University of Darmstadt.

1.5.2. Multi-method provenance analysis

The composition of a sandstone is rarely the exact image of the source rocks contributing to the detritus. A sediment is altered by many different processes on its way from source to sink (Figure 1-4): weathering in the source area, breaking and abrasion, sorting during transport, addition of intraclasts, weathering during alluvial storage, recycling, sorting during deposition and processes acting during burial diagenesis (e.g. Morton and Hallsworth, 1999; Weltje and von Eynatten, 2004). This makes it difficult to trace back the provenance of the sediment and to ascribe features to a certain cause or process. Since none of the various methods that can deliver provenance information yields unique results, it is necessary to use several methods on the same samples parallel. Figure 1-5 gives an overview over the methods used in this thesis and their systematics. In the following, the methods and how they complement each other are described in brief.

Petrography

Thin sections of the sandstones, the basement and boulders were studied under a polarizing microscope at the Institute of Applied Geosciences, Technical University of Darmstadt. The samples from boulders and the basement were studied only qualitatively to determine the rock type, whereas for the sandstone samples, the proportions of quartz, feldspar and lithic fragments were counted. Details on the counting procedure are given in Section 2.3. These proportions give information on the sediment's mineralogical maturity, which is essentially influenced by chemical alteration during surface weathering (in the source area, at temporal storage during transport, or in the outcrop) or during diagenesis (Morton and Hallsworth, 1999; Garzanti, 2017). The textural maturity, i.e. roundness of the mineral grains and degree of sorting, can be assessed during petrography as well. It is influenced by processes acting during transport, such as transport medium, hydrodynamics and to a minor degree transport distance (Morton and Hallsworth, 1999; Garzanti et al., 2015; Garzanti, 2017). The matrix content can further reveal information on the transport process and depositional environment (e.g. beach sand vs. moraine deposits). While petrography provides rather a first approach on the nature of the samples and a bunch of possible processes that acted on the sediment, an advantage is that primary and secondary signals (such as authigenic phases that grew during diagenesis) can be separated.
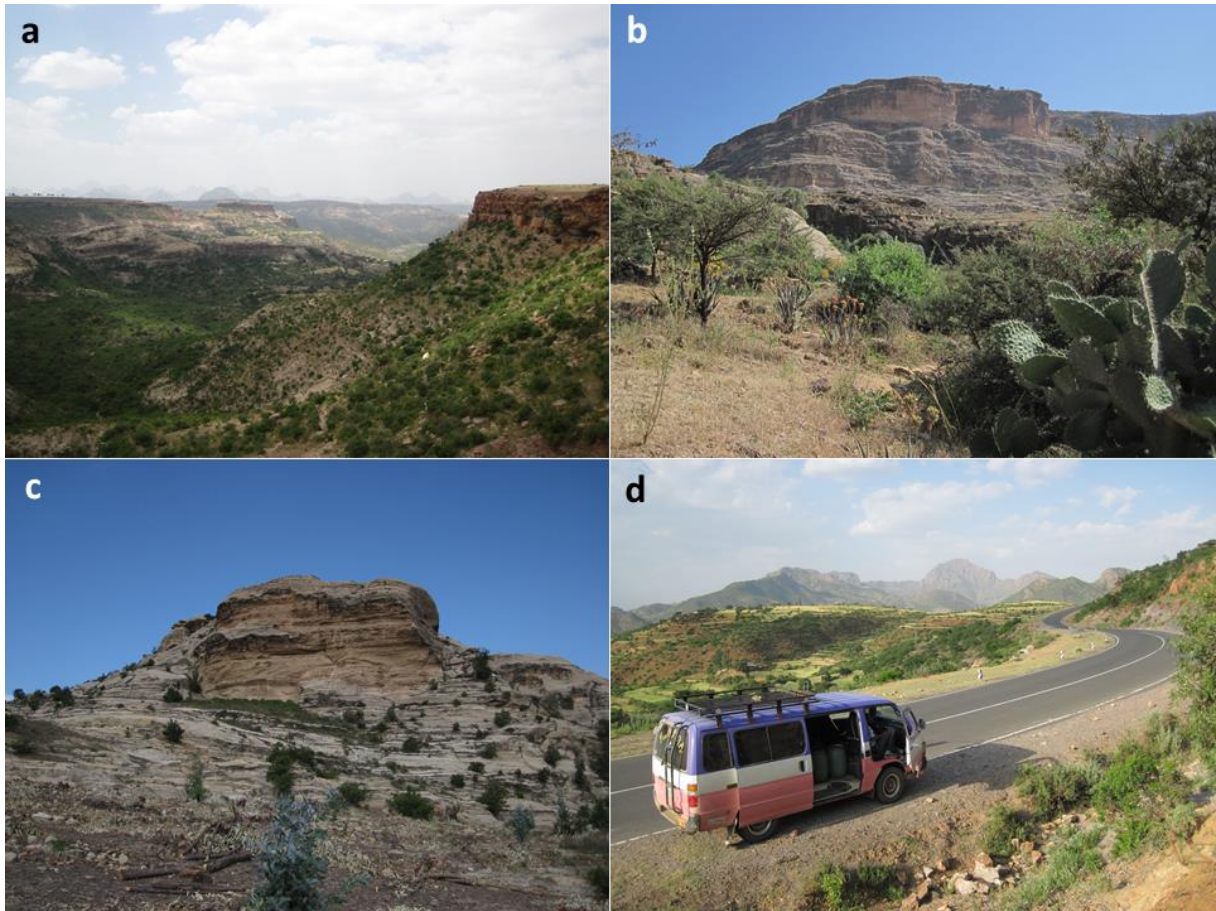
Figure 1-3: Impressions of the landscape in northern Ethiopia, where most of the samples were taken, from the field trip in October 2015. a) near Edaga Robi; b) near Zalambassa; c) near Atsbi; d) near Adwa.

Bulk geochemistry

Bulk geochemical analyses where carried out using X-ray fluorescence spectroscopy (XRF) and inductively coupled plasma mass spectrometry (ICP-MS) at the Geoscience Centre, University of Göttingen. Analyses were conducted on powders of sandstone, basement and boulder samples. Details on the procedure are given in Section 2.3. Major elements and certain trace elements were determined by XRF; further trace element, including rare earth elements (REE) were measured by ICP-MS. By analysis of the major elements, information from petrography can be confirmed and quantified. For example, the degree of chemical weathering (or diagenetic modification) can be assessed by the chemical index of alteration (CIA) introduced by Nesbitt and Young (1982). Major and trace elements can point to the presence of certain minerals or mineral groups. A high proportion of Al, for instance, is often associated with a high clay or feldspar content, whereas a high P content may point to apatite. Zr and Th may indicate the presence of heavy minerals, such as zircon or monazite. Furthermore, the major and trace element compositions of the studied sandstone samples are compared to those of the underlying basement to test a possible provenance from the local basement. Many of the studied elements are, however, highly mobile and thus easily affected by processes altering the sediment, including weathering in the outcrop, from which the sample is taken. The interpretation should, therefore, be done with caution. An element group, which is less mobile, is the group of rare earth elements (McLennan, 1989). The pattern of REE in a sandstone sample, normalized to the composition of a standard chondrite, gives first hints to the parent rocks, from which the sediment stems. For instance, rocks from differentiated and undifferentiated magmas feature different REE patterns (McLennan et al., 1993).
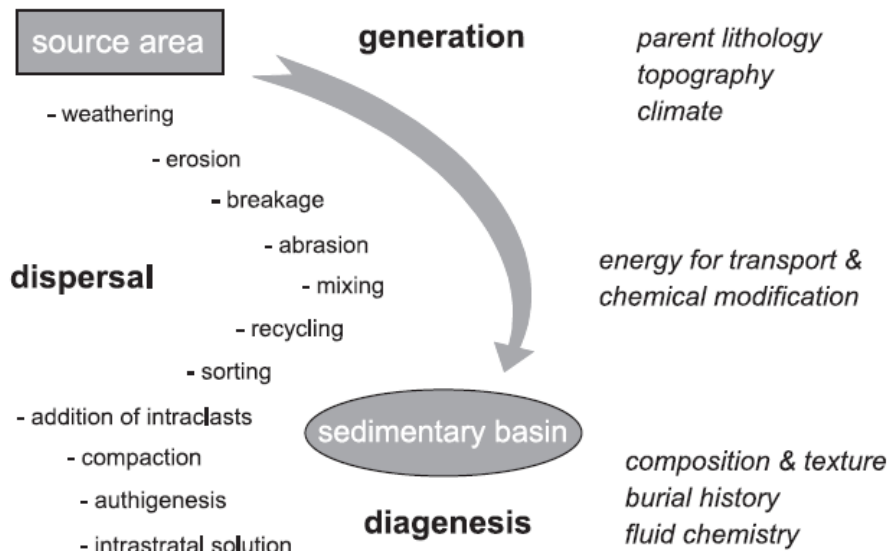
Figure 1-4: Processes altering a sediment on its pathway from source to sink and controlling factors for these processes (Figure from Weltje and von Eynatten (2004)).

Conventional heavy mineral analysis

Heavy minerals are minerals with a specific density higher than around 2.8 g/cm³ (Mange and Maurer, 1992). They can be rock forming in their parent rock (such as amphiboles, pyroxenes and micas) or accessory (such as zircon, apatite or tourmaline). In clastic sediments they usually make up less than 1 wt-% of the sediment (Mange and Maurer, 1992). Heavy minerals are often specific in origin and can be diagnostic for a certain source rock or rock type (e.g. metamorphic rocks, felsic igneous rocks, etc.). Some metamorphic minerals, such as andalusite, sillimanite and kyanite, even stand for certain pressure and temperature conditions. By conventional heavy mineral analysis, a study of the heavy mineral assemblage, i.e. counting the proportions of the various heavy minerals in the sample, is meant. Since the minerals have different potentials of being altered by physical and chemical processes (e.g. Morton and Hallsworth, 1999; Garzanti, 2017) and different hydrodynamic behaviours (e.g. Rubey, 1933; Garzanti et al., 2008), the study of mineral proportions may be misleading. Therefore, pairwise indices comparing the proportions of minerals with similar typical grain size, hydrodynamic behaviour and resistance to alteration can be used to assess, for instance, the influence of metamorphic versus magmatic parent rocks (e.g. Morton and Hallsworth, 1994). For conventional heavy mineral analysis, the grain size fraction of 63–125 µm has been used to ensure comparability with previous studies (Morton et al., 2011; Bassis et al., 2016a). Some samples were further studied in their 40–63 and 125–250 µm fractions to reveal the influence of the studied grain size window (for details see Section 4.3). The heavy minerals have been separated from the light ones using a liquid with a density of 2.8 g/cm³ and scatter mounts of the obtained heavy mineral concentrates were studied under a polarizing microscope at the Institute of Applied Geosciences, Technical University of Darmstadt. For some samples the heavy mineral proportions were additionally determined using Raman spectroscopy at the Geoscience Centre, University of Göttingen.

Mineral chemistry

The bulk of the heavy minerals in a sandstone is still significantly influenced by the above-described processes of alteration affecting a sediment on its way from source to sink. Therefore, for many minerals it is still not possible to discriminate, whether their presence/absence or ratios are due to certain source rocks that are involved, or due to later alteration. In most cases, it is probably a combination of both. To overcome this problem and get isolated provenance information, the study of single mineral species is

a powerful complementary technique (e.g. von Eynatten and Dunkl, 2012). The elemental or isotope composition of some heavy mineral species reflects certain chemical, pressure or temperature conditions during formation, which may point to a certain host rock type. In this thesis, the chemical compositions of rutile and garnet are studied. Rutile is one of the most stable heavy minerals and very resistant to physical and chemical alteration. Its chemical composition is dependent on the metamorphic temperature during formation and also on whether the mineral grows in a metafelsic or a metamafic host rock (e.g. Triebold et al., 2007; Meinhold, 2010; Triebold et al., 2012). Garnet chemical composition depends on host rock lithology, temperature and pressure conditions as well (Morton, 1987; Mange and Morton, 2007). For this thesis, rutile and garnet grains were hand-picked from the heavy mineral concentrates of ten samples under a binocular microscope, mounted in epoxy and polished. The chemical compositions were studied using electron microprobe analysis at the Geoscience Centre, University of Göttingen.
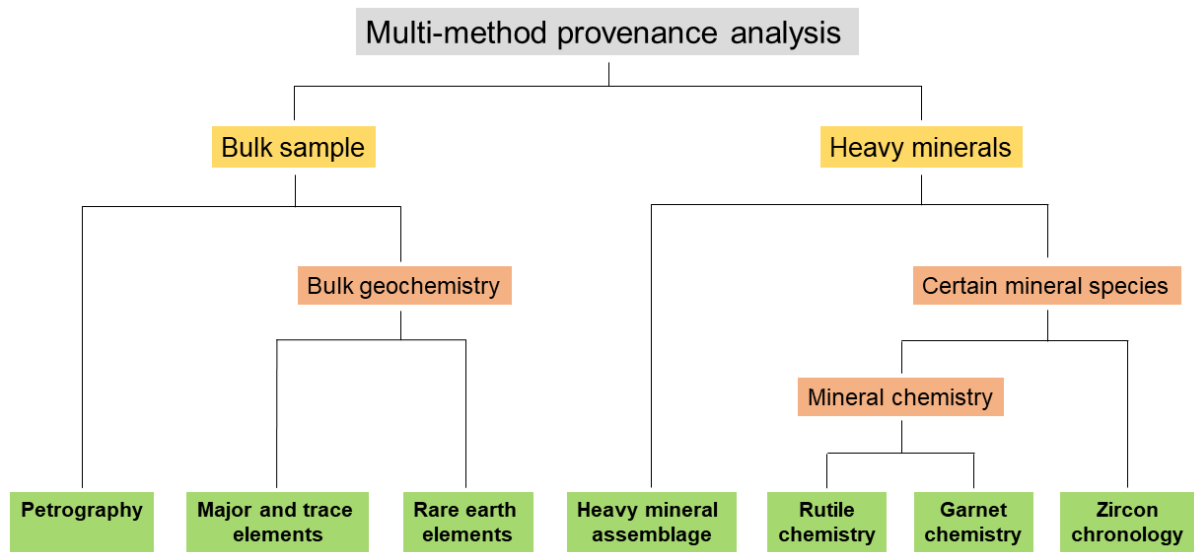
Figure 1-5: Overview of the methods used in this thesis and their systematics.

Detrital zircon chronology

Another suite of provenance methods applied to single mineral species is the radiometric dating of minerals. In this thesis, U–Pb dating of detrital zircons is applied. Zircon, similar to rutile, is one of the most stable heavy minerals and very resistant to physical and chemical alteration. Furthermore, zircon is an abundant heavy mineral in many kinds of source rocks. During growth, it incorporates U, but no or little Pb (Roberts and Spencer, 2015). When the mineral cools below the closure temperature of the U–Pb system, no exchange with the environment can take place anymore and during radioactive decay of U, the daughter product Pb becomes trapped and enriched in the crystal. The decay reactions used here are

$$^{206}Pb_{mineral} = {}^{206}Pb_0 + {}^{238}U_{mineral}(e^{\lambda_{238}t} - 1) \text{ and}$$
$$^{207}Pb_{mineral} = {}^{207}Pb_0 + {}^{235}U_{mineral}(e^{\lambda_{235}t} - 1).$$

Knowing the decay constant values, the crystallisation age t of the zircon can be determined by measuring the proportions of $^{206}Pb/^{238}U$ and $^{207}Pb/^{235}U$ in a zircon crystal. A common diagram for the U–Pb dating of zircon and monazite is the Concordia diagram. Plotting the ratios of $^{206}Pb/^{238}U$ and $^{207}Pb/^{235}U$ of many zircons of different age against each other after subtraction of the initial lead content yields a curve, along which the ages determined from the $^{206}Pb/^{238}U$ and $^{207}Pb/^{235}U$ ratio, respectively, are the same. A zircon grain which plots on the Concordia curve has been a closed system since its

crystallisation and its age can unequivocally be determined. A zircon grain plotting besides the curve is discordant due to diffusion of radiogenic Pb out of the crystal. If this lead loss occurred during a single (metamorphic) event, the intersections with the Concordia curve indicate the original crystallisation age and the age of lead loss (Okrusch and Matthes, 2005). However, the closure temperature of zircon regarding its U–Pb system is very high with $\geq 900\,°C$ (Lee et al., 1997). This means that the U–Pb system can survive most metamorphic and post-depositional processes without being modified and lead loss due to a single metamorphic event is rare. In most cases, lead loss of discordant zircons occurs continuously due to damage of the crystal structure by its own radioactivity and the crystallisation age cannot be determined (Okrusch and Matthes, 2005). For provenance analysis, the age populations of zircons in the studied sand(stone) samples can be linked to potential source rocks if the ages of these source rocks are known. A problem with the study of ancient rocks is, however, that the source rocks may not be present anymore nowadays. For this thesis, as for rutile and garnet chemistry, zircons were hand-picked from the heavy mineral concentrates of 11 sandstone samples under a binocular microscope, mounted in epoxy and polished. The measurement of U and Pb isotopes was performed using laser ablation inductively coupled plasma mass spectrometry (LA-ICP-MS) at the Institute of Mineralogy, University of Münster.

1.5.3. Statistical analysis of obtained data

Some data obtained in this thesis (e.g. bulk geochemistry, mineral chemistry and zircon chronology) were statistically evaluated to explore the internal variability of the datasets and compare them to literature data.

The data from petrographic and heavy mineral point counting, geochemical and mineral chemical analyses belong to the class of compositional data meaning that they contain relative information, are non-negative and sum up to a whole, e.g. 1 or 100% (Pawlowsky-Glahn and Egozcue, 2006). Standard statistical methods cannot readily be applied to this class of data, since such methods are designed for data in the real space that range from $-\infty$ to $+\infty$ and can lead to spurious effects when applied to parts of a composition (Pawlowsky-Glahn and Egozcue, 2006). The sample space for compositional data, however, is the simplex with the respective dimension (e.g. Egozcue et al., 2011). A way to transform compositional data from the simplex to the real space is taking log-ratios, that is, the logarithms of ratios of components (Aitchison, 1982; 1986). Aitchison (1982) introduced the additive and the centred log-ratio transformations. For the former, one of the components is taken as the denominator, all others are divided by this one and the natural logarithms are taken. For the latter, the components are divided by the geometric mean of the whole composition and the natural logarithm is taken. Egozcue et al. (2003) later introduced the isometric log-ratio transformation, which is more complicated to perform and the ratios more complex to interpret, but has some advantages when processing the data further (Pawlowsky-Glahn and Egozcue, 2006; Tolosana-Delgado, 2012).

In this study, centred log-ratio transformation (clr) is applied to prepare data for principal component analysis (PCA) as suggested by Tolosana-Delgado (2012). This method (PCA) reduces the dimensions of a multivariate dataset to principal components (PC) still containing the most important information and aiming to find the best summary of the data with a limited number of PCs (Lever et al., 2017). The PCs are linear combinations of the original variables of the dataset and can be seen as the directions in the dataset that explain a maximal amount of variance (Lever et al., 2017). There are as many PCs for a dataset as it contains variables and they are constructed in a way that the first PC represents the direction of the maximum variance within the dataset, the second PC the second largest amount of variance and so on. The result of a PCA can be displayed in a biplot of the first two PCs, making it possible to visualize the most important information contained in the dataset in two dimensions (Figure 1-6 a). In a clr-biplot the origin represents the centre (geometric mean) of the dataset (von Eynatten et al., 2003).

Both the samples and the variables are represented in the biplot (Figure 1-6 a). Variables are displayed as arrows pointing to their clr-loadings in the first two PCs (Tolosana-Delgado, 2012). The length of an arrow represents the variance of the corresponding clr-transformed variable, i.e. long arrows imply large variance, short arrows imply small variance (Tolosana-Delgado, 2012). A small angle between an arrow and one of the axes implies high influence of the respective variable on the corresponding PC (von Eynatten et al., 2003). A collinear set of arrows means that the respective variables are correlated, orthogonal arrows indicate that their pairs of log-ratios are uncorrelated (Tolosana-Delgado, 2012). The samples are displayed as points in the biplot. The distance between data points is a measure of similarity, that is, strong clustering of data points/samples implies that these samples have strong similarities in composition (von Eynatten et al., 2003). During interpretation of a compositional PCA biplot it must be kept in mind that only a portion of the total variability of the dataset is explained by the two-dimensional projection. The calculated percentage of variability represented by the two PCs of a biplot is a measure of strength of the biplot for data interpretation (von Eynatten et al., 2003). It is also possible to combine different datasets in one PCA, as it is done in Section 5.2. In this case, it is necessary to standardize the variables so that they have unit variance to account for the different units in the datasets (Lever et al., 2017).

For geochronological data, PCA is inappropriate. Vermeesch (2013), therefore, suggests multidimensional scaling (MDS) to facilitate multi-sample comparison of geochronological data. MDS is a superset of PCA and makes less assumptions about the data (Vermeesch, 2013). MDS is used in this study to compare detrital zircon age spectra obtained for the two studied formations to data from the literature. This technique produces a simple two-dimensional map (Figure 1-6 b) in which "similar" samples plot close together and "dissimilar" samples plot far apart (Vermeesch and Garzanti, 2015). The Kolmogorov–Smirnov statistics can be used as a dissimilarity measure (Vermeesch, 2013; Vermeesch and Garzanti, 2015). The MDS algorithm produces an R-dimensional configuration of points for which the Euclidian distance between two points approximates the disparity between the respective samples (Vermeesch, 2013). For R = 2, the result can be visualized as a map. For the most general case, making least assumptions about the data, *non-metric* MDS is used. The goal here is not to approximate the dissimilarities themselves, but rather their relative ranks (Vermeesch, 2013). The solution for non-metric MDS is not found analytically but numerically (Vermeesch, 2013). As for PCA, it is important to note that MDS makes an abstraction of the data and does not always cover all the details of complex datasets (Vermeesch, 2013).
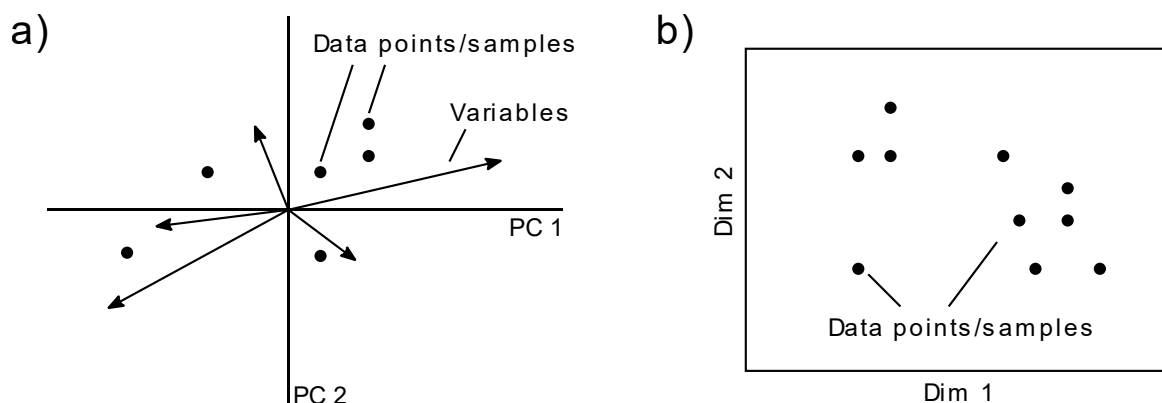

Figure 1-6: Simple sketch of a) a typical principal component analysis (PCA) biplot and b) a multidimensional scaling (MDS) map.

2. Provenance of sandstones in northern Ethiopia during Late Ordovician and Carboniferous–Permian Gondwana glaciations: petrography and geochemistry of the Enticho Sandstone and the Edaga Arbi Glacials

Anna Lewin[a], Guido Meinhold[b,c], Matthias Hinderer[a], Enkurie L. Dawit[d], Robert Bussert[e]

[a]Institut für Angewandte Geowissenschaften, Fachgebiet Angewandte Sedimentologie, Technische Universität Darmstadt, Schnittspahnstraße 9, 64287 Darmstadt, Germany
[b]Abteilung Sedimentologie / Umweltgeologie, Geowissenschaftliches Zentrum Göttingen, Universität Göttingen, Goldschmidtstraße 3, 37077 Göttingen, Germany
[c]School of Geography, Geology and the Environment, Keele University, Keele, Staffordshire, ST5 5BG, UK
[d]Department of Geology, University of Gondar, P.O. Box 196, Gondar, Ethiopia
[e]Institut für Angewandte Geowissenschaften, Fachgebiet Explorationsgeologie, Technische Universität Berlin, Ackerstraße 76, 13355 Berlin, Germany

Abstract

We compare Ethiopian glaciogenic sandstone of the Late Ordovician and Carboniferous–Permian Gondwana glaciations petrographically and geochemically to provide insight into provenance, transport and weathering characteristics. Although several studies deal with the glacial deposits in northern Africa and Arabia, the distribution of ice sheets and continent-wide glacier dynamics during the two glaciations remain unclear. Provenance data on Ethiopian Palaeozoic sedimentary rocks are scarce. The sandstones of the Late Ordovician glaciation are highly mature with an average quartz content of 95% and an average chemical index of alteration of 85, pointing to intense weathering and reworking prior to deposition. No evidence for sediment recycling was found. In contrast, the Carboniferous–Permian glaciogenic sandstones are less mature with an average quartz content of 75%, higher amounts of feldspar and rock fragments and a chemical index of alteration of 62. Trace and rare earth element concentrations indicate a higher input of juvenile material, most probably from proximal sources. Comparison with stratigraphically corresponding formations in Saudi Arabia shows similar geochemical patterns for the Upper Ordovician, but major differences in the Carboniferous–Permian. This supports previous assumptions of a large, uniform sediment dispersal system during the Late Ordovician glaciation, in which a combination of long transport paths and exceptionally strong weathering prior to the glaciation produced mature sandstone. During the Carboniferous–Permian, the glacial systems seem to have been more localised and glacial abrasion exposed fresh basement material.

2.1. Introduction

During the amalgamation of the Gondwana supercontinent in the Neoproterozoic (between 650 Ma and 600 Ma), the East African Orogen was formed – one of the largest accretionary orogens in Earth's history (Stern, 1994; Collins and Pisarevsky, 2005; Squire et al., 2006). In Northeast Africa, a stable platform developed after the consolidation of the newly formed continent, on which a vast blanket of Palaeozoic sand was deposited (Garfunkel, 2002; Avigad et al., 2005). The sediment transport direction is generally assumed to have been towards the margin of northern Gondwana (e.g. Meinhold et al., 2011; Morag et al., 2011). However, the exact provenance of the sediment and its pathways are still poorly understood. Palaeozoic sedimentary rocks in Ethiopia are related to the two major Gondwana glaciations: 1) the Late Ordovician glaciation and the following transgression, probably up to early Silurian and 2) the Carboniferous–Permian glaciation (Saxena and Assefa, 1983; Kumpulainen et al., 2006; Bussert and Schrank, 2007; Kumpulainen, 2007; Bussert, 2010) with a large hiatus between them.

Although several studies deal with the glacial deposits in northern Africa and Arabia (Ghienne, 2003; Le Heron et al., 2009; Bussert, 2010; Keller et al., 2011), the distribution of ice sheets and continent-wide glacier dynamics remain unclear. For the Late Ordovician glaciation, a scenario of a large ice sheet covering the whole Saharan region or even whole central Gondwana is proposed (e.g. Ghienne et al., 2007; Le Heron and Craig, 2008). During the Carboniferous–Permian glaciation, a more complex spatial and temporal pattern of ice sheets is likely. Different authors propose a system of several local ice centres that developed asynchronously across Gondwana (e.g. Eyles, 1993; Fielding et al., 2008). The late Palaeozoic topography in northern Gondwana was influenced by the Hercynian tectonic event and by thermal uplift prior to the formation of the Zagros rift zone that later formed the Neo-Tethys ocean (Sharland et al., 2001). In such elevated areas mountain glaciers may have formed in the Carboniferous–Permian (Konert et al., 2001; Bussert and Schrank, 2007; Le Heron et al., 2009). In southern Libya (Morton et al., 2011) and Saudi Arabia (Knox et al., 2007; Bassis et al., 2016a), provenance changes were identified during the Carboniferous based on heavy minerals, pointing to re-organisation of the sediment dispersal system. A comparative field study on deposits of both Gondwana glaciations in Saudi Arabia has been carried out by Keller et al. (2011); detailed petrographic and bulk-rock geochemical data on these formations were provided by Bassis et al. (2016b). Though, in these studies, common glacial and proglacial sedimentary features can be found in both formations, the sedimentary rocks of the Late Ordovician glaciation are significantly more quartzose than those of the late Palaeozoic glaciation. The high maturity of lower Palaeozoic sedimentary rocks of northern Gondwana – untypical for post-orogenic sediment – was also discussed by Garfunkel (2002) and Avigad et al. (2005). Recycling of older sedimentary units cannot be ruled out, but Avigad et al. (2005) suggested strong chemical weathering under a corrosive Cambrian–Ordovician atmosphere in a vegetation-free landscape to be the reason for this high sandstone maturity. Strong chemical weathering is indicated by the highest marine $^{87}Sr/^{86}Sr$ level in Earth's history during that time (e.g. Squire et al., 2006) and may have been enhanced by acidic precipitation due to Ordovician volcanism (Keller and Lehnert, 2010). Morag et al. (2011) assumed a far distant sediment source for lower Palaeozoic sedimentary rocks in Israel and Jordan based on pre-Pan-African detrital zircon ages. In Ethiopia, sedimentological and palynological studies on Palaeozoic glacial successions have been carried out by Dow et al. (1971), Beyth (1972a; 1972b), Saxena and Assefa (1983), Bussert and Schrank (2007), Bussert and Dawit (2009) and Bussert (2010; 2014), providing evidence that two different glaciations are recorded. Geochemical and heavy mineral data to assess the provenance of these sedimentary rocks are lacking so far. A likely proximal source area is the Arabian–Nubian Shield, which forms the northernmost part of the East African Orogen and reaches south to the northern Ethiopian basement (Figure 2-1). It consists of Neoproterozoic juvenile arcs, younger sedimentary and volcanic basins, voluminous granitoid intrusions and minor remobilised pre-Neoproterozoic crust and further contains ophiolite (Stern, 1994; Meert, 2003; Johnson et al., 2011; Stern et al., 2012). Potential distal source areas are the Archean cratons and the Proterozoic mobile belts in the centre of Gondwana (Figure 2-1).

In this study, we provide petrographic and geochemical data for the two Palaeozoic glaciogenic successions in Ethiopia in order to:
- Differentiate both formations based on petrography and geochemistry making it possible to assign unknown samples to one of them,
- Show that different weathering and transport conditions prevailed during both glacial periods,
- Point out a change in regional correlation with Saudi Arabia (Keller et al., 2011; Bassis et al., 2016a; 2016b) between the two glaciations, reflecting different extents of the palaeo-ice sheets.
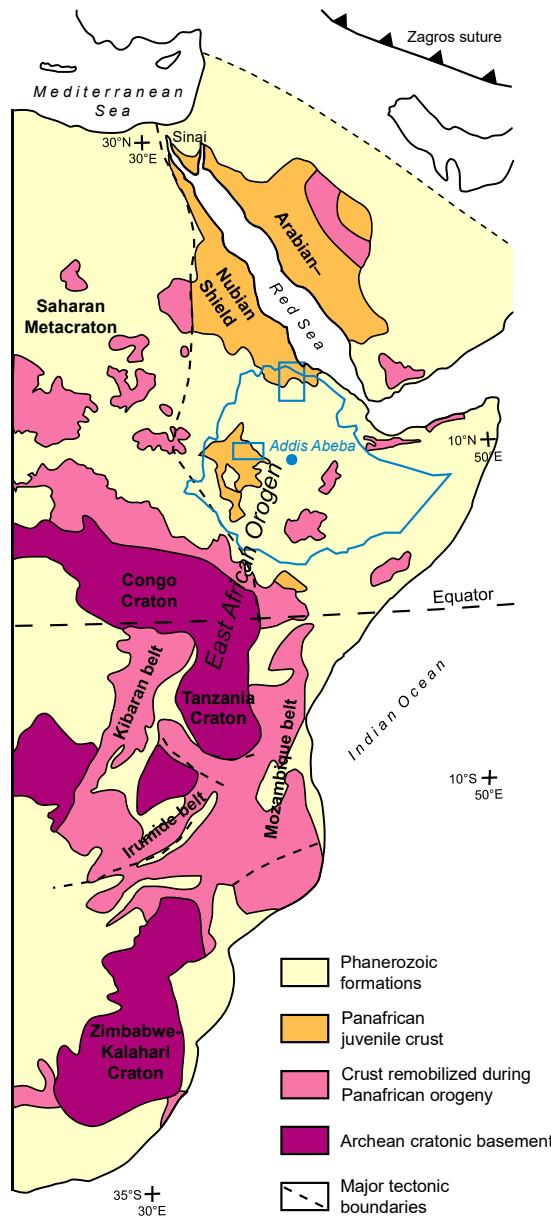
Figure 2-1: Eastern Africa and Arabia with occurrences of Precambrian rocks and major tectonic units. The outline of Ethiopia and the study regions are indicated in blue.

2.2. Geological setting

Palaeozoic sedimentary rocks crop out in the northern Ethiopian province Tigray around the Mekelle Basin and to a minor extent in the Blue Nile region in the west of the country (Kazmin, 1972; Garland, 1980; Tsige and Hailu, 2007). The Palaeozoic units comprise sediments of the two major Gondwana glaciations in the Upper Ordovician and the Carboniferous–Permian (Saxena and Assefa, 1983; Kumpulainen et al., 2006; Bussert and Schrank, 2007; Kumpulainen, 2007; Bussert, 2010). They overlie Neoproterozoic basement rocks and are in turn overlain by Mesozoic clastic and carbonate sediments (Beyth, 1972a; Tefera et al., 1996; Dawit, 2010).

The basement in Ethiopia represents the junction of the Mozambique Belt in the south and the Arabian–Nubian Shield in the North (Kazmin et al., 1978; Tefera et al., 1996; Stern et al., 2012; Figure 2-1). In the southern part of the Ethiopian basement, Neoproterozoic low-grade metavolcanic and metasedimentary rocks record submarine volcanism and marine sedimentation at the northern rim of the

closing Mozambique Ocean (Kazmin et al., 1978; Miller et al., 2003; Miller et al., 2009). In northern Ethiopia, the basement comprises two main units: the metavolcanic/metavolcaniclastic Tsaliet Group and the overlying Tambien Group, a slate and metacarbonate succession, both of up to greenschist facies (Beyth, 1972b; Alene et al., 2006). Syn- and post-tectonic granites and diorites intruded both units (Beyth, 1972b; Kazmin et al., 1978; Tefera et al., 1996).
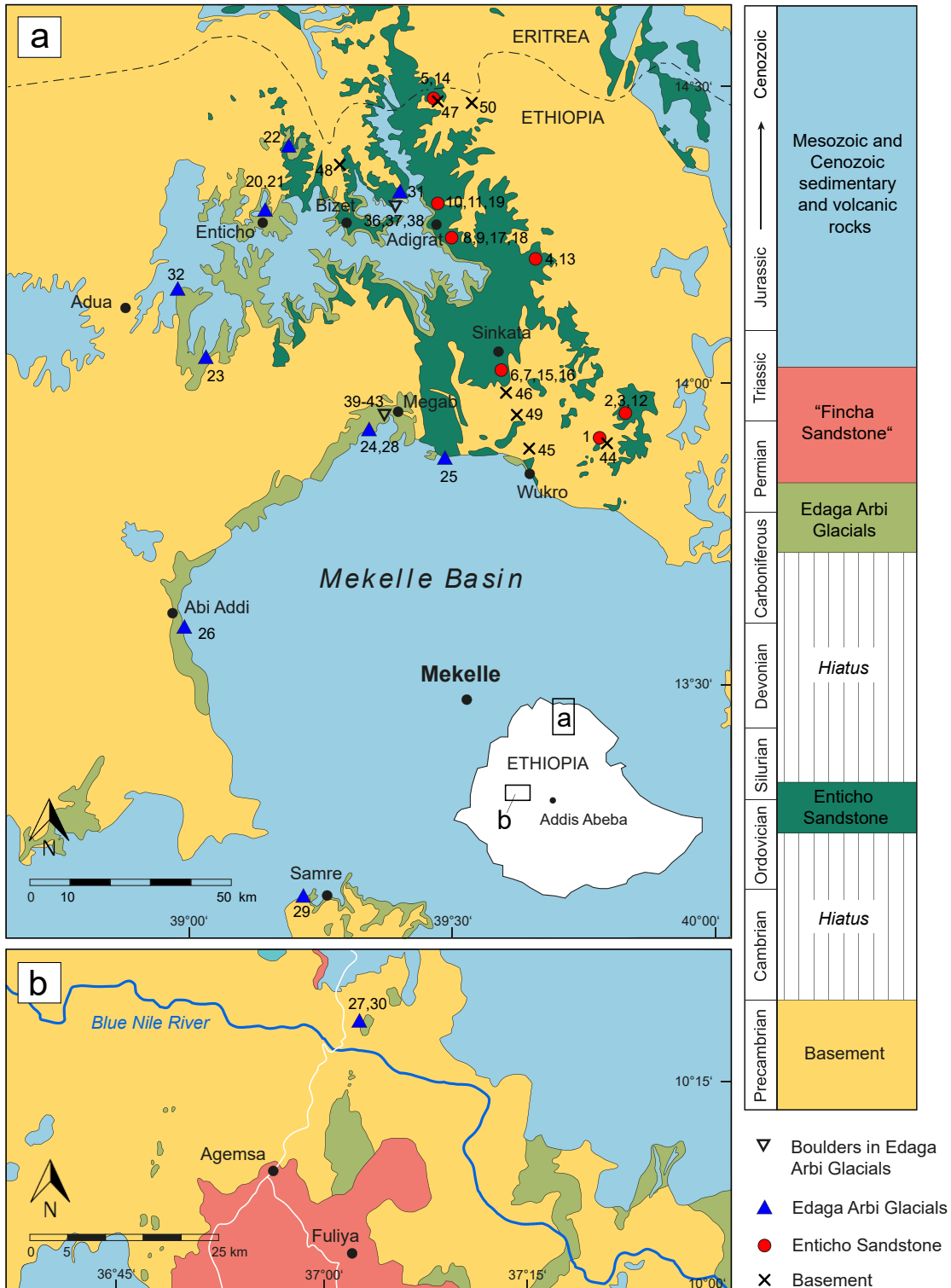
Figure 2-2 Geological maps of the study areas showing the sampling locations. Numbers next to the sampling locations correspond to those in Table Table 2-1. (a) Northern Ethiopia, modified after Arkin et al. (1971), Garland et al. (1978), Bussert (2014). (b) Blue Nile region, modified after Tsige and Hailu (2007), Dawit (2014). The term "Fincha Sandstone" is taken from Dawit (2014).

The Palaeozoic glacial deposits of Ethiopia were first described by Dow et al. (1971) and Beyth (1972a; 1972b) as two facies (tillite facies – Edaga Arbi Glacials and sandstone facies – Enticho Sandstone), which interfinger laterally and both, in places, lie unconformably on the basement. They assigned both facies to one glacial episode. Later, early Palaeozoic trace fossils (e.g. *Arthrophycus alleghaniensis*) were found in the upper part of the Enticho Sandstone and gave a minimum age for the underlying glaciogenic deposits (Saxena and Assefa, 1983; Kumpulainen et al., 2006). In the Edaga Arbi Glacials, Carboniferous–Permian palynomorphs provide age control (Bussert and Schrank, 2007; Bussert, 2014).

The Enticho Sandstone unconformably overlies the Neoproterozoic basement and has a thickness of up to 200 m (Saxena and Assefa, 1983; Dawit, 2010). Bussert and Dawit (2009) provide detailed facies descriptions. It consists of basal tillite, a lower glaciogenic sandstone unit and an upper shallow marine sandstone unit. The tillite is exposed only in the area east of Wukro (Figure 2-2). Its matrix is red medium sand. Clasts are angular boulders of metavolcanics, metapelites and conglomerates, probably from the local basement and well-rounded quartz pebbles, which may be recycled (Figure 2-3 g). Since large volumes of sandstone are not present in the local basement, the matrix material may have been transported from further away. Associated with the tillite are soft sediment deformation structures in underlying sandstone (Figure 2-3 h) and in the tillite itself, which may represent shallow marine push-moraine or grounding line complexes (Dawit, 2010). The glaciogenic unit consists mainly of massive, partly large-scale cross-bedded fine- to medium-grained sandstone, with intercalated gravel beds (Figure 2-3 f) interpreted to represent pulses of glacial outwash (Bussert and Dawit, 2009; Dawit, 2010). The shallow marine unit comprises well-sorted sandstones with bipolar cross-bed sets and rhythmic mud drapes suggesting a tide-dominated shallow marine depositional setting (Bussert and Dawit, 2009; Dawit, 2010). The Enticho Sandstone occurs along the eastern rim of the Mekelle Basin (Figure 2-2 a).

The Edaga Arbi Glacials unconformably overlie the Enticho Sandstone and, in places, lie directly on the basement (e.g. Beyth, 1972b). They crop out along the western and southwestern margin of the Mekelle Basin and to a minor extent in the Blue Nile region in western Ethiopia (Figure 2-2). Their thickness is around 200 m in northern Ethiopia, but significant lateral thickness variations occur (Bussert, 2010). Bussert and Dawit (2009) and Bussert (2014) give detailed descriptions of the sediment facies. The Edaga Arbi Glacials consist of tillite at the base overlain by laminated clay- and siltstones, which contain scattered out-sized clasts and lenses of sandstone (Beyth, 1972b; Bussert and Dawit, 2009; Bussert, 2014). In the tillite, mostly rounded boulders of granitoid, metabasic and metasedimentary rock are found and often exhibit striated surfaces (Figure 2-3 c). Outsized clasts in rhythmic lamination of sandstone and silt- to claystone (Figure 2-3 b) are interpreted as dropstones (Bussert and Dawit, 2009; Bussert, 2014). The sandstone lenses may represent channelized glacial outwash deposits or hyperpycnal sediment flows (Bussert and Dawit, 2009; Bussert, 2014). Bussert (2014) proposed a model for the generation of this succession with initial glacier advance and deposition of tillites, followed by the formation of subaerial and subaqueous outwash fans during the glacier retreat and the final suspension settling of silt and clay in calm water of a proglacial lake or fjord. Periodic hyperpycnal sediment flows and the deposition of dropstones interrupted the suspension settling. The association of the Edaga Arbi Glacials with glacial landforms on the basement surface, such as roche moutonnées, rock drumlins as well as glacial striae confirms a glacial origin (Bussert, 2010). In the Blue Nile region (Figure 2-2 b) Permian–Triassic continental sandstones partly overlie the Edaga Arbi Glacials (Dawit, 2014). The Palaeozoic succession is – unconformably in northern Ethiopia – overlain by the Mesozoic Adigrat Sandstone, the Antalo Limestone, Agula Shale and Amba Aradam Formation (Beyth, 1972b; Dawit, 2010).
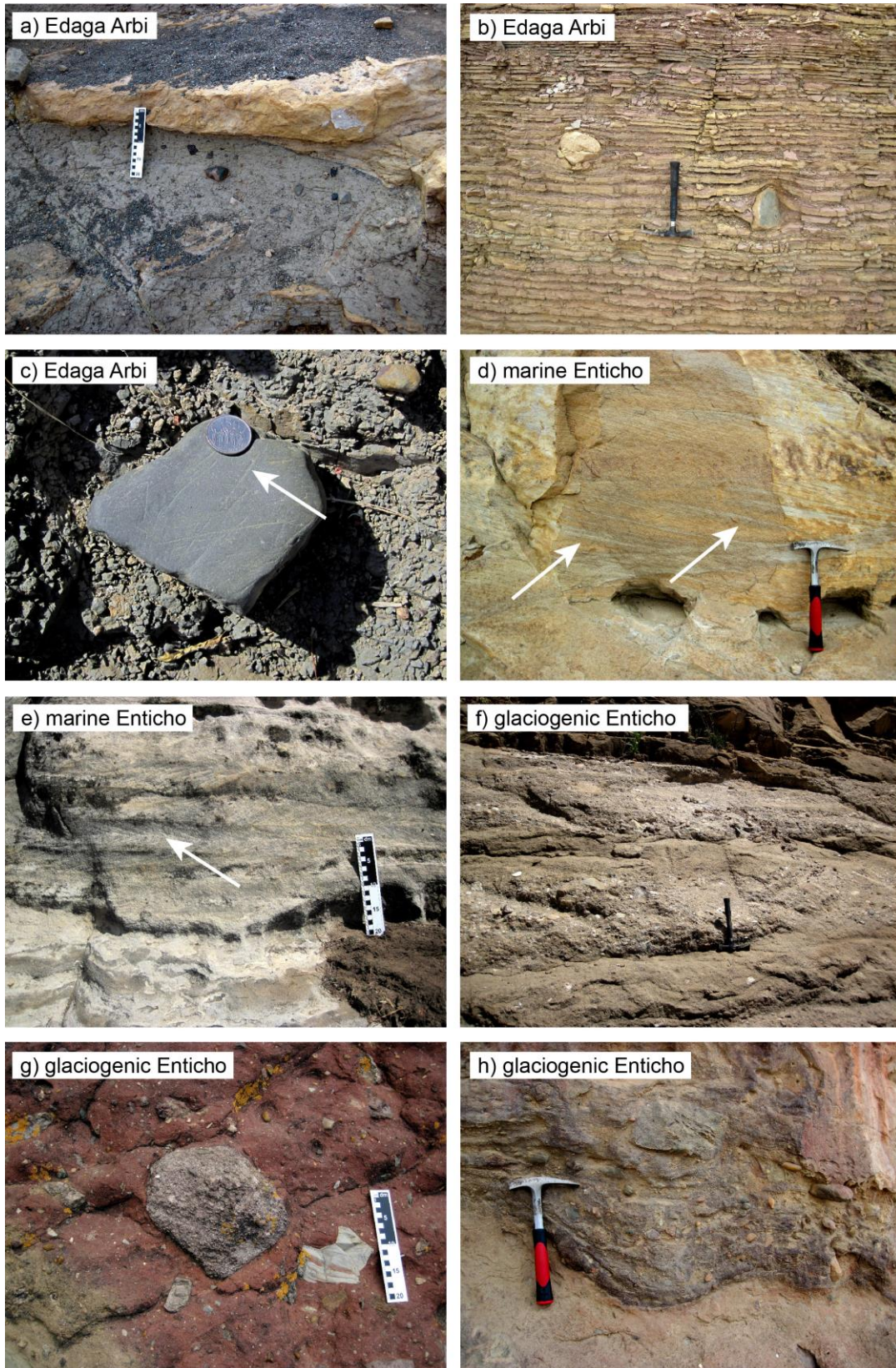
Figure 2-3: Field photographs. (a) Sandstone lens above tillite with muddy matrix and rounded clasts of various compositions at the base of the Edaga Arbi Glacials. (b) Dropstones in rhythmically laminated sandstone and silt- to claystone in Edaga Arbi Glacials. (c) Striated boulder in tillite at the base of Edaga Arbi Glacials. (d) Rhythmic mud drapes on cross-beds in marine part of the Enticho Sandstone indicating intertidal environment. (e) Herringbone cross-lamination in marine part of Enticho Sandstone indicating tidal environment. (f) Alternation of gravel beds and sandstone in glaciogenic part of Enticho Sandstone. (g) Tillite at the base of glaciogenic Enticho Sandstone. (h) Soft-sediment deformation structures in sandstone underlying tillite in the basal part of Enticho Sandstone.

2.3. Sampling and methods

Thirty-two sandstone samples were taken from surface outcrops, 19 from the Enticho Sandstone and 13 from the Edaga Arbi Glacials. The focus of the sampling campaign was on northern Ethiopia since Palaeozoic glacial sediments are more abundant there. In the Blue Nile region in the west of the country, glacial sediments could be identified at only one locality (Figure 2-2 b). In addition to the sedimentary rocks, 7 samples from the local basement of northern Ethiopia were studied, as well as 11 samples from boulders in tillite of the Edaga Arbi Glacials. Figure 2-2 shows the sample locations; Table 2-1 provides the corresponding coordinates. Sampling sites were chosen in order to cover a laterally extensive area based on previous stratigraphic and sedimentological work of R. Bussert and E. L. Dawit (Bussert and Schrank, 2007; Bussert and Dawit, 2009; personal communication). We paid attention to select sampling sites where there is biostratigraphic control on the sediments. Furthermore, we distinguished the Enticho Sandstone and Edaga Arbi Glacials based on homo-/heterogeneity in grain size and mineralogy and on sedimentary structures: the outcrops of the Enticho Sandstone – apart from the tillite at the base of one outcrop (see Section 2) – appear uniform in grain size and mineralogy (highly quartzose). The Edaga Arbi Glacials are much more heterogeneous (see Section 2.2). In the Edaga Arbi Glacials, we mainly sampled from the sandy lenses. Three samples are from the tillite matrix (Table 2-1). One sample was taken with highly uncertain stratigraphic assignment (sample Eda-5, Table 2-1). For reasons of comparability, we focused on the fine-grained parts of the sandstones during sampling, i.e. a dominating grain size of 63–250 µm, using the grain-size comparator chart for field work by Stow (2005).

Petrography
Thin sections were prepared from all samples. The samples from basement and tillite boulders were studied only qualitatively in to determine the rock type. The framework composition of the sandstone samples was assessed by point-counting of 300 grains per sample using the "traditional" counting method (e.g. Decker and Helmold, 1985). In contrast to the Gazzi-Dickinson method (e.g. Ingersoll et al., 1984; Zuffa, 1985), minerals within lithic fragments are counted as the type of fragment they occur in. We used this method to make sure that information conveyed by the type of lithic fragment is not lost. However, only few lithic fragments are present in the samples so that the choice of the counting method does not have a significant effect on the result. The matrix content was estimated based on the comparison chart of Folk (1951) with an upper grain-size limit for the matrix of 30 µm. Sorting and roundness of the framework grains were estimated according to Powers (1953). For sandstone classification, we used the scheme of McBride (1963; Fig. 2-4). We did not use the scheme of Dott (1964) that includes wackes, even though many samples have a high matrix content (Table A 3). This is, because in many cases it cannot be decided whether the matrix is primary or secondary.

Major and trace element geochemistry
For geochemical analysis, ~50 g of each of the 50 samples were pulverised to a particle size <63 µm using an agate vibratory disc mill. Geochemical analyses were carried out at the Geoscience Centre at the University of Göttingen, Germany. Concentrations of major elements and selected trace elements were determined by X-ray fluorescence analysis (XRF) on fusion tablets. For each sample 2.8 g of rock powder were mixed with 5.6 g of a di-lithium tetraborate/lithium metaborate fluxing agent (Spectromelt® A12, Merck) and 0.64 g lithium fluoride and fused in platinum crucibles at 1250 °C. XRF analysis was performed using a PANalytical AXIOS Advanced sequential X-ray fluorescence spectrometer equipped with a rhodium target tube for sample excitation and the software SuperQ 4 for data processing. Further trace elements, including rare earth elements (REE) were quantified using inductively coupled plasma mass spectrometry (ICP-MS) on the dissolved sample. For each sample 100 mg of rock powder were digested in the following steps using a PicoTrace® acid sample digestion system: (1) pre-reaction with 2 ml HNO_3 at 50 °C overnight, (2) first pressure phase with 3 ml HF (40%)

and 3 ml HClO$_4$ (70 %) at 150 °C for 8 hours, (3) evaporation at 180 °C for 16 hours, (4) second pressure phase with 10 ml double de-ionised water, 2 ml HNO$_3$ and 0.5 ml HCl at 150 °C for 4 hours. The resulting solution was diluted to 100 ml with ultrapure water. Analysis was performed using a ThermoElectron VG PlasmaQuad 2 quadrupole ICP-MS. Measurements were calibrated to the standard JA-2 of the Geological Survey of Japan.

Table 2-1: Samples, corresponding locations and geographic coordinates (WGS84). The stratigraphic assignment is based on biostratigraphic evidence (B) or lithofacies characteristics (LF) in the outcrop or it is uncertain (U).

#	Sample	Formation	Age	Location	North(°)	East(°)	Position within Fm.	Facies/ Lithology	Strati-graphic assignment
1	Enti-4	Enticho	Upper Ordovician	Atsbi south	13.83465	039.71262	Base	Tillite matrix	U
2	Enti-5	Enticho	Upper Ordovician	Atsbi north	13.88828	039.74783	Base	Glacial	B
3	Enti-7	Enticho	Upper Ordovician	Atsbi north	13.88842	039.74259	Base	Glacial	B
4	Enti-9	Enticho	Upper Ordovician	Wollwello	14.22037	039.65014	Base	Glacial	B
5	Enti-13	Enticho	Upper Ordovician	Zalambassa	14.49285	039.41911	Base	Glacial	LF
6	S1	Enticho	Upper Ordovician	Sinkata	13.96861	039.61167	Base	Glacial	B
7	S2	Enticho	Upper Ordovician	Sinkata	13.96861	039.61167	Base	Glacial	B
8	Nib-1	Enticho	Upper Ordovician	Adigrat south	14.25194	039.48972	Base	Glacial	B
9	Nib-2	Enticho	Upper Ordovician	Adigrat south	14.25194	039.48972	Base	Glacial	B
10	North-1	Enticho	Upper Ordovician	Adigrat north	14.31333	039.46000	Base	Glacial	B
11	North-2	Enticho	Upper Ordovician	Adigrat north	14.31333	039.46000	Base	Glacial	B
12	Enti-6	Enticho	Upper Ordovician	Atsbi north	13.88842	039.74827	Top	Marine	B
13	Enti-10	Enticho	Upper Ordovician	Wollwello	14.21839	039.64994	Top	Marine	B
14	Enti-12	Enticho	Upper Ordovician	Zalambassa	14.49627	039.41911	Top	Marine	LF
15	S3	Enticho	Upper Ordovician	Sinkata	13.97056	039.61111	Top	Marine	B
16	S4	Enticho	Upper Ordovician	Sinkata	13.97056	039.61111	Top	Marine	B
17	Nib-3	Enticho	Upper Ordovician	Adigrat south	14.25222	039.49583	Top	Marine	B
18	Nib-4	Enticho	Upper Ordovician	Adigrat south	14.25222	039.49583	Top	Marine	B
19	North-3	Enticho	Upper Ordovician	Adigrat north	14.31944	039.45889	Top	Marine	B
20	Eda-2	Edaga Arbi	Carboniferous-Permian	Enticho	14.28166	039.14725	Base	Tillite matrix	B
21	Eda-3	Edaga Arbi	Carboniferous-Permian	Enticho	14.27929	039.14836	Base	Sand lens	U
22	Eda-4	Edaga Arbi	Carboniferous-Permian	Edaga Robi	14.38906	039.18161	Base	Tillite matrix	U
23	Eda-6	Edaga Arbi	Carboniferous-Permian	Edaga Arbi west	14.05667	039.07095	Base	Sand lens	LF
24	Eda-8	Edaga Arbi	Carboniferous-Permian	Megab south	13.90944	039.32301	Base	Sand lens	B
25	Eda-10	Edaga Arbi	Carboniferous-Permian	Dugum	13.84957	039.49003	Base	Sand lens	LF
26	Eda-11	Edaga Arbi	Carboniferous-Permian	Abi Addi	13.61842	039.00042	Base	Sand lens	LF
27	Hu-1	Edaga Arbi	Carboniferous-Permian	Bure, Blue Nile	10.31057	037.05068	Base	Sand lens	LF
28	Eda-9	Edaga Arbi	Carboniferous-Permian	Megab south	13.90915	039.32235	Top	Sand lens	B
29	Eda-12	Edaga Arbi	Carboniferous-Permian	Samre	13.17844	039.19745	Top	Sand lens	B
30	Hu-2	Edaga Arbi	Carboniferous-Permian	Bure, Blue Nile	10.31057	037.05068	Top	Sand lens	LF
31	Eda-1	Edaga Arbi	Carboniferous-Permian	Adigrat west	14.31171	039.40472	Uncertain	Tillite matrix	LF
32	Eda-5	Uncertain	Uncertain	Adwa east	14.19102	038.93957	Uncertain	Sand lens	U
33	Bas-1		Unknown	Megab	13.93496	039.36520		Metabasite	
34	Bas-2		Unknown	Megab	13.93496	039.36520		(Meta)basite	
35	Gn-1		Unknown	Megab	13.93496	039.36520		Paragneiss	
36	Gr-3	Boulders	Unknown	Adigrat west	14.31171	039.40472		Granitoid	
37	Gr-4	in	Unknown	Adigrat west	14.31171	039.40472		Granitoid	
38	Gr-5	Edaga	Unknown	Adigrat west	14.31171	039.40472		Granitoid	
39	Gr-6	Arbi	Unknown	Megab	13.93496	039.36520		Granitoid	
40	Gr-7	tillite	Unknown	Megab	13.93496	039.36520		Granitoid	
41	Gr-8		Unknown	Megab	13.93496	039.36520		Granitoid	
42	Gr-9		Unknown	Megab	13.93496	039.36520		Diorite/Gabbro	
43	Gr-10		Unknown	Megab	13.93496	039.36520		Diorite/Gabbro	
44	Neop-1	Basement	Neoproterozoic	Atsbi south	13.83374	039.71132		Metagreywacke	
45	Neop-2	Basement	Neoproterozoic	Negash	13.83561	039.61442		Metatillite	
46	Neop-3	Basement	Neoproterozoic	near Negash	13.94186	039.59876		Metabasite	
47	Neop-4	Basement	Neoproterozoic	Zalambassa	14.49276	039.41899		Metapelite	
48	Neop-5	Basement	Neoproterozoic	Road Debre Damo – Enticho	14.37729	039.27883		Metagreywacke	
49	Gr-1	Basement pluton	Neoproterozoic	Negash highschool	13.89164	039.60517		Granitoid	
50	Gr-2	Basement pluton	Neoproterozoic	Sebea	14.46629	039.48225		Granitoid	

The Eu anomaly of the sandstone samples was calculated as suggested by McLennan (1989):

$$\frac{Eu}{Eu^*} = \frac{Eu_N}{(Sm_N * Gd_N)^{0.5}}$$

The subscript *N* indicates chondrite-normalised values (see Figure 2-6). To put the degree of weathering and leaching into numbers, we calculated the frequently used chemical index of alteration as proposed by Nesbitt and Young (1982):

$$CIA = \frac{Al_2O_3}{(Al_2O_3 + CaO^* + Na_2O + K_2O)} * 100.$$

The molecular proportions of the respective oxides are used. CaO* is the amount of CaO incorporated in silicates. Therefore, out of the Edaga Arbi Glacials only five samples without carbonate cementation are considered. To get an idea of the tectonic signature of the sandstones we used the tectonic setting discrimination diagrams of Verma and Armstrong-Altrin (2013) based on discriminant functions employing major oxides and trace elements.

For statistical analysis of the data, their compositional nature – vectors of non-negative values summing up to a whole – was taken into account. Standard multivariate statistical methods are designed for data in the real space whereas the sample space of compositional data is the simplex with the respective dimension (Aitchison, 1982; Egozcue et al., 2011). To transform compositional data from the simplex to the real space, Aitchison (1986) introduced the principle of log-ratio transformation, that is, taking the logarithms of ratios of components. In this study, we used the centred log-ratio (clr) transformation to perform a principal component analysis (PCA) of the major and trace element data. This means that parts of a composition (e.g., element concentrations of a sample) are transformed by taking the natural logarithm of the ratio of the respective part and the geometric mean of the whole composition (Aitchison, 2003). We performed a second PCA not considering the highly mobile elements K, Rb, Ba, Sr, Mn and Na. The high variability of these elements masks the provenance signal. Moreover, Ca and Mg are excluded, because they are probably influenced by carbonate cement. The major and trace element data of the local basement and tillite boulders were used for comparison. For the use of log-ratios the data set must not contain any zeros. Therefore, those have to be replaced by small values. We chose a multiplicative zero replacement using 0.65 times the detection limit, as suggested by Martín-Fernández et al. (2003), since only very few values are below the detection limits of the XRF and ICP-MS.

2.4. Results

Petrography
According to the classification scheme of McBride (1963) the glaciogenic facies of the Enticho Sandstone is quartzarenite to subarkose with an average composition of 90.5% quartz, 7.4% feldspar and 1.4% lithic fragments. The marine facies is quartzarenite with an average composition of 99.0% quartz, 0.2% feldspar and 0.3% lithic fragments (Figure 2-4, Table A 3). The lithic fragments are mostly plutonic or sedimentary. The sedimentary lithoclasts are fine sand- to siltstone, sometimes with metamorphic overprint, indicated by foliation. As expected, grain size and roundness are more variable in the glaciogenic than in the marine unit (Figure 2-5 b, c, Table A 3). The average matrix content is 16% with an average in the glaciogenic unit of 20% and 11% in the marine unit. Accessory minerals are mostly zircon, tourmaline, rutile and some opaque phases. The sandstones in the Edaga Arbi Glacials are subarkose to arkose with an average composition of 74.8% quartz, 18.9% feldspar and 3.3% lithic fragments (Figure 2-4, Table A 3). Most lithic fragments are plutonic or sedimentary, as in the Enticho Sandstone, but few volcanic lithics were also counted (Table A 3). Apart from zircon, tourmaline, rutile and opaque phases, garnet is an additional accessory mineral. The sandstones in the Edaga Arbi Glacials are generally heterogeneous in composition and texture with variable roundness and moderate sorting (Figure 2-5 a, Table A 3). The average matrix content is 20%. 4 of 13 analysed samples of the Edaga Arbi Glacials are strongly cemented with calcite with 20–25% of the thin section area, 4 samples contain up to 5% calcite cement and the remaining 5 samples contain almost no calcite. No indicators for

significant sediment recycling, such as abraded quartz overgrowths or abundant sedimentary lithoclasts were found in either of the two formations.

The samples taken from the basement include two metagreywackes, one metatillite, one metapelite, one metabasite and two granites. The boulders sampled from the tillite at the base of the Edaga Arbi Glacials are classified as six granitoids, two diorites/gabbros two metabasites and one paragneiss (Table 2-1).
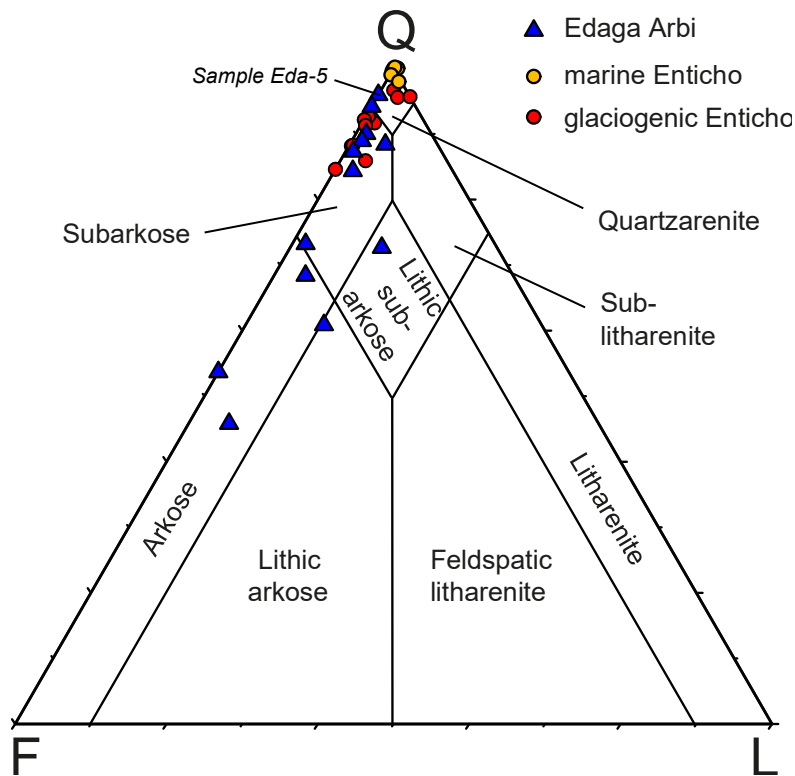
Figure 2-4: Sandstone classification diagram after McBride (1963). Q = quartz, F = feldspar, L = lithic fragments (thin section point-counting).

Bulk-rock geochemistry

The Enticho Sandstone, especially the marine unit, is depleted in the mobile elements Rb, Ba, K and Sr but enriched in Th and Zr compared to the average upper continental crust (Figure 2-6). Its elemental composition is highly variable, especially in the mobile elements. The REE pattern is typical for sedimentary rocks of upper crustal origin (Figure 2-6; McLennan et al., 1993). The chondrite-normalised La_N/Yb_N, which quantifies the LREE enrichment, is on average 10.7. The Eu anomaly is pronounced (i.e. <1) in the Enticho Sandstone with a mean Eu/Eu* for the glaciogenic facies of 0.8 and 0.7 for the marine facies. The CIA is on average 92 for marine facies and 78 for the glaciogenic facies (Table A 4). The elemental composition of the Edaga Arbi Glacials is more uniform. The depletion in mobile elements and the Zr enrichment is less than for the Enticho Sandstone. The chondrite-normalised La_N/Yb_N is on average 5.9 and the mean Eu/Eu* 0.9. The average CIA is 62 (Table A 4). Sample Eda-5, with uncertain stratigraphic assignment, differs from the Edaga Arbi Glacials sandstone by high depletion in mobile elements, Zr enrichment (Figure 2-6) and a high CIA of 95.

In the PCA biplot of major and trace elements (Figure 2-7 a), a clear separation between the two formations as well as between the glaciogenic and the marine facies becomes obvious: along the rays of Ni and Th (enriched in Enticho Sandstone) versus Ca, Mg and Na (enriched in Edaga Arbi Glacials) the two formations can be distinguished. Along the rays K, Rb, Ba and Sr (enriched in glaciogenic) versus

P, Y, V, Sc and HREE (enriched in marine), different facies separate. Sample Eda-5 has a similar composition to the Enticho Sandstone. The first three PCs (Figure 2-7 b, c) of the principal component analysis excluding mobile elements and carbonate cement influence together explain 74% of the total variability. Again, a separation of the two formations is possible with the Enticho Sandstone being enriched in Th, Zr, Hf, U, Si and depleted in P and Al compared to the Edaga Arbi Glacials. This separation is facies-independent since no clustering of marine and glaciogenic Enticho Sandstone is visible. No patterns related to stratigraphic or geographic sampling position were detected (not shown in Fig. 7).
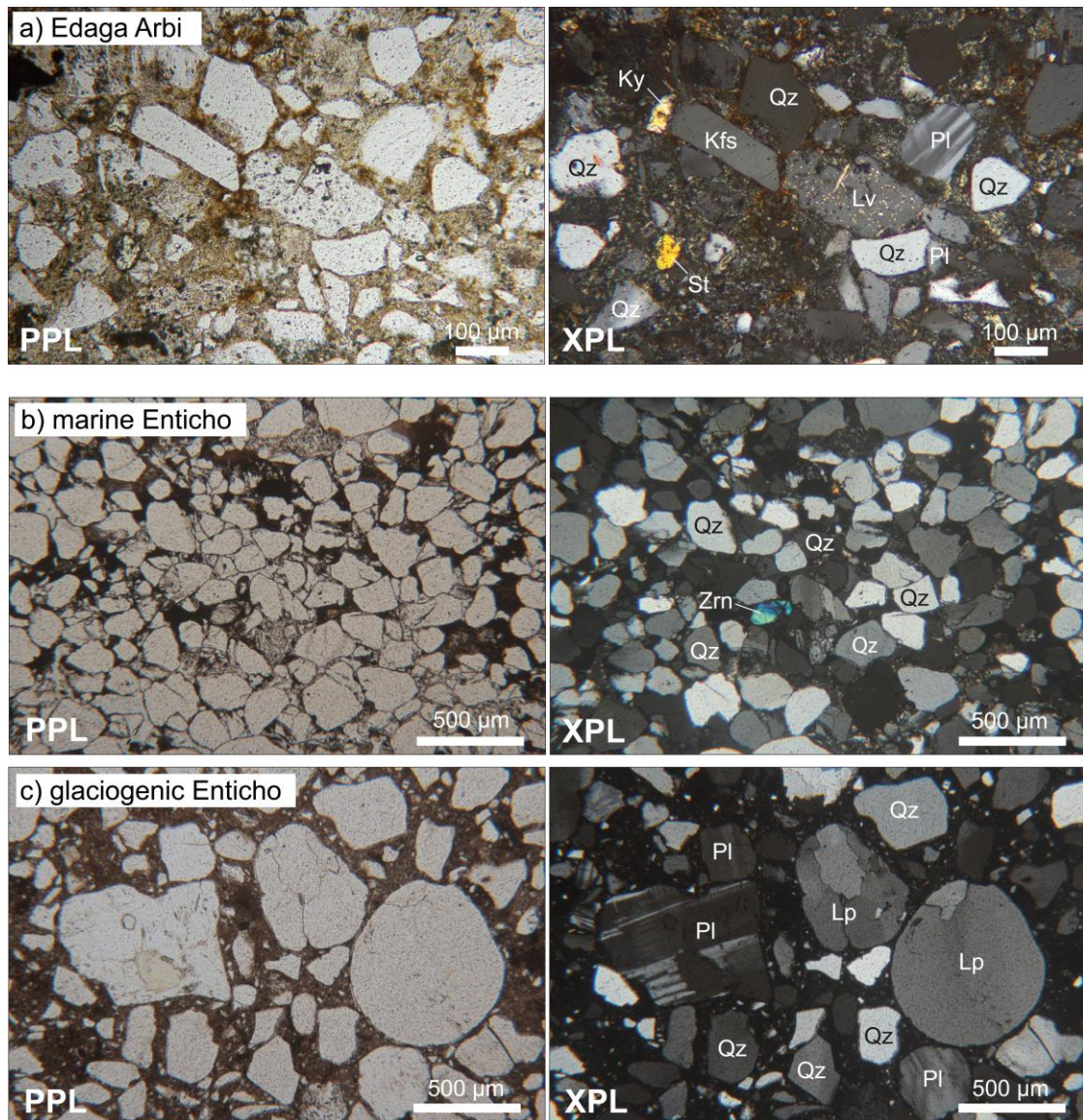
Figure 2-5: Thin section photomicrographs of the Edaga Arbi Glacials and the marine and glaciogenic units of the Enticho Sandstone. Qz = quartz, Pl = plagioclase, Kfs = potassium feldspar, Lp = plutonic lithic fragment, Lv=(meta)volcanic lithic fragment, St = staurolite, Ky = kyanite, Zrn = zircon (mineral abbreviations after Kretz (1983); Whitney and Evans (2010)). PPL = plane-polarised light, XPL = cross-polarised light.

In the tectonic setting discrimination diagram of Verma and Armstrong-Altrin (2013) based on major oxide concentrations, the Enticho Sandstone plots in the "continental rift" field, the Edaga Arbi Glacials in the "continental rift" and "collision" fields (Figure 2-8 a). In the active versus passive margin diagram of Verma and Armstrong-Altrin (2016; Figure 2-8 b) based on major oxides and selected trace elements, the Enticho Sandstone is assigned to a passive margin setting whereas the Edaga Arbi Glacials plot

partly in the active and partly in the passive margin field. The Th/Sc and Zr/Sc ratios are generally higher for the Enticho Sandstone than for the Edaga Arbi Glacials (Figure 2-9). Significant Zr enrichment that would lead to a deviation from the compositional trend is not clearly visible for either of the formations. A plot of the Th/Sc versus Zr/Sc ratios of the samples grouped geographically into north, centre and south (Figure 2-9 b) reveals a trend towards higher Th/Sc and higher Zr/Sc ratios along the assumed transport direction from south to north for both formations.
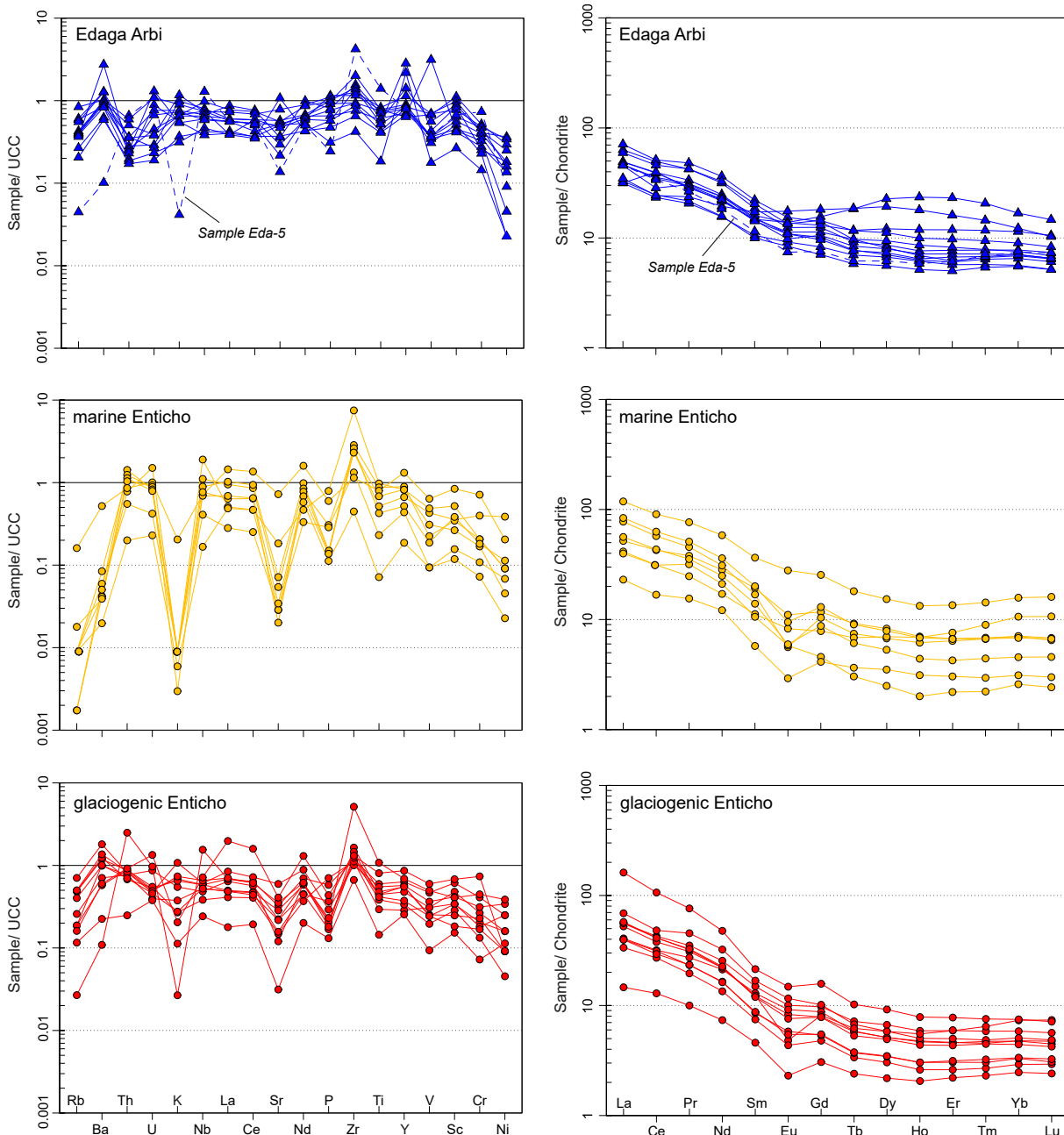
Figure 2-6: Selected major and trace element concentrations normalised to the average upper continental crust (UCC; normalising values from McLennan (2001)) are shown on the left side. Rare earth element concentrations normalised to average CI chondrites (normalising values from Taylor and McLennan (1985)) are shown on the right side.

Of the basement samples, the granites are enriched in Nb, HREE and Y and depleted in Cr and Ni compared to the centre of the data set plotted in Figure 2-10. The metasediments are enriched in V, Sc, Fe, Ni and Cr and depleted in Zr, Th, Hf and U, similar to the metabasite (Figure 2-10). The overall composition of the basement samples resembles that of the Edaga Arbi Glacials (Figure 2-10). Of the

boulders sampled from tillite at the base of the Edaga Arbi Glacials, the granitoids have similar compositions to the granites in the basement (Figure 2-10 a). The diorites/gabbros have variable compositions, one being rich in P and the other in Fe and Sc (Figure 2-10 a). Of the basalts, one is enriched in HREE, Nb and Y, the other in V, Sc and Cr. The composition of the paragneiss is close to the centre of the data set with slight enrichment in Fe, Sc and Cr.
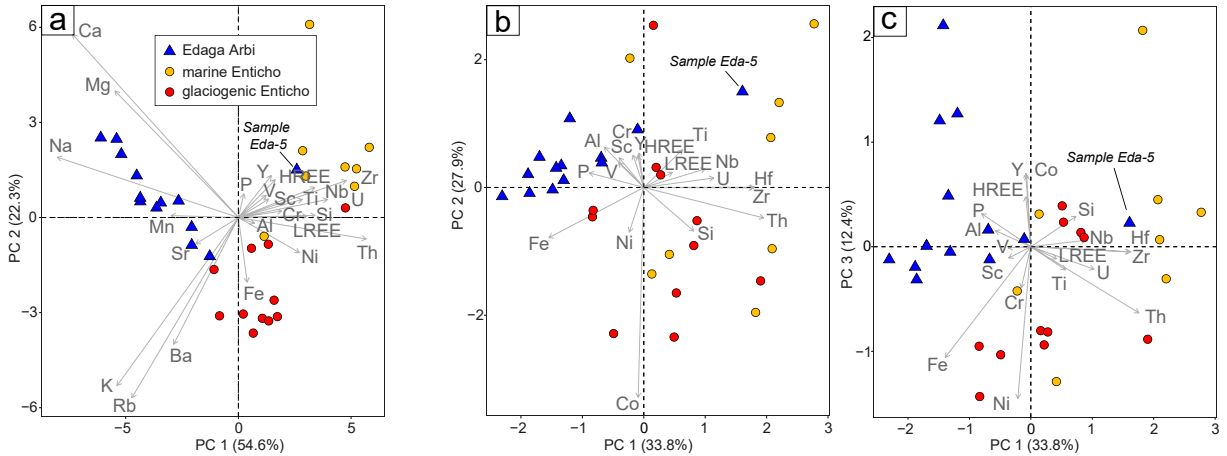
Figure 2-7: Compositional biplots of (a) the first two principal components of a principal component analysis (PCA) based on the clr-transformed concentrations of the major and trace elements considered in Fig. Figure 2-6 with the sum of LREE and HREE, (b) the first and second and (c) the first and third principal components of a PCA based on the clr-transformed concentrations of a subset of the elements considered in Fig. Figure 2-6, which is assumed to be less affected by diagenesis and leaching.

2.5. Discussion

When interpreting bulk-rock geochemical data, grain-size effects have to be considered (e.g., Rollinson, 1993; von Eynatten et al., 2012). The grain-size distribution of a sediment is influenced by transport processes, such as hydraulic sorting and comminution (e.g., Rubey, 1933; Garzanti et al., 2008; von Eynatten et al., 2012) and by the inherited grain size of the respective minerals in the parent rock (Morton and Hallsworth, 1994). Even though we collected samples of the same major grain size, the degree of sorting of framework grains and the matrix content differ (Section 2.4; Table A 3). Therefore, for instance, the high contents of Mg, Ca, Na and K in the glacial samples (Figure 2-7 a) are probably not only related to (little) weathering and (strong) diagenesis but also to the poor sorting and higher matrix content of the glacial samples as compared to the marine (Table A 3). To account for the facies differences, we plotted the glaciogenic and marine facies of the Enticho Sandstone separately in the respective diagrams (Figure 2-4, Figure 2-6 to 2-10).
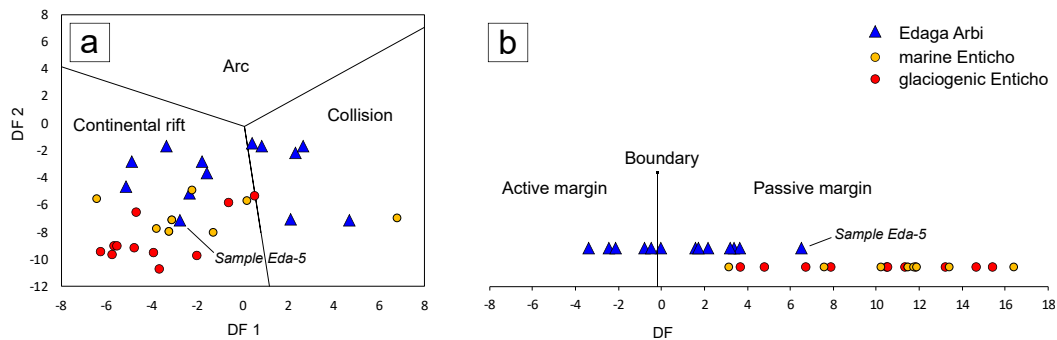
Figure 2-8: Tectonic setting discrimination diagrams after Verma and Armstrong-Altrin (2013; 2016). (a) Discriminant functions (DF) based on major oxides (SiO_2, TiO_2, Al_2O_3, Fe_2O_3, MnO, MgO, CaO, Na_2O, K_2O, P_2O_5; Verma and Armstrong-Altrin, 2013). (b) Discriminant function based on major oxides and selected trace elements (SiO_2, TiO_2, Al_2O_3, Fe_2O_3, MnO, MgO, CaO, Na_2O, K_2O, P_2O_5, Cr, Nb, Ni, V, Y, Zr; Verma and Armstrong-Altrin, 2016).

A clear distinction of the two formations is possible, particularly in terms of their major and trace element compositions (e.g. Figure 2-7, Figure 2-8). This makes it possible to assign stratigraphically uncertain samples: sample Eda-5 was tentatively assigned to the Edaga Arbi Glacials by sedimentological characteristics in the field but without biostratigraphic evidence. Based on the geochemical characteristics it is likely that it belongs to the Enticho Sandstone instead. Furthermore, the samples taken from an outcrop in Enticho (samples Eda-2 and Eda-3) – originally the type location of the Enticho Sandstone – can be assigned to the Edaga Arbi Glacials based on their petrography and chemical composition (Table A 3, Table A 4).
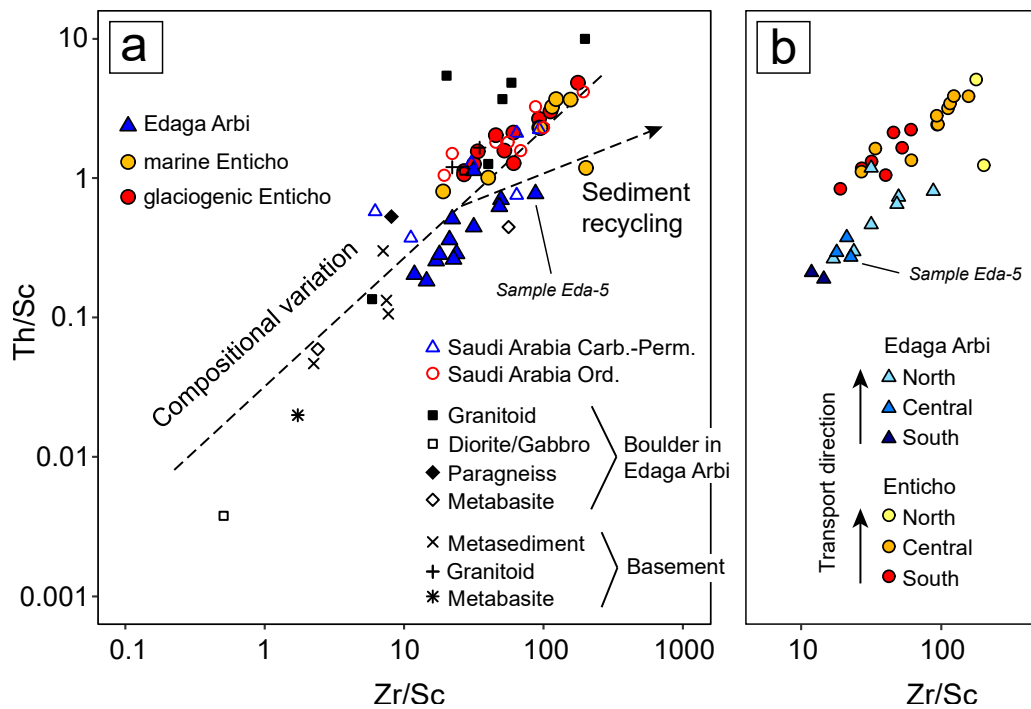
Figure 2-9: Th/Sc versus Zr/Sc diagram after McLennan et al. (1993). (a) Samples analysed in this study, stratigraphically equivalent units from Saudi Arabia (Bassis et al., 2016b), boulders in tillite of the Edaga Arbi Glacials (granitoid, diorite/gabbro, metabasite and gneiss) and local basement (granitoid, metabasite and metasedimentary rocks; this study). (b) Samples analysed in this study grouped by their geographic position.

The high variability in Ca, Mg, Na, K, Rb and Ba (Figure 2-7 a) in the data set reflects the high mobility of these elements, which are present in the glaciogenic sedimentary rocks but leached from the marine. The enrichment of Si in the Enticho Sandstone (Figure 2-7) indicates a higher quartz content, which is in agreement with petrographic observations (Figure 2-4, Table A 3) and points to high maturity. The negative correlation of Al and Si (Figure 2-7 b) indicates transport processes that remove clay minerals and feldspars and destroy lithic fragments and thus relatively enrich quartz in the Enticho Sandstone. Similarly, the negative correlation of P and Th (Figure 2-7 b, c) suggests weathering under acidic conditions, in which apatite is destroyed and Th persists and which affected the Enticho Sandstone more than the Edaga Arbi Glacials. This is supported by the higher CIA values for the Enticho Sandstone (Table A 4). The correlations of Hf, Th, U and Nb with Zr and Ti in the Enticho Sandstone (Figure 2-7 b, c) suggests that these elements are carried zircon and rutile. The presence of these stable heavy minerals is an additional indicator for maturity. The high maturity of the Enticho Sandstone is probably a consequence of (1) intense chemical weathering in the source area prior to the glaciation and (2) long transport and/or marine reworking, in which clay minerals produced during weathering are removed from the sediment. Intense chemical weathering in northern Gondwana under a corrosive Neoproterozoic to pre-glacial Ordovician atmosphere was suggested by, e.g., Avigad et al. (2005). The assignment of the Enticho Sandstone to "continental rift" and "passive margin" settings based on major

and trace element composition (Figure 2-8; Verma and Armstrong-Altrin, 2013; 2016) is related to the higher maturity as well.

For the Edaga Arbi Glacials, on the other hand, Al enrichment indicates a higher content of feldspar and clay minerals and thus a lower maturity (Figure 2-7 b, c). Since Eu is enriched in plagioclase, the less pronounced anomaly in the Edaga Arbi Glacials (Figure 2-6) corresponds to a higher feldspar content as well. This is in accordance with the petrographic observations (Figure 2-4, Table A 3). The higher concentration of HREE in the Edaga Arbi Glacials is probably related to the presence of garnet. The tendency of the Edaga Arbi Glacials to "collision" and "active margin" signatures (Figure 2-8) points to fresher, less reworked material deposited in the Carboniferous–Permian and does not have to indicate different tectonic settings.
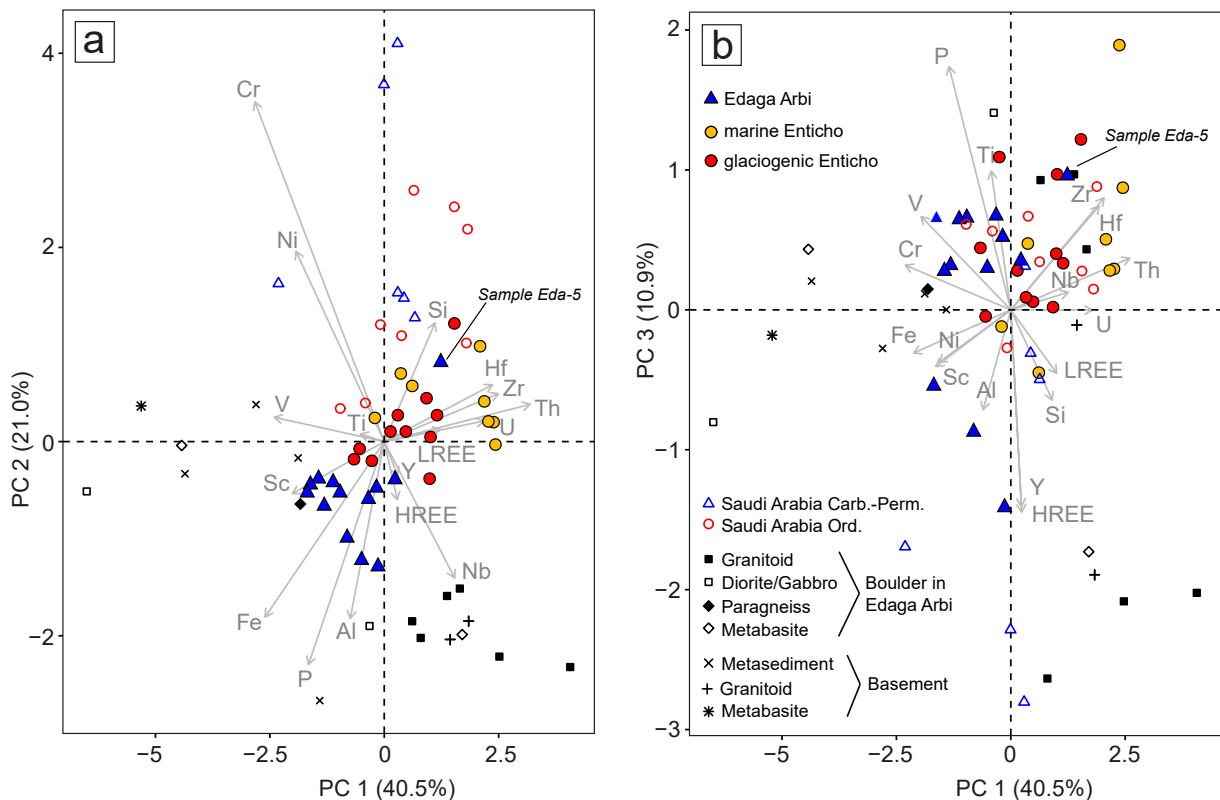
Figure 2-10: Compositional biplots of (a) the first and second and (b) the first and third principal components of a principal component analysis (PCA) based on the clr-transformed concentrations of the major and trace elements in Fig. Figure 2-7 (b, c) comparing the samples analysed in this study with stratigraphically equivalent samples from Bassis et al. (2016b), local basement samples and boulders in tillite of the Edaga Arbi Glacials (this study). Co is left out, because it was not measured by Bassis et al. (2016b). Carb. = Carboniferous, Perm. = Permian, Ord.= Ordovician.

Neither petrography nor the Th/Sc and Zr/Sc ratios give hints to sedimentary recycling being an important process for one of the formations. The few fine-grained and foliated sedimentary lithoclasts may be due to local erosion of slates from the Neoproterozoic basement. The south-north trend of Th/Sc and Zr/Sc ratios in both formations (Figure 2-9 b) may be due to progressive enrichment of stable heavy minerals, such as zircon, along the transport path. Zircon is a major carrier of Zr and Th (Figure 2-7). Another possibility would be the admixture of felsic material.

The enrichment of the Enticho Sandstone in Zr, Hf, Th, U, Nb and the light REE (Figure 2-5, Figure 2-7) points to felsic source rocks. The pronounced negative Eu anomaly (Figure 2-5) indicates evolved crustal material as a source. Possible source areas are the Archean cratons (Congo craton, Tanzania

craton) or the Meso- and Neoproterozoic mobile belts (Kibaran Belt, Irumide Belt, Mozambique Belt) in the inner part of Gondwana (Figure 2-1). A distal source area in central Gondwana has also been proposed for Cambrian–Ordovician sandstone in Israel and Jordan: Based on detrital zircon ages, Kolodner et al. (2006) infer a progressive southward migration of the source area during the Cambrian–Ordovician. Hf isotopic data in Neoproterozoic zircons of these formations are incompatible with the local Arabian Nubian Shield. This led Morag et al. (2011) to the assumption that the source region might be within the remobilised crustal areas further south (Figure 2-1). If this trend extends to the Upper Ordovician, a distal source area in the inner part of Gondwana for the Enticho Sandstone is likely.

In the Edaga Arbi Glacials, the relative enrichment of V and Cr and the higher proportion of HREE indicates a higher influence of mafic and garnet-bearing source material (e.g. Bhatia and Crook, 1986; McLennan et al., 1993). For example, smectite – commonly a weathering product of mafic precursor minerals – can be rich in Cr and V (Chamley et al., 1979). Garnet is a major carrier of HREE (Harangi et al., 2001). The poor Eu anomaly (Figure 2-6) indicates contribution of juvenile source material (McLennan et al., 1993). Similarly, the lower Th/Sc of the Edaga Arbi Glacials compared to the Enticho Sandstone points to a higher influence of undifferentiated crustal material (McLennan et al., 1993). A proximal source area composed mainly of juvenile crust would be the Arabian–Nubian Shield, which is the northernmost edge of the East African Orogen (Johnson et al., 2011). Ophiolites in the ANS, as described for instance by Meert (2003), Johnson et al. (2011) and Stern et al. (2012), could be the source for mafic input in the Edaga Arbi Glacials. Volcanic rock fragments in the Edaga Arbi Glacials may indicate Late Palaeozoic volcanism, as speculated by Sacchi et al. (2007). However, it cannot be said with certainty that the rock fragments are not metamorphically overprinted and older. Metavolcanic rocks are abundant in the Neoproterozoic basement and are a likely source for these fragments. The similar overall composition of the local basement samples and the Edaga Arbi Glacials (Figure 2-10) supports the assumption of a local source for these and a different source area for the Enticho Sandstone.

Petrographic and chemical compositions of glacial successions of Upper Ordovician and Carboniferous–Permian sandstone in Saudi Arabia are similar to those obtained in Ethiopia: a signature of old crustal material in the early Palaeozoic and a higher influence of juvenile material in the late Palaeozoic (Bassis et al., 2016b). In the PCA biplot (Figure 2-10), however, the Carboniferous–Permian samples from Saudi Arabia plot far away from the corresponding samples of this study, whereas the Upper Ordovician samples are grouped with the corresponding. Therefore, for the early Palaeozoic a common provenance for the glacial sandstones of both areas is likely, whereas in the late Palaeozoic the sediments were probably supplied from different local sources (Figure 2-11). This supports the assumption of a large North-Gondwanan ice sheet in the Late Ordovician (Ghienne et al., 2007; Le Heron and Craig, 2008) and more local glacial systems during the Carboniferous–Permian glaciation (Eyles, 1993; Fielding et al., 2008).

2.6. Conclusions

The petrographic and geochemical comparison of sandstones deposited during the two Gondwana glaciations in the Late Ordovician and the Carboniferous–Permian reveals clear differences: The Upper Ordovician Enticho Sandstone is highly mature with a major and trace element composition typical for an old differentiated crustal provenance. In contrast, the sandstone of the Carboniferous–Permian Edaga Arbi Glacials is less mature with a geochemical signature of more juvenile source material. Its major and trace element composition resembles that of the local basement. Stratigraphically equivalent formations in Saudi Arabia show similar patterns for the Late Ordovician but significant differences for the Carboniferous–Permian. The distinct petrographic and geochemical differences between the two formations make it possible to assign stratigraphically uncertain samples.

The high maturity of the Upper Ordovician Enticho Sandstone is probably a consequence of strong chemical weathering in the source area before the glaciation combined with long transport by the glaciers and reworking in a shallow marine environment after the glaciation. The material is possibly sourced from Archean cratons and/or Meso- and Neoproterozoic mobile belts in central Gondwana, such as the Congo and Tanzania cratons or the Kibaran, Irumide or Mozambique belts. The Edaga Arbi Glacials have a proximal source, most likely the Arabian–Nubian Shield. These findings support previous models of a large ice sheet covering northern Gondwana in the Late Ordovician, leading to a regional mixture and homogenisation of source material and a complex pattern of local glaciers in the Carboniferous–Permian.
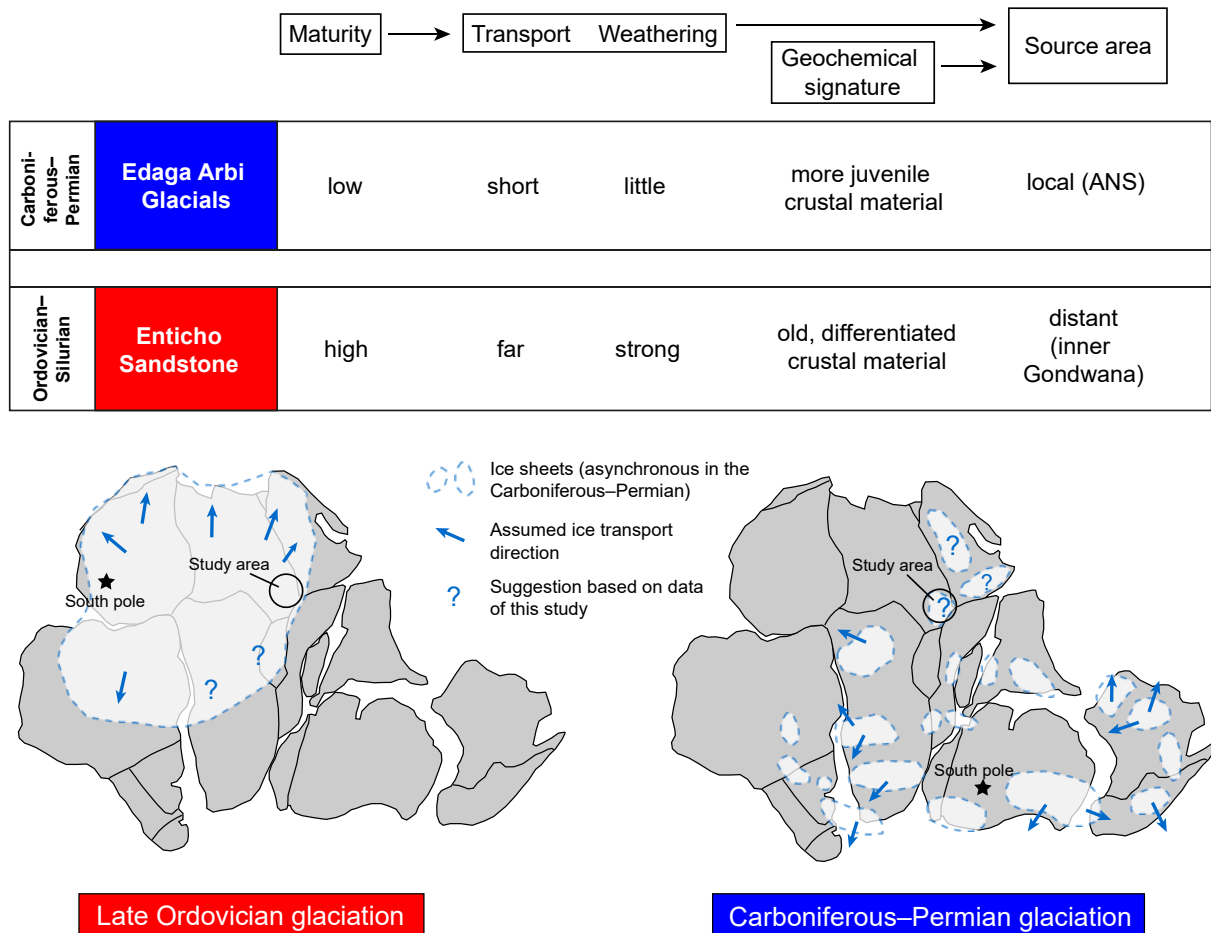
Figure 2-11: Summary of the main findings of this study for the two Gondwana glaciations in Ethiopia. Gondwana palaeogeography and south pole positions from Torsvik and Cocks (2013). Ice sheet locations and transport directions for the Late Ordovician are after Ghienne et al. (2007), Le Heron and Craig (2008) and Torsvik and Cocks (2013); for the Carboniferous–Permian they are after Bussert and Schrank (2007), Fielding et al. (2008) and Isbell et al. (2012).

Acknowledgements

3. Provenance of Ordovician–Silurian and Carboniferous–Permian glaciogenic successions in Ethiopia revealed by detrital zircon U–Pb geochronology

Anna Lewin[1], Guido Meinhold[2,3], Matthias Hinderer[1], Enkurie L. Dawit[4], Robert Bussert[5] & Jasper Berndt[6]

[1]Institut für Angewandte Geowissenschaften, Technische Universität Darmstadt, Schnittspahnstraße 9, 64287 Darmstadt, Germany
[2]School of Geography, Geology and the Environment, Keele University, Keele, Staffordshire, ST5 5BG, UK
[3]Geowissenschaftliches Zentrum Göttingen, Abteilung Sedimentologie / Umweltgeologie, Universität Göttingen, Goldschmidtstraße 3, 37077 Göttingen, Germany
[4]Department of Geology, University of Gondar, P.O. Box 196, Gondar, Ethiopia
[5]Institut für Angewandte Geowissenschaften, Technische Universität Berlin, Ernst-Reuter-Platz 1, 10587 Berlin, Germany
[6]Institut für Mineralogie, Westfälische Wilhelms-Universität Münster, Corrensstraße 24, 48149 Münster, Germany

Abstract

Palaeozoic sedimentary successions in northern Ethiopia contain evidence for two Gondwana glaciations during the Late Ordovician and Carboniferous–Permian. We compare sediments of the two glaciations regarding their detrital zircon U–Pb ages. The main age group for both formations is Pan-African (*c.* 550–700 Ma). However, the remaining spectra are different: The Upper Ordovician–Lower Silurian Enticho Sandstone is characterised by a Stenian–Tonian (*c.* 1 Ga) zircon population. The Carboniferous–Permian Edaga Arbi Glacials contain a prominent *c.* 800 Ma population. The Stenian–Tonian zircons are likely derived from the centre of the East African Orogen and were supplied via the Gondwana super-fan system. This material was transported by the Late Ordovician glaciers and formed the Enticho Sandstone. Tonian (*c.* 800 Ma) zircons are abundant in the Ethiopian basement and represent the earliest formation stage of the southern Arabian–Nubian Shield. Glaciers of the Late Palaeozoic Ice Age must have cut deeply into the basement for efficient erosion. No recycling of the Enticho Sandstone by the Edaga Arbi Glacials took place on a grand scale — probably because sedimentation of the former was limited to northern Ethiopia, whereas the source area for the latter was to the south.

3.1. Introduction

The Gondwana supercontinent comprised Archean to Mesoproterozoic cratons surrounded by Neoproterozoic mobile belts. These belts include juvenile crust and crust that was reactivated in the orogenic processes (e.g. Stern, 1994; Burke et al., 2003; Collins and Pisarevsky, 2005; Figure 3-1). The East African Orogen (EAO), which formed between 650 and 600 Ma at the suture of East and West Gondwana, is regarded as one of the largest accretionary orogens in the Earth's history (Stern, 1994; Collins and Pisarevsky, 2005; Squire et al., 2006). In northern Africa, a vast peneplain developed after the consolidation of the newly formed continent, on which a blanket of Palaeozoic sandstone was deposited (Garfunkel, 2002; Avigad et al., 2005). The direction of sediment transport during the early Palaeozoic is generally assumed to the north towards the margin of Gondwana (e.g. Meinhold et al., 2011; Morag et al., 2011; Avigad et al., 2012). The high maturity of the North Gondwana Lower Palaeozoic sandstones is striking. It can be attributed either to long transport distance and/or multiple recycling (e.g. Garfunkel, 2002; Morag et al., 2011) or strong chemical weathering at the time of deposition (e.g. Avigad et al., 2005).
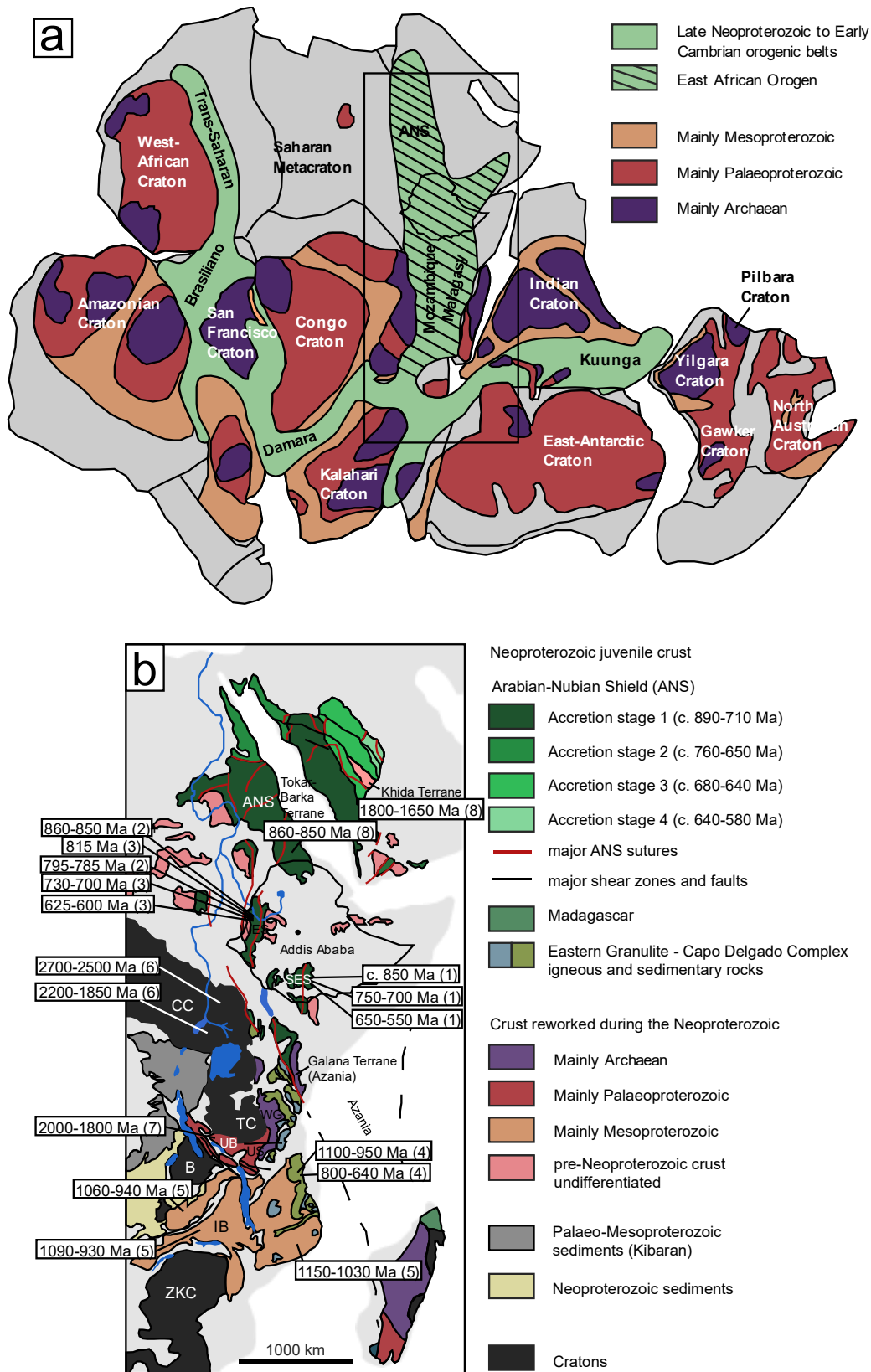
Figure 3-1: (a) Map of Gondwana showing the overall geological setting (modified after Torsvik and Cocks, 2013). (b) Map of Eastern Africa and Arabia showing exposures of Precambrian rocks and major tectonic units (modified after Fritz et al, 2013). ANS, Arabian–Nubian Shield; B, Bangweulu; CC, Congo Craton; IB, Irumide Belt; SES, Southern Ethiopian Shield; TC, Tanzania Craton; UB, Ubendian Belt; US, Usagaran Belt; WES, Western Ethiopian Shield; WG, Western Granulite Belt; ZKC, Zimbabwe–Kalahari Craton. References for age information: (1) Teklay et al. (1998); (2) Woldemichael et al. (2010); (3) Kebede et al. (2001); (4) Kröner et al. (2003); (5) Bingen et al. (2009); (6) Mänttäri (2014); (7) Fritz et al. (2013); (8) Johnson et al. (2011).

Based on the similarity of detrital zircon U–Pb age spectra throughout Gondwana, Squire et al. (2006) postulated the existence of large sediment fans that brought detritus from the EAO towards the continental margins. In a compilation of detrital zircon age spectra from Cambrian–Ordovician sandstones of North Africa and NW Arabia, Meinhold et al. (2013) extended the super-fan model to the northern Gondwana margin. Ethiopia would hence lie more proximal along the sediment path. Here, the Palaeozoic is mainly composed of sedimentary rocks related to the two Gondwana glaciations: (1) the Enticho Sandstone, deposited during the Late Ordovician (Hirnantian) glaciation and the following transgression, probably up to the early Silurian; and (2) the Edaga Arbi Glacials that formed during the Carboniferous–Permian glaciation. The Late Ordovician glaciation was short-lived and affected large parts of Gondwana synchronously (e.g. Eyles, 1993; Ghienne et al., 2007; Le Heron and Craig, 2008; Le Heron et al., 2018). A more complex spatial and temporal pattern of ice sheets is likely for the Late Palaeozoic Ice Age (LPIA) that affected Ethiopia in the Carboniferous–Permian (e.g. Eyles, 1993; Bussert and Schrank, 2007; Fielding et al., 2008; Bussert, 2014).

We analysed 11 sandstone samples from the Upper Ordovician–lower Silurian Enticho Sandstone and the Carboniferous–Permian Edaga Arbi Glacials for their detrital zircon U–Pb ages to link them to potential source areas. Our aim was to test the Gondwana super-fan hypothesis (Squire et al., 2006; Meinhold et al., 2013) at a more proximal location and to review the assumption of a distant provenance for the Enticho Sandstone and a proximal provenance for the Edaga Arbi Glacials (Lewin et al., 2018).

3.2. Geological setting

In Ethiopia, outcrops of the Palaeozoic successions are present around the Mekelle Basin in the Tigray province of northern Ethiopia and, to a minor extent, in the Blue Nile region in the west of the country (Kazmin, 1972; Garland, 1980; Tsige and Hailu, 2007; Figure 3-2). Sedimentological and palynological studies on these successions have been carried out by Dow et al. (1971), Beyth (1972a; 1972b), Saxena and Assefa (1983), Bussert and Schrank (2007), Bussert and Dawit (2009), Bussert (2014) and Dawit (2014). The two formations studied here overlie the Neoproterozoic basement and are overlain by uppermost Palaeozoic and Mesozoic sediments (Beyth, 1972b; Tefera et al., 1996; Dawit, 2010; 2014; Figure 3-2).

The basement in Ethiopia represents the junction of the Arabian–Nubian Shield in the north and the Mozambique Belt in the south, together making up the EAO (Kazmin, 1972; Tefera et al., 1996; Stern et al., 2012; Figure 3-1). The Arabian–Nubian Shield comprises a collage of Neoproterozoic juvenile arcs, younger sedimentary and volcanic basins, voluminous granitoid intrusions and a few enclaves of pre-Neoproterozoic crust (Johnson et al., 2011). Woldemichael et al. (2010) described the evolution of the Arabian–Nubian Shield in a supercontinent cycle from the break-up of Rodinia to the amalgamation of Gondwana, with early rifting beginning at c. 900–860 Ma. With the opening of the Mozambique Ocean, a passive margin formed in the area and early intrusions were emplaced at c. 860–830 Ma. Subduction and back-arc formation began at 830–750 Ma, followed by terrane accretion, metamorphism and syntectonic intrusions. The ocean closed at c. 750–650 Ma with further accretion and intrusions. Between 650 and 550 Ma, the assembly of the Arabian–Nubian Shield was in its final stage and metamorphism as well as post-tectonic intrusions occurred. The rocks of the Arabian–Nubian Shield were metamorphosed at low-grade greenschist facies (Beyth, 1972b; Alene et al., 2006; Stern, 2008).

By contrast, the Mozambique Belt to the south comprises medium- to high-grade gneisses and amphibolites as well as granulites. Here, the Ediacaran collision between East and West Gondwana was most intense. Mountains rose to a great height and were eroded in the Late Ediacaran and Early Palaeozoic (Stern et al., 2012). The Mozambique Belt contains large amounts of Archean to

Mesoproterozoic crust that was reworked during Neoproterozoic metamorphism and anatexis, although subordinate amounts of juvenile Neoproterozoic igneous rocks are present (Stern, 2008; Johnson et al., 2011; Fritz et al., 2013).
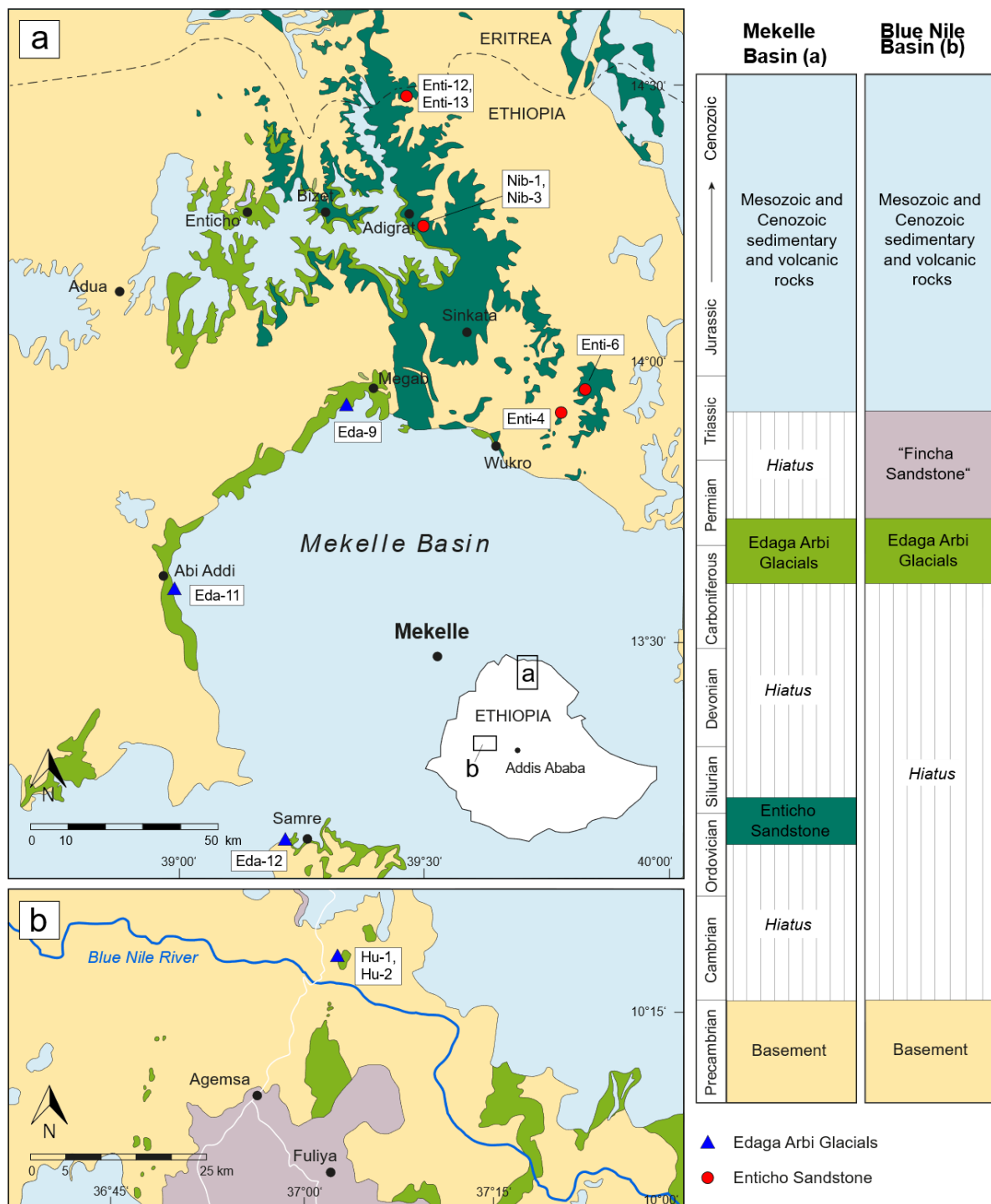
Figure 3-2: Maps of the study areas showing the sampling locations. (a) Northern Ethiopia, modified after Arkin et al. (1971), Garland et al. (1978), Bussert (2014). (b) Blue Nile region, modified after Tsige and Hailu (2007), Dawit (2014). The term 'Fincha Sandstone' is taken from Dawit (2014).

The basement of northern Ethiopia is considered to be part of the Arabian–Nubian Shield because it consists mainly of juvenile Neoproterozoic crustal material (Alene et al., 2000; Beyth et al., 2003; Fritz et al., 2013). The arc phase is represented by effusive flows and diverse volcaniclastic rocks of the upper

Tonian Tsaliet Group (Beyth, 1972b; Miller et al., 2009). When magmatism ceased, the marine siliciclastic and carbonate succession of the Cryogenian Tambien Group was deposited (Alene et al., 2006; Avigad et al., 2007; Miller et al., 2009). Both units experienced greenschist facies metamorphism and the intrusion of syn- and post-tectonic granitoids and diorites (Beyth, 1972b; Kazmin et al., 1978; Tefera et al., 1996). In western and southern Ethiopia, the basement can be regarded as the transition between the Arabian–Nubian Shield and the Mozambique Belt because it shows features of both; the crust is mainly juvenile Neoproterozoic with an age range indistinguishable from that of the Arabian–Nubian Shield (Teklay et al., 1998; Stern et al., 2012). The basement also includes a significant proportion of ophiolitic and volcano-sedimentary units (Woldemichael et al., 2010; Stern et al., 2012). High-grade metamorphic rocks are abundant in western and southern Ethiopia (Yibas et al., 2002; Woldemichael et al., 2010; Stern et al., 2012) and Archean protoliths have been recognized in the Alghae Terrane in southern Ethiopia (Stern et al., 2012). The east Ethiopian basement, however, represents a separate crustal domain. Here, the granitoid chemistry, zircon ages and Nd–Sr isotopes point to considerable reworking of pre-Neoproterozoic crust (Teklay et al., 1998). These characteristics extend to northern Somalia and perhaps even to the southernmost Arabian Peninsula because similar basement has also been found in southern Yemen (Windley et al., 1996; Teklay et al., 1998).

The Phanerozoic sediment cover in Ethiopia starts with the Upper Ordovician–Lower Silurian Enticho Sandstone. Cambrian or Early Ordovician sediments are missing. The Enticho Sandstone occurs north of the Mekelle Basin (Figure 3-2 a) and has a thickness of up to 300 m (e.g. Saxena and Assefa, 1983; Dawit, 2010). It consists of a lower glaciogenic unit and an upper shallow marine unit (Bussert and Dawit, 2009). The glaciogenic part comprises massive and largescale cross-bedded sandstones and conglomerates, assumed to be (subaerial or subaqueous) meltwater deposits. Foreset dips indicate a transport direction towards the south-east (Bussert and Dawit, 2009), although, in places, the transport directions are towards the north (Kumpulainen, 2007; Bussert and Dawit, 2009). Diamictites occur rarely (Bussert and Dawit, 2009; Dawit, 2010). In the upper part, well-sorted sandstones with bipolar cross-bed sets point to a tide dominated shallow marine depositional setting (Bussert and Dawit, 2009; Dawit, 2010). Locally, a mudstone unit separates the glaciogenic and shallow marine sandstones. The age of the Enticho Sandstone was constrained by body and trace fossils, as well as palynoflora (cryptospores). Saxena and Assefa (1983) assigned an Ordovician age based on fossil siphonophorid impressions. Bussert and Dawit (2009) discovered *Arthrophycus alleghaniensis*, an ichnospecies that is largely restricted to the early Silurian, in the upper, shallow marine unit (Seilacher, 2007; Buatois and Mángano, 2011). Additional biostratigraphic evidence comes from recently discovered cryptospores, colonial algae and phosphatic-shelled inarticulate brachiopods from the lower glaciogenic unit of the Enticho Sandstone. These were assigned by Brocke et al. (2015) as post-Hirnantian (latest Ordovician–early Silurian).

The Edaga Arbi Glacials are mainly exposed along the western and southwestern margin of the Mekelle Basin and to a minor extent in the Blue Nile region in western Ethiopia (Figure 3-2 b). Their thickness is up to 200 m in northern Ethiopia, but significant lateral variations occur (Bussert, 2010). The Edaga Arbi Glacials lie unconformably on top of the Enticho Sandstone and, in places, directly on the basement (e.g. Beyth, 1972b). They are laminated claystones and siltstones containing scattered outsized clasts, lenses of sandstone and a polymict glacial conglomerate at the base (Beyth, 1972b; Bussert and Dawit, 2009; Bussert, 2014). The occurrence is often in north–south oriented troughs and channels that carve into the basement with an inferred transport direction from south to north (Bussert, 2010). The following model for the generation of this succession has been proposed by Bussert (2014): (1) initial glacier advance led to the deposition of tillites; (2) outwash fans (subaerial and subaqueous) formed during glacial retreat; and (3) fines settled from the water column in a proglacial lake or fjord-like environment, interrupted by periodic hyperpycnal sediment flows and the deposition of dropstones. In the Blue Nile

region (Figure 3-2 b), Permian–Triassic continental sedimentary rocks partly overlie the glacial sediments presumed to be equivalent to the Edaga Arbi Glacials (Dawit, 2014). A more detailed facies description of the Enticho Sandstone and the Edaga Arbi Glacials is given by Bussert and Dawit (2009), Bussert (2014) and Lewin et al. (2018). The age of the Edaga Arbi Glacials is constrained by the rich and well-preserved microfloral assemblages, including *Potonieisporites sp.*, *Plicatipollenites sp.*, *Cycadopytes cymbatus* and *Microbaculispora sp.* (Bussert and Schrank, 2007). These palynotaxa are known from the Early Permian glacial sequences across the whole Gondwana region and are used for stratigraphic correlations (Kemp et al., 1977; Backhouse, 1991; Stephenson et al., 2003).

3.3. Methods

Sandstone samples were mainly collected from surface outcrops in northern Ethiopia, where Palaeozoic glaciogenic sedimentary rocks are abundant. In the Blue Nile region, in the west of the country, such sandstones could only be sampled in one locality (Figure 3-2 b). The choice of sampling sites was based on previous stratigraphic and sedimentological work (Bussert and Schrank, 2007; Bussert and Dawit, 2009). Four sections were sampled that were biostratigraphically constrained (Bussert and Dawit, 2009; Brocke et al., 2015). The other sampled sections were assigned to one of the two formations by lithofacies characteristics. The field classification was confirmed by geochemical analyses, which are well suited to distinguish between the two formations and assign unknown samples (Lewin et al., 2018). Eleven samples were chosen for detrital zircon geochronology: six samples from the Enticho Sandstone and five from the Edaga Arbi Glacials (Table 3-1). This choice was made to cover a large geographical and stratigraphic spread within each formation.

Table 3-1: Sample information. Locations are given in geographical coordinates (WGS84). The stratigraphic assignment to one of the two studied formations is based on biostratigraphic evidence (B) or lithofacial characteristics (LF) in the outcrop or, in one case, uncertain (U). Detailed information on the petrography and geochemistry of each sample is given in Lewin et al. (2018). Last three columns: summary of detrital zircon ages of samples analysed in this study. The full dataset is given in the supplementary material.

Sample	Longitude (°)	Latitude (°)	Formation	Strati-graphic assignment	Lithology	Ages deter-mined	Concor-dant ages	% concor-dant ages
Enti-4	039.71262	13.83465	Enticho	U	Diamictite	54	48	89
Enti-6	039.74827	13.88842	Enticho	B	Sandstone	85	82	96
Enti-12	039.42093	14.49627	Enticho	LF	Sandstone	85	66	78
Enti-13	039.41911	14.49275	Enticho	LF	Sandstone	86	74	86
Nib-1	039.48972	14.25194	Enticho	B	Sandstone	85	76	89
Nib-3	039.49583	14.25222	Enticho	B	Sandstone	86	75	87
Eda-9	039.32235	13.90915	Edaga Arbi	B	Sandstone	89	73	82
Eda-11	039.00042	13.61842	Edaga Arbi	LF	Sandstone	85	80	94
Eda-12	039.19745	13.17844	Edaga Arbi	B	Sandstone	73	69	95
Hu-1	037.05068	10.31057	Edaga Arbi	LF	Sandstone	47	41	87
Hu-2	037.05068	10.31057	Edaga Arbi	LF	Sandstone	77	72	94

To prepare for zircon analysis, 1–2 kg of each sample was disaggregated using a jaw-crusher followed by a mortar and pestle and then wet sieved. Heavy minerals were separated from the 63–125 μm grain size fraction using sodium polytungstate with a density of 2.85 g ml^{-1}. We chose this grain size fraction to ensure comparability with existing data from Palaeozoic sandstones in Libya. Zircon grains were randomly hand-picked from the heavy mineral concentrates, mounted in epoxy resin and polished to expose the interior of the grains. Cathodoluminescence images of the grains were taken to reveal the internal structures prior to analysis. We analysed 80 zircons per sample because this appears to produce a robust number of ages for deciphering the sources of natural detrital samples (e.g. Sláma and Košler,

2012). For samples Enti-4 and Hu-1, the zircon fertility was too low to analyse 80 grains and only 54 and 47 grains, respectively, could be dated (Table 3-1). If the zircon grains had inherited cores, then the measuring spot was set, where possible, on the outer rim to consistently date the latest event.

Zircon U–Pb analyses were performed at the Institute of Mineralogy at the University of Münster using a ThermoFisher Element 2 single-collector inductively coupled plasma mass spectrometer coupled with a Photon Machines Analyte G2 laser ablation system. The laser spot size was 25 μm. Masses of 202 (to determine ^{204}Hg interference with ^{204}Pb), 204, 206, 207 and 238 were measured. Common Pb correction was performed after Stacey and Kramers (1975) if the common ^{206}Pb fraction of the total ^{206}Pb exceeded 1%. The GJ-1 reference zircon (Jackson et al., 2004) was used for calibration by bracketing ten unknowns with three analyses of the reference zircon. To further ensure the reproducibility and precision of the U–Pb ages, the 91500 reference zircon (Wiedenbeck et al., 1995) was regularly analysed. The measured isotopic ratios matched the published values of Wiedenbeck et al. (1995).

Data processing was carried out with an in-house Excel spreadsheet (Kooijman et al., 2012). As a result of the lower precision of ^{207}Pb/^{206}Pb values for young zircons, the data were filtered based on two criteria: (1) agreement in the U–Pb ages ((^{206}Pb/^{238}U)/(^{207}Pb/^{235}U)) in the range 90–110% for grains younger than 1200 Ma; and (2) 90–110% concordance in terms of (^{206}Pb/^{238}U)/(^{207}Pb/^{206}Pb) for grains older than 1200 Ma. Zircons younger than 1200 Ma are quoted by their ^{206}Pb/^{238}U age, whereas the ^{207}Pb/^{206}Pb age is used for zircons older than 1200 Ma. This age was chosen due to the natural gap of zircon ages in the analysed samples. The R-package Provenance (Vermeesch et al., 2016) was used for visualization of the zircon age spectra as kernel density estimates and for multi-sample comparison in multidimensional scaling maps, as suggested by Vermeesch (2013).

3.4. Results

In total, 852 zircon grains were dated in 11 samples from the studied formations, of which 756 were 90–110% concordant using the respective data filters described earlier. In the Enticho Sandstone, 481 grains were analysed, of which 421 (88%) were concordant, and in the Edaga Arbi Glacials 371 grains, of which 335 (90%) were concordant (Table 3-1). Most zircons are prismatic or short prismatic in shape and subrounded to well rounded. They mostly exhibit oscillatory (magmatic) zoning in the cathodoluminescence images (Figure 3-3). Very few zircons are unzoned and thus probably metamorphic in origin or metamorphically overprinted.

Five main age groups can be defined in detrital zircons of the Enticho Sandstone and the Edaga Arbi Glacials (Figures 3-4 to 3-6): Pan-African (700–550 Ma), Tonian (900–700 Ma), Stenian–Tonian (1200–900 Ma), Palaeoproterozoic (2500–1600 Ma) and Archaean (>2500 Ma). The Pan-African population is ubiquitous in both formations and comprises c. 40% of the zircon grains. The Tonian age group is very prominent in the Edaga Arbi Glacials (45% of all zircon grains on average; Figure 3-5), yet less important in the Enticho Sandstone (22% of all zircon grains on average; Figure 3-6). An exception is sample Nib-1, which shows a well-defined peak of Tonian aged zircons (Figure 3-4). By contrast, the Stenian–Tonian age population is characteristic of the Enticho Sandstone (Figure 3-4, Figure 3-6), where it comprises 19% of all ages, in contrast with the Edaga Arbi Glacials with 5% of the ages in this group.

The ratios of Tonian to Stenian–Tonian ages is on average 1.2 in the Enticho Sandstone (range 1.0–1.6) and 13.1 in the Edaga Arbi Glacials (range 5.0–22.0) and can be used to discriminate between the age spectra of both formations. No stratigraphic pattern in zircon age spectra was detected within the formations. Mesoproterozoic ages older than Stenian are rare in both formations and comprise only five

of the 756 concordant ages. The Palaeoproterozoic and Archaean age populations are more prominent in the Enticho Sandstone than in the Edaga Arbi Glacials. The former contains, on average, 9% Palaeoproterozoic and 5% Archaean zircons, whereas in the latter 4% of the zircons are Palaeoproterozoic and 1% Archaean in age. The proportion of Palaeoproterozoic to Archaean zircons varies with the geographical position of the samples (Figure 3-6). Four per cent of the zircons in both formations are younger than 550 Ma (Figure 3-6).
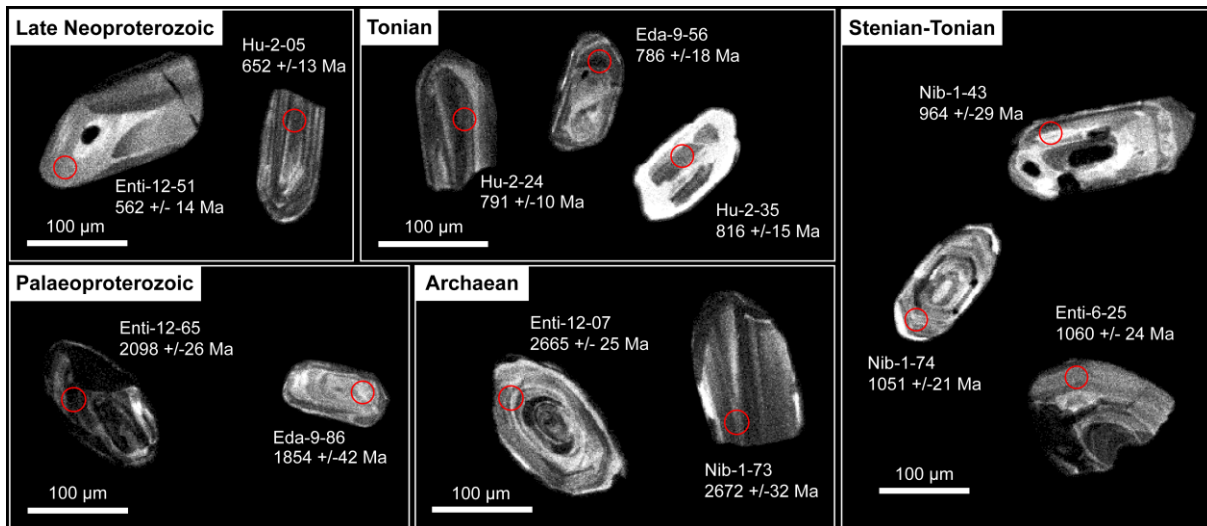
Figure 3-3: Cathodoluminescence images of representative zircons of the defined age groups. Pan-African, 700–550 Ma; Tonian, 900–700 Ma; Stenian–Tonian, 1200–900 Ma; Palaeoproterozoic, 2500–1600 Ma; Archaean, >2500 Ma.

3.5. Discussion

Enticho Sandstone

The largest zircon population in the Enticho Sandstone is of Pan-African age (700–550 Ma; Figure 3-4, Figure 3-6). Rocks of this age are ubiquitous in the whole EAO and record syn- and post-collisional magmatism associated with the final assembly of Gondwana (e.g. Fritz et al., 2013). It is thus hard to assign a particular provenance to these zircons. Of greater interest is the Stenian–Tonian (1200–900 Ma) age group because it is characteristic of the Enticho Sandstone (Figure 3-4, Figure 3-6). In the basement of the Arabian–Nubian Shield, zircons of this age are found in Neoproterozoic metasediments in Sinai, the Elat area in southern Israel and also in Cryogenian diamictites in Ethiopia (Avigad et al., 2007; Be'eri-Shlevin et al., 2009; Morag et al., 2012). Be'eri-Shlevin et al. (2009) postulate a tract of c. 1 Ga old crust incorporated in the Arabian–Nubian Shield and conclude a proximal provenance for the upper Neoproterozoic and lower Palaeozoic sediments. Similar considerations are made by Avigad et al. (2007) on the origin of c. 1 Ga zircons in the Cryogenian diamictites in Ethiopia. It may thus be possible that the Stenian–Tonian zircon population in the Enticho Sandstone is derived from such metasediments or the postulated former crustal tract. The nearest crust with an age of c. 1 Ga still existing in North–East Africa, however, is reported from the Central Saharan Belt (Toteu et al., 2001; De Wit et al., 2005) and the Irumide Belt and plutons in the Ubendian Belt, both part of the Mozambique Belt in Tanzania and Mozambique (Bingen et al., 2009; De Waele et al., 2009; Fritz et al., 2013).
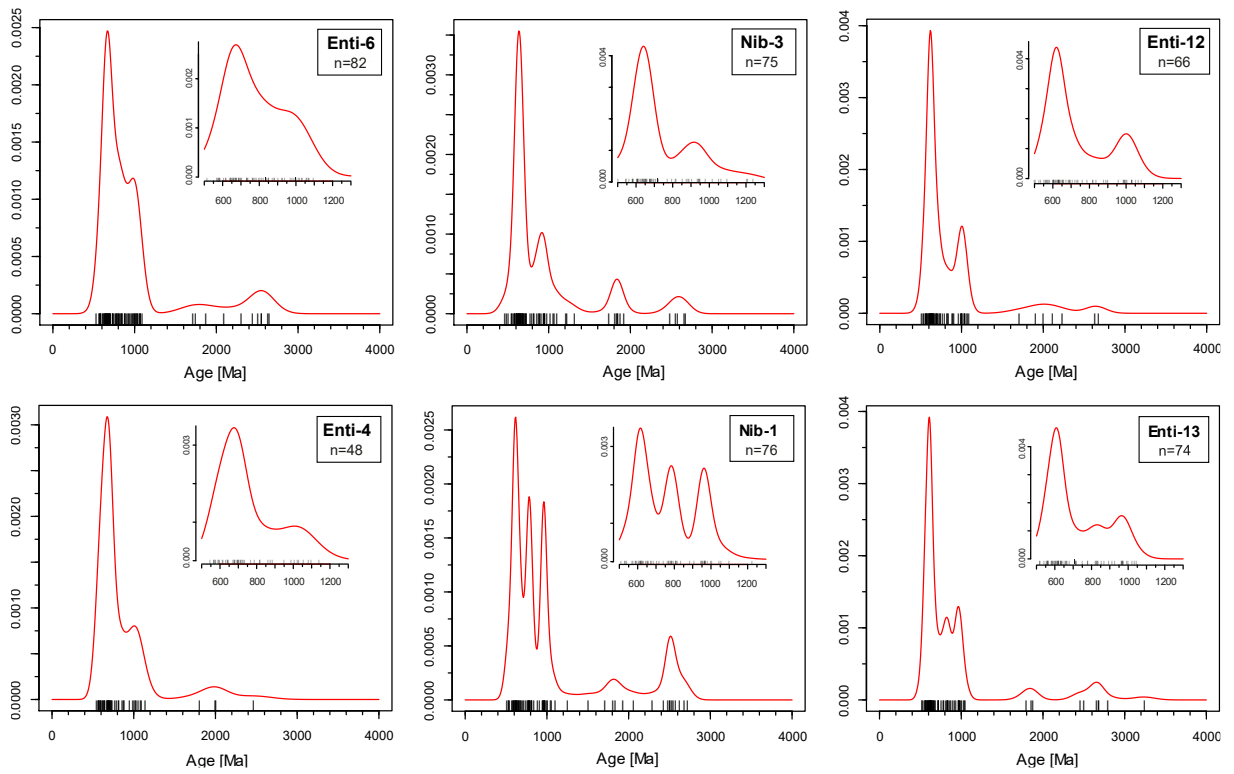
Figure 3-4: Kernel density estimate plots of the zircon age spectra in samples of the Enticho Sandstone. Inset shows a close-up of the 1300–500 Ma age range. Samples are arranged from left to right according to their geographical location from south to north, with the lower row from the glaciogenic basal part of the formation and the upper row from the shallow marine upper part.
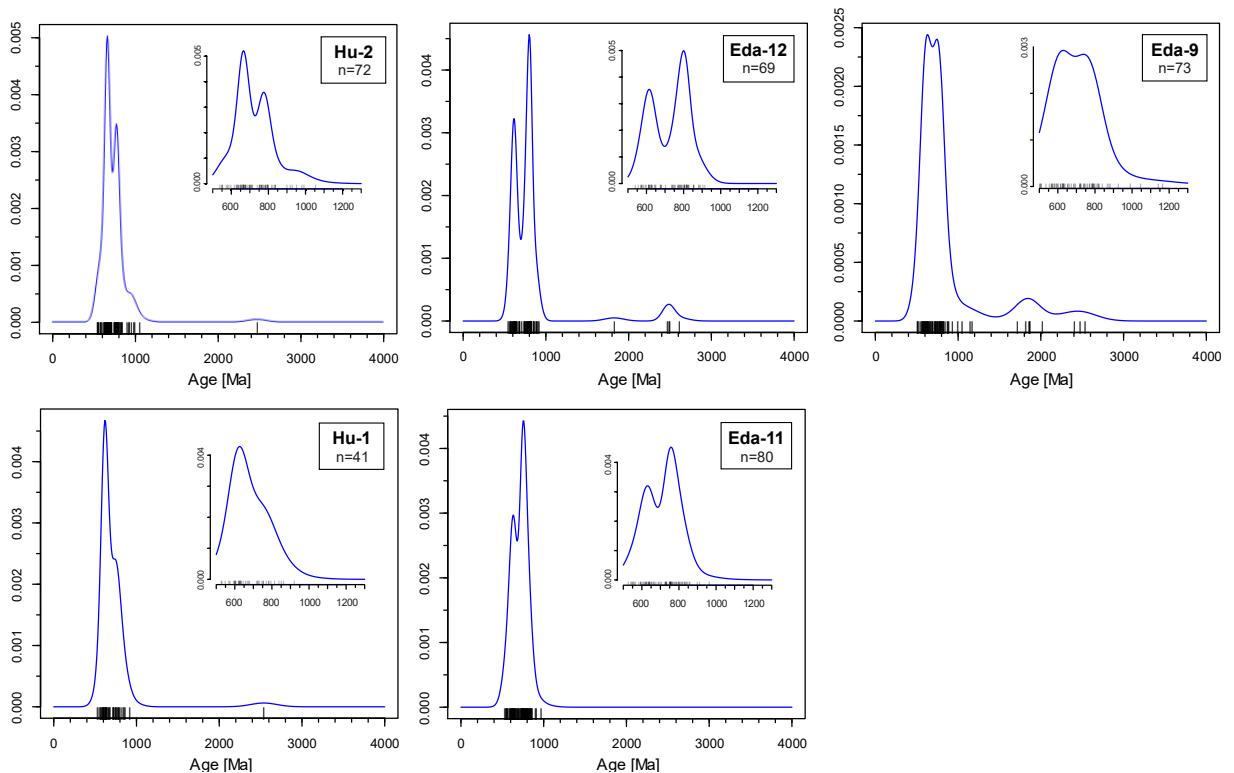
Figure 3-5: Kernel density estimate plots of the zircon age spectra in samples of the Edaga Arbi Glacials. Inset shows a close-up of the 1300–500 Ma age range. Samples are arranged from left to right according to their geographical location from south to north, with the lower row from the basal part of the formation and the upper row from the middle to upper part.
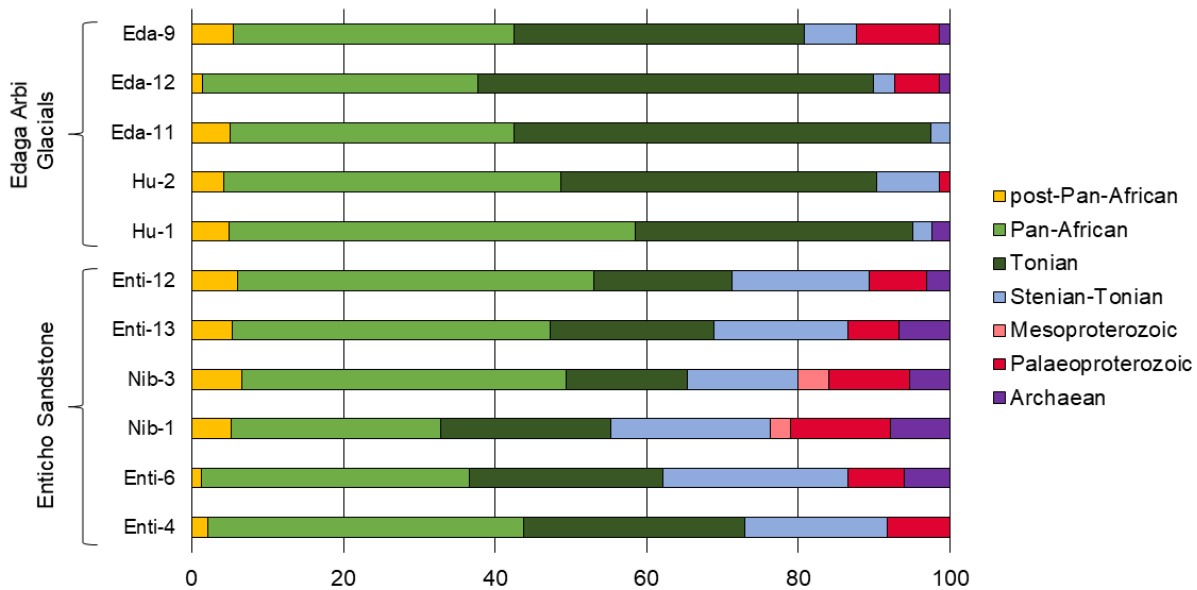
Figure 3-6: Bar chart showing the distribution of the defined age groups in the analysed samples. Samples of the respective formations are arranged from bottom to top according to their geographical location from south to north.

According to the super-fan hypothesis (Squire et al., 2006; Meinhold et al., 2013), c. 1 Ga zircons were transported from regions in the centre of the EAO (the Mozambique Belt) towards the continental margin of Gondwana during the early Palaeozoic. The high similarity between the Upper Ordovician–Lower Silurian sandstones in Ethiopia and Libya can be revealed in a multidimensional scaling map of the detrital zircon age spectra (Figure 3-7). The Algerian Hirnantian sandstone, however, is not part of the cluster. We did not consider age-equivalent deposits outside the Gondwana mainland because the palaeogeographical position of the peri-Gondwana terranes is highly uncertain. The differences are mainly in the presence or absence of c. 1 Ga zircons, which can be used as a tracer for areas within reach of the super-fan system (Meinhold et al., 2013). The boundary between this East African–Arabian zircon province and the West African province has also been illustrated by Linnemann et al. (2004) and statistically highlighted by Stephan et al. (2019). The remarkable accordance of the detrital zircon age spectra in sandstones from Libya and Ethiopia makes a common provenance within the Gondwana super-fan system, which led to regional homogenization of the detritus, more likely than a derivation of the Stenian–Tonian zircons from the local basement of Ethiopia.

When also including zircon ages from older sandstones (Cambrian–Ordovician) of northern Africa in the multidimensional scaling map (Figure 3-8), a spatial clustering appears rather than a temporal clustering. The Enticho Sandstone clusters with Cambrian–Ordovician sandstones from Israel and Jordan and the Libyan sandstones are in the vicinity, whereas the Algerian and Moroccan sandstones are further away in the plot, implying the least similarity of the age spectra. The high similarity of the Cambrian–Ordovician age spectra with those of the Hirnantian glaciogenic sandstones leads to the assumption that no change in provenance occurred with the onset of glaciation. Rather, the glaciers reworked the sediment delivered by the super-fan system, which was strongly weathered in the source area or during transport and temporal storage (Garfunkel, 2002; Avigad et al., 2005). A cannibalization of pre-Hirnantian sediments by the Hirnantian glaciers is also suggested by Ghienne et al. (2018) for the Upper Ordovician sandstones in Morocco, although these cannibalized sediments probably did not belong to the super-fan system (Figure 3-8).

Because no Cambrian or Lower to Middle Ordovician sedimentary rocks exist in Ethiopia, the area was probably a site of sediment bypass or erosion during this period and was still elevated in the aftermath

of the Pan-African Orogeny. If erosion took place, it was probably minor compared with the whole super-fan material: a prominent population of c. 800 Ma zircons, the signature for the Ethiopian basement, is not present in the super-fan sediments (Meinhold et al., 2013). Alternatively, the Ethiopian basement, rich in c. 800 Ma zircons, may only have been exhumed later and covered by a blanket of detrital material transported in the super-fan system. The Hirnantian glaciation probably extended eastwards to northern Ethiopia, as witnessed by the tillite from which sample Enti-4 was taken (see also Bussert and Dawit, 2009). Massive amounts of sediment were transported to Ethiopia through glaciers or ice streams and meltwater and were released and deposited during meltdown of the ice sheet. The lower part of the Enticho Sandstone is interpreted to represent outwash fan deposits (Bussert and Dawit, 2009).
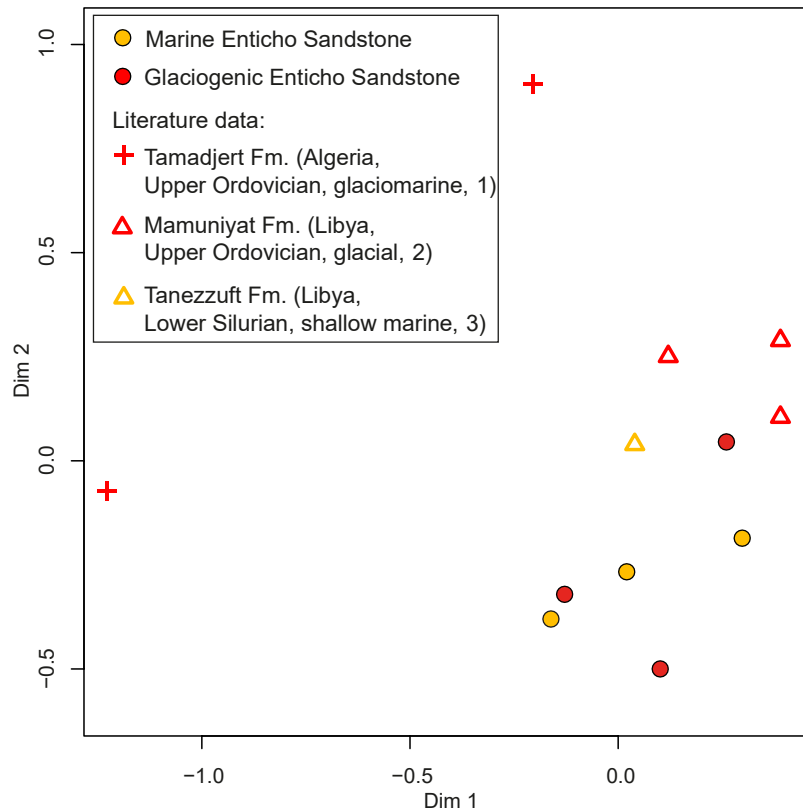
Figure 3-7: Non-metric multidimensional scaling map for the Ordovician–Silurian period. Only Precambrian ages (>541 Ma) are used here due to the low reliability of younger ages (see discussion for details). Published data: (1) Linnemann et al. (2011); (2) Morton et al. (2012); and (3) Meinhold et al. (2011).

The post-glacial transgression provided increased accommodation space to store sediment and to allow deposition of the upper, shallow marine part of the Enticho Sandstone. The original depositional site of the super-fan sediments that were reworked and transported to Ethiopia during the glaciation remains unclear. Assuming an ice spreading centre in mid- to northern Africa (e.g. Ghienne et al., 2007; Le Heron and Craig, 2008), these sediments may have come from the NW – that is, the area of Libya. This transport direction would agree with foreset dips towards the SE, as observed in meltwater deposits by Bussert and Dawit (2009).

A considerable population of Palaeoproterozoic to Archaean zircons is present in the Enticho Sandstone (Figure 3-4, Figure 3-6). Such pre-Neoproterozoic zircons are also detected in increasing amounts up-section in the Cambrian–Ordovician successions in Libya, Israel and Jordan and are interpreted to record the southwards migration of river systems associated with the Gondwana super-fan system (Kolodner et al., 2006; Meinhold et al., 2013). Based on the Hf isotopic signatures of zircons in Cambrian–

Ordovician sandstones in Israel and Jordan, Morag et al. (2011) postulated that a large proportion of the material was sourced from ancient terranes outside the Arabian–Nubian Shield. This was confirmed by Ben Dor et al. (2018) analysing Sr and Nd isotopes in the feldspars and clays of such sandstones. This supports a distant provenance of the material in the Enticho Sandstone and the recycling of super-fan sediments. However, the proportion of the oldest zircon populations varies with the geographical position of the samples, with the highest proportion in samples Nib-1 and Nib-3 (Figure 3-6). Hence it cannot be ruled out that these older zircons are a local phenomenon. Hargrove et al. (2006) reported inherited Palaeoproterozoic and Archaean zircons in magmatic rocks of the Arabian–Nubian Shield in Saudi Arabia, which may also be the case in the Ethiopian Neoproterozoic basement.
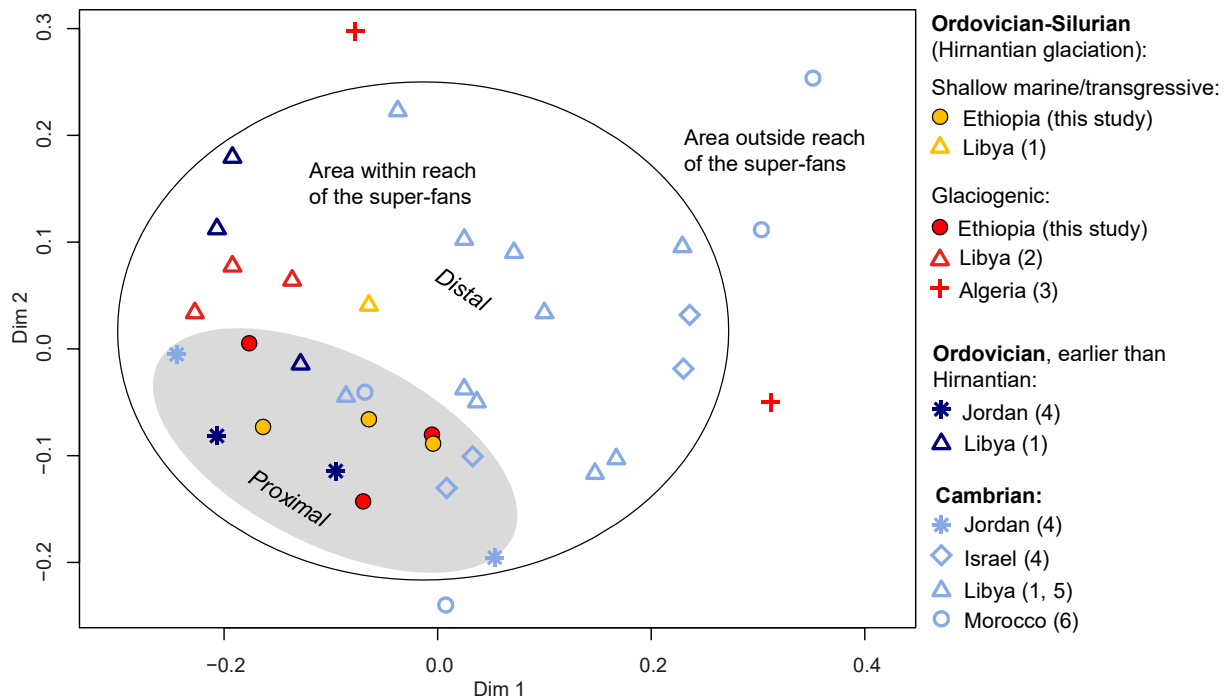
Figure 3-8: Non-metric multidimensional scaling map comparing the detrital zircon age spectra of Ordovician–Silurian sandstones analysed in this study with published data from Ordovician–Silurian and Cambrian–Lower Ordovician sandstones. Only Precambrian ages (>541 Ma) are used here due to the low reliability of younger ages (see discussion for details). Published data: (1) Meinhold et al. (2011); (2) Morton et al. (2012); (3) Linnemann et al. (2011); (4) Kolodner et al. (2006); (5) Altumi et al. (2013); and (6) Avigad et al. (2012). Note that the published data are those compiled by Meinhold et al. (2013) augmented by those from Altumi et al. (2013).

Avigad et al. (2017) analysed detrital rutile U–Pb cooling ages in Cambrian–Ordovician sandstones in Israel and Jordan and one sample from the Enticho Sandstone in Ethiopia. They found younger cooling ages in the Ethiopian sandstone than in the samples from Israel and Jordan and ascribed this to a change in the drainage system and supply from new crustal vestiges. The detrital zircon age spectrum of that sample is, however, very similar to the spectra in the Edaga Arbi Glacials (Figure 3-5), with a prominent age peak at c. 800 Ma and only a few c. 1 Ga old zircons, leading to a high ratio of Tonian to Stenian–Tonian ages. The Ethiopian sample analysed by Avigad et al. (2017) might therefore be of Carboniferous–Permian and not Ordovician–Silurian age.

Edaga Arbi Glacials
In addition to the Pan-African (700–550 Ma) 'background signal', the Tonian (c. 800 Ma) age group is very pronounced in the Carboniferous–Permian Edaga Arbi Glacials (Figure 3-5, Figure 3-6). This age coincides with the earliest stage of formation of the Arabian–Nubian Shield when Rodinia broke up. Woldemichael et al. (2010) postulated magmatism in western Ethiopia associated with the opening of

the Mozambique Ocean and constrained the pulses of magmatism at 860–850 and 795–785 Ma. Kebede et al. (2001) dated the granitoids of the Western Ethiopian Shield to an age of 815 Ma. In the Southern Ethiopian Shield, magmatic episodes can be defined at 890–840 and 790–700 Ma (Teklay et al., 1998; Yibas et al., 2002; Stern et al., 2012). They overlap in age with the arc and back-arc magmatism of the Tsaliet Group in North–East Ethiopia and Eritrea (Avigad et al., 2007). Johnson et al. (2011) assigned protolith ages of 870–840 Ma to the Tokar–Barka terrane in the north Ethiopian–Eritrean basement. Altogether, 900–700 Ma magmatic rocks are abundant in the local and regional basement and are thus the most likely source for the zircons of this age in the Edaga Arbi Glacials. This agrees with earlier considerations of a local provenance for this formation based on sandstone petrography and geochemistry (Lewin et al., 2018).

The glaciers of the LPIA in North–East Africa were probably of the local mountain glacier type (Konert et al., 2001; Bussert and Schrank, 2007; Le Heron et al., 2009). Uplift of the Ethiopian basement probably occurred due to Carboniferous Hercynian tectonism (Al-Husseini, 1992; Sharland et al., 2004). On the Arabian Peninsula, this tectonism caused north–south-oriented faults, sags and swells (Al-Husseini, 2004). The Edaga Arbi Glacials in northern Ethiopia are presumed to have been deposited in a large north-north-east trending trough in which glacial erosion may have followed and reinforced this pre-glacial topography (Bussert, 2014). Another reason for uplift could be thermal up-doming prior to the formation of the Zagros rift zone, which later formed the Neo-Tethys ocean (Sharland et al., 2001). Bussert (2010) studied erosional landforms associated with the LPIA in northern Ethiopia and proposed a landscape of areal scouring, in which wet-based ice carved deeply into the basement. This would have enabled the efficient erosion of c. 800 Ma zircon bearing rocks, which may also have provided the rutiles analysed by Avigad et al. (2017). In the Enticho Sandstone, sample Nib-1 also contains a notable age peak of c. 800 Ma (Figure 3-4). The assignment of this sample to the Enticho Sandstone is through biostratigraphy and is further confirmed by geochemical analysis (Lewin et al., 2018) and the ratio of Tonian to Stenian–Tonian zircons of 1.1. This leads to the assumption that the Ordovician glaciers were locally able to erode the basement effectively due to differences in topography or in glacier dynamics.

Few concordant Phanerozoic zircon ages are present in the two studied formations, mainly in the range 520–450 Ma. Almost all these young zircons are corrected for common Pb, so they may be over-corrected, leading to younger ages. However, we cannot exclude magmatic activity in the area at that time. There is no clear evidence for early Palaeozoic magmatism in Ethiopia, although Sacchi et al. (2007) identified fresh volcanic clasts in Palaeozoic tillite in northern Ethiopia. It is doubtful whether this tillite is of Ordovician or Carboniferous–Permian age. In the explanations of the geological map of the Mekelle area from 1970, a black lava layer is described that lies on top of the basement peneplain and is interpreted to have formed before the Mesozoic (Levitte, 1970). Even though it is described as ultrabasic, it may have delivered minor amounts of zircon to the Palaeozoic sediments. Middle Ordovician volcanic ash beds (K-bentonites) have been reported in Libya (Ramos et al., 2003) and ascribed to volcanic activity in northern Gondwana during that time. Such volcanic products could have provided an additional or alternative source. Cambrian post-collisional plutons in the Arabian–Nubian Shield have been reported by Fritz et al. (2013), although it is unknown whether they were exposed at the times of deposition of the studied formations.

The preservation of mainly glaciation-related sediments in the Palaeozoic of Ethiopia is striking. As an explanation, we propose a combination of increased sediment delivery by glaciers, ice streams and meltwater and increased accommodation space at the time of deposition. The melting ice sheet released large amounts of sediment towards the end of the Hirnantian glaciation and accommodation space was created in the area of Ethiopia through the following transgression. The later isostatic rebound may have caused uplift of the area, leading to another period of nondeposition. Sea-level fall has also accompanied

Silurian–early Devonian Palaeotethys rifting (Torsvik and Cocks, 2011). In the Carboniferous–Permian, Hercynian tectonism produced a complex local geomorphology. Areas that were uplifted, glaciated and eroded were close to local depressions in which proglacial lakes provided numerous depocentres for the accumulation of sediment.

A remaining question is why no major recycling of the Enticho Sandstone by the Edaga Arbi Glacials has taken place. This may be because the deposition of the Enticho Sandstone was limited to northern Ethiopia (Kazmin, 1972; Tefera et al., 1996). The source area of the Edaga Arbi Glacials was probably to the south and a northwards transport direction was inferred by Bussert (2010) based on the orientation and geometry of palaeo-landforms such as roches moutonnées. Sedimentary rocks presumed to be equivalent to the Edaga Arbi Glacials are also present in the Blue Nile area (samples Hu-1 and Hu-2, showing the same zircon age signature as other samples from the Edaga Arbi Glacials) and in other parts of Ethiopia (e.g. Bussert and Dawit, 2009, and references therein).

3.6. Conclusions

The U–Pb dating of detrital zircons in the Upper Ordovician (Hirnantian) to lower Silurian Enticho Sandstone and the Carboniferous–Permian Edaga Arbi Glacials in northern Ethiopia reveals distinct differences in the age spectra of both formations. Differences exist mainly in the Tonian (900–700 Ma) age population, which is characteristic of the Edaga Arbi Glacials, and the Stenian–Tonian (1200–900 Ma) group, which is prominent in the Enticho Sandstone. We can therefore rule out recycling of the Enticho Sandstone by the Edaga Arbi Glacials on a grand scale.

The Stenian–Tonian zircons are correlative with characteristic populations of this age in Hirnantian sandstones in Libya and Cambrian–Ordovician sandstones in Libya, Israel and Jordan. Following the hypothesis of a Gondwana super-fan system in the Early Palaeozoic that can be traced by c. 1 Ga zircons, the Enticho Sandstone can be regarded as super-fan sediments reworked by the Late Ordovician glaciers and during the subsequent transgression. The Tonian zircon population, which is prominent in the Carboniferous–Permian Edaga Arbi Glacials, is probably derived from the local basement of Ethiopia. Here, 900–700 Ma magmatic rocks are abundant and represent the earliest formation stage of the southern Arabian–Nubian Shield. These basement rocks must have been uplifted and exposed for efficient erosion by the glaciers of the LPIA.

The preservation of mainly glaciation-related sediments in the Palaeozoic of Ethiopia is probably a consequence of (1) the high sediment supply due to the erosional and transport potential of glaciers, ice streams and meltwater and (2) the creation of accommodation space during these times. For the Enticho Sandstone, the latter resulted from base-level rise due to postglacial transgression that reached southwards (in present day coordinates) as far as Ethiopia. For the Edaga Arbi Glacials, accommodation space was created in proglacial lakes in local depressions. Because the deposition of the Enticho Sandstone was probably limited to northern Ethiopia and the inferred source area of the Edaga Arbi Glacials is to the south, no major recycling of the former by the latter took place.

Acknowledgements

4. Heavy minerals as provenance indicator in glaciogenic successions: An example from the Palaeozoic of Ethiopia

Anna Lewin[a], Guido Meinhold[b,c], Matthias Hinderer[a], Enkurie L. Dawit[d], Robert Bussert[e], Nils Keno Lünsdorf[b]

[a]Technische Universität Darmstadt, Material- und Geowissenschaften, Institut für Angewandte Geowissenschaften, Schnittspahnstraße 9, 64287 Darmstadt, Germany
[b]School of Geography, Geology and the Environment, Keele University, Keele, Staffordshire, ST5 5BG, United Kingdom
[c]Geowissenschaftliches Zentrum Göttingen, Abteilung Sedimentologie / Umweltgeologie, Universität Göttingen, Goldschmidtstraße 3, 37077 Göttingen, Germany
[d]Department of Geology, University of Gondar, P.O. Box 196, Gondar, Ethiopia
[e]Institut für Angewandte Geowissenschaften, Technische Universität Berlin, Ernst-Reuter-Platz 1, 10587 Berlin, Germany

Abstract

We use heavy minerals and rutile and garnet chemical compositions to constrain the provenance of two glaciogenic sandstone formations that build up the Palaeozoic succession in Ethiopia. The heavy mineral assemblage of the Upper Ordovician–lower Silurian Enticho Sandstone is dominated by ultra-stable minerals, implying high maturity of the sediment. Variable amounts of garnet are present as well. The Carboniferous–Permian Edaga Arbi Glacials contain mainly less stable heavy minerals, such as garnet and apatite, suggesting little chemical alteration. A combination of magmatic and metamorphic source rocks is likely for both formations. Rutile and garnet chemistry point to mainly amphibolite-facies and to a lesser extent granulite-facies metamorphic source rocks with generally slightly higher metamorphic temperatures for detrital heavy minerals in the Enticho Sandstone. We conclude that the Enticho Sandstone is mainly the product of reworked mature Cambrian–Ordovician sediment, which may have been supplied via the Gondwana super-fan system. Locally, glaciers of the Late Ordovician glaciation eroded fresh basement material, delivering the garnet. For the Edaga Arbi Glacials, a rather proximal provenance is likely. The potential source area is the southern hinterland, where Precambrian low-to higher grade metamorphic rocks of the Arabian–Nubian Shield occur at the transition to the Mozambique Belt.

4.1. Introduction

Two glaciations affected the supercontinent Gondwana in the Palaeozoic: The Late Ordovician (Hirnantian) glaciation was short-lived and reconstructions propose a large ice sheet covering much of northern Gondwana (e.g. Eyles, 1993; Ghienne et al., 2007; Le Heron and Craig, 2008; Le Heron et al., 2018). The Late Palaeozoic Ice Age (LPIA) affected Ethiopia in the Carboniferous–Permian (Bussert and Schrank, 2007) and is considered more complex in its spatial and temporal extend (e.g. Eyles, 1993; Fielding et al., 2008). The Palaeozoic sedimentary succession in Ethiopia is the product of these two glaciations and comprises the Upper Ordovician–lower Silurian Enticho Sandstone and the Carboniferous–Permian Edaga Arbi Glacials. Sedimentological and palynological studies of the two formations by Dow et al. (1971), Beyth (1972a; 1972b) Saxena and Assefa (1983), Bussert and Schrank (2007), Bussert and Dawit (2009) and Bussert (2010; 2014) provide stratigraphic control and evidence that two different glaciations are recorded.

Petrographic and bulk geochemical analyses (Lewin et al., 2018) reveal a very high mineralogical maturity for the Enticho Sandstone, which is striking for glaciogenic sediments. In contrast, the Edaga Arbi Glacials are less mature and more variable in composition. These trends have also been observed in age-equivalent formations in Saudi Arabia (Keller et al., 2011; Bassis et al., 2016b). In the Lower Palaeozoic, high maturity is a common feature of sandstones in northern Gondwana (Garfunkel, 2002; Avigad et al., 2005; Morag et al., 2011). The high similarity of early Palaeozoic sedimentary rocks across Gondwana, not only in maturity, but also in their detrital zircon age spectra, led Squire et al. (2006) to propose a model of large sediment fans that transported masses of detritus from the East African Orogen in the centre of Gondwana (Figure 4-1) towards the continental margins. The long transport, possibly in combination with strong chemical weathering under a corrosive Cambrian–Ordovician atmosphere, may have led to the high maturity (Avigad et al., 2005; Morag et al., 2011). The super-fan hypothesis was confirmed for northern Gondwana by Meinhold et al. (2013) and Stephan et al. (2019). Detrital zircon ages in the Enticho Sandstone in Ethiopia are very similar to those of the presumed super-fan sediments, suggesting that the formation contains reworked super-fan material (Lewin et al., 2020).
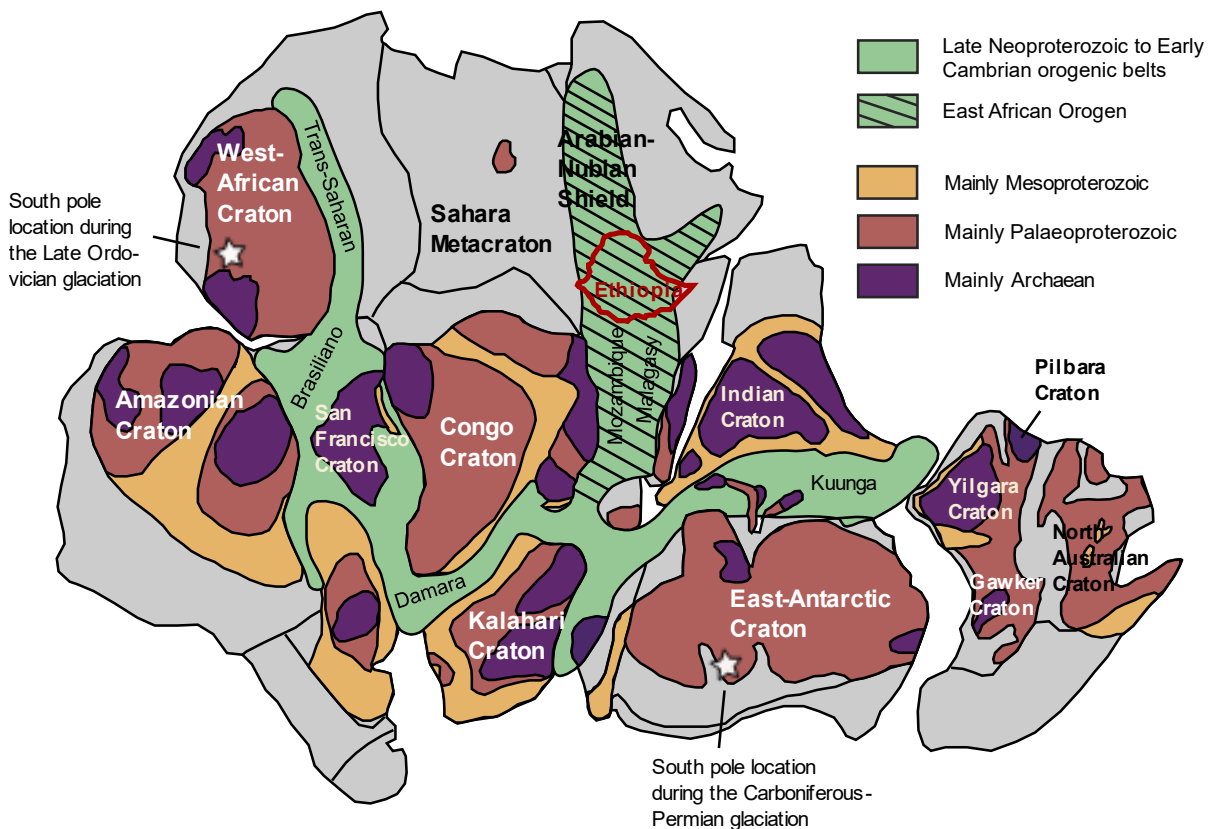
Figure 4-1: Map of Gondwana showing the overall geological setting (modified after Torsvik and Cocks, 2013; Avigad et al., 2017).

For the Edaga Arbi Glacials, the low maturity and zircon ages similar to those in the Arabian–Nubian Shield make a local provenance likely (Lewin et al., 2018; 2020). A re-organisation of the sediment dispersal system during the Carboniferous is also inferred for southern Libya (Morton et al., 2011) and Saudi Arabia (Knox et al., 2007; Bassis et al., 2016a) based on changes in the heavy mineral spectra. Heavy mineral data for the Ethiopian Palaeozoic sandstones are missing so far.

Heavy minerals in sediments and sedimentary rocks are widely used to infer the sediments' provenance by assigning the minerals and their parageneses to certain source rock lithologies, for which they are

characteristic. Because the heavy mineral assemblage in a sediment is not only influenced by source rock lithology, but also by processes operating during weathering, transport, deposition and diagenesis (e.g. Morton and Hallsworth, 1994), single grain geochemical analyses on specific mineral species are a powerful complementary technique (von Eynatten and Dunkl, 2012). Rutile is one of the ultra-stable heavy minerals and very resistant to physical and chemical alterations. Furthermore, its trace element composition is dependent on the metamorphic temperature conditions during growth and the lithology of the host rock, making it a good candidate for provenance studies (e.g. Triebold et al., 2007; Meinhold, 2010; Triebold et al., 2012). Similarly, garnet composition depends on host rock lithology and pressure and temperature conditions during growth and its use in provenance analysis is well established (e.g. Morton, 1987; Mange and Wright, 2007; Krippner et al., 2014; Stutenbecker et al., 2017).

In this study we use the heavy mineral assemblages and rutile and garnet chemistry to further constrain the provenance of the two Palaeozoic sandstone formations in Ethiopia. This study tests the assumption that the Enticho Sandstone contains reworked material from the Gondwana super-fan system and that the Edaga Arbi Glacials originate from proximal source areas in the Arabian–Nubian Shield. We also examine whether a regional correlation of changes in the heavy mineral spectra from early to late Palaeozoic with sedimentary rocks in Libya and Saudi Arabia is possible. This allows a better understanding of the Palaeozoic sediment dispersal system of northern Gondwana and the influence of the two glaciations.

4.2. Geological setting

Both the Upper Ordovician–Lower Silurian Enticho Sandstone and the Carboniferous–Permian Edaga Arbi Glacials are exposed around the Mekelle Basin in the northern Ethiopian province Tigray (Kazmin, 1972; Garland et al., 1978; Tsige and Hailu, 2007; Figure 4-2). The Enticho Sandstone lies unconformably on the Neoproterozoic metamorphic basement. In some areas, also the Edaga Arbi Glacials lie unconformably on the Neoproterozoic basement while in others on the Enticho Sandstone. Both the Enticho Sandstone and the Edaga Arbi Glacials and are overlain by Mesozoic sediments (Beyth, 1972b; Tefera et al., 1996; Dawit, 2010; Figure 4-2). In addition, glacial sediments corresponding to the Edaga Arbi Glacials occur in the Blue Nile region in western Ethiopia (Figure 4-2 b).

The basement in Ethiopia is part of the East African Orogen, comprising the Arabian–Nubian Shield in the north and the Mozambique Belt in the south (Kazmin, 1972; Tefera et al., 1996; Stern et al., 2012; Figure 4-1). The Arabian–Nubian Shield is composed of mainly juvenile Neoproterozoic crust, which experienced greenschist- to amphibolite-facies metamorphism (e.g. Johnson et al., 2011). In the Mozambique Belt, amphibolite- to granulite-facies metamorphic grades can be found, ascribed to the intense Ediacaran collision between East and West Gondwana (Stern et al., 2012). The basement of northern Ethiopia is considered to belong to the Arabian–Nubian Shield (e.g. Stern et al., 2012; Johnson, 2014). The upper Tonian Tsaliet Group consists of effusive flows and diverse volcaniclastic rocks (Beyth, 1972b; Miller et al., 2009). The Cryogenian Tambien Group is made of marine siliciclastic and carbonate rocks deposited in post-magmatism basins (Alene et al., 2006; Avigad et al., 2007; Miller et al., 2009). Both units were metamorphically overprinted to greenschist-facies grade and syn- and post-tectonic granitoids and diorites intruded (Beyth, 1972b; Kazmin et al., 1978; Tefera et al., 1996). The Western and Southern Ethiopian Shields contain high-grade metamorphic rocks of the Mozambique Belt (Yibas et al., 2002; Woldemichael et al., 2010; Stern et al., 2012).

The Palaeozoic sedimentary succession starts with the Upper Ordovician–lower Silurian Enticho Sandstone. Cambrian, Lower and Middle Ordovician sediments are missing. Body and trace fossils as

well as palynoflora (cryptospores) constrain the age of the formation (Saxena and Assefa, 1983; Bussert and Dawit, 2009; Brocke et al., 2015); its thickness is up to 300 m (Saxena and Assefa, 1983; Dawit, 2010). The lower part is glaciogenic. Massive, large-scale trough or sigmoidal cross-bedded sandstones and conglomerates occur, which are interpreted as subaqueous meltwater deposits. Diamictite occurs in one location, which is probably a tillite. In the upper part of the Enticho Sandstone, well-sorted sandstones with bipolar cross-bed sets indicate a tidal deposition in a shallow sea (Bussert and Dawit, 2009; Dawit, 2010).

Between the Upper Ordovician–lower Silurian Enticho Sandstone and the Carboniferous–Permian Edaga Arbi Glacials there is a long hiatus; middle Silurian to middle Carboniferous rocks are not preserved. The Edaga Arbi Glacials have a thickness of up to 200 m in northern Ethiopia (Bussert, 2010) and lie unconformably either on the Enticho Sandstone or directly on the basement (e.g. Beyth, 1972b). They are biostratigraphically constrained by their well-preserved microfloral assemblage (Bussert and Schrank, 2007). At the base, a polymict conglomerate probably represents a tillite; it is followed by laminated claystones and siltstones with scattered out-sized clasts and lenses of sandstone, interpreted as suspension settle-outs in a pro-glacial lake or fjord-like environment, with periodic hyperpycnal sediment flows and the deposition of dropstones (Beyth, 1972b; Bussert and Dawit, 2009; Bussert, 2014). For a more detailed facies description of the two studied formations and field photographs we refer to Bussert and Dawit (2009), Bussert (2014) and Lewin et al. (2018).

4.3. Sampling and methods

The selection of sampling sites was based on previous stratigraphic and sedimentological work and priority was given to sections that are biostratigraphically constrained (Bussert and Schrank, 2007; Bussert and Dawit, 2009; Brocke et al., 2015). In other sections, the assignment to one of the two formations was through lithofacies characteristics in the field and could be confirmed by geochemical analyses (Lewin et al., 2018; Table 4-1). Only one sample (Eda-5) was erroneously classified in the field and could be assigned to the Enticho Sandstone by bulk geochemistry. We chose 20 samples from the Enticho Sandstone and 11 samples from the Edaga Arbi Glacials for heavy mineral analysis (Table 4-1). The selection was made to cover a large spatial and stratigraphic range.

Approximately 1 kg of sample material was disaggregated using a jaw crusher followed by mortar and pestle. The material was treated with 10% acetic acid to dissolve carbonate, which was found in many samples as cement, especially in the Edaga Arbi Glacials. Furthermore, a mixture of sodium citrate, sodium bicarbonate and sodium dithionite (60 g, 8 g and 20 g, respectively, in 1 L of water) was used to remove iron oxide coating, which was especially strong in samples of the Enticho Sandstone. After being placed in an ultrasonic bath for five minutes, the samples were wet sieved to obtain the grain size fractions 40–63 µm, 63–125 µm and 125–500 µm. For further analyses, we focused on the grain size interval of 63–125 µm to ensure comparability with corresponding data from previous studies in Libya (Morton et al., 2011) and Saudi Arabia (Bassis et al., 2016a). The other grain size intervals were additionally considered in four samples during conventional heavy mineral analysis to assess the influence of chosen grain size windows on the heavy mineral assemblage (Table A 8). These samples were selected due to their relatively large grain size variation compared to the other samples and to cover a large geographical spread. Heavy mineral separation was done using sodium polytungstate with a density of 2.8 g/cm³ in a separatory funnel. The separation procedure was performed two times per sample to ensure proper separation of the heavy and the light minerals.
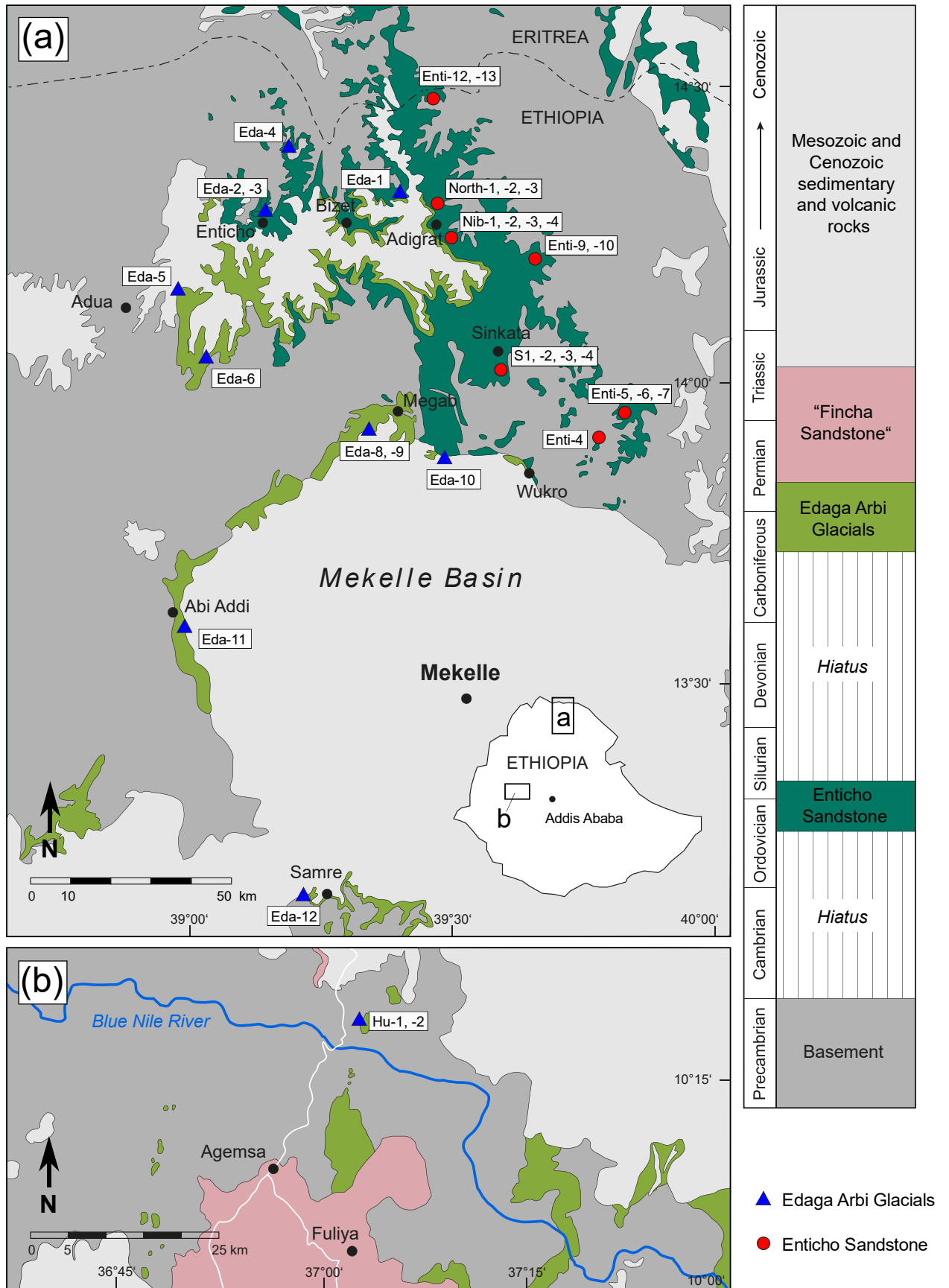
Figure 4-2: Maps of the study areas showing the sampling locations (after Lewin et al., 2018). (a) Northern Ethiopia, modified after Arkin et al. (1971), Garland et al. (1978), Bussert (2014). (b) Blue Nile region, modified after Tsige and Hailu (2007), Dawit (2014). The term "Fincha Sandstone" is taken from Dawit (2014).

Table 4-1: Sample information. Locations are given in geographical coordinates (WGS84). The stratigraphic assignment (Strat) to one of the two studied formations is based on biostratigraphic evidence (B), lithofacies characteristics (LF) in the outcrop or geochemical analyses (C). Detailed information on the petrography and geochemistry of each sample is given in Lewin et al. (2018). HMA-o – heavy mineral analysis using an optical microscope, HMA-r – heavy mineral analysis using Raman spectroscopy, HMA*-r – heavy mineral analysis with both optical microscopy and Raman spectroscopy, rtl – rutile chemical analysis, grt – garnet chemical analysis.

#	Sample	Formation	Age	Location	North(°)	East(°)	Facies/ Lithology	Strat.	Methods
1	Enti-4	Enticho	Upper Ordovician	Atsbi south	13.83465	039.71262	Tillite matrix	C	HMA*-r, rtl, grt
2	Enti-5	Enticho	Upper Ordovician	Atsbi north	13.88828	039.74783	Glacial	B	HMA-r, grt
3	Enti-7	Enticho	Upper Ordovician	Atsbi north	13.88842	039.74259	Glacial	B	HMA-o
4	Enti-9	Enticho	Upper Ordovician	Wollwello	14.22037	039.65014	Glacial	B	HMA-r, grt
5	Enti-13	Enticho	Upper Ordovician	Zalambassa	14.49275	039.41911	Glacial	LF	HMA-r, rtl
6	S1	Enticho	Upper Ordovician	Sinkata	13.96861	039.61167	Glacial	B	HMA-o
7	S2	Enticho	Upper Ordovician	Sinkata	13.96861	039.61167	Glacial	B	HMA-o
8	Nib-1	Enticho	Upper Ordovician	Adigrat south	14.25194	039.48972	Glacial	B	Rtl
9	Nib-2	Enticho	Upper Ordovician	Adigrat south	14.25194	039.48972	Glacial	B	HMA-r, grt
10	North-1	Enticho	Upper Ordovician	Adigrat north	14.31333	039.46000	Glacial	B	HMA-o
11	North-2	Enticho	Upper Ordovician	Adigrat north	14.31333	039.46000	Glacial	B	HMA-o
12	Enti-6	Enticho	Upper Ordovician	Atsbi north	13.88842	039.74827	Marine	B	HMA-r, rtl
13	Enti-10	Enticho	Upper Ordovician	Wollwello	14.21839	039.64994	Marine	B	HMA-o
14	Enti-12	Enticho	Upper Ordovician	Zalambassa	14.49627	039.41911	Marine	LF	HMA*-r, rtl
15	S3	Enticho	Upper Ordovician	Sinkata	13.97056	039.61111	Marine	B	HMA-o
16	S4	Enticho	Upper Ordovician	Sinkata	13.97056	039.61111	Marine	B	HMA-o
17	Nib-3	Enticho	Upper Ordovician	Adigrat south	14.25222	039.49583	Marine	B	Rtl
18	Nib-4	Enticho	Upper Ordovician	Adigrat south	14.25222	039.49583	Marine	B	HMA-o
19	North-3	Enticho	Upper Ordovician	Adigrat north	14.31944	039.45889	Marine	B	HMA-o
20	Eda-5	Enticho	Upper Ordovician	Adwa east	14.19102	038.93957	Sand lens	C	HMA-r
21	Eda-2	Edaga Arbi	Carboniferous-Permian	Enticho	14.28166	039.14725	Tillite matrix	B	HMA*-r, rtl
22	Eda-3	Edaga Arbi	Carboniferous-Permian	Enticho	14.27929	039.14836	Sand lens	C	HMA-r, rtl
23	Eda-4	Edaga Arbi	Carboniferous-Permian	Edaga Robi	14.38906	039.18161	Tillite matrix	C	HMA-o
24	Eda-6	Edaga Arbi	Carboniferous-Permian	Edaga Arbi west	14.05667	039.07095	Sand lens	LF	HMA-o
25	Eda-8	Edaga Arbi	Carboniferous-Permian	Megab south	13.90944	039.32301	Sand lens	B	HMA-o
26	Eda-9	Edaga Arbi	Carboniferous-Permian	Megab south	13.90915	039.32235	Sand lens	B	HMA-r, rtl, grt
27	Eda-10	Edaga Arbi	Carboniferous-Permian	Dugum	13.84957	039.49003	Sand lens	LF	HMA-o
28	Eda-11	Edaga Arbi	Carboniferous-Permian	Abi Addi	13.61842	039.00042	Sand lens	LF	HMA-r, rtl, grt
29	Eda-12	Edaga Arbi	Carboniferous-Permian	Samre	13.17844	039.19745	Sand lens	B	HMA-r, grt
30	Hu-1	Edaga Arbi	Carboniferous-Permian	Bure, Blue Nile	10.31057	037.05068	Sand lens	LF	HMA*-r, grt
31	Hu-2	Edaga Arbi	Carboniferous-Permian	Bure, Blue Nile	10.31057	037.05068	Sand lens	LF	HMA-r, grt

Conventional heavy mineral analysis

For optical analysis of the heavy mineral assemblage, representative subsamples of the heavy mineral concentrates obtained with a micro-riffle splitter were mounted on glass slides embedded in Cargille Meltmount^{TM} with a refraction index of 1.662. Mineral species were identified using a polarizing microscope and 200 translucent grains per sample were counted where possible. Since the grain size windows analysed are narrow, no area-sensitive counting method was used and all grains encountered under the microscope were counted until 200 counts were reached. The proportions of translucent and opaque minerals were assessed based on 100 counts per sample.

Raman spectroscopy

To confirm the results from the optical analysis of the heavy mineral assemblages, we applied a semi-automatic identification and counting method based on Raman spectroscopy at the Geoscience Centre of the University of Göttingen (Lünsdorf et al., 2019) to 15 of the samples (Table 4-1). The samples were chosen to cover all different minerals and assemblages identified during optical analysis. Representative subsamples of the respective heavy mineral concentrates were embedded in epoxy resin and polished to reveal the grains' interior on a flat surface. High-resolution mosaic images of the mounts were taken using a Zeiss Axio Imager M2m polarizing microscope with the ZEN Pro software at high magnification (50x, 0.75 NA) in transmitted and reflected light. Measuring spots were selected on these mosaics using the Coordsetter software introduced by Lünsdorf et al. (2019) and the coordinates were transferred to a Horiba Scientific XploRA PLUS Raman microscope. Raman spectroscopy was performed with a laser wavelength of 532 nm, laser power of 25% (of 100 mW) and circular polarization (lambda/4 retarder plate). The following measurement parameters were used; spectral grating: 1200 gr/mm, spectrometer position: 1310 cm^{-1}, objective: 50x, 0.5 NA, LWD, exposure time: 0.1 s

(min.)/30 s (max.), number of accumulations: 1, max. intensity: 5000 cts. Automated identification of heavy mineral species was done with an in-house program using a modified version of the RRUFF database in combination with the segmental hit quality index approach (Lünsdorf et al., 2019). Depending on the quality of the mount and the proportions of translucent and opaque grains, between 87 and 937 translucent minerals per sample were confidently identified (Table A 7).

Electron microprobe analysis
Rutile chemical analyses were performed on six samples from the Enticho Sandstone and four samples from the Edaga Arbi Glacials; garnet chemical analyses were performed on four samples from the Enticho Sandstone and five samples from the Edaga Arbi Glacials. The choice was made based on the amount of the respective mineral in the heavy mineral concentrate. Rutile and garnet grains were randomly handpicked under a binocular microscope from the heavy mineral concentrates of the 63–125 µm grain size fraction, embedded in epoxy resin and polished to expose the grains' interior on a flat surface. The mounts were carbon-coated to ensure conductivity. Chemical analyses of the mineral grains were performed with a JEOL JXA 8900 RL electron microprobe equipped with five wavelength dispersive spectrometers at the Geoscience Centre of the University of Göttingen. Rutile was analysed with a beam current of 80 nA and an accelerating voltage of 25 kV. A counting time of 200 s was used for Al, Cr, Nb, V and Zr, 100 s were used for Fe, Si, Sn and W and 15 s for Ti. Garnet was analysed with a beam current of 20 nA and an accelerating voltage of 15 kV. The counting times per spot were 15 s for Al, Ca, Fe, Mg and Si and 30 s for Cr, Mn and Ti. Detection limits and standard errors are given in the supplementary material together with the analytical data.

To visualise the datasets obtained from electron microprobe analyses and their variability, a principal component analysis (PCA) was performed with the centred log-ratio transformed chemical data for rutile and garnet, respectively. The log-ratio transformation is necessary to account for the compositional nature of the data (Aitchison, 1986). Values below the detection limit were replaced by 0.65 times the detection limit, as suggested by Martín-Fernández et al. (2003), to make sure that the dataset for log-ratio transformation does not contain any zeros.

Rutile growth temperature was assessed using the latest Zr-in-rutile thermometer introduced by Tomkins et al. (2007) in the α-quartz field after the following equation:

$$T(°C) = ((83.9 + 0.410\ P) / (0.1428 - R\ \ln(Zr[ppm]))) - 273.$$

R is the gas constant with 0.0083144 kJ K^{-1}. A default pressure P of 10 kbar was used, as proposed by Triebold et al. (2012) for detrital rutile with unknown growth pressure conditions. The dependency of Cr and Nb concentrations in rutile on host rock chemistry was used to deduce the proportions of metamafic and metafelsic rutiles with the following Cr–Nb separation line after Triebold et al. (2012):

$$x = 5\ (Nb[ppm] - 500) - Cr[ppm].$$

Here, rutiles from metamafic rocks yield negative values for x, while for rutiles from metafelsic rocks x is positive.

The assignment of detrital garnet to certain source lithologies is difficult given the complex control of garnet composition by host rock chemical composition and pressure and temperature during formation (e.g. Krippner et al., 2014; Tolosana-Delgado et al., 2018). To account for the overlap of compositional fields of garnets from different host rock lithologies and the need for robust multivariate statistical methods for garnet classification, Tolosana-Delgado et al. (2018) proposed a new discrimination

scheme, which is applied in this study. It is hierarchical, based on linear discriminant analysis and gives a set of probabilities for a garnet grain of belonging to one of the five host rock categories: igneous rocks, ultramafic rocks or eclogite-, amphibolite- and granulite-facies metamorphic rocks.

4.4. Results

Heavy mineral analysis

The full data set obtained during optical heavy mineral analysis and Raman spectroscopy is available in the supplementary material to this article (Table A 7). The proportions of heavy minerals with respect to the bulk of the respective grain size fractions used for separation are low. Heavy mineral yields vary between 0.01 wt% and 3.94 wt% of the respective grain size fractions with most yields below 1 wt% (Table A 7). No systematic difference between the two formations is visible in the heavy mineral yield. The ratio between translucent and opaque grains is highly variable and no pattern is observable (Table A 7). An overview of photomicrographs of the most common heavy minerals in the studied samples is given in Figure 4-3. The analysis of the heavy mineral assemblages reveals distinct differences between samples of the Enticho Sandstone and the Edaga Arbi Glacials. The heavy mineral suite of the Enticho Sandstone, especially the upper, marine, subunit, is dominated by the ultra-stable minerals zircon, rutile and tourmaline (Figure 4-4). The lower glaciogenic subunit contains significant amounts of garnet and in some samples apatite and staurolite (Figure 4-4). The highest garnet content in the Enticho Sandstone is found in sample Enti-4, which is taken from the basal tillite. Moreover, monazite is a common mineral in the Enticho Sandstone.
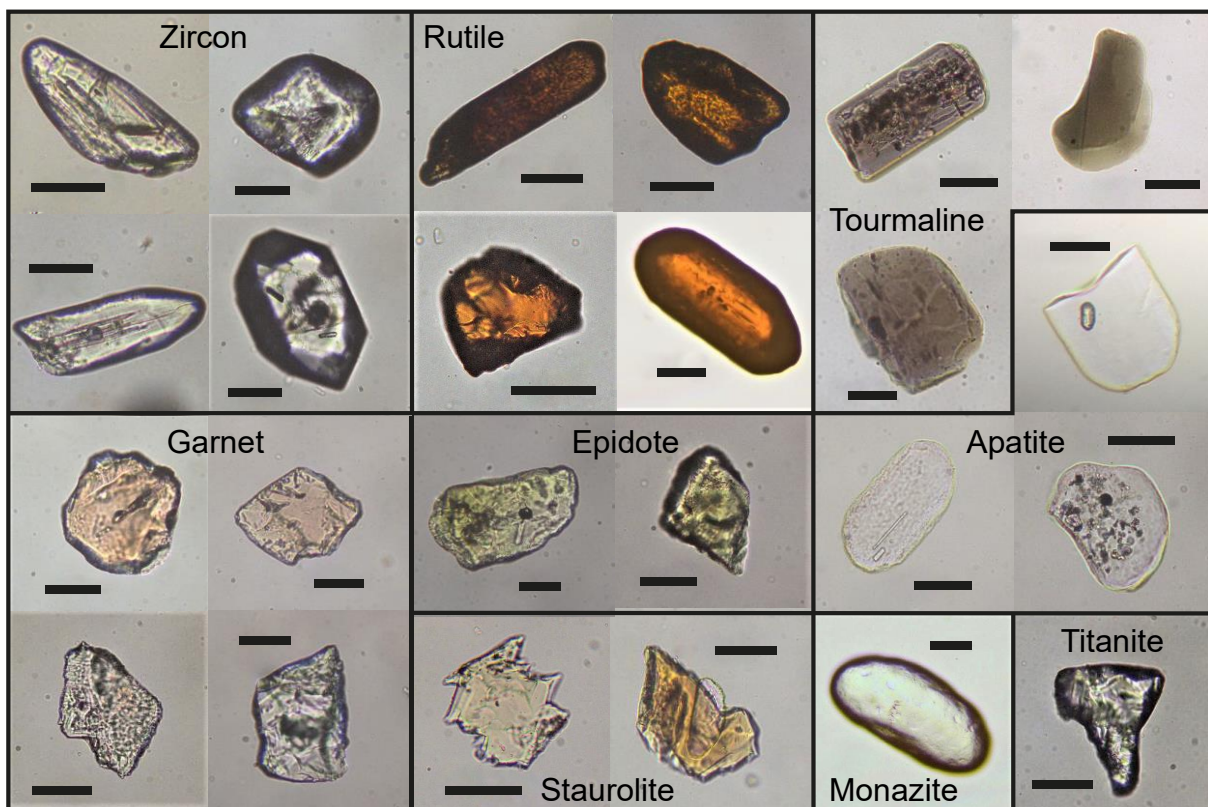
Figure 4-3: Photomicrographs of the most common heavy minerals in the studied samples. The bars represent 50 μm, respectively.

In the Edaga Arbi Glacials, the proportion of the ultra-stable heavy minerals is much lower. Instead, apatite and garnet make up the largest heavy mineral groups, but with strongly varying relations (Figure 4-4). Garnet contents range from zero to 86% and apatite contents from 7 to 77.1% (Figure 4-4, Table A 7). Remarkable is the exceptionally high epidote content in two samples from the Edaga Arbi Glacials

(Eda-6 with 45% and Eda-12 with 50.6%). Regarding the TiO_2 polymorphs (rutile, anatase and brookite), differentiated by Raman spectroscopy, rutile constitutes more than 80% in most studied samples (Table A 7). However, some samples, especially in the Edaga Arbi Glacials, contain considerable amounts of anatase and brookite intergrowths.

For four samples, two from each formation, the heavy mineral assemblages in the grain size fractions 40–63 μm and 125–250 μm were analysed additionally to reveal the influence of the chosen grain size window (Figure 4-5). Generally, the same heavy mineral assemblage can be observed within different grain size fractions of one sample, but with varying proportions of the respective minerals. It is evident that zircon preferentially occurs in the finest grain size fraction, whereas tourmaline and garnet are more abundant in the largest grain size fraction. An exception is sample Enti-4, where staurolite and monazite occur in the largest fraction, which are not present in the two finer fractions. Figure 4-5 also reveals differences in heavy mineral identification optically and using Raman spectroscopy; the 63–125 μm fraction of these four samples was counted with both methods. The result is similar, however, tourmaline and minerals of the epidote group are generally overestimated during optical counting, whereas garnet is underestimated (Figure 4-5).
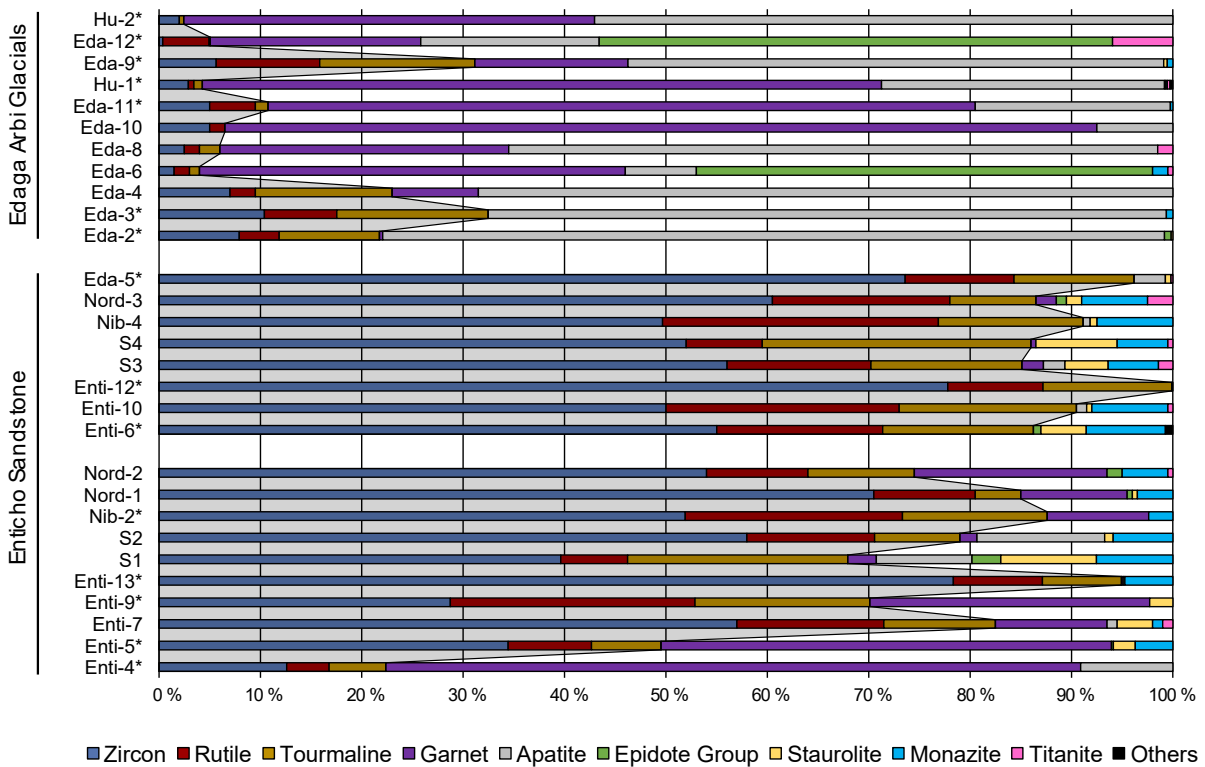
Figure 4-4: Heavy mineral assemblages in the 63–125 μm grain-size fractions of the studied samples. For samples marked with an asterisk (*) the heavy minerals were identified using Raman spectroscopy, for the other samples with a polarising microscope. The samples are arranged according to their stratigraphic order as inferred during field work.

The two studied formations can well be discriminated using heavy mineral indices (e.g. Morton and Hallsworth, 1994; Table 4-2). The dominance of the ultra-stable heavy minerals in the Enticho Sandstone is shown in the zircon–tourmaline–rutile (ZTR) index of 79.7 on average. In the Edaga Arbi Glacials ZTR is on average 13.4. On the other hand, the high proportions of garnet and apatite in the Edaga Arbi Glacials are reflected in a garnet–tourmaline index (GTi) of 88.3 and an apatite–tourmaline

index (ATi) of 88.7. In the Enticho Sandstone these indices are on average 17.3 and 14.6, respectively. The rutile–zircon index (RZi) is higher in the Edaga Arbi Glacials with a mean of 43.0, while in the Enticho Sandstone RZi is 20.4 on average. The staurolite–tourmaline index (STi) is higher in the Enticho Sandstone (14.4) than in the Edaga Arbi Glacials (0.9; Table 4-2).
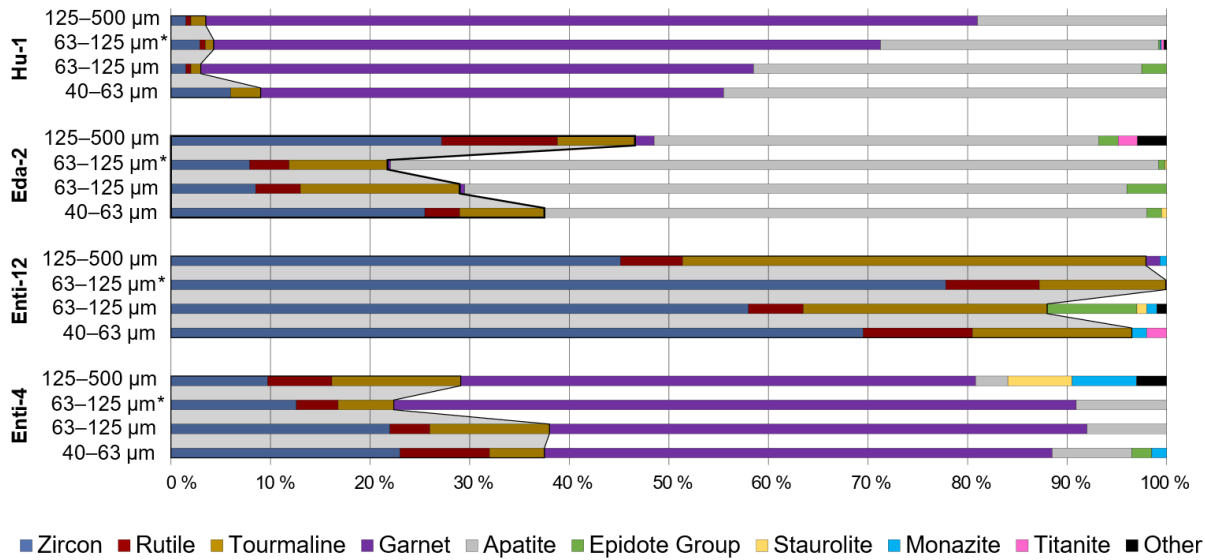
Figure 4-5: Comparison of the heavy mineral assemblages in the grain-size fractions 40–63 µm, 63–125 µm and 125–250 µm for four samples. Note that the 63–125 µm fraction was studied by both optical microscopy and Raman spectroscopy (*).

Table 4-2: Heavy mineral indices (Morton and Hallsworth, 1994): ZTR = zircon + rutile + tourmaline; RZi = 100 rutile / (rutile + zircon); GZi = 100 garnet / (garnet + zircon); ATi = 100 apatite / (apatite + tourmaline); STi = 100 staurolite / (staurolite + tourmaline). Samples marked with an asterisk (*) are studied with Raman spectroscopy, other samples using optical microscopy.

Sample	Formation	ZTR	RZi	GZi	ATi	STi
Enti-4*	Enticho Sandstone	22.4	25.0	84.5	61.9	0.0
Enti-5*	Enticho Sandstone	49.5	19.3	56.3	0.0	23.9
Enti-6*	Enticho Sandstone	86.2	22.9	0.0	0.0	23.1
Enti-7	Enticho Sandstone	82.5	20.3	16.2	8.3	24.1
Enti-9*	Enticho Sandstone	70.1	45.7	49.0	0.0	11.8
Enti-10	Enticho Sandstone	90.5	31.5	0.0	5.4	2.8
Enti-12*	Enticho Sandstone	99.9	10.8	0.1	0.0	0.0
Enti-13*	Enticho Sandstone	94.9	10.1	0.2	0.0	0.0
S1	Enticho Sandstone	67.9	14.3	6.7	30.3	30.3
S2	Enticho Sandstone	79.0	17.9	2.8	60.0	9.1
S3	Enticho Sandstone	85.1	20.2	3.7	12.5	22.2
S4	Enticho Sandstone	86.0	12.6	1.0	0.0	23.2
Nib-2*	Enticho Sandstone	87.6	29.2	16.2	0.0	0.0
Nib-4	Enticho Sandstone	91.2	35.4	0.0	4.5	4.5
Nord-1	Enticho Sandstone	85.0	12.4	13.0	0.0	10.0
Nord-2	Enticho Sandstone	74.5	15.6	26.0	0.0	0.0
Nord-3	Enticho Sandstone	86.5	22.4	3.2	0.0	15.0
Eda-2*	Edaga Arbi Glacials	21.7	33.3	4.0	88.6	1.6
Eda-3*	Edaga Arbi Glacials	32.5	40.7	0.0	81.7	0.0
Eda-4	Edaga Arbi Glacials	23.0	26.3	54.8	83.5	0.0
Eda-5*	Enticho?	96.2	12.7	0.0	20.7	4.4
Eda-6	Edaga Arbi Glacials	4.0	50.0	96.6	87.5	0.0
Eda-8	Edaga Arbi Glacials	6.0	37.5	91.9	97.0	0.0
Eda-9*	Edaga Arbi Glacials	31.1	64.4	72.8	77.5	2.3
Eda-10	Edaga Arbi Glacials	6.5	23.1	94.5	100.0	0.0
Eda-11*	Edaga Arbi Glacials	10.8	47.4	93.3	93.9	0.0
Eda-12*	Edaga Arbi Glacials	5.1	92.3	98.2	99.3	0.0
Hu-1*	Edaga Arbi Glacials	4.3	16.0	95.8	97.1	0.0
Hu-2*	Edaga Arbi Glacials	2.4	0.0	95.3	99.2	0.0
Enticho mean		*79.7*	*20.4*	*17.3*	*14.6*	*14.4*
Edaga Arbi mean		*13.4*	*43.0*	*88.3*	*88.7*	*0.9*

Rutile chemistry

The PCA biplot of the rutile chemical data (Figure 4-6) gives a first overview of the variability within the data set. The colour code by formation reveals clustering of the samples from the Enticho Sandstone and the Edaga Arbi Glacials, respectively. Rutiles from the Enticho Sandstone are enriched in Zr, V and Nb, whereas rutiles from the Edaga Arbi Glacials contain more Al and Fe (Figure 4-6). A group of rutiles from the Enticho Sandstone is enriched in Fe as well and is dominated by rutiles in sample Enti-6 (Figure 4-6). When looking at the first and third principal component (Figure 4-6 b), a group of rutile grains in the Enticho Sandstone is striking that is significantly depleted in Al compared to all other grains. This group is not from one single sample but contains grains from all analysed Enticho Sandstone samples (Figure 4-6).

According to the Zr-in-rutile thermometry after Tomkins et al. (2007), most analysed rutiles have grown under amphibolite-/eclogite-facies thermal conditions (ca. 500–750 °C for metapelitic rutiles, following Zack et al., 2004), while both formations contain also granulite-facies rutiles (>750 °C, following Zack et al., 2004; Figure 4-7). The proportion of granulite-facies rutiles is higher in the Enticho Sandstone (mean: 17.7%, range: 10.6–22.7%) than in the Edaga Arbi Glacials (mean: 15.8%, range: 7.0–33.3%). According to the source rock lithological assessment using the Cr and Nb contents most of the rutile grains in both formations are probably from metafelsic host rocks (Figure 4-7). The Edaga Arbi Glacials contain a higher proportion of rutile grains that might be derived from metamafic sources (mean: 39.8%, range: 28.9–48.7%) than the Enticho Sandstone (mean: 27.0%, range: 16.7–34.0%).

Garnet chemistry

Garnet chemical analyses yield similar compositions for garnets from the Enticho Sandstone and from the Edaga Arbi Glacials. In a PCA biplot no clear clustering is visible (Figure A 3). However, garnets in the Enticho Sandstone appear to be slightly more Mn-rich (spessartine), while garnets in the Edaga Arbi Glacials are more Fe-rich (almandine). According to the garnet classification scheme after Tolosana-Delgado et al. (2018) most garnets are derived from metamorphic rocks. Both formations contain also a significant amount of garnets classified as from felsic igneous rocks, which is higher in the Enticho Sandstone (11.5%) than in the Edaga Arbi Glacials (5.9%; Figure 4-8). Only one garnet grain in a sample from the Enticho Sandstone is classified with the highest probability as from an ultramafic source. The metamorphic garnets are mostly classified as derived from amphibolite-facies and to a minor extent from granulite-facies metamorphic rocks (Figure 4-8). Only a few metamorphic garnets are with high probabilities from eclogite-facies sources. The proportion of metamorphic garnets probably from granulite-facies rocks is higher in the Enticho Sandstone (average: 29%, range 16.7–43.8%) than in the Edaga Arbi Glacials (average: 16.9%, range: 8.9–34.0%; Figure 4-8). Within the formations, inter-sample variations can be observed. In the Enticho Sandstone, samples Enti-4 and Enti-5 contain more high-grade metamorphic garnets than the other samples (Figure 4-8 a). In the Edaga Arbi Glacials, a tendency to high metamorphic grades can be observed for sample Eda-9 (Figure 4-8 b).

4.5. Discussion

Enticho Sandstone (Ordovician–Silurian)

The very high proportion of ultra-stable heavy minerals (ZTR; Figure 4-4) and monazite, hence the very high mineralogical maturity, is untypical for glaciogenic sediments. In an ice-house climate chemical weathering is poor. An explanation for the high maturity can be the recycling of older sediments or sedimentary rocks that have undergone substantial diagenetic modification dissolving unstable minerals (Garzanti, 2017). Typical indicators for recycled sedimentary rocks, such as abraded quartz overgrowth or sedimentary lithoclasts, have not been identified during petrographic analyses. However, if the
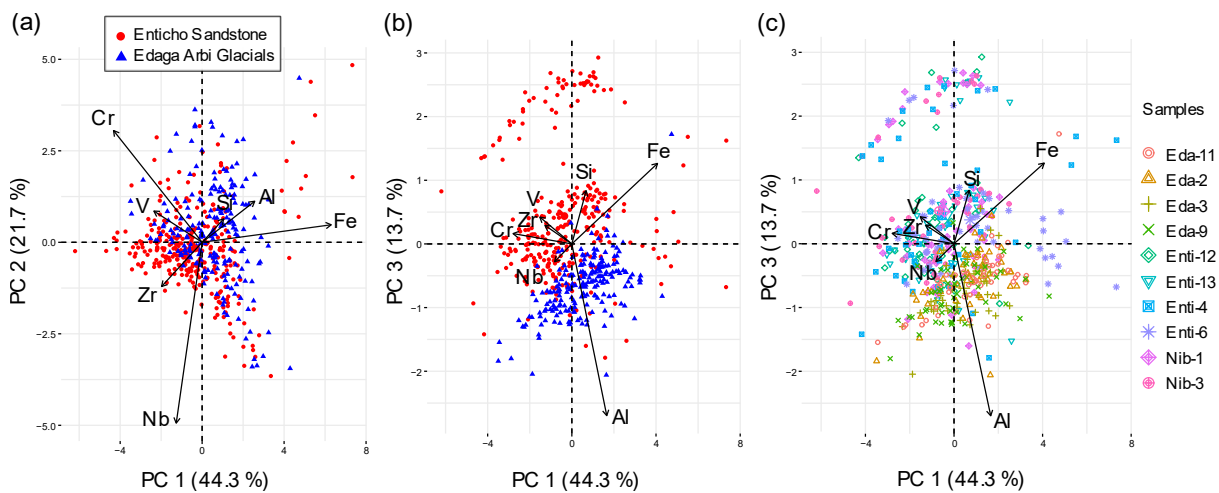
Figure 4-6: PCA biplot based on the centred log-raio (clr) transformed concentrations of the measured trace elements in rutile from Enticho Sandstone and Edaga Arbi Glacials. (a) First and second principal component. (b) First and third principal component. (c) First and third principal component with colour-code by sample.

sediment incorporated and transported by the glaciers and meltwater of the Hirnantian glaciation was not significantly lithified, such indicators are less pronounced. As parent sediment for the Enticho Sandstone, the Cambrian–Ordovician quartzarenites that covered much of northern Gondwana (Garfunkel, 2002; Avigad et al., 2005) are a likely candidate. It is unlikely that these sediments have been buried to a depth in which substantial diagenetic dissolution of unstable minerals took place before they were taken up by the Hirnantian glaciers. However, the high maturity of the parent sediment may have been caused by strong chemical surface weathering due to warm and humid climate conditions combined with a low relief and low sedimentation rates in the aftermath of the Pan-African orogeny under a corrosive Cambrian–Ordovician atmosphere, as suggested by Avigad et al. (2005). The Enticho Sandstone may thus represent reworked Cambrian–Ordovician sediments leading to its strikingly high maturity. This assumption is also made for Hirnantian glaciogenic sandstones in Saudi Arabia (Hussain et al., 2004; Knox et al., 2007; Bassis et al., 2016a; 2016b).

The glaciogenic basal part of the Enticho Sandstone, however, does also contain substantial amounts of less stable minerals, mainly garnet. This is particularly true for sample Enti-4, which was taken from the basal tillite (Figure 4-4). High proportions of garnet have also been observed in Hirnantian sandstones in Israel (Weissbrod and Bogoch, 2007) and ascribed to proximal sources since glacio-fluvial channels cut deeply into the basement. In Libya, an increase in garnet content, together with an increase in RZi is observed at the base of the Tanezzuft Formation (Meinhold et al., 2011; Morton et al., 2012), which is equivalent to the shallow marine part of the Enticho Sandstone (Figure 4-9 b). This shift is ascribed to the final pulse of the Hirnantian glaciation, during which glaciers have cut deeply into the hinterland and brought new material, which was then reworked during transgression. In the Enticho Sandstone, there are numerous indications of several glacier advance-retreat cycles, such as large and intense deformation structures in the glaciogenic sediments and the occurrence of tunnel valleys filled with glaciogenic sediments and eroded into older glaciogenic sediments. The unstable heavy minerals in the basal glaciogenic sediments may thus have been derived from intensive erosion during the first glacier advance. The subsequent glacial advances probably did not erode these glaciogenic sediments down to the basement, so that fresh basement material was not admixed during the subsequent advances. In Saudi-Arabia, Hirnantian sandstones are devoid of garnet (Bassis et al., 2016a), so glacial erosion of the basement was probably geographically variable. The absence of garnet in the shallow marine upper part of the Enticho Sandstone may be a consequence of selective removal during diagenesis. Corrosive pore fluids could penetrate the well-sorted and highly permeable marine sandstone better than the less

permeable glaciogenic part of the formation. Corroded garnet surfaces that could be observed during optical investigation of the heavy mineral concentrates (Figure 4-3, lower left image) further indicate such dissolution effects. The interpretation of the garnet content as a provenance signal should, therefore, be taken with caution.
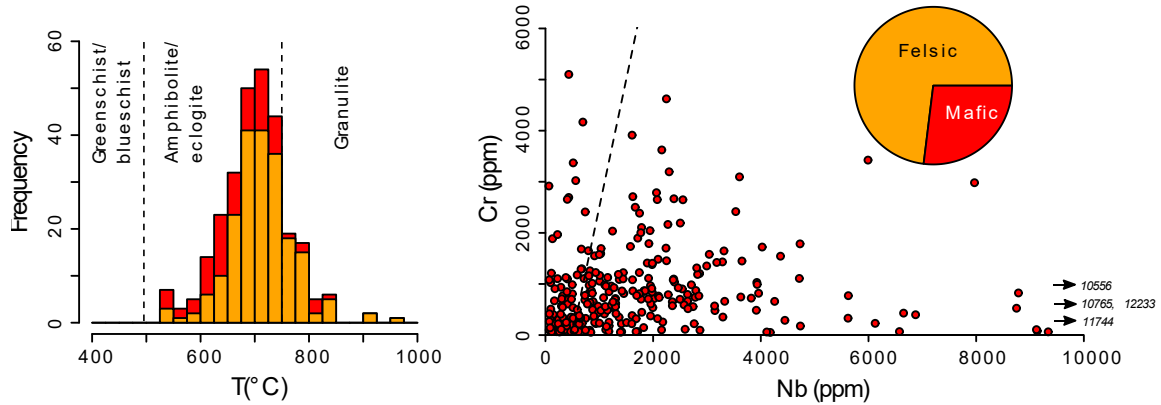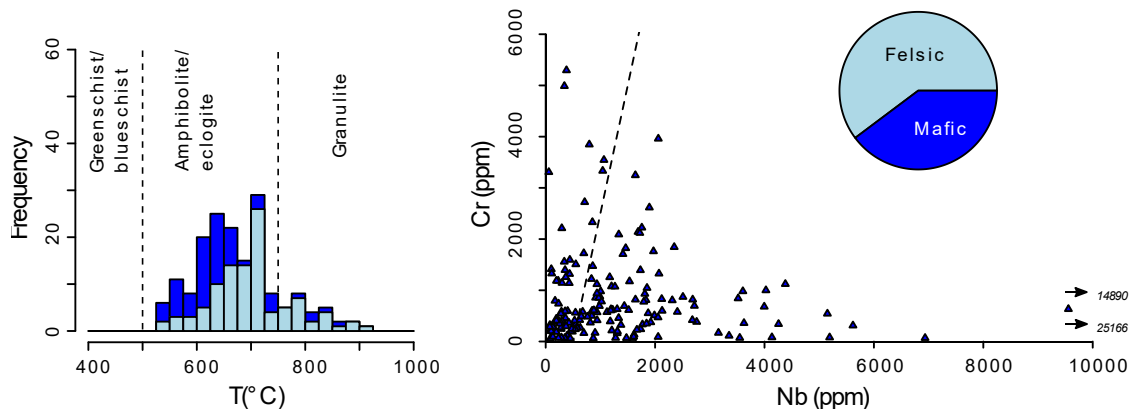
Figure 4-7: Left: histograms of the calculated formation temperatures from Zr-in-rutile thermometry after Tomkins et al. (2007). Approximate temperature boundaries of metamorphic facies for metapelitic rutile following Zack et al. (2004). Right: Cr–Nb crossplot and pie charts for classification of rutiles derived from metamafic and metafelsic source rocks after Triebold et al. (2012).

Despite the above-mentioned differences in garnet content, the heavy mineral assemblages in Ethiopia, Saudi Arabia and Libya are largely similar in the Ordovician–Silurian succession, as illustrated in the heavy mineral index cross plots (Figure 4-9). This supports the hypothesis of continent-scale homogenisation of the sediment in the early Palaeozoic. RZi is notably higher in some Libyan samples, likely implying a higher influence of metamorphic sources (Figure 4-9). In the Enticho Sandstone, the ratio of metamorphic and magmatic sources, as mirrored in RZi, is rather constant with little variation between the samples (Figure 4-9). Rutile and garnet chemical analyses point to mainly amphibolite-facies metamorphic source rocks, while both provide evidence for a certain contribution of granulite-facies sources as well (Figure 4-7, Figure 4-8). For rutile, the ratio of granulite-facies to amphibolite-facies grains is quite constant from sample to sample in the Enticho Sandstone, while garnet displays significant inter-sample variations (Figure 4-10). In samples Enti-4 and Enti-5 the proportion of garnets probably from granulite-facies sources is much higher than in the other samples (Figure 4-10). These samples are those with the highest garnet content, so that the ratio may be more reliable than for the other samples. Post-depositional dissolution may have affected different garnet-types differently. Additionally, it must be noted that the ratios are based on probabilities that grains grew under the

respective metamorphic conditions and not on a distinct classification (Tolosana-Delgado et al., 2018). If the inter-sample differences are not an artefact, they indicate that in the Enticho Sandstone there have been geographical differences in the contribution of different source areas and that garnet and rutile are, at least partly, from different sources.
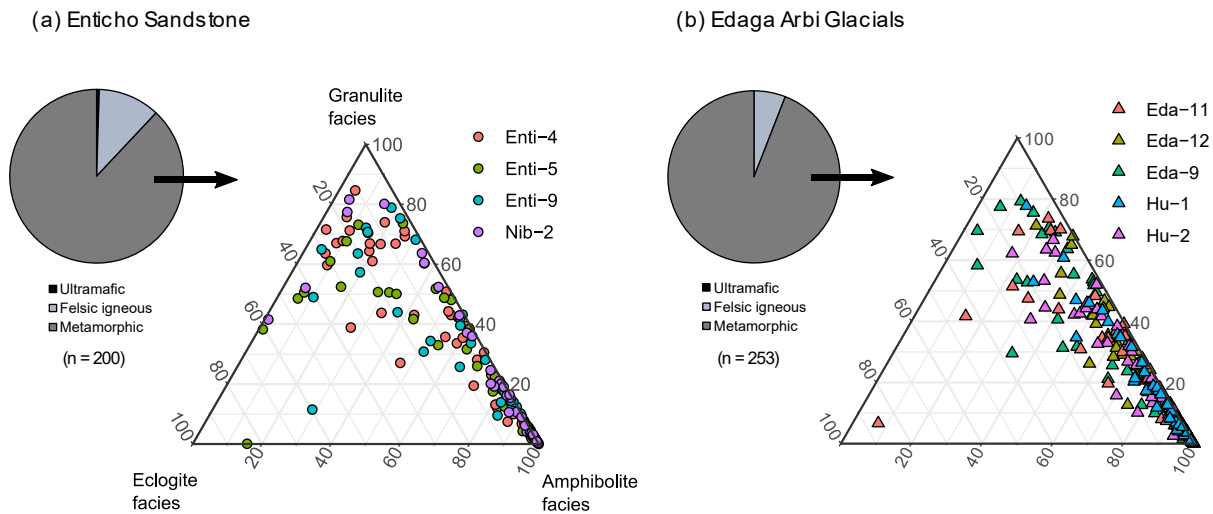
Figure 4-8: Garnet classification after Tolosana-Delgado et al. (2018) using the prior "global". For the pie charts, garnets were assigned to one class if the highest probability was calculated for the respective class, even if it was < 50 %. Ternary diagrams further classify the metamorphic garnets.

Rutile, as a chemically and physically very stable heavy mineral, can have been sourced from the reworked sediment incorporated in the Enticho Sandstone. The original provenance of this material is unclear, but following the Gondwana super-fan hypothesis, it may have originated in the central part of the East African Orogen (Mozambique Belt). Amphibolite- to granulite-facies metamorphic rocks are abundant there (e.g. Stern et al., 2012; Fritz et al., 2013) and may have supplied the rutile. The group of Fe-rich rutiles in sample Enti-6 (Figure 4-6) shows that differences in provenance exist within the Enticho Sandstone. Since this sample is taken from the shallow marine upper part of the formation, it may indicate that locally different material is brought to the basin during the transgression.

The garnet is probably derived from fresh basement material, which was eroded by the glaciers of the Hirnantian glaciation. The local basement in northern Ethiopia comprises mainly greenschist-facies metamorphic rocks (Beyth, 1972b; Kazmin et al., 1978; Tefera et al., 1996), but in the vicinity of intrusions, higher temperatures may have led to amphibolite-facies metamorphism. Reconstructions of the Hirnantian ice sheet assume the ice spreading centre to be in north-west Africa (Ghienne et al., 2007; Le Heron and Craig, 2008; Torsvik and Cocks, 2013), making a western provenance likely. Amphibolite- to granulite-facies rocks are present in the Sahara Metacraton (e.g. Abdelsalam et al., 2002) and may have supplied the garnet. Garnet chemistry further reveals a certain proportion of garnets that originate with high probability from felsic igneous rocks (Figure 4-8). Such rocks are, however, abundant in all parts of the East African Orogen and elsewhere in northern and central Gondwana, making it difficult to deduce any source area.

Summarizing, the heavy mineral assemblage of the Enticho Sandstone is probably a consequence of 1) reworking of mature sand by glaciers of the Hirnantian glaciation, 2) admixing garnet-rich material eroded by the glaciers from the basement and 3) post-depositional modification by dissolution of chemically unstable minerals, especially in the well-sorted and highly permeable marine part of the formation. The reworked mature sediments may have belonged to the postulated super-fans that transported large amounts of material towards the Gondwana margins during the early Palaeozoic

(Squire et al., 2006; Meinhold et al., 2013; Stephan et al., 2019), a hypothesis that is also underlined by detrital zircon age spectra in the Enticho Sandstone (Lewin et al., 2020). The variably admixed fresh basement material that delivered the garnet may origin from sources in the Sahara Metacraton. A northwesterly source area for the Enticho Sandstone is supported by palaeocurrent directions derived from the dip direction of foreset beds within cross-bedded sandstone (Bussert and Dawit, 2009).
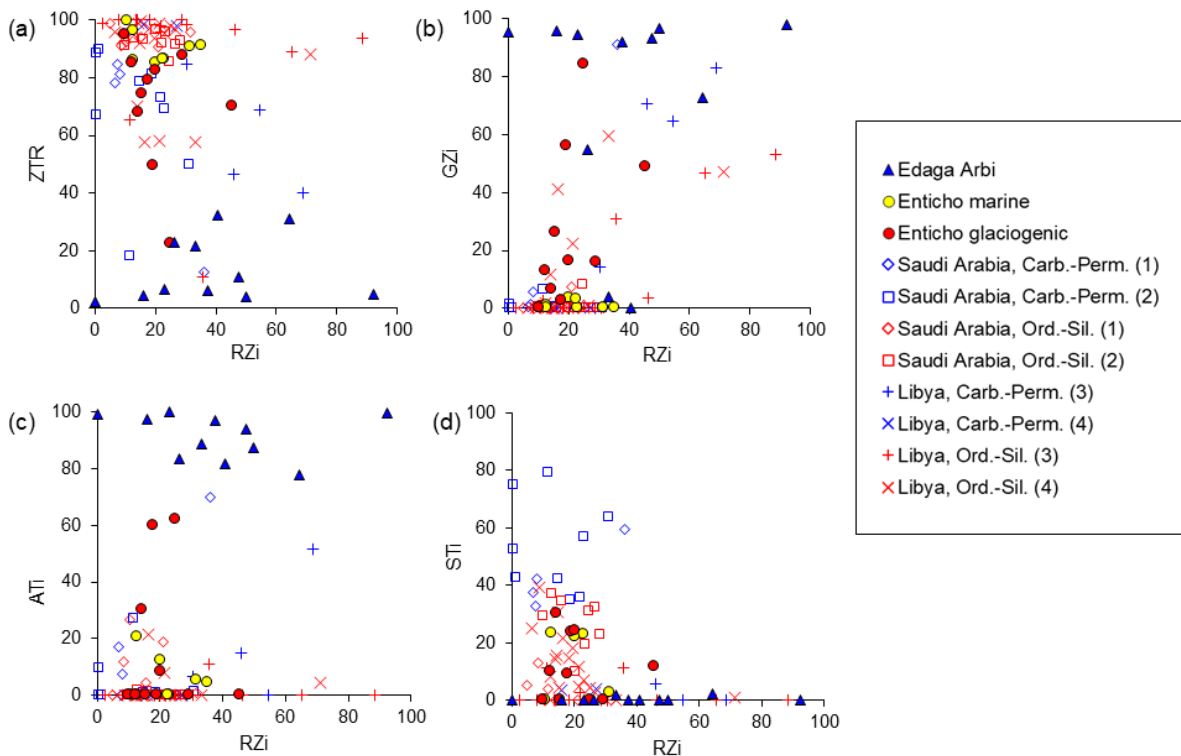
Figure 4-9: Cross-plots of heavy mineral indices for the studied formations (Table 2) and for stratigraphically corresponding formations in Saudi Arabia and Libya. (1) Bassis et al. (2016a), (2) Knox et al. (2007), (3) Morton et al. (2011), (4) Morton et al. (2012).

Edaga Arbi Glacials (Carboniferous–Permian)

In the Edaga Arbi Glacials, apatite and garnet, and in two samples epidote, are present with very high proportions (Figure 4-4). This means that 1) the formation cannot be (solely) the product of recycling of the Enticho Sandstone and 2) very little chemical alteration of the sediment must have taken place. Besides the generally low influence of chemical weathering in glacial environments, it may indicate short transport of the material, with little time for temporal storage and weathering. Furthermore, the potential of post-depositional intrastratal dissolution was lower in the Edaga Arbi Glacials, because the sandstone is poorly sorted with significant proportions of clay. The clay may have filled the pores avoiding the penetration of corrosive fluids (see also petrographic description in Lewin et al., 2018).

An increase in garnet content in the Upper Palaeozoic is also observed in Libya at the base of the Carboniferous Mrar Formation (Morton et al., 2011) and in Saudi Arabia in the Carboniferous–Permian glaciofluvial Juwayl Formation (Bassis et al., 2016a) and interpreted as a change in provenance. The comparison of heavy mineral indices of the Upper Palaeozoic sandstones in these regions to the Edaga Arbi Glacials (Figure 4-9), however, reveals substantial differences. In all plots presented in Figure 4-9, the Edaga Arbi Glacials differ significantly from all other formations. The heavy mineral assemblage is thus not regionally correlative and probably the result of local provenance and sedimentary conditions. Striking is particularly the high abundance of apatite and the absence of staurolite in the Edaga Arbi

Glacials as compared to stratigraphically equivalent formations in Saudi Arabia and Libya (Figure 4-9). Apatite is abundant in many magmatic and metamorphic rocks and widespread in the northern Ethiopian basement. This is supported by geochemical analyses of some samples from the local basement that revealed relative enrichment in phosphorus (Lewin et al., 2018; Figure 2-10 a). The high epidote content in two samples, Eda-6 and Eda-12 (Figure 4-4), may also be due to a very proximal provenance of the material and could be derived from the greenschist-facies metavolcanics of the Tsaliet Group (Beyth, 1972b; Miller et al., 2009).
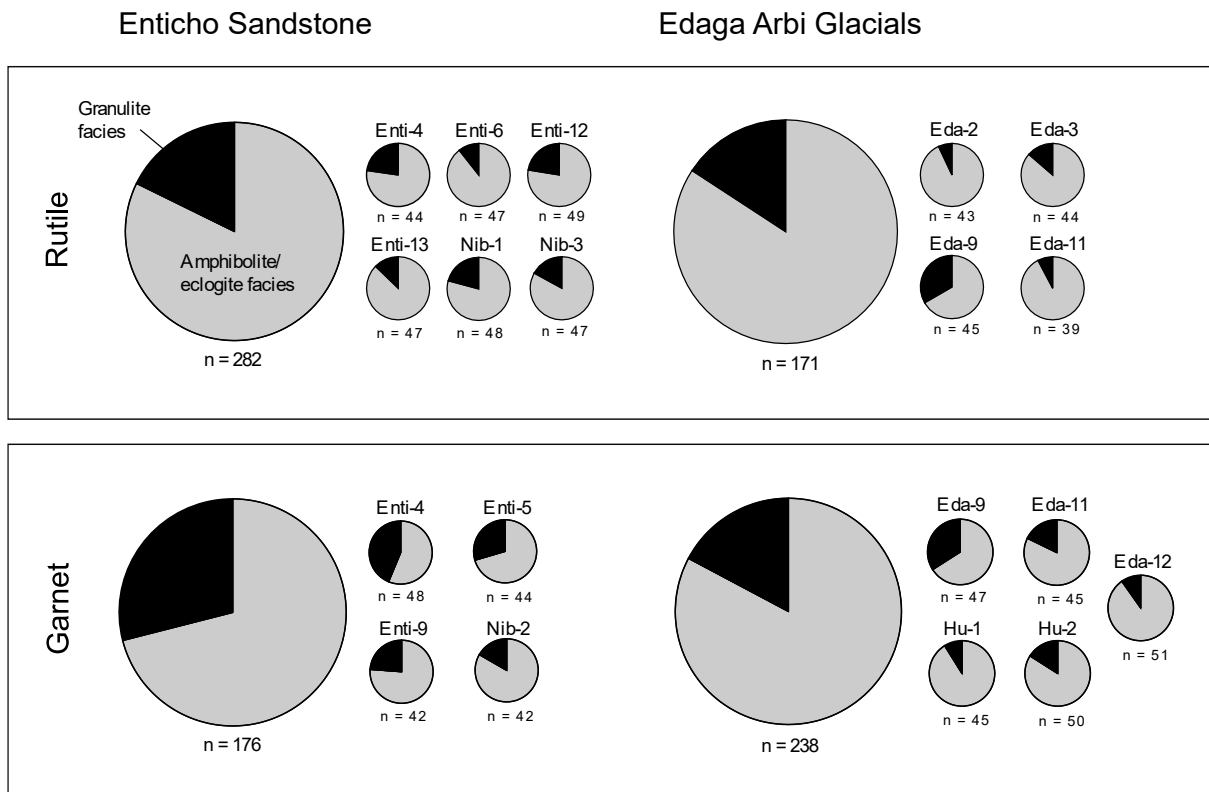
Figure 4-10: Comparison of the proportions of amphibolite/eclogite-facies and granulite-facies rutiles and garnets for the two studied formations, respectively, as inferred from Zr-in-rutile thermometry after Tomkins et al. (2007) and the garnet classification scheme after Tolosana-Delgado et al. (2018). Large pie charts show the respective total proportions for the whole formation, which are broken down to the single samples in the small pie charts.

Garnet and rutile chemistry indicate mainly amphibolite- but also granulite-facies metamorphic rocks as sources, though to a smaller proportion as in the Enticho Sandstone (Figure 4-7, Figure 4-8, Figure 4-10). The ratio of granulite- and amphibolite-facies garnet and rutile is similar so that both minerals could be derived from the same source rocks (Figure 4-10). The separation of rutile in both formations according to its chemical composition, as revealed in the PCA biplot (Figure 4-6), indicates that rutile in the Edaga Arbi Glacials is, at least partly, derived from a different source area than rutile in the Enticho Sandstone. This is also indicated by the different proportions of rutile assigned to metamafic and metafelsic host rocks by their Cr–Nb contents with a higher proportion of metamafic rutiles in the Edaga Arbi Glacials (Figure 4-7). The greenschist-facies metamorphism of the local basement in northern Ethiopia, as discussed above, questions a very local provenance for the rutile and garnet in the Edaga Arbi Glacials. The transport direction is inferred from south to north based on the orientation and geometry of palaeo-landforms, such as roche moutonnées (Bussert, 2010). The amphibolite- and granulite-facies garnets and rutiles may thus be derived from the high-grade metamorphic rocks in the Southern and Western Ethiopian Shields (Yibas et al., 2002; Woldemichael et al., 2010; Stern et al., 2012). Striking is the exceptionally high proportion of granulite-facies rutiles and garnets in sample Eda-

9 (Figure 4-10). Raman spectroscopy of this sample revealed that it contains also significant amounts of anatase and brookite, which may have led to erroneous results of Zr-in-rutile thermometry. However, for Raman spectroscopy, random grain mounts were analysed and we assume that during picking of rutile grains for microprobe analysis rutile is selected intuitively. An analysis of the picked rutile trace element composition after Triebold et al. (2010) resulted in rutile being the dominant TiO_2 polymorph in the mounts for single-grain analysis (99.4% of all grains, in sample Eda-9 98%). Furthermore, garnet chemistry shows a similar proportion of granulite-facies grains in sample Eda-9, which is much higher than in the other samples (Figure 4-8, Figure 4-10). This leads to the assumption of geographic (and maybe also stratigraphic) differences in provenance within the Edaga Arbi Glacials. Such differences are also indicated by the generally less uniform and systematic heavy mineral assemblage in the Edaga Arbi Glacials compared to that of the Enticho Sandstone (Figure 4-4) and by the variations in RZi (Figure 4-9).

A rather proximal provenance for the Edaga Arbi Glacials is in accordance with earlier findings from petrographic and geochemical analyses and detrital zircon geochronology (Lewin et al., 2018; Lewin et al., 2020) and supports the assumption of a complex pattern of ice sheets during the Late Palaeozoic Ice Age (e.g. Eyles, 1993; Fielding et al., 2008). In north-east Africa, complex local geomorphology evolved during 'Hercynian' tectonism (Al-Husseini, 1992; Sharland et al., 2001), leading to mountain glaciers during the Late Palaeozoic Ice Age (Konert et al., 2001; Bussert and Schrank, 2007; Le Heron et al., 2009). Alternatively, thermal up-doming prior to the formation of the Zagros rift zone, which later formed the Neo-Tethys ocean, could have caused basement uplift (Sharland et al., 2001). The glaciers then could effectively erode material from the uplifted areas and transport it to nearby depocentres, leading to the immature heavy mineral assemblage found in the Edaga Arbi Glacials.

The findings show that no major recycling of the Enticho Sandstone by the Edaga Arbi Glacials took place. This is probably because the deposition of the Enticho Sandstone was limited to northern Ethiopia (Kazmin, 1972; Tefera et al., 1996), while the inferred source area of the Edaga Arbi Glacials is to the south.

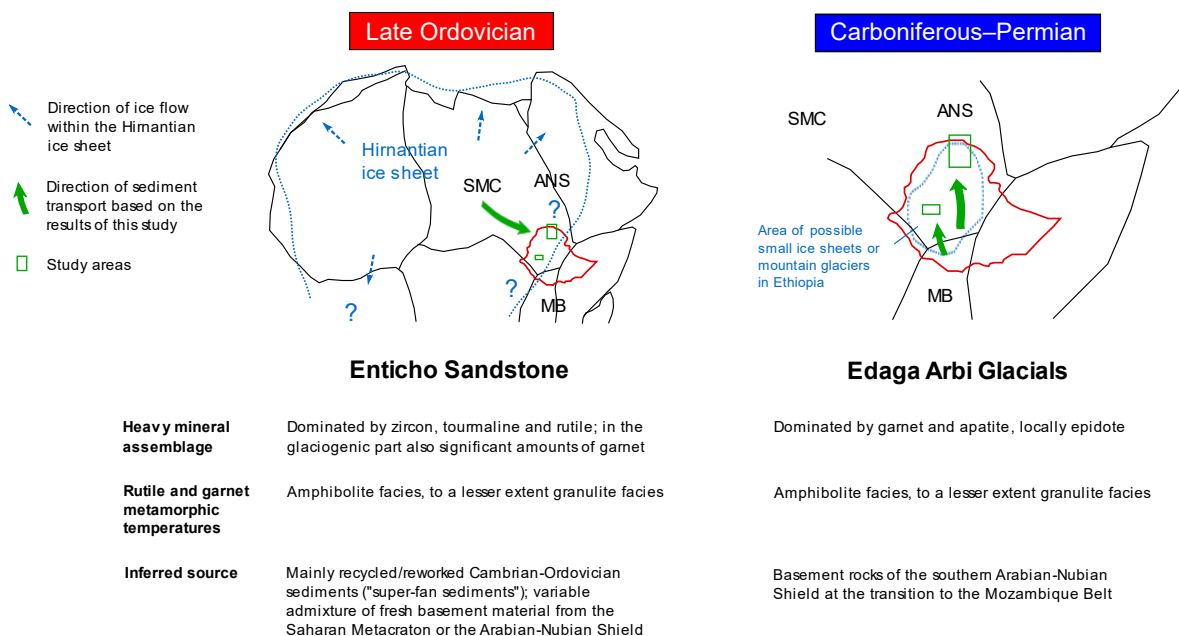|	Enticho Sandstone	Edaga Arbi Glacials
Heavy mineral assemblage	Dominated by zircon, tourmaline and rutile; in the glaciogenic part also significant amounts of garnet	Dominated by garnet and apatite, locally epidote
Rutile and garnet metamorphic temperatures	Amphibolite facies, to a lesser extent granulite facies	Amphibolite facies, to a lesser extent granulite facies
Inferred source	Mainly recycled/reworked Cambrian-Ordovician sediments ("super-fan sediments"); variable admixture of fresh basement material from the Saharan Metacraton or the Arabian-Nubian Shield	Basement rocks of the southern Arabian-Nubian Shield at the transition to the Mozambique Belt

Figure 4-11: Overview over the main findings of this study. Extent and ice flow directions for the Hirnantian ice sheet are after Ghienne et al. (2007), Le Heron and Craig (2008) and Torsvik and Cocks (2013). The contour of Ethiopia is given in red. SMC – Saharan Metacraton, ANS – Arabian–Nubian Shield, MB – Mozambique Belt.

4.6. Conclusions

A summary of the main findings of this study is given in Figure 4-11. The study of heavy minerals in the Ordovician–Silurian Enticho Sandstone and the Carboniferous–Permian Edaga Arbi Glacials revealed significant differences in the heavy mineral assemblages. The Enticho Sandstone is characterised by a highly mature heavy mineral assemblage, which is uncommon for glaciogenic sediments. We, therefore, conclude that it is composed of recycled material of older sediments. Additionally, various proportions of garnet, especially in the tillite, indicate an admixture of fresh basement material through glacial erosion. Heavy mineral assemblage and rutile and garnet chemical analyses point to magmatic and metamorphic source rocks with metamorphic temperatures of mainly amphibolite-, but also granulite-facies grade. Garnet and rutile are not necessarily derived from the same metamorphic host rocks. The recycled/reworked sediments incorporated in the Enticho Sandstone may have been part of the Gondwana super-fan system that transported large amounts of sediment from the inner part of the continent to the margins. The original provenance of the material remains unclear. The fresh basement material delivering the garnet could originate from the Sahara Metacraton.

The heavy mineral assemblage of the Edaga Arbi Glacials is dominated by less stable minerals, mainly garnet and apatite. Therefore, very little chemical weathering of the sediment must have taken place. We assume a more proximal provenance for the Edaga Arbi Glacials. The source area is characterised by magmatic and metamorphic rocks as well. Rutile and garnet chemistry indicate mainly amphibolite metamorphic temperatures, while also granulite-facies host rocks were inferred. Rutile in the Edaga Arbi Glacials and the Enticho Sandstone are probably from different host rocks, as inferred from differences in trace element compositions. The local basement in northern Ethiopia experienced only greenschist-facies metamorphism, but higher metamorphic grades were reached in the southern Arabian–Nubian Shield (Western and Southern Ethiopian Shields). This agrees with an assumed transport direction of the Edaga Arbi Glacials from south to north. Since the deposition of the Enticho Sandstone was probably limited to northern Ethiopia, no recycling by the Edaga Arbi Glacials took place.

These findings confirm previous assumptions of reworked mature sediment as the major constituent of the Enticho Sandstone and a proximal provenance for the Edaga Arbi Glacials. They also support previous models for the two glaciations with a large ice sheet covering northern Gondwana in the Late Ordovician and a complex pattern of local glaciers in the Carboniferous–Permian.

Acknowledgements

5. Synthesis

5.1. Comparison and validity of methods

In this thesis, methods on different scales were applied, from bulk sample to certain mineral species. An overview of the methods used is given in Section 1.5 and Figure 1-5. In the following, a short synopsis of the validities and informative values of the respective methods in answering the research questions shall be given.

The petrographic study of thin sections provided the basis for further steps in provenance analysis. It helped to get a general understanding of the nature of the samples, their texture and main constituents and mineralogical and textural maturity. It also helped to assess the relevance of matrix and authigenic phases. The bulk geochemical analyses of major and trace elements mainly confirmed the results of petrography and heavy mineral analysis. It turned out as an excellent tool to distinguish the two studied formations. With this, samples of uncertain stratigraphic classification can be assigned to one formation, as has been shown by the example of sample Eda-5, originally classified as belonging to the Edaga Arbi Glacials in the field. Using the geochemical data, it could clearly be assigned to the Enticho Sandstone. The typical diagrams for assessment of the tectonic setting in which the sediments were deposited (e.g. Verma and Armstrong-Altrin, 2013; 2016) did not provide much additional information to the mere assessment of the geochemical data via multivariate statistical methods (e.g. PCA) but are another tool for discrimination of the two formations. The measurement of rare earth elements (REE) could provide the first hint to differences in provenance of the two formations by their different patterns in the relation of heavy and light REE and in Eu anomaly. The conventional heavy mineral analysis was able to confirm the previous findings on maturity, assess the influence of chemical weathering and diagenetic modification and give further insights into provenance. In the heavy mineral assemblages, the strongest differences between the two formations were revealed. Especially with Raman spectroscopy, efficient determination of heavy mineral species was possible and the operator bias could be reduced. The conventional heavy mineral analysis further provided the basis for single grain analyses, e.g. if the necessary number of grains of a certain mineral species could be reached. Rutile and garnet chemical analysis yielded rather similar results for the two formations. Furthermore, the information obtained is not directly assignable to a certain source terrain but rather to a type of (metamorphic) rock, all of which are present in many places in possible source areas. However, slight differences in rutile chemistry between the two formations indicated that the rutiles were (partly) from different sources. Moreover, the indicated metamorphic grades higher than greenschist-facies could rule out a major provenance from the directly underlying basement for the Edaga Arbi Glacials. The tool which could most precisely indicate a certain source (area) in this study was detrital zircon chronology. Impressive differences between the two formations could be revealed and the sources could be constrained.

To sum up, the most helpful methods for addressing the research questions of this thesis were thin section petrography, REE analysis, conventional heavy mineral analysis and detrital zircon chronology. Major and trace element analysis turned out as a tool to distinguish the two formations clearly and assign unknown samples (chemostratigraphy). This evaluation is, of course, only valid for this certain study with its specific research questions. In other cases, another combination of provenance methods may be most useful. An overview of the used methods, the characteristic results for the respective formation and the kind of information that is revealed by the methods is given in Table 5-1.

Table 5-1: Overview of the methods used in this study, the characteristic results for the two formations from Ethiopia, the kind of information that could be revealed by the respective method and an evaluation of the helpfulness to answer the research questions of this thesis (the more + the more helpful the method was).

Category	Method	Characteristics in Enticho Sandstone	Characteristics in Edaga Arbi Glacials	Information revealed	Eva-luation
Bulk sample	Petrography	Quartzarenite (especially marine part), subarkose; well sorted and rounded in marine part, poorly in glaciogenic	Subarkose, lithic subarkose, arkose; variable roundness, moderate sorting	Mineralogical maturity, textural maturity; *Chemical alteration (weathering, diagenesis), transport mode*	++
	Major and trace elements	CIA of 92 (marine part) / 78 (glaciogenic part); relative enrichment in Zr, Th, Hf, U	CIA of 62; relative enrichment in Al, P, Sc, V	Mineralogical maturity; *Chemical alteration (weathering, diagenesis)*	+
	Rare earth elements	Strong enrichment in LREE, strong Eu anomaly	Less enrichment in LREE (flat pattern), little to no Eu anomaly	Mineralogical maturity, provenance; *Chemical alteration (weathering, diagenesis), type of source rocks*	++
Heavy minerals	Conventional heavy mineral analysis	ZTR of 79.7; variable amounts of garnet (especially in glaciogenic part)	ZTR of 13.4; high amounts of garnet and apatite, but with strongly varying relations	Mineralogical maturity, provenance; *Chemical alteration (weathering, diagenesis), type of source rocks*	++
	Rutile chemistry	Relatively enriched in Zr, V and Nb, temperature mainly amphibolite-facies, host rock lithology mainly felsic	Relatively enriched in Al and Fe, temperature mainly amphibolite-facies, host rock lithology mainly felsic, slightly higher mafic contribution than for Enticho Sandstone	Provenance; *Metamorphic temperature and lithology (felsic/mafic) of source rocks*	+
	Garnet chemistry	Most garnets metamorphic (mainly amphibolite-facies, some granulite-facies), some felsic igneous	Most garnets metamorphic (mainly amphibolite-facies, less granulite-facies than in Enticho Sandstone), less felsic igneous than in Enticho Sandstone	Provenance; *Type and metamorphic grade of source rocks*	+
	Zircon chronology	Characteristic Stenian–Tonian (1200–900 Ma) population, ratio of Tonian to Stenian–Tonian zircons is 1.2	Characteristic Tonian (900–700 Ma) population, ratio of Tonian to Stenian–Tonian zircons is 13.1	Provenance; *Age of source rocks*	+++

5.2. Multi-method provenance analysis

In a principal component analysis (PCA; explanation in Section 1.5.3) results obtained from different methods can be combined. A final PCA has been carried out, summarizing the most significant parameters characterising the two studied formations, as inferred from the three articles (Sections 2, 3 and 4). Biplots of this PCA are presented in Figure 5-1. They contain data from petrography, bulk geochemistry including REE and conventional heavy mineral analysis. Since data from mineral chemistry and zircon chronology have only been obtained from few samples, they were not integrated. All data integrated in the PCA are compositional making it necessary to transform them by centred log-ratio transformation before the operation (see explanation in Section 1.5.3). Furthermore, the variables have been standardized to unit variance to account for the different units (Lever et al., 2017).

Two biplots are presented for the integrated PCA (Figure 5-1). In Figure 5-1 a, all parameters are summarized that have been identified as characterising the two studied formations most. In Figure 5-1 b, the apatite and garnet contents, which have a large influence on the variability structure, are left out to enhance the visibility of the remaining variability. The two studied formations can be separated very well. The separation is mainly along the line ZTR–Ap (Figure 5-1 a). This is the direction of variability in mineralogical maturity: the highly mature Enticho Sandstone is characterised by high amounts of the ultra-stable heavy mineral assemblage zircon-tourmaline-rutile (ZTR). This is accompanied by a high

Th content, a trace element, which is often present in stable heavy minerals such as zircon or monazite. Furthermore, the Enticho Sandstone is characterised by an enrichment in quartz and Zr, underlining the high mineralogical maturity (Figure 5-1 a). On the other hand, the enrichment of the Edaga Arbi Glacials in apatite indicates lower mineralogical maturity and little influence of chemical weathering. Furthermore, the high Al proportions in Edaga Arbi Glacials point to higher amounts of feldspar and clays. Garnet is enriched in samples from both the Edaga Arbi Glacials and the glaciogenic part of the Enticho Sandstone (Figure 5-1 a). In the latter, diagenetic modification and garnet dissolution had a much lower effect than in the marine subunit due to lower permeability (see discussion in Section 4.5). Interestingly, the rays of garnet and apatite contents are orthogonal to each other implying that the variables are uncorrelated. However, it must be kept in mind that the biplot in Figure 5-1 a explains only 65.1% of the total variance of the displayed dataset.

In the biplot without the apatite and garnet contents (Figure 5-1 b) the two formations are again separated along a "mineralogical maturity axis" represented by ZTR and Th versus P. The latter indicates the high apatite content in the Edaga Arbi Glacials. The relative enrichment of Fe, Ni, Sc and HREE in the Edaga Arbi Glacials points to a higher influence of mafic source rocks. This is also indicated by rutile chemistry, though not very pronounced (see next paragraph). In the second biplot (Figure 5-1 b), the samples of the glaciogenic and marine parts of the Enticho Sandstone appear largely in clusters. Interestingly, most samples of the glaciogenic subunit cluster along the rays of quartz content and LREE. This is difficult to interpret, because the quartz content is generally higher in the marine subunit (Figure 2-4). Both subunits show similar enrichment in LREE, while the sample with the strongest enrichment is in the glaciogenic part (Figure 2-6). It may be that the relative enrichment in Zr and Th in the marine subunit is so high that these two variables mainly influence the clustering of the two subunits. Again, it must be noted that the biplots are only a projection onto a plane and explain only part of the variability of the dataset (in Figure 5-1 b it is only 59.6%), so the relations should not be overinterpreted. The same holds true for the Eu anomaly (Eu/Eu*), which is not very indicative in the biplots.
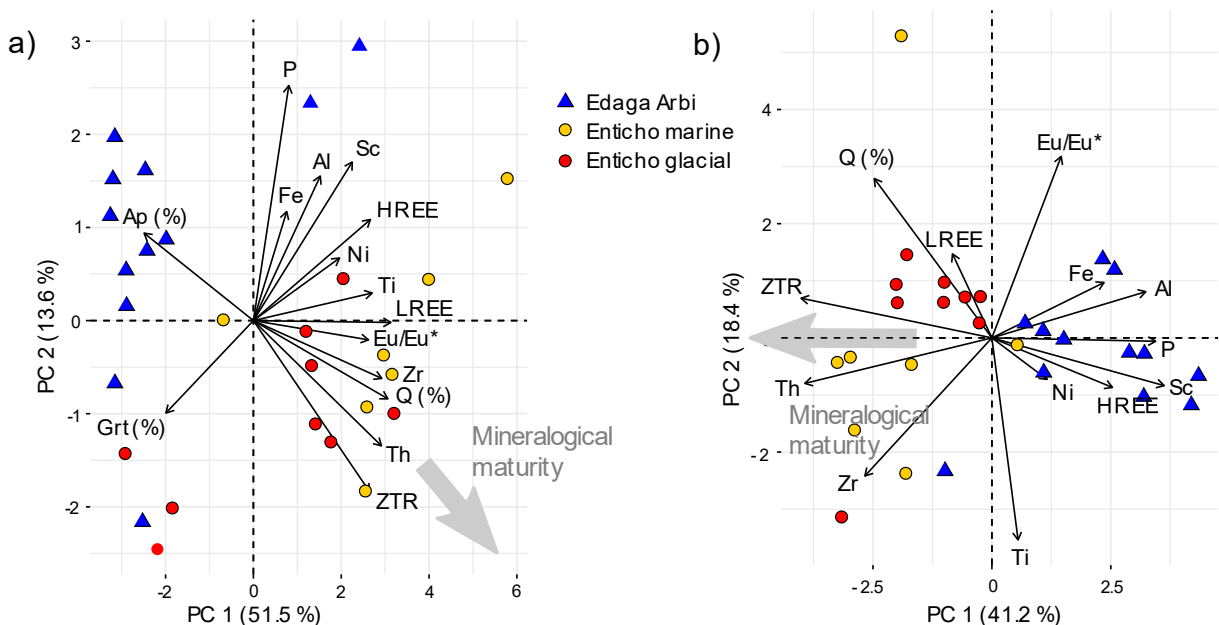
Figure 5-1: (a) Biplot of a the first and second principal component of a principal component analysis combining data from different methods obtained for all studied samples. (b) Biplot of the first and second principal component of a principal component analysis of the parameters in (a) leaving out the garnet (Grt) and apatite (Ap) contents of the respective samples to enhance visibility of the variabilities in the remaining variables. For both plots, all variables have been standardized to unit variance to account for the different scales.

Mineral chemical analyses and zircon chronology are not included into the final PCA because they have been conducted only on few samples. These are the indicators that are typically independent from weathering and sorting effects because only one mineral type is investigated. Rutile and garnet chemistry yield rather similar results for both formations. Rutile and garnet metamorphic temperatures are similar (mainly amphibolite-facies but also granulite-facies), with a slight tendency in the Enticho Sandstone towards higher temperatures. This supports the assumption that material transported via the Gondwana super-fan system from the centre of the EAO, where metamorphism was strong, is contained in the Enticho Sandstone. Rutile Cr-Nb analysis yields contribution of mainly metafelsic host rocks, but also metamafic host rocks for both formations. However, there is a slight tendency to more mafic input for the Edaga Arbi Glacials, which confirms the assumption of a higher influence of the ANS. Chemical differences between rutiles from the two formations are indicated by a PCA of the measured elements, showing that rutiles from the Enticho Sandstone are enriched in Zr, V and Nb, whereas rutiles from the Edaga Arbi Glacials generally contain more Al and Fe (Figure 4-6). Hence, rutiles of the two formations are probably from – at least partly – different sources. For garnet, no such clustering appears.

The differences in heavy mineral assemblages between the two studied formations become clearly visible in the heavy mineral charts in Section 4 (Figure 4-4). They are largest in ZTR – characteristic for the Enticho Sandstone – and garnet and apatite content – characteristic for the Edaga Arbi Glacials (while the glaciogenic part of the Enticho Sandstone does also contain significant amounts of garnet). These characteristics indicate mainly differences in chemical alteration. Apatite is highly sensitive and garnet moderately sensitive to surficial weathering (Velbel, 1984; Bateman and Catt, 2007; van Loon and Mange, 2007; Morton et al., 2012). However, indirectly they may indicate differences in provenance, because when transport distance is short, there are few occasions for weathering during transport and temporal storage on the way. It may even be that the material contained in the Enticho Sandstone originally contained as much garnet and apatite as is now found in the Edaga Arbi Glacials but was so strongly weathered that almost all these minerals were leached. Such strong alteration, however, needs time, supporting the hypothesis that the Enticho Sandstone contains recycled material that was strongly weathered on the North Gondwana peneplain before taken up and transported by the glaciers of the Hirnantian ice age. The garnet in the glaciogenic part of the Enticho Sandstone is probably derived from glacially eroded basement material (Saharan Metacraton and/or Nubian Shield) that was admixed in variable amounts to the recycled super-fan sediments (see also discussion in Section 4.5). It is unlikely that this garnet comes from the recycled super-fan sediments, since they were so strongly weathered that garnet should have been largely removed. Furthermore, pre-Hirnantian sandstones in Libya (Morton et al., 2011) and Israel (Weissbrod and Bogoch, 2007), assumed to belong to the super-fan sediments, contain only very small amounts of garnet, much less than the Enticho Sandstone. The strong difference in garnet content between the glaciogenic and the marine part of the Enticho Sandstone is probably highly affected by dissolution during burial diagenesis, to which garnet is susceptible (Morton and Hallsworth, 2007; Andò et al., 2012).

Zircon chronology shows unequivocal differences between the two studied formations. These are mainly in their characteristic populations of Tonian (900–700 Ma, typical for zircons in the Edaga Arbi Glacials) and Stenian–Tonian (1200–900 Ma, typical for zircons in the Enticho Sandstone). The relation of these two populations is a useful indicator to separate the two formations. The Stenian–Tonian population is characteristic for the Gondwana super-fan system in North–East Africa and the Arabian Peninsula (Meinhold et al., 2013; Stephan et al., 2019). The age spectra in the Enticho Sandstone are correlative with Cambrian–Ordovician sandstones in Libya, Israel, Jordan and Saudi Arabia (Kolodner et al., 2006; Meinhold et al., 2011; Morton et al., 2012; Altumi et al., 2013; Meinhold et al., in revision), indicating a common origin in the Gondwana super-fan system and a recycling of super-fan sediments by the Hirnantian glaciers. Zircon chronology of sample Enti-4 could confirm its belonging to the

Enticho Sandstone, as inferred from field relationships. This is an important finding, since it is the only location where tillite was found in this formation. It underlies glaciofluvial/glaciomarine deposits of the Enticho Sandstone. This evidences that glaciers of the Hirnantian glaciation reached the study area. The Tonian population is characteristic for the local basement of the southern Nubian Shield (see Section 3).

Geographic inter-sample trends within the respective formations are almost not present. The only geographic pattern is the variation in Th/Sc and Zr/Sc, which both become higher from south to north for both formations (Figure 2-9). The progressive enrichment of Th and Zr may be due to the enrichment in stable heavy minerals such as zircon along the transport path. However, a transport from south to north is only assumed for the Edaga Arbi Glacials (Bussert, 2010). For the Enticho Sandstone, palaeo-transport indicators, such as foreset dips of meltwater deposits point to varying directions, mainly towards the south-east or the north (Kumpulainen, 2007; Bussert and Dawit, 2009). A general provenance of the material from the (north-)west is likely, because the ice spreading centre of the Hirnantian ice sheet is assumed to have been in North-West Africa, which also corresponds to the direction of tunnel valleys (Ghienne et al., 2007; Le Heron and Craig, 2008). Locally, transport directions may have varied due to differences in ice dynamics or topography. Another explanation for the Th and Zr enrichment from south to north could be progressive marine reworking towards the north due to the transgression. The stratigraphic inter-sample variations within the respective formations are mainly between the glaciogenic basal part of the Enticho Sandstone and the marine upper part. They can be attributed to facies differences rather than to provenance changes with stratigraphy. Within the Edaga Arbi Glacials, no systematic stratigraphic pattern could be observed in any of the studied parameters.

A comparison of data obtained in this study with stratigraphically corresponding formations in other regions of northern Africa and the Arabian Peninsula complemented the provenance interpretations for the Enticho Sandstone and the Edaga Arbi Glacials. Bulk geochemical data of this study was compared to data from Saudi Arabia in a PCA biplot (Figure 2-10) yielding similarities in the Ordovician–Silurian samples and dissimilarities in the Carboniferous–Permian samples. Comparing heavy mineral indices (Figure 4-9), stratigraphically equivalent sandstones in Saudi Arabia, Libya and Ethiopia are rather similar in the Ordovician–Silurian, while stronger differences occur in the Carboniferous–Permian. These patterns point to a large-scale sedimentary dispersal system with strong regional homogenisation of sediment and continent-wide provenance patterns in the Early Palaeozoic (Gondwana super-fan system and large ice-sheet of the Hirnantian glaciation). In the Late Palaeozoic, however, sediment dispersal systems were more complex and provenance was more locally confined. Comparing detrital zircon age spectra of the Enticho Sandstone to those in Hirnantian sandstones form Libya and Algeria could prove the belonging of the Enticho Sandstone to the East African–Arabian zircon province sensu Stephan et al. (2019), as do the Libyan sandstones. This zircon province is assumed to represent a super-fan (Meinhold et al., 2013; Meinhold et al., in revision). Including pre-Hirnantian Palaeozoic sandstones of North-East Africa and the Middle East in the comparison revealed that no change in provenance occurred with the onset of the glaciation but the glaciogenic sandstones contain recycled super-fan material (see Figure 3-8 and Section 3.5). Recycling of pre-Hirnantian sediments by Hirnantian glaciers and a higher influence of fresh basement sources during the Late Palaeozoic Ice Age is also assumed for the Saudi Arabian succession (Hinderer et al., 2009; Keller et al., 2011; Bassis et al., 2016a). Meinhold et al. (in revision) compared detrital zircon age spectra in Saudi Arabian glaciogenic sandstones with those in Ethiopia and found high similarities in the Hirnantian spectra. A spatial correlation could be observed: the northernmost samples from Ethiopia resemble most those of the northern study area in Saudi Arabia, whereas those form the southern study area cluster with the Ethiopian samples further south. Hence, slight changes in provenance or spatial differences probably occurred during the Hirnantian glaciation (Meinhold et al., in revision). For the Carboniferous–Permian sandstones, a clearer clustering appears between Saudi Arabia and Ethiopia in a multidimensional

scaling map. However, the samples from both countries are still in close vicinity to each other leading to the assumption that the Saudi Arabian sandstones contain major amounts of material from the Nubian Shield, as do the Ethiopian (Meinhold et al., in revision).

Altogether, the integrated provenance analysis using several complementary methods reveals substantial differences between the two studied formations in several parameters. It shows that the lower Palaeozoic Enticho Sandstone is highly mature – unusual for glaciogenic sediments – and that this high maturity is probably due to recycling of sediments that have been transported in the Gondwana super-fan system and strongly weathered in the source area and on the North Gondwana peneplain before taken up by glaciers and ice streams of the Hirnantian ice sheet. The material was transported to the study area from the North-West. It is likely that glacial erosion admixed material from the basement of the Saharan Metacraton (and maybe also the Nubian Shield). For the Edaga Arbi Glacials, a much lower maturity is indicated by the used methods and a less distal provenance from Neoproterozoic basement rocks of the Nubian Shield in the southern hinterland is likely.

5.3. Final synoptic provenance model for the two studied formations as inferred from the results of this thesis

Taking into account all results obtained in this study and the discussion and conclusions of all three articles, a final provenance model for the two studied formations is inferred, which is presented in Figure 5-2. The regional configuration and depositional models for the Enticho Sandstone and the Edaga Arbi Glacials are drawn in Figure 5-2 b, c and e. The depositional models result from observations made in the field and previous studies of Robert Bussert and Enkurie L. Dawit (Bussert and Dawit, 2009; Bussert, 2010; Bussert, 2014). Figure 5-2 a and d represent literature information and theoretical considerations on regional evolution before and between deposition of the two studied formations.

Cambrian–Ordovician (Fig. 5-2 a)
After the Pan-African orogeny in the Neoproterozoic, which led to the final amalgamation of the supercontinent Gondwana, the hypothetical "Gondwana super-fan system" transported large amounts of detritus from the respective orogens, especially the East-African Orogen, to the continental margins (Squire et al., 2006; Meinhold et al., 2013). On the northern margin of the continent, a large peneplain existed, on which the sediments were deposited (e.g. Garfunkel, 2002). The study area was no major site of deposition by that time, probably because it was still elevated as part of the orogen. The climate was warm and humid and the atmosphere corrosive leading to strong chemical weathering in the source areas and the sediments stored on the peneplain (Avigad et al., 2005).

Late Ordovician (Hirnantian, Fig. 5-2 b)
During the Hirnantian glaciation, a giant ice sheet developed with its centre in North-West Africa (Ghienne et al., 2007; Le Heron and Craig, 2008). The ice reached the study area, as witnessed by tillite in northern Ethiopia (sample Enti-4). Ice streams or glaciers and associated meltwater transported super-fan material south–east to the study area. Since the material was strongly weathered before, unusually mature glaciogenic sediments result. Variable amounts of basement material (from the Saharan Metacraton and maybe also the Nubian Shield) were admixed to the recycled super-fan sediments, supplying minerals such as garnet (see Section 4). The tillite may represent a terminal moraine, marginal moraine or basal till, whereas the sandstones are probably from subaerial or subaqueous outwash fans (Bussert and Dawit, 2009). Most of the glaciogenic part of the Enticho Sandstone are meltwater deposits and a thick succession could be observed in the field. Probably, large amounts of sediment were deposited in a short time interval. Therefore, it is likely that these sediments were mainly released during the final meltdown of the ice sheet, when high amounts of meltwater were produced.

a) Cambrian-Ordovician

SMC
ANS
MB
~50-55° S

Super-fans transported detritus from East African Orogen; strong chemical weathering of the sediments in the source area and on the North Gondwana peneplain; study area no major site of deposition.

Enticho Sandstone

b) Late Ordovician (Himantian)

Himantian ice sheet
SMC
ANS
MB
~45° S

Ice streams, glaciers and meltwater transported super-fan sediments to the study area.

Depositional model:

Outwash fans
Subglacial till
Terminal moraine

c) Early Silurian

ANS
SMC
MB
~45° S

Post-glacial transgression reached the study area and seawater reworked glacial sediments.

d) Mid-Silurian to mid-Carboniferous

SMC
ANS
MB
~45-70° S

Period of non-deposition and erosion, probably due to a consecutive combination of isostatic rebound, eustatic sea-level fall and updoming prior to Neo-Tethys rifting.

Edaga Arbi Glacials

e) Carboniferous-Permian

SMC
ANS
Area of possible small ice sheets or mountain glaciers in Ethiopia
MB
~40-55° S

Complex topography evolved due to tectonic segmentation of North-East Africa and the Arabian Peninsula during rifting and opening of the Neo-Tethys. In uplands, mountain glaciers or small ice sheets formed and sediment was eroded and transported into nearby depressions.

Depositional model:

Dropstones
Hyperpycnal sediment flows
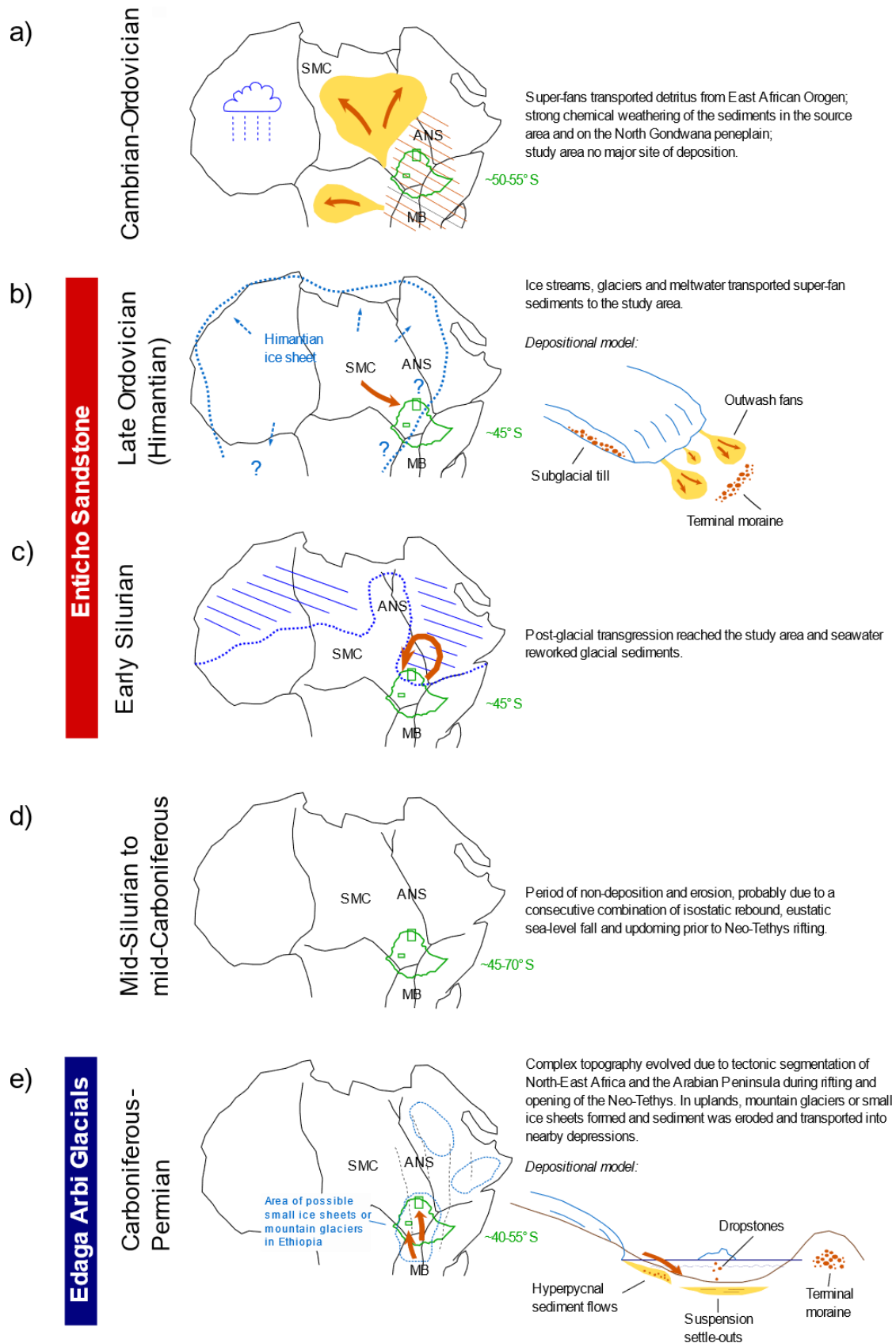Suspension settle-outs
Terminal moraine

Figure 5-2: Final model of the provenance and depositional settings of the two studied formations and considerations of regional setting during these times and the phases before and between. The time slices b, c and e are inferred based on the results of this study, literature and personal discussions on the depositional environments of the two studied formations (Bussert and Schrank, 2007; Bussert and Dawit, 2009; Bussert, 2010; 2014). Extent of the transgression in c is after Luening et al. (2000). Assumed ice sheets on the Arabian Peninsula in e are after Bussert and Schrank (2007), Fielding et al. (2008) and Isbell et al. (2012). Time slices a and d illustrate hypotheses based on literature and theoretical considerations (Squire et al.,

Early Silurian (Fig. 5-2 c)

The post-glacial transgression in the Early Silurian reached the study area and seawater reworked the upper part of the sediment sequence. Fines were washed out and the material became well sorted. The study area was probably in the tidal zone, as witnessed by bipolar cross-bed sets observed in the field.

Mid-Silurian to Mid-Carboniferous (Fig. 5-2 d)

No sediments of this time interval are present in the study area. Initially, the area may have become a site of non-deposition due to isostatic rebound after the meltdown of the Hirnantian ice sheet. Eustatic sea-level fall occurred in the latest Silurian–Early Devonian (Craig et al., 2008) and is ascribed to Palaeotethys rifting (Torsvik and Cocks, 2011). Crustal up-doming prior to Neo-Tethys rifting starting in the latest Devonian (Torsvik and Cocks, 2013) further led to uplift at the northern Gondwana margin. Part of the Late Ordovician to Early Silurian succession of the Enticho Sandstone must have been eroded, as indicated by channels and troughs to which sedimentation of Late Palaeozoic sediments in central and southern Ethiopia is limited. Furthermore, the Edaga Arbi Glacials contain mainly fresh basement material, hence, little sediment must have been available to be incorporated. Erosion is also indicated by a clastic pulse in the Palaeozoic succession of Saudi Arabia in the Devonian (Al-Ajmi et al., 2015).

Late Carboniferous to Early Permian (Fig. 5-2 e)

In the Late Palaeozoic, a complex local geomorphology evolved. Uplift of the Ethiopian basement may have occurred due to the Carboniferous "Hercynian event" (Al-Husseini, 1992; Sharland et al., 2004). In uplifted areas, mountain glaciers or small ice sheets formed. Material of the uplifted local or regional basement to the south (Arabian–Nubian Shield at the transition to the Mozambique Belt, e.g. Western and Southern Ethiopian Shields) was eroded and transported to nearby depressions. The cold climate and short transport left little room for significant weathering of the material. The tillite probably represents moraine material. The fines and dropstones are thought to have been deposited in proglacial lakes or fjords, in which episodic hyperpycnal sediment flows interrupted the settling-out and deposited sand bodies (Bussert, 2014). A similar setting with lake sediments containing dropstones is observed in the Saudi Arabian Juwayl Formation (Hinderer et al., 2009; Keller et al., 2011). The dropstones are assumed to be sourced from the southern hinterland, which has been uplifted (Hinderer et al., 2009; Keller et al., 2011). A vast glacial lake or a series of lakes probably existed in south-eastern Saudi Arabia and Oman and in Ethiopia (Keller et al., 2011). No recycling of Ordovician–Silurian sediments is evidenced in the Carboniferous–Permian succession. This may be either because the sedimentation of the Enticho Sandstone was limited to northern Ethiopia, whereas the source area of the Edaga Arbi Glacials was to the south. Another possibility is that all Ordovician–Silurian sediments in the south have been eroded in the time interval before the Edaga Arbi Glacials formed.

5.4. Conclusions

Provenance analysis of ancient rocks – in comparison to modern sediments – faces difficulties, e.g. due to diagenetic overprint and leaching of minerals. A direct connection to potential parent rocks and areas cannot easily be drawn and it is not even known if the parent rocks still exist. Despite these difficulties, using a combination of different methods, valuable new insights could be revealed on the provenance

of the two studied formations and the study showed once more that provenance analysis of ancient rocks is possible and helpful for the reconstruction of past sedimentary systems.

Thin section petrography provided the basis for further analyses and revealed first insights into mineralogical and textural composition and maturity. The maturity patterns could be confirmed by bulk geochemistry, which furthermore turned out as an excellent tool to distinguish the two formations and assign unknown samples (chemostratigraphy). Analysis of the REE provided first insights into provenance. Conventional heavy mineral analysis revealed extreme differences between the two formations, especially in the ultrastable versus unstable and metastable minerals, and provided further constraints on chemical weathering and diagenetic modification. Rutile and garnet chemistry did not turn out as very helpful for distinction of the two formations but provided some further constraints to provenance. The most helpful method for provenance interpretation was detrital zircon chronology.

For the Upper Ordovician–lower Silurian Enticho Sandstone, a relation to the Gondwana super-fan system can be drawn, particularly by means of detrital zircon age spectra, which contain the typical fingerprint for the super-fan sediments. The spectra can be correlated with those of Hirnantian sandstones in Libya and Cambrian–Ordovician sandstones in Libya, Israel, Jordan and Saudi Arabia. It is concluded that the material of the Enticho Sandstone is mainly the product of recycling of super-fan sediments stored and strongly weathered on the North Gondwana peneplain. The material was then transported to the study area by ice streams, glaciers and meltwater of the Hirnantian glaciation. By this, unusually mature glaciogenic deposits could be produced. The original source of the material remains unknown and may be in the centre of the East African Orogen, from which the super-fans are assumed to have come off. Variable admixture of material from the basement of the Saharan Metacraton and/or the Nubian Shield is indicated by the presence of garnet. The super-fan model as well as models of a large ice sheet covering North Africa in the Hirnantian, reaching south-east until Ethiopia and transporting material from its centre to the margin in the study area can be confirmed.

For the upper Carboniferous–lower Permian Edaga Arbi Glacials, a more proximal provenance is concluded based on major and trace element signatures and zircon age spectra resembling those of the local basement. Large amounts of garnet and apatite point to little time for weathering and alteration during temporal storage along the transport path. Geochemical and heavy mineral signatures are significantly different from those in stratigraphically equivalent formations in North-East Africa and the Arabian Peninsula. Hence, a more complex supply pattern existed, probably resulting from a rejuvenation of topography in the Late Palaeozoic in the course of rifting and opening of the Neo-Tethys ocean along the continental margin of North-East Gondwana. However, an exclusive provenance from the directly underlying basement is unlikely, since detrital rutile and garnet indicate higher metamorphic temperatures than reached in the local basement. This agrees with a previously assumed source area of the Edaga Arbi Glacials to the south, where the Arabian–Nubian Shield merges the Mozambique Belt (e.g. Western and Southern Ethiopian Shields) and higher metamorphic temperatures were reached. Variable admixture of the local basement, however, is likely as well. The data of this thesis confirm previous assumptions of a complex local pattern of ice sheets and glaciers during the Late Palaeozoic Ice Age.

Strikingly, no major recycling of the Enticho Sandstone by the Edaga Arbi Glacials has taken place. This was either because the deposition of the Enticho Sandstone was limited to northern Ethiopia and the source area for the Edaga Arbi Glacials was to the south or due to complete erosion of the Enticho Sandstone in the source area of the Edaga Arbi Glacials before the Late Palaeozoic Ice Age.

Another interesting aspect is the almost exclusive preservation of glaciation-related sediments in the Palaeozoic of the study area and the long hiatus between the Enticho Sandstone and the Edaga Arbi Glacials. An explanation could be the increased accommodation space and sediment supply during the glacial periods. The glaciers formed troughs and valleys that could take up sediments. Further accommodation space is provided during the transgression. For the Edaga Arbi Glacials, proglacial lakes in local depressions offered space for sediment deposition. The sediment supply during the glacial periods was high due to erosion and transport of massive amounts of sediment by ice streams, glaciers and meltwater. Before the deposition of the Enticho Sandstone, the study area was probably still elevated as part of the East African Orogen. The Silurian–Carboniferous hiatus can be explained by a decrease in accommodation space due to uplift of the area, leading to erosion.

5.5. Outlook

To improve statistical analysis of the two studied formations and make it possible to detect geographic or stratigraphic patterns within one formation, it would be helpful to complement the analyses performed so that there are more samples, on which all methods are applied. This could provide further insights into variations in provenance and glacier dynamics in the course of the respective glaciations.

To further constrain the provenance of the two studied formations, complementary single-grain analyses, e.g. Hf isotopes in detrital zircons could be used. Detrital rutile U–Pb chronology can provide insights into cooling and exhumation of the source area following Avigad et al. (2017). For the Enticho Sandstone, however, it must be kept in mind that it mainly contains recycled material and the sediment pathway is uncertain. This makes it difficult to use the data to correlate provenance patterns in the Cambrian–Ordovician succession of northern Gondwana as it is done by Avigad et al. (2017).

Zircon chronology of the basement in the study area and the Western and Southern Ethiopian Shields (assumed source region for the Edaga Arbi Glacials) can provide more specific provenance information for the Edaga Arbi Glacials and enable an assessment of the contributions of the directly underlying basement versus the southern hinterland. This is of importance to further constrain the ice sheet extent in the study area during the Late Palaeozoic Ice Age.

A remaining question, which was not in the focus of this thesis but may be interesting for future studies, is the question of Palaeozoic volcanism in the study area. Cambrian–Ordovician zircons dated in this thesis may origin from such volcanic rocks or from post-orogenic plutons in the Arabian–Nubian Shield. Lithic fragments in the Edaga Arbi Glacials, of which it is uncertain if they are volcanic or metavolcanic, underline this question. It can, therefore, be of interest to further study lithic fragments in the two formations to address the topic.

Finally, to continue reconstruction of the sediment dispersal system in northern Gondwana and its evolution, the study of provenance data can be extended to younger stratigraphic ages in Ethiopia. Samples of the Permian–Triassic Fincha Sandstone have been taken during the second field trip, which took place in the Blue Nile region in western Ethiopia and are studied in another PhD project at the Institute of Applied Geosciences in Darmstadt. Provenance studies of the Palaeozoic–Mesozoic sedimentary successions in Eritrea and Sudan would be of interest for regional correlation and broadening of the geographical scope.

References

Abdelsalam, M.G., Liégeois, J.-P., Stern, R.J., 2002. The Saharan Metacraton. Journal of African Earth Sciences 34, 119-136.

Aitchison, J., 1982. The Statistical Analysis of Compositional Data. Journal of the Royal Statistical Society. Series B (Methodological) 44, 139-177.

Aitchison, J., 1986. The Statistical Analysis of Compositional Data. Chapman & Hall, London, New York.

Aitchison, J., 2003. A Concise Guide to Compositional Data Analysis, University of Glasgow, Department of Statistics.

Akarish, A.I.M., El-Gohary, A.M., 2008. Petrography and geochemistry of lower Paleozoic sandstones, East Sinai, Egypt: Implications for provenance and tectonic setting. Journal of African Earth Sciences 52, 43-54.

Al-Ajmi, H.F., Keller, M., Hinderer, M., Filomena, C.M., 2015. Lithofacies, depositional environments and stratigraphic architecture of the Wajid Group outcrops in southern Saudi Arabia. GeoArabia 20, 49-94.

Al-Husseini, M.I., 1992. Upper Palaeozoic tectono-sedimentary evolution of the Arabian and adjoining plates. Journal of the Geological Society 149, 419-129.

Al-Husseini, M.I., 2004. Pre-Unayzah unconformity, Saudi Arabia. In: M.I. Al-Husseini (Ed.), Carboniferous, Permian and Early Triassic Arabian Stratigraphy. GeoArabia Special Publication 3, pp. 15-59.

Alene, M., Jenkin, G.R.T., Leng, M.J., Darbyshire, D.P.F., 2006. The Tambien Group, Ethiopia: An early Cryogenian (ca. 800–735Ma) Neoproterozoic sequence in the Arabian–Nubian Shield. Precambrian Research 147, 79-99.

Alene, M., Ruffini, R., Sacchi, R., 2000. Geochemistry and Geotectonic Setting of Neoproterozoic Rocks from Northern Ethiopia (Arabian-Nubian Shield). Gondwana Research 3, 333-347.

Altumi, M.M., Elicki, O., Linnemann, U., Hofmann, M., Sagawe, A., Gärtner, A., 2013. U–Pb LA-ICP-MS detrital zircon ages from the Cambrian of Al Qarqaf Arch, central-western Libya: Provenance of the West Gondwanan sand sea at the dawn of the early Palaeozoic. Journal of African Earth Sciences 79, 74-97.

Amireh, 1991. Mineral composition of the Cambrian-Cretaceous Nubian series of Jordan: Provenance, tectonic setting and climatological implications. Sedimentary Geology 71, 99-119.

Andò, S., Garzanti, E., Padoan, M., Limonta, M., 2012. Corrosion of heavy minerals during weathering and diagenesis: A catalog for optical analysis. Sedimentary Geology 280, 165-178.

Arkin, Y., Beyth, M., Dow, D.B., Levitte, D., Temesgen, H., Tsegaye, H., 1971. Geological Map of Mekele Area, sheet ND 37-11. Geological Survey of Ethiopia, Addis Ababa.

Avigad, D., Gerdes, A., Morag, N., Bechstädt, T., 2012. Coupled U–Pb–Hf of detrital zircons of Cambrian sandstones from Morocco and Sardinia: Implications for provenance and Precambrian crustal evolution of North Africa. Gondwana Research 21, 690-703.

Avigad, D., Kolodner, K., McWilliams, M., Persing, H., Weissbrod, T., 2003. Origin of northern Gondwana Cambrian sandstones revealed by detrital zircon SHRIMP dating. Geology 31, 227-230.

Avigad, D., Morag, N., Abbo, A., Gerdes, A., 2017. Detrital rutile U-Pb perspective on the origin of the great Cambro-Ordovician sandstone of North Gondwana and its linkage to orogeny. Gondwana Research 51, 17-29.

Avigad, D., Sandler, A., Kolodner, K., Stern, R., McWilliams, M., Miller, N., Beyth, M., 2005. Mass-production of Cambro–Ordovician quartz-rich sandstone as a consequence of chemical weathering of Pan-African terranes: Environmental implications. Earth and Planetary Science Letters 240, 818-826.

Avigad, D., Stern, R.J., Beyth, M., Miller, N., McWilliams, M.O., 2007. Detrital zircon U–Pb geochronology of Cryogenian diamictites and Lower Paleozoic sandstone in Ethiopia (Tigrai): Age constraints on Neoproterozoic glaciation and crustal evolution of the southern Arabian–Nubian Shield. Precambrian Research 154, 88-106.

Backhouse, J., 1991. Permian palynostratigraphy of the Collie Basin, Western Australia. Review of Palaeobotany and Palynology 67, 237-314.

Bassis, A., Hinderer, M., Meinhold, G., 2016a. New insights into the provenance of Saudi Arabian Palaeozoic sandstones from heavy mineral analysis and single-grain geochemistry. Sedimentary Geology 333, 100-114.

Bassis, A., Hinderer, M., Meinhold, G., 2016b. Petrography and geochemistry of Palaeozoic quartz-rich sandstones from Saudi Arabia: implications for provenance and chemostratigraphy. Arabian Journal of Geosciences 9, 400.

Bateman, R.M., Catt, J.A., 2007. Provenance and palaeoenvironmental interpretation of superficial deposits with particular reference to post-depositional modification of heavy mineral assemblages. In: M. Mange, D.T. Wright (Eds.), Heavy minerals in use. Developments in Sedimentology. Elsevier, Amsterdam, Netherlands, pp. 151-188.

Be'eri-Shlevin, Y., Katzir, Y., Whitehouse, M.J., Kleinhanns, I.C., 2009. Contribution of pre Pan-African crust to the formation of the Arabian Nubian Shield: new secondary ionization mass spectrometry U–Pb and O studies of zircon. Geology 37, 899-902.

Beerling, D.J., Berner, R.A., 2005. Feedbacks and the coevolution of plants and atmospheric CO2. Proceedings of the National Academy of Science of the United States of America 102, 1302-1305.

Ben Dor, Y., Harlavan, Y., Avigad, D., 2018. Provenance of the great Cambrian sandstone succession of northern Gondwana unravelled by strontium, neodymium and lead isotopes of feldspars and clays. Sedimentology 65, 2595-2620.

Berner, R.A., 1998. The carbon cycle and CO2 over Phanerozoict ime: the role of land plants. Philosophical transactions of the royal society of London B 353, 75-82.

Beyth, M., 1972a. Paleozoic-Mesozoic sedimentary basin of the Mekele Outlier, Northern Ethiopia. AAPG Bulletin 56, 2426-2439.

Beyth, M., 1972b. To the geology of central-western Tigre, PhD thesis, Rheinische Friedrich-Wilhelms-Universität Bonn, Bonn.

Beyth, M., Avigad, D., Wetzel, H.U., Matthews, A., Berhe, S.M., 2003. Crustal exhumation and indications for Snowball Earth in the East African Orogen: north Ethiopia and east Eritrea. Precambrian Research 123, 187-201.

Bhatia, M.R., Crook, K.A.W., 1986. Trace element characteristics of graywackes and tectonic setting discrimination of sedimentary basins. Contributions to Mineralogy and Petrology 92, 181-193.

Bingen, B., Jacobs, J., Viola, G., Henderson, I.H.C., Skår, Ø., Boyd, R., Thomas, R.J., Solli, A., Key, R.M., Daudi, E.X.F., 2009. Geochronology of the Precambrian crust in the Mozambique belt in NE Mozambique, and implications for Gondwana assembly. Precambrian Research 170, 231-255.

Brenchley, P.J., Carden, G.A., Hints, L., Kaljo, D., Marshall, J.D., Martma, T., Meidla, T., Nolvak, J., 2003. High-resolution stable isotope stratigraphy of Upper Ordovician sequences: Constraints on the timing of bioevents and environmental changes associated with mass extinction and glaciation. Geological Society of America Bulletin 115, 89-104.

Brenchley, P.J., Marshall, J.D., Carden, G.A., Robertson, D.B., Long, D.G., Meidla, T., Hints, L., Anderson, T.F., 1994. Bathymetric and isotopic evidence for a short-lived Late Ordovician glaciation in a greenhouse period. Geology 22, 295-298.

Brocke, R., Bussert, R., Dawit, E.L., 2015. First discovery of Early Palaeozoic post-glacial (post-Hirnantian/latest Ordovician-early Silurian) mudstones and cryptospores in northern Ethiopia. In: J. Wagner, K. Elger (Eds.), Annual Meeting of DGGV and DMG, 4-7 October 2015. 2015, Berlin. GFZ German Research Centre for Geosciences, Potsdam, p. 100.

Buatois, L.A., Mángano, M.G., 2011. Ichnology: Organism–Substrate Interactions in Space and Time. Cambridge University Press, Cambridge, UK.

Burke, K., MacGregor, D.S., Cameron, N.R., 2003. Africa's petroleum systems: four tectonic 'Aces' in the past 600 million years. In: T.J. Arthur, D.S. MacGregor, N.R. Cameron (Eds.), Petroleum Geology of Africa: New Themes and Developing Technologies. Geological Society of London Special Publication 207, pp. 21-60.

Bussert, R., 2010. Exhumed erosional landforms of the Late Palaeozoic glaciation in northern Ethiopia: Indicators of ice-flow direction, palaeolandscape and regional ice dynamics. Gondwana Research 18, 356-369.

Bussert, R., 2014. Depositional environments during the Late Palaeozoic ice age (LPIA) in northern Ethiopia, NE Africa. Journal of African Earth Sciences 99, 386-407.

Bussert, R., Dawit, E.L., 2009. Unexpected diversity: New results on the stratigraphy and sedimentology of Palaeozoic and Mesozoic siliciclastic sediments in Northern Ethiopia. Zentralblatt für Geologie und Paläontologie Teil I, 181-198.

Bussert, R., Schrank, E., 2007. Palynological evidence for a latest Carboniferous-Early Permian glaciation in Northern Ethiopia. Journal of African Earth Sciences 49, 201-210.

Chamley, H., Debrabant, P., Foulon, J., d'Argoud, G.G., Latouche, C., Maillet, N., Maillot, H., Sommer, F., 1979. Mineralogy and geochemistry of Cretaceous and Cenozoic Atlantic sediments off the Iberian Peninsula (Site 398, DSDP LEG 47B). In: F.H. Laughter (Ed.), Leg 47, Part 2 of the cruises of the drilling vessel Glomar Challenger, Vigo, Spain to Brest, France; April-May 1976. Initial Reports of the Deep Sea Drilling Project. Texas A&M University, Ocean Drilling Program, College Station, Texas, United States.

Collins, A.S., Pisarevsky, S.A., 2005. Amalgamating eastern Gondwana: The evolution of the Circum-Indian Orogens. Earth-Science Reviews 71, 229-270.

Craig, J.L., Rizzi, C., Said, F., Thusu, B., Lüning, S., Asbali, A.I., Keeley, M.L., Bell, J.F., Durham, M.J., Eales, M.H., Beswetherick, S., Hamblett, C., 2008. Structural Styles and Prospectivity in the Precambrian and Palaeozoic Hydrocarbon Systems of North Africa. In: M.J. Salem, K.M. Oun, A.S. Essed (Eds.), The Geology of East Libya. Gutenberg Press, Malta, pp. 51-122.

Crowell, J.C., 1983. Ice ages recorded on Gondwanan continents. Transactions of the Geological Society of South Africa 86, 237-262.

Dawit, E.L., 2010. Adigrat Sandstone in Northern and Central Ethiopia: Stratigraphy, Facies, Depositional Environments and Palynology, PhD thesis, Berlin Technical University, Berlin.

Dawit, E.L., 2014. Permian and Triassic microfloral assemblages from the Blue Nile Basin, central Ethiopia. Journal of African Earth Sciences 99, 408-426.

De Waele, B., Fitzsimons, I.C.W., Wingate, M.T.D., Tembo, F., Mapani, B., Belousova, A., 2009. The geochronological framework of the Irumide Belt: a prolonged crustal history along the margin of the Bangweulu Craton. American Journal of Science 309, 132-187.

De Wit, M.J., Bowring, S.A., Dudas, F., Kamga, G., 2005. The great Neoproterozoic central Saharan Arc and the amalgamation of the North African Shield. GAC-MAC-CSPG-CSSS Joint Meeting, May 15-18, 2005, Halifax, Nova Scotia, Canada, Abstracts 42-43.

Decker, J., Helmold, K.P., 1985. The effect of grain size on detrital modes: a test of the Gazzi-Dickinson point-counting method - discussion. Journal of Sedimentary Petrology 55, 618-620.

Dott, R.H., 1964. Wacke, graywacke and matrix - what approach to immature sandstone classification? Journal of Sedimentary Petrology 34, 625-632.

Dow, D.B., Beyth, M., Hailu, T., 1971. Palaeozoic glacial rocks recently discovered in northern Ethiopia. Geological Magazine 108, 53-60.

Egozcue, J., Barceló-Vidal, C., Martín-Fernández, J.A., Jarauta-Bragulat, E., Díaz-Barrero, J.L., Mateu-Figueras, G., 2011. Elements of Simplicial Linear Algebra and Geometry. In: V. Pawlowsky-Glahn, A. Buccianti (Eds.), Compositional Data Analysis: Theory and Applications. John Wiley & Sons, Ltd, Chichester, West Sussex, UK, pp. 139-157.

Egozcue, J.J., Pawlowsky-Glahn, V., Mateu-Figueras, G., Barceló-Vidal, C., 2003. Isometric Logratio Transformations for Compositional Data Analysis. Mathematical Geology 35, 279-300.

Eyles, N., 1993. Earth's glacial record and its tectonic setting. Earth Science Reviews 35, 1-248.

Fielding, C.R., Frank, T.D., Isbell, J.L., 2008. The late Paleozoic ice age—A review of current understanding and synthesis of global climate patterns. The Geological Society of America Special Paper 441, 343-354.

Folk, R.L., 1951. A comparison chart for visual percentage estimation. Journal of Sedimentary Petrology 21, 32-33.

Fritz, H., Abdelsalam, M., Ali, K.A., Bingen, B., Collins, A.S., Fowler, A.R., Ghebreab, W., Hauzenberger, C.A., Johnson, P.R., Kusky, T.M., Macey, P., Muhongo, S., Stern, R.J., Viola, G., 2013. Orogen styles in the East African Orogen: A review of the Neoproterozoic to Cambrian tectonic evolution. Journal of African Earth Sciences 86, 65-106.

Garfunkel, Z., 2002. Early Paleozoic sediments of NE Africa and Arabia: Products of continental-scale erosion, sediment transport and deposition. Israel Journal of Earth Sciences 51, 135-156.

Garland, C.R., 1980. Geology of the Adigrat Area. Ministry of Mines, Energy and Water Resources, Geological Survey of Ethiopia, Memoir 1, Addis Abeba, pp. 51.

Garland, C.R., Akililu, A., Assefa, A., Amenti, A., Beyth, M., Dow, D.B., Temesgen, H., Tsegaye, H., 1978. Geological Map of Adigrat, Sheet ND37-7, Geological Survey of Ethiopia, Addis Ababa.

Garzanti, E., 2017. The Maturity Myth In Sedimentology and Provenance Analysis. Journal of Sedimentary Research 87, 353-365.

Garzanti, E., Andò, S., Vezzoli, G., 2008. Settling equivalence of detrital minerals and grain-size dependence of sediment composition. Earth and Planetary Science Letters 273, 138-151.

Garzanti, E., Resentini, A., Andò, S., Vezzoli, G., Pereira, A., Vermeesch, P., Lancaster, N., 2015. Physical controls on sand composition and relative durability of detrital minerals during ultra-long distance littoral and aeolian transport (Namibia and southern Angola). Sedimentology 62, 971-996.

Ghienne, J.-F., 2003. Late Ordovician sedimentary environments, glacial cycles, and post-glacial transgression in the Taoudeni Basin, West Africa. Palaeogeography, Palaeoclimatology, Palaeoecology 189, 117-145.

Ghienne, J.-F., Benvenuti, A., El Houicha, M., Girard, F., Kali, E., Khoukhi, Y., Langbour, C., Magna, T., Míková, J., Moscariello, A., Schulmann, K., 2018. The impact of the end-Ordovician glaciation on sediment routing systems: A case study from the Meseta (northern Morocco). Gondwana Research 63, 169-178.

Ghienne, J.-F., Le Heron, D.P., Moreau, J., Denis, M., Deynoux, M., 2007. The Late Ordovician glacial sedimentary system of the North Gondwana platform. In: M.J. Hambrey, P. Christoffersen, N.F. Glasser, B. Hubbard (Eds.), Glacial Sedimentary Processes and Products. International Association of Sedimentologists Special Publication 39, pp. 295-319.

Harangi, S., Downes, H., Kósa, L., Szabó, C., Thirlwall, M.F., Mason, P.R.D., Mattey, D., 2001. Almandine Garnet in Calc-alkaline Volcanic Rocks of the Northern Pannonian Basin (Eastern–Central Europe): Geochemistry, Petrogenesis and Geodynamic Implications. Journal of Petrology 42, 1813–1843.

Hargrove, U.S., Stern, R.J., Kimura, J.I., Manton, W.I., Johnson, P.R., 2006. How juvenile is the Arabian–Nubian Shield? Evidence from Nd isotopes and pre-Neoproterozoic inherited zircon in the Bi'r Umq suture zone, Saudi Arabia. Earth and Planetary Science Letters 252, 308-326.

Hinderer, M., Keller, M., Al-Ajmi, H., Rausch, R., 2009. Tales of two glaciations in the Paleozoic of SW Saudi Arabia: Implications for ice shield dynamics and paleogeography of the SW Arabian platform and adjacent areas. ILP Task Force on Sedimentary Basins, International Workshop, December 6-11, 2009, Abu Dhabi, United Arab Emirates.

Hussain, M., Babalola, L.O., Hariri, M.M., 2004. Heavy minerals in the Wajid Sandstone from Abha-Khamis Mushayt area, southwestern Saudi Arabia: implications on provenance and regional tectonic setting. GeoArabia 9, 77-102.

Ingersoll, R.V., Bullard, T.F., Ford, R.L., Grimm, J.P., Pickle, J.D., Sares, S.W., 1984. The effect of grain size on detrital modes: a test of the Gazzi-Dickinson point-counting method. Journal of Sedimentary Petrology 54, 103-116.

Isbell, J.L., Henry, L.C., Gulbranson, E.L., Limarino, C.O., Fraiser, M.L., Koch, Z.J., Ciccioli, P.L., Dineen, A.A., 2012. Glacial paradoxes during the late Paleozoic ice age: Evaluating the equilibrium line altitude as a control on glaciation. Gondwana Research 22, 1-19.

Jackson, S.E., Pearson, N.J., Griffin, W.L., Belousova, E.A., 2004. The application of laser ablation-inductively coupled plasma-mass spectrometry to in situ U–Pb zircon geochronology. Chemical Geology 211, 47-69.

Johnson, P.R., 2014. An Expanding Arabian-Nubian Shield Geochronologic and Isotopic Dataset: Defining Limits and Confirming the Tectonic Setting of a Neoproterozoic Accretionary Orogen. The Open Geology Journal 8, 3-33.

Johnson, P.R., Andresen, A., Collins, A.S., Fowler, A.R., Fritz, H., Ghebreab, W., Kusky, T., Stern, R.J., 2011. Late Cryogenian–Ediacaran history of the Arabian–Nubian Shield: A review of depositional, plutonic, structural, and tectonic events in the closing stages of the northern East African Orogen. Journal of African Earth Sciences 61, 167-232.

Kazmin, V., 1972. Geological Map of Ethiopia. Geological Survey of Ethiopia, Addis Abeba.

Kazmin, V., Shifferaw, A., Balcha, T., 1978. The Ethiopian basement: Stratigraphy and Possible Manner of Evolution. Geol. Rundschau 67, 531-546.

Kebede, T., Kloetzli, U.S., Koeberl, C., 2001. U/Pb and Pb/Pb zircon ages from granitoid rocks of Wallagga area: constraints on magmatic and tectonic evolution of Precambrian rocks of western Ethiopia. Mineralogy and Petrology 71, 251-271.

Keller, M., Hinderer, M., Al-Ajmi, H., Rausch, R., 2011. Palaeozoic glacial depositional environments of SW Saudi Arabia: process and product, Geological Society London Special Publication 354, pp. 129-152.

Keller, M., Lehnert, O., 2010. Ordovician paleokarst and quartz sand: Evidence of volcanically triggered extreme climates? Palaeogeography, Palaeoclimatology, Palaeoecology 296, 297-309.

Kemp, E.M., Balme, B.E., Helby, R.J., Kyle, R.A., Playford, G., Price, P.L., 1977. Carboniferous and Permian palynostratigraphy in Australia and Antarctica, a review. BMR Journal of Australian Geology and Geophysics 2, 177-208.

Knox, R.W.O.B., Franks, S.G., Cocker, J.D., 2007. Stratigraphic evolution of heavy-mineral provenance signatures in the sandstones of the Wajid group (Cambrian to Permian), southwestern Saudi Arabia. GeoArabia 12, 65-96.

Kolodner, K., Avigad, D., McWilliams, M., Wooden, J.L., Weissbrod, T., Feinstein, S., 2006. Provenance of north Gondwana Cambrian–Ordovician sandstone: U–Pb SHRIMP dating of detrital zircons from Israel and Jordan. Geological Magazine 143, 367-391.

Konert, G., Afifi, A.M., Al-Hajri, S.A., Droste, H.J., 2001. Paleozoic stratigraphy and hydrocarbon habitat of the Arabian Plate. GeoArabia 6, 407-442.

Kooijman, E., Berndt, J., Mezger, K., 2012. U-Pb dating of zircon by laser ablation ICP-MS: recent improvements and new insights. European Journal of Mineralogy 24, 5-21.

Kretz, R., 1983. Symbols of rock-forming minerals. American Mineralogist 68, 277-279.

Krippner, A., Meinhold, G., Morton, A.C., von Eynatten, H., 2014. Evaluation of garnet discrimination diagrams using geochemical data of garnets derived from various host rocks. Sedimentary Geology 306, 36-52.

Kröner, A., Muhongo, S., Hegner, E., Wingate, M.T.D., 2003. Single-zircon geochronology and Nd isotopic systematics of Proterozoic high-grade rocks from the Mozambique belt of southern Tanzania (Masasi area): implications for Gondwana assembly. Journal of the Geological Society, London 160, 745-757.

Kumpulainen, R.A., 2007. The Ordovician glaciation in Eritrea and Ethiopia. In: M.J. Hambrey, P. Christoffersen, N.F. Glasser, B. Hubbard (Eds.), Glacial Sedimentary Processes and Products. International Association of Sedimentologists Special Publication 39, pp. 321-342.

Kumpulainen, R.A., Uchman, A., Woldehaimanot, B., Kreuser, T., Ghirmay, S., 2006. Trace fossil evidence from the Adigrat Sandstone for an Ordovician glaciation in Eritrea, NE Africa. Journal of African Earth Sciences 45, 408-420.

Laboun, A.A., 2010. Paleozoic tectono-stratigraphic framework of the Arabian Peninsula. Journal of King Saud University - Science 22, 41-50.

Le Heron, D.P., Craig, J., 2008. First-order reconstructions of a Late Ordovician Saharan ice sheet. Journal of the Geological Society 165, 19-29.

Le Heron, D.P., Craig, J., Etienne, J.L., 2009. Ancient glaciations and hydrocarbon accumulations in North Africa and the Middle East. Earth-Science Reviews 93, 47-76.

Le Heron, D.P., Sutcliffe, O.E., Bourgig, K., Craig, J., Visentin, C., Whittington, R.J., 2004. Sedimentary architecture of Upper Ordovician tunnel valleys, Gargaf Arch, Libya: Implications for the genesis of a hydrocarbon reservoir. GeoArabia 9, 137-160.

Le Heron, D.P., Sutcliffe, O.E., Whittington, R.J., Craig, J., 2005. The origins of glacially related soft-sediment deformation structures in Upper Ordovician glaciogenic rocks: implication for ice-sheet dynamics. Palaeogeography, Palaeoclimatology, Palaeoecology 218, 75-103.

Le Heron, D.P., Tofaif, S., Melvin, J., 2018. The Early Palaeozoic glacial deposits of Gondwana: overview, chronology and controversies. In: J. Menzies, J.J.M. van der Meer (Eds.), Past Glacial Environments. Elsevier, Amsterdam, Netherlands, pp. 47-73.

Lee, J.K.W., Williams, I.S., Ellis, D.J., 1997. Pb, U and Th diffusion in natural zircon. Nature 390, 159-162.

Lever, J., Krzywinski, M., Altman, N., 2017. Principal component analysis. Nature Methods 14, 641-642.

Levitte, D., 1970. The Geology of Mekele. Report on the Geology of the Central Part of Sheet ND 37-11, Addis Ababa, Ethiopia.

Lewin, A., Meinhold, G., Hinderer, M., Dawit, E.L., Bussert, R., 2018. Provenance of sandstones in Ethiopia during Late Ordovician and Carboniferous–Permian Gondwana glaciations: Petrography and geochemistry of the Enticho Sandstone and the Edaga Arbi Glacials. Sedimentary Geology 375, 188-202.

Lewin, A., Meinhold, G., Hinderer, M., Dawit, E.L., Bussert, R., Berndt, J., 2020. Provenance of Ordovician–Silurian and Carboniferous–Permian glaciogenic successions in Ethiopia revealed by detrital zircon U–Pb geochronology. Journal of the Geological Society 177, 141-152.

Linnemann, U., McNaughton, N.J., Romer, R.L., Gehmlich, M., Drost, K., Tonk, C., 2004. West African provenance for Saxo-Thuringia (Bohemian Massif): Did Armorica ever leave pre-Pangean Gondwana? U/Pb-SHRIMP zircon evidence and the Nd-isotopic record. International Journal of Earth Sciences 93, 683-705.

Linnemann, U., Ouzegane, K., Drareni, A., Hofmann, M., Becker, S., Gärtner, A., Sagawe, A., 2011. Sands of West Gondwana: An archive of secular magmatism and plate interactions — A case study from the Cambro-Ordovician section of the Tassili Ouan Ahaggar (Algerian Sahara) using U–Pb–LA-ICP-MS detrital zircon ages. Lithos 123, 188-203.

López-Gamundí, O.R., Buatois, L.A., 2010. Introduction: Late Paleozoic glacial events and postglacial transgressions in Gondwana. The Geological Society of America Special Paper 468, v-viii.

Luening, S., Craig, J., Loydell, D.K., Storch, P., Fitches, B., 2000. Lower Silurian 'hot shales' in North Africa and Arabia: regional distribution and depositional model. Earth-Science Reviews 49, 121-200.

Lünsdorf, K., Kalies, J., Ahlers, P., Dunkl, I., von Eynatten, H., 2019. Semi-Automated Heavy-Mineral Analysis by Raman Spectroscopy. Minerals 9, 385.

Mange, M., Maurer, H.F.W., 1992. Heavy minerals in colour. Chapman and Hall, London, UK.

Mange, M., Morton, A.C., 2007. Geochemistry of heavy minerals. In: M. Mange, D.T. Wright (Eds.), Heavy minerals in use. Developments in Sedimentology. Elsevier, Amsterdam, Netherlands, pp. 345-391.

Mange, M.A., Wright, D.T., 2007. Heavy minerals in use. Developments in Sedimentology. Elsevier, Amsterdam, Netherlands, 1283 pp.

Mänttäri, I., 2014. Mesoarchaean to Neoproterozoic U–Pb and Sm–Nd ages from Uganda. In: T. Lehto, E. Katto (Eds.), GTK Consortium Geological Surveys in Uganda 2008−2012. Geological Survey of Finland Special Paper 56, pp. 121-164.

Martín-Fernández, J.A., Barceló-Vidal, C., Pawlowsky-Glahn, V., 2003. Dealing with zeros and missing values in compositional data sets using nonparametric imputation. Mathematical Geology 35, 253-278.

McBride, E.F., 1963. A classification of common sandstones. Journal of Sedimentary Petrology 33, 664-669.

McLennan, S.M., 1989. Rare earth elements in sedimentary rocks: influence of provenance and sedimentary processes. In: B.R. Lipin, G.A. McKay (Eds.), Reviews in Mineralogy 21. The Mineralogical Society of America, Washington D.C., pp. 169-196.

McLennan, S.M., 2001. Relationships between the trace element composition of sedimentary rocks and upper continental crust. Geochemistry, Geophysics, Geosystems 2, Paper number 2000GC000109.

McLennan, S.M., Hemming, S., McDaniel, D.K., Hanson, G.N., 1993. Geochemical approaches to sedimentation, provenance, and tectonics. Geological Society of America Special Paper 284, 21-40.

Meert, J.G., 2003. A synopsis of events related to the assembly of eastern Gondwana. Tectonophysics 362, 1-40.

Meinhold, G., 2010. Rutile and its applications in earth sciences. Earth-Science Reviews 102, 1-28.

Meinhold, G., Bassis, A., Hinderer, M., Lewin, A., Berndt, J., in revision. Detrital zircon provenance of north Gondwana Palaeozoic sandstones from Saudi Arabia. Geological Magazine.

Meinhold, G., Morton, A.C., Avigad, D., 2013. New insights into peri-Gondwana paleogeography and the Gondwana super-fan system from detrital zircon U–Pb ages. Gondwana Research 23, 661-665.

Meinhold, G., Morton, A.C., Fanning, C.M., Frei, D., Howard, J.P., Phillips, R.J., Strogen, D., Whitham, A.G., 2011. Evidence from detrital zircons for recycling of Mesoproterozoic and Neoproterozoic crust recorded in Paleozoic and Mesozoic sandstones of southern Libya. Earth and Planetary Science Letters 312, 164-175.

Miller, N.R., Alene, M., Sacchi, R., Stern, R.J., Conti, A., Kröner, A., Zuppi, G., 2003. Significance of the Tambien Group (Tigrai, N. Ethiopia) for Snowball Earth events in the Arabian–Nubian Shield. Precambrian Research 121, 263-283.

Miller, N.R., Stern, R.J., Avigad, D., Beyth, M., Schilman, B., 2009. Cryogenian slate-carbonate sequences of the Tambien Group, Northern Ethiopia (I): Pre-"Sturtian" chemostratigraphy and regional correlations. Precambrian Research 170, 129-156.

Montañez, I.P., Poulsen, C.J., 2013. The Late Paleozoic Ice Age: An Evolving Paradigm. Annual Review of Earth and Planetary Sciences 41, 629-656.

Morag, N., Avigad, D., Gerdes, A., Belousova, E., Harlavan, Y., 2011. Detrital zircon Hf isotopic composition indicates long-distance transport of North Gondwana Cambrian-Ordovician sandstones. Geology 39, 955-958.

Morag, N., Avigad, D., Gerdes, A., Harlavan, Y., 2012. 1000–580 Ma crustal evolution in the northern Arabian–Nubian Shield revealed by U–Pb–Hf of detrital zircons from late Neoproterozoic sediments (Elat area, Israel). Precambrian Research 208, 197-212.

Morton, A., Hallsworth, C., 2007. Stability of detrital heavy minerals during burial diagenesis. In: M. Mange, D.T. Wright (Eds.), Heavy minerals in use. Developments in Sedimentology. Elsevier, Amsterdam, Netherlands, pp. 215-245.

Morton, A., Whitham, A., Howard, J., Fanning, M., Abutarruma, Y., El Dieb, M., Elkatarry, F., Hamhoom, A., Lüning, S., Phillips, R., Thusu, B., 2012. Using heavy minerals to test the stratigraphic framework of the Al Kufrah Basin. In: M. Salem, A. Abadi (Eds.). Fourth Symposium on the Sedimentary Basins of Libya. The Geology of Southern Libya. Earth Science Society of Libya, Tripoli, pp. 33-76.

Morton, A.C., 1987. Influences of provenance and diagenesis on detrital garnet suites in the Palaeocene Forties Sandstone, central North Sea. Journal of Sedimentary Petrology 57, 1027-1032.

Morton, A.C., Hallsworth, C., 1994. Identifying the provenance-specific features of detrital heavy mineral assemblages in sandstones. Sedimentary Geology 90, 241-256.

Morton, A.C., Hallsworth, C.R., 1999. Processes controlling the composition of heavy mineral assemblages in sandstones. Sedimentary Geology 124, 3-29.

Morton, A.C., Meinhold, G., Howard, J.P., Phillips, R.J., Strogen, D., Abutarruma, Y., Elgadry, M., Thusu, B., Whitham, A.G., 2011. A heavy mineral study of sandstones from the eastern Murzuq Basin, Libya: Constraints on provenance and stratigraphic correlation. Journal of African Earth Sciences 61, 308-330.

Nesbitt, H.W., Young, G.M., 1982. Early proterozoic climates and plate motions inferred from major element chemistry of lutites. Nature 299, 715-717.

Okrusch, M., Matthes, S., 2005. Mineralogie. Eine Einführung in die spezielle Mineralogie, Petrologie und Lagerstättenkunde. Springer, Berlin, Heidelberg, Germany, New York, USA.

Pawlowsky-Glahn, V., Egozcue, J.J., 2006. Compositional data and their analysis: an introduction. In: A. Buccianti, G. Mateu-Figueras, V. Pawlowsky-Glahn (Eds.), Compositional Data Analysis in the Geosciences: From Theory to Practice. Geological Society, London, Special Publications 264, pp. 1-10.

Powell, C.M., Veevers, J.J., 1987. Namurian uplift in Australia and South America triggered the main Gondwana glaciation. Nature 326, 177-179.

Powers, M.C., 1953. A new roundness scale for sedimentary particles. Journal of Sedimentary Petrology 23, 117-119.

Prokoph, A., Shields, G.A., Veizer, J., 2008. Compilation and time-series analysis of a marine carbonate $\delta18O$, $\delta13C$, 87Sr/86Sr and $\delta34S$ database through Earth history. Earth-Science Reviews 87, 113-133.

Ramos, E., Navidad, M., Marzo, M., Bolatti, N., 2003. Middle-Ordovician K-bentonite beds in the Murzuq Basin (Central Libya). In: G.L. Albanesi, M.S. Beresi, S.H. Peralta (Eds.), Ordovician from the Andes. Serie Correlación Geológica 17. Instituto Superior de Correlación Geológica, Universidad Nacional de Tucumán, Argentina, pp. 203-207.

Roberts, N.M.W., Spencer, C.J., 2015. The zircon archive of continent formation through time. Geological Society, London, Special Publications 389, 197-225.

Rösel, D., Boger, S.D., Möller, A., Gaitzsch, B., Barth, M., Oalmann, J., Zack, T., 2014. Indo-Antarctic derived detritus on the northern margin of Gondwana: evidence for continental-scale sediment transport. Terra Nova 26, 64-71.

Rubey, W.W., 1933. Settling velocities of gravel, sand and silt particles. American Journal of Science 25, 325-338.

Sabaou, N., Ait-Salem, H., Zazoun, R.S., 2009. Chemostratigraphy, tectonic setting and provenance of the Cambro-Ordovician clastic deposits of the subsurface Algerian Sahara. Journal of African Earth Sciences 55, 158-174.

Sacchi, R., Alene, M., Barbieri, M., Conti, A., 2007. On the Palaeozoic Tillite of the Adigrat Group (Tigrai, Ethiopia). Periodico di Mineralogia 76, 241-251.

Saxena, G.N., Assefa, G., 1983. New evidence on the age of the glacial rocks of northern Ethiopia. Geological Magazine 120, 549-554.

Seilacher, A., 2007. Trace Fossil Analysis. Springer, Berlin, Germany.

Sharland, P.R., Archer, R., Casey, D.M., Davies, R.B., Hall, S.H., Heward, A.P., Horbury, A.D., Simmons, M.D., 2001. Arabian Plate Sequence Stratigraphy. GeoArabia Special Publication, 2. Gulf PetroLink, Bahrain.

Sharland, P.R., Casey, D.M., Davies, R.B., Simmons, M.D., Sutcliffe, O.E., 2004. Arabian Plate Sequence Stratigraphy - revisions to SP2. GeoArabia 9, 199-214.

Sláma, J., Košler, J., 2012. Effects of sampling and mineral separation on accuracy of detrital zircon studies. Geochemistry Geophysics Geosystems 13, 1-17.

Squire, R.J., Campbell, I.H., Allen, C.M., Wilson, C.J.L., 2006. Did the Transgondwanan Supermountain trigger the explosive radiation of animals on Earth? Earth and Planetary Science Letters 250, 116-133.

Stacey, J.S., Kramers, J.D., 1975. Approximation of terrestrial lead isotope evolution by a two-stage model. Earth and Planetary Science Letters 26, 207-221.

Stephan, T., Kroner, U.W.E., Romer, R.L., 2019. The pre-orogenic detrital zircon record of the Peri-Gondwanan crust. Geological Magazine 156, 281-307.

Stephenson, M.H., Osterloff, P.L., Filatoff, J., 2003. Palynological biozonation of the Permian of Oman and Saudi Arabia: progress and challenges. GeoArabia 8, 467-496.

Stern, R.J., 1994. Arc assembly and continental collision in the Neoproterozoic East African Orogen: Implications for the consolidation of Gondwanaland. Annual Review of Earth and Planetary Sciences 22, 319-351.

Stern, R.J., 2008. Neoproterozoic crustal growth: The solid Earth system during a critical episode of Earth history. Gondwana Research 14, 33-50.

Stern, R.J., Ali, K.A., Abdelsalam, M.G., Wilde, S.A., Zhou, Q., 2012. U–Pb zircon geochronology of the eastern part of the Southern Ethiopian Shield. Precambrian Research 206-207, 159-167.

Stow, D.A.V., 2005. Sedimentary Rocks in the Field - A Colour Guide. CRC Press, Taylor & Francis Group, Boca Raton, USA.

Stutenbecker, L., Berger, A., Schlunegger, F., 2017. The potential of detrital garnet as a provenance proxy in the Central Swiss Alps. Sedimentary Geology 351, 11-20.

Sutcliffe, O.E., Dowdeswell, J.A., Whittington, R.J., Theron, J.N., Craig, J., 2000. Calibrating the Late Ordovician glaciation and mass extinction by the eccentricity cycles of Earth's orbit. Geology 28, 967-970.

Tawfik, H.A., Ghandour, I.M., Maejima, W., Armstrong-Altrin, J.S., Abdel-Hameed, A.-M.T., 2017. Petrography and geochemistry of the siliciclastic Araba Formation (Cambrian), east Sinai, Egypt: implications for provenance, tectonic setting and source weathering. Geological Magazine 154, 1-23.

Taylor, S.R., McLennan, S.M., 1985. The Continental Crust: Its Composition and Evolution. Blackwell Scientific Publication, Oxford, United Kingdom.

Tefera, M., Chernet, T., Haro, W., 1996. Explanation of the geological map of Ethiopia. Ethiopian Ministry of Mines and Energy Bulletin 3, Addis Ababa.

Teklay, M., Kroener, A., Mezger, K., Oberhaensl, R., 1998. Geochemistry, Pb-Pb single zircon ages and Nd-Sr isotope composition of Precambrian rocks from southern and eastern Ethiopia: implications for crustal evolution in East Africa. Journal of African Earth Sciences 26, 207-227.

Tolosana-Delgado, R., 2012. Uses and misuses of compositional data in sedimentology. Sedimentary Geology 280, 60-79.

Tolosana-Delgado, R., von Eynatten, H., Krippner, A., Meinhold, G., 2018. A multivariate discrimination scheme of detrital garnet chemistry for use in sedimentary provenance analysis. Sedimentary Geology 375, 14-26.

Tomkins, H.S., Powell, R., Ellis, D.J., 2007. The pressure dependence of the zirconium-in-rutile thermometer. Journal of Metamorphic Geology 25, 703-713.

Torsvik, T.H., Cocks, L.R.M., 2011. The Palaeozoic palaeogeography of central Gondwana. Geological Society, London, Special Publications 357, 137-166.

Torsvik, T.H., Cocks, L.R.M., 2013. Gondwana from top to base in space and time. Gondwana Research 24, 999-1030.

Toteu, S.F., van Schmus, W.R., Penaye, J., Michard, A., 2001. New U–Pb and Sm–Nd data from north-central Cameroon and its bearing on the pre-Pan African history of central Africa. Precambrian Research 108, 45-73.

Triebold, S., Luvizotto, G.L., Tolosana-Delgado, R., Zack, T., von Eynatten, H., 2010. Discrimination of TiO2 polymorphs in sedimentary and metamorphic rocks. Contributions to Mineralogy and Petrology 161, 581-596.

Triebold, S., von Eynatten, H., Luvizotto, G.L., Zack, T., 2007. Deducing source rock lithology from detrital rutile geochemistry: An example from the Erzgebirge, Germany. Chemical Geology 244, 421-436.

Triebold, S., von Eynatten, H., Zack, T., 2012. A recipe for the use of rutile in sedimentary provenance analysis. Sedimentary Geology 282, 268-275.

Tsige, L., Hailu, F., 2007. Geological Map of the Bure Area, sheet NC 37-5. Geological Survey of Ethiopia, Addis Ababa.

van Loon, A.J., Mange, M., 2007. 'In situ' dissolution of heavy minerals through extreme weathering, and the application of the surviving assemblages and their dissolution characteristics to correlation of Dutch and German Silver Sands. In: M. Mange, D.T. Wright (Eds.), Heavy minerals in use. Developments in Sedimentology. Elsevier, Amsterdam, Netherlands, pp. 189-213.

Vaslet, D., 1990. Upper Ordovician glacial deposits in Saudi Arabia. IUGS Episodes 13, 147-161.

Veizer, J., Ala, D., Azmy, K., Bruckschen, P., Buhl, D., Bruhn, F., Carden, G.A.F., Diener, A., Ebneth, S., Godderis, Y., Jasper, T., Korte, C., Pawellek, F., Podlaha, O.G., Strauss, H., 1999. 87Sr/86Sr, δ13C and δ18O evolution of Phanerozoic seawater. Chemical Geology 161, 59-88.

Velbel, M.A., 1984. Natural weathering mechanisms of almandine garnet. Geology 12, 631-634.

Verma, S.P., Armstrong-Altrin, J.S., 2013. New multi-dimensional diagrams for tectonic discrimination of siliciclastic sediments and their application to Precambrian basins. Chemical Geology 355, 117-133.

Verma, S.P., Armstrong-Altrin, J.S., 2016. Geochemical discrimination of siliciclastic sediments from active and passive margin settings. Sedimentary Geology 332, 1-12.

Vermeesch, P., 2013. Multi-sample comparison of detrital age distributions. Chemical Geology 341, 140-146.

Vermeesch, P., Garzanti, E., 2015. Making geological sense of 'Big Data' in sedimentary provenance analysis. Chemical Geology 409, 20-27.

Vermeesch, P., Resentini, A., Garzanti, E., 2016. An R package for statistical provenance analysis. Sedimentary Geology 336, 14-25.

Villas, E., Vizcaïno, D., Álvaro, J.J., Destombes, J., Vennin, E., 2006. Biostratigraphic control of the latest-Ordovician glaciogenic unconformity in Alnif (Eastern Anti-Atlas, Morocco), based on brachiopods. Geobios 39, 727-737.

von Eynatten, H., Barceló-Vidal, C., Pawlowsky-Glahn, V., 2003. Composition and discrimination of sandstones: statistical evaluation of different analytical methods. Journal of Sedimentary Research 73, 47-57.

von Eynatten, H., Dunkl, I., 2012. Assessing the sediment factory: The role of single grain analysis. Earth-Science Reviews 115, 97-120.

Weissbrod, T., Bogoch, R., 2007. Distribution pattern and provenance implications of the heavy minerals in Neoproterozoic to Mesozoic siliciclastic successions in the Arabo-Nubian Shield and its

northern periphery: a review. In: M.A. Mange, D.T. Wright (Eds.), Heavy minerals in use. Developments in Sedimentology. Elsevier, Amsterdam, Netherlands, pp. 647-676.

Weissbrod, T., Nachmais, J., 1986. Stratigraphic significance of heavy minerals in the Late Precambrian-Mesozoic clastic sequence ("Nubian Sandstone") in the Near East. Sedimentary Geology 47, 263-291.

Weltje, G.J., von Eynatten, H., 2004. Quantitative provenance analysis of sediments: review and outlook. Sedimentary Geology 171, 1-11.

Whitney, D.L., Evans, B.W., 2010. Abbreviations for names of rock-forming minerals. American Mineralogist 95, 185-187.

Wiedenbeck, M., Allé, P., Corfu, F., Griffin, W.L., Meier, M., Oberli, F., von Quadt, A., Roddick, J.C., Spiegel, W., 1995. Three natural zircon standards for U-Th-Pb, Lu-Hf, trace element and REE analyses. Geostandards Newsletter 19, 1-23.

Windley, B.F., Whitehouse, M.J., Ba-Bttat, M.A.O., 1996. Early Precambrian gneiss terranes and Pan-African island arcs in Yemen: crustal accretion of the eastern Arabian Shield. Geology 24, 131-134.

Woldemichael, B.W., Kimura, J.-I., Dunkley, D.J., Tani, K., Ohira, H., 2010. SHRIMP U–Pb zircon geochronology and Sr–Nd isotopic systematic of the Neoproterozoic Ghimbi-Nedjo mafic to intermediate intrusions of Western Ethiopia: a record of passive margin magmatism at 855 Ma? International Journal of Earth Sciences 99, 1773-1790.

Yibas, B., Reimold, W.U., Armstrong, R., Koeberl, C., Anhaeusser, C.R., Phillips, D., 2002. The tectonostratigraphy, granitoid geochronology and geological evolution of the Precambrian of southern Ethiopia. Journal of African Earth Sciences 34, 57-84.

Zack, T., Moraes, R., Kronz, A., 2004. Temperature dependence of Zr in rutile: empirical calibration of a rutile thermometer. Contributions to Mineralogy and Petrology 148, 471-488.

Zuffa, G.G., 1985. Optical analyses of arenites: influence of methodology on compositional results. In: G.G. Zuffa (Ed.), Provenance of Arenites. Nato Science Series. Springer Netherlands.

Appendix

Appendix to Chapter 1

Table A 1: List of all taken samples, geographical information and lithological description of the hand sample prior to further analysis. Abbreviations: vf – very fine; f – fine; m – medium; c – coarse; vc – very coarse; sst – sandstone; mst – mudstone; qz – quartz; akf – alkali feldspar

#	Sample name	Location name	Location North (°)	Location East (°)	Elevation (m+NN)	Description	Remarks
1	Enti-1	Atsbi South	13.83197	039.71230	2723	Red-grey m to f sst; rounded; moderately to well sorted; many black components (rock fragments? Tourmaline?); laminated, lot of mica on bedding planes; red weathering colour	Tufflayer in marine Sst?
2	Enti-2	Atsbi South	13.83195	039.71207	2714	Yellowish-brown m sst; subrounded-rounded, well sorted; mainly qz, few rock fragments, some white material between grains (kaolinite); fine, horizontal lamination	Shallow marine
3	Enti-3	Atsbi South	13.83262	039.71320	2705	Light red-white m sst; rounded; moderately to well sorted; reddish clayey material in interstices; poorly cemented, crumbly	Glacial sst, ca. 2 m below contact to shallow marine
4	Enti-4	Atsbi South	13.83465	039.71262	2685	Red; matrix: f to coarse sst, poorly sorted, subrounded, mainly qz; clasts: f to c gravel, qz, sst, mst (qz often well rounded, mst and sst clasts less rounded)	Tillite
5	Enti-5	Atsbi North	13.88828	039.74783	2761	Yellow c to m sst; subrounded-rounded; poorly sorted; many rock fragments (also akf, rose-orange); a lot of clayey yellow cement in the interstices, crumbly	Glacial sst, ca. 5 m below the mudstone with the cryptospores
6	Enti-6	Atsbi North	13.88842	039.74827	2775	Red-brown m sst; very well sorted (except for few slightly coarser rock fragments); well rounded; mainly qz; poorly cemented, soft and crumbly	Marine sst above mudstone with cryptospores (ca. 1 m above transgression unconformity)
7	Enti-7	Atsbi North	13.88842	039.74259	2740	Yellow m sst; very well rounded and sorted; mainly qz, little fsp, some dark material (organic matter?); yellowish clay as cement, crumbly	Base of the glacial sst
8	Enti-8	Negash	13.83882	039.60846	2101	Yellow-brown m to c sst; very well rounded, well sorted (except for few slightly coarser rock fragments); mainly qz; poorly cemented, crumbly	Glacial part of Enticho Sandstone
9	Enti-9	Wollwello	14.22037	039.65014	2783	Orange-brown m to vc sst; poorly sorted, rounded; orange clay as cement, crumbly	Glacial sst, ca. 1 m above basement (metapelite)
10	Enti-10	Wollwello	14.21839	039.64994	2848	White-yellowish f sst; well rounded, well sorted; slight, fine horizontal lamination recognisable; not so much clay in interstices; poorly cemented, soft	Marine sst, intertidal; at top of outcrop, ca. 50 m above mudstone with cryptospores (which separates glacial and marine Enticho)
11	Enti-11	Zalam-bassa	14.49694	039.42136	2383	White m to c sst; subrounded, poorly sorted; mainly qz, kaolinite in interstices, poorly cemented, soft	Marine, top

Table A 1 continued.

#	Sample name	Location name	Location North (°)	Location East (°)	Elevation (m+NN)	Description	Remarks
12	Enti-12	Zalam-bassa	14.49627	039.42093	2325	White m sst; well rounded, well sorted, qz with kaolinite in interstices; fine lamination (partly slightly cross-bedded); very poorly cemented	Base of marine sst
13	Enti-13	Zalam-bassa	14.49275	039.41911	2189	Yellow c sst; well rounded, well sorted; mainly qz; poorly cemented with some yellowish clay	Base of the glacial sst, ca. 2m above contact to basement
14	Enti-14	Road Sebea - Adigrat	14.39174	039.44908	2319	Light grey/yellow m to c sst; poorly sorted, rounded; mainly qz, some kaolinitised akf in interstices, some yellow clay; alternating grey and yellow layers of app. 5 cm thickness, poorly cemented	Glacial sst.
15	Enti-15	Debre Damo	14.37533	039.29246	2195	Reddish-grey f sst; well rounded, well sorted; dark red spots (iron weathering); some reddish clay as cement; poorly cemented	Glacial sst., ca. 20m below boundary to marine
16	Enti-16	Debre Damo	14.37717	039.29315	2139	White m to c sst; mostly medium-grained rounded qz, many subrounded rock fragments; kaolinite in interstices, poorly cemented, soft	Glacial sst., ca. 60m below boundary to marine
17	Eda-1	Adigrat West	14.31171	039.40472	2408	Light brown m sst; poorly sorted, subrounded; sub-arkose? → 15-20% fsp; ca. 15% rock fragments; poorly cemented by clay, kaolinite in the interstices, crumbly	Tillite, most north-eastern Edaga Arbi, muddy to middle sandy matrix with many clasts
18	Eda-2	Enticho	14.28166	039.14725	2027	Yellowish-white f sst; well rounded, well sorted; clayey cemented (abrasion), but still relatively hard and sharp-edged; slight iron weathering? → red spots on surface; fine dark laminae (< 1mm) → organic matter?	Tillite, directly above the mudstone with Permo-Carboniferous pollen and spores
19	Eda-3	Enticho	14.27929	039.14836	2007	Light brown f sst; well rounded, well sorted; iron weathering? → red spots on the surface	Sandstone, 20m below E-Eda-2, probably also Edaga Arbi, but could also be relict Enticho
20	Eda-4	Edaga Robi	14.38906	039.18161	2026	Light brown to yellow f sst; well sorted, well rounded; clayey cement, soft	Sandy section in tillite at the base of Edaga Arbi
21	Eda-5	Adwa East	14.19102	038.93957	2155	White-beige f sst; well rounded, moderately sorted; some rock fragments (ca. 5%); kaolinite in interstices; probably cemented with silica because very hard and sharp-edged	Sandstone, ca. 3m above contact to mudstone, mudstone directly above the basement
22	Eda-6	Edaga Arbi West	14.05667	039.07095	2013	Light brown vf sst; very well rounded, very well sorted; little clay because hard and sharp-edged with little abrasion	Slidden sandy channel fill in mudstone with dropstones

Table A 1 continued.

#	Sample name	Location name	Location North (°)	Location East (°)	Elevation (m+NN)	Description	Remarks
23	Eda-7	Megab	13.93496	039.36520	2046	Light orange-brown vf sst; very well rounded, very well sorted; some dark components (rock fragments? Minerals?); partly clay-cemented but not crumbly; lens-shaped hollows (clay? Carbonate?)	Back-up sample! Like E-Eda-8, with worse grain size! sandy channel fill in tillites with muddy matrix
24	Eda-8	Megab South	13.90944	039.32301	1857	Reddish-brown vf sst; very well sorted, very well rounded; stiff and sharp-edged, carbonaceous	sandy channel fill in tillites with muddy matrix; at the base of the formation
25	Eda-9	Megab South	13.90915	039.32235	1860	Light-grey f sst; very well sorted and rounded; thin dark layers, same grain size as light areas (organic matter?); partly iron-bearing (red spots on surface and reddish coloured bedding planes	Large sst block, fallen from sst plateau ca. 70m further up (elevation is the one of the find spot)
26	Eda-10	Dugum	13.84957	039.49003	1967	Light-red m sst; subrounded, moderately to well sorted; partly clay-cemented, kaolinite in interstices (sub-arkose?), crumbly	Sandy channel fill in mudstone, rather at the base of the formation, but no basement contact; most eastern Edaga Arbi outcrop
27	Eda-11	Abyi Addi	13.61842	039.00042	1826	Intensively red f sst; well-rounded and sorted; rel. well cemented but clay bearing (not very sharp-edged), carbonaceous	Sandy channel fill in muddy Edaga Arbi glacials; rel. strongly weathered; ca. 5m above basement contact
28	Eda-12	Samre	13.17844	039.19745	1848	Light-brown to grey vf sst; very well sorted and rounded (probably); rel. sharp-edged → well cemented; little clay (little abrasion)	Sandy channel fill in muddy Edaga Arbi glacials, ca. 1,5m, quite fine-grained
29	Eda-13	Near Samre	13.18945	039.19981	1962	Light-grey (almost white) vf sst; very well rounded and sorted; clay-cemented; finely laminated	Unknown sst horizon between Edaga Arbi and Adigrat sst with bones
30	Eda-14	Gravel road Samre – Abyi Addi	13.50532	039.04365	1493	Red-white f to c sst; poorly sorted, subrounded; many rock fragments (often coarser than the qz), a lot of fsp (intact and kaolinitised); iron weathering; crumbly; may be carbonatic (some shiny white minerals in interstices, could be calcite (test with HCl!)	"Mount Robert" (here first palynomorphs found); sandy turbidites in muddy Edaga Arbi
31	Eda-15	Asphalt road Abyi Addi - Megab	13.85940	039.25177	1727	Diamictite → poorly sorted; matrix: orange-brown f sst; clasts: f to m gravel, subangular, qz, fst, f to m sst (white), mudstone (grey)	Sandy diamictite with many clasts (also reworked basement) → base of Edaga Arbi
						Sandstone samples provided by R. Bussert (TU Berlin), taken during a field trip 2014	
32	S1-14	Sinkata	13.96861	039.61167		Enticho Sandstone, glaciogenic part, orange-brown; a lot of reddish clay	Ca. 2 m above basement contact
33	S2-14	Sinkata	13.96861	039.61167		Enticho Sandstone, glaciogenic part, light brown	Ca. 7 m below unconformity to marine sandstone

#	Sample name	Location name	Location North (°)	Location East (°)	Elevation (m+NN)	Description	Remarks
34	S3-14	Sinkata	13.97056	039.61111		Enticho Sandstone, marine part, light grey, lot of clay	Ca. 1.5 m above unconformity
35	S4-14	Sinkata	13.97056	039.61111		Enticho Sandstone, marine part, yellowish-white	Ca. 20 m above unconformity
36	Nib1-14	Adigrat South	14.25194	039.48972		Enticho Sandstone, glaciogenic part, light brown	Ca. 10 m above basement contact
37	Nib2-14	Adigrat South	14.25194	039.48972		Enticho Sandstone, glaciogenic part, light orange, a lot of clay	Ca. 10 m below unconformity to marine sst
38	Nib3-14	Adigrat South	14.25222	039.49583		Enticho Sandstone, marine part, white	In the upper area of the formation
39	Nib4-14	Adigrat South	14.25222	039.49583		Enticho Sandstone, marine part, white, little clay	At the top of the formation
40	Nord1-14	Adigrat North	14.31333	039.46000		Enticho Sandstone, glaciogenic part, yellow, lot of clay	Base of the glacial sst
41	Nord2-14	Adigrat North	14.31333	039.46000		Enticho Sandstone, glaciogenic part, grey, lot of clay	Top of the glacial sst
42	Nord3-14	Adigrat North	14.31944	039.45889		Enticho Sandstone, marine part, yellowish-white, not a lot of material	Rel. at the base of the marine sst
43	Hu-1/2014	Blue Nile Region	10.31057	037.05068		Edaga Arbi Glacials	Ca. 10 km N of Fuliya
44	Hu-2/2014	Blue Nile Region	10.31057	037.05068		Edaga Arbi Glacials	Ca. 10 km N of Fuliya
						Samples from the basement and boulders in Edaga Arbi tillite	
45	Gr-1	Negash Highschool	13.89164	039.60517	2372	Granite, f to m crystalline (0.5-2 mm); isotropic structure, anhedral grains; 30% qz, 30% plag, 30% akf, 10% biotite; moderately weathered	Basement, post-orogenic (undeformed) granite (Late Neoproterozoic/Early Cambrian?) → corresponds to "Mareb granite" mentioned in Miller et al. (2009), age 610 Ma
46	Gr-2	Sebea	14.46629	039.48225	2064	Light yellowish granite, f to m crystalline (0.5-3 mm); ca. 30-40% qz, 60-70% fsp (already quite weathered, probably mainly plag), no mica	Basement, probably Neoproterozoic granite
47	Gr-3	Adigrat West	14.31171	039.40472	2408	m crystalline granite (2-5mm); mainly akf (45%) and qz (45%), 10% of black minerals (biotite, px?), some muscovite	Boulder, ca. 30cm, angled, coarse-crystalline, akf rich
48	Gr-4	Adigrat West	14.31171	039.40472	2408	F to m crystalline granite (0.5-2mm), anhedral, ca. 60% akf, 20% qz, 20% biotite (could also be some px or amph)	Large boulder, ca. 60cm, subrounded, fine-crystalline, biotite-rich

#	Sample name	Location name	Location North (°)	Location East (°)	Elevation (m+NN)	Description	Remarks
49	Gr-5	Adigrat West	14.31171	039.40472	2408	Boulder, ca. 60% qz, 1-3mm, anhedral; 20% akf, 1-3mm, subhedral; 10% plag, 1mm, anhedral, 10% biotite, subhedral, 1mm	Well-rounded boulder, ca. 15cm, middle crystalline
50	Gr-6	Megab	13.93496	039.36520	2046	f to c crystalline granite; 45% akf 1-15mm, subhedral, 35% qz, 1-3mm anhedral, 20% biotite, 0.5-2mm, anhedral	Boulder, very large akf crystals
51	Gr-7	Megab	13.93496	039.36520	2046	M crystallinie (1-3mm), 40% qz, 40% akf, 10% plag, 10% biotite; all crystals anhedral and isometric	Boulder, tpyical granite
52	Gr-8	Megab	13.93496	039.36520	2046	F crystalline granite (0.25-1mm); ca. 40% qz, 40% akf, 20% biotite; crystals anhedral and isometric	Boulder, fine-crystalline
53	Gr-9	Megab	13.93496	039.36520	2046	Granite? Diorite? Gabbro? Minerals not well recognisable because weathered → wait for TS! Large fsp crystals (plag? 2-3mm, anhedral), surrounded by greenish-dark material (qz+px+biotite?)	Boulder, dark, greenish
54	Gr-10	Megab	13.93496	039.36520	2046	Well-rounded qz diorite boulder, black; no fresh facette → wait for TS!	Boulder, qz-diorite
55	Neop-1	Atsbi South	13.83374	039.71132	2668	Fine, grey matrix, 30% rock fragments of 0.5-1mm size, subrounded; ca. 5% black minerals (→ TS); sharp edges	Basement, metagreywacke
56	Neop-2	Negash	13.83561	039.61442	2081	Very fine-grained dark grey matrix, foliated, foliation bent around clasts; clasts: 0.5-7mm, subrounded to subangular, basalt (? Or black limestone?), mono and poly-qz, fsp, sandstone	Basement, Metatillite → corresponds to " Negash Diamictite" in Avigad et al. 2007
57	Neop-3	Near Negash	13.94186	039.59876	2409	Very fine-crystalline (tight), dark grey-green; 5-10% actinolite (small black needles, ca. 0.5-1mm long with preferred orientation) → greenschist-facies; very small plag-crystals (<0.5mm); greenish veins	Metabasite, rel. highly metamorphic, actinolith bearing
58	Neop-4	Zalam-bassa	14.49276	039.41899	2186	Clay slate, reddish-grey, very fine-grained, well sorted; rough foliation (1-2cm), sharp-edged	Basement, metapelite, at contact to glacial sst.
59	Neop-5	Road Debre Damo-Enticho	14.37729	039.27883	1875	ca. 50% plagioclase, 1-5mm, subhedral; dark grey matrix with black components (glass? Magnetite?), foliated	Basement, metagreywacke

Table A 1 continued.

#	Sample name	Location name	Location North (°)	Location East (°)	Elevation (m+NN)	Description	Remarks
60	Gn-1	Megab	13.93496	039.36520	2046	Paragneiss (→ a lot of mica, fine-medium grained (</= 1mm)), ca. 40% qz, 30% biotite, 20% plagioclase, 10% muscovite	Boulder, paragneiss
61	Bas-1	Megab	13.93496	039.36520	2046	Basalt with fine-crystalline, black-green matrix, large (up to 1cm) subhedral plagioclase, no preferred orientation	Boulder, basalt with up to 1cm sized fsp
62	Bas-2	Megab	13.93496	039.36520	2046	Basalt with very fine-crystalline black matrix and small (up to 3mm) sub- to anhedral plagioclase	Boulder basalt, black, tight with very small fsp
63	Neop-6	Road from Fincha to the north	09.77737	037.35017	1593	Basement, orthogneiss	Under the bridge (Fincha river); contact basement – Permo-Triassic sandstone
64	Neop-7	Road from Fincha to the north	09.77737	037.35017	1593	Basement, mafic dyke	Under the bridge (Fincha river); contact basement – Permo-Triassic sandstone
65	Neop-8	after Agemsa, north of Fuliya	10.19705	036.97737	1661	Basement, granite	Granite blocks on a field, but seems to crop out here
66	Neop-9	after Agemsa, north of Fuliya	10.24793	036.99155	1560	Basement, granite	Roadworks, fresh
67	Neop-10	North of Blue Nile Bridge	10.29327	037.02072	972	Basement, migmatite gneiss, dark	
68	Neop-11	Between Kuch and Blue Nile River	10.38512	037.00663	1605	Basement, gabbro	In dried river bed (small, steep)
69	Neop-12	Between Kuch and Blue Nile River	10.38563	037.00717	1619	Basement, felsic aplite	In dried river bed (small, steep)
70	Neop-13	Between Kuch and Blue Nile River	10.38550	037.01012	1673	Basement, (ortho?)gneiss	In dried river bed (small, steep)
71	Neop-14	Between Kuch and Blue Nile River	10.38827	037.01285	1638	Basement, metabasite	In dried river bed (small, steep), near contact basement – Permo-Triassic sandstone; strongly chloritised, only trace element analysis

Table A 2: Overview of the samples analysed in this thesis and which methods have been applied to which sample (X if the respective method has been applied to the sample). X* in the column thin section petrography indicates that the respective samples were only studied qualitatively without point counting. In the column HMA (Heavy mineral analysis) R indicates analysis by Raman spectroscopy while O indicates optical analysis with a polarising microscope.

#	Formation	Sample	Thin section petrography	Bulk geo-chemistry	HMA	Rutile chemistry	Garnet chemistry	Zircon chrono-logy
1	Enticho Sandstone	Enti-4	X	X	R	X	X	X
2	Enticho Sandstone	Enti-5	X	X	R		X	
3	Enticho Sandstone	Enti-6	X	X	R	X		X
4	Enticho Sandstone	Enti-7	X	X	O			
5	Enticho Sandstone	Enti-9	X	X	R		X	
6	Enticho Sandstone	Enti-10	X	X	O			
7	Enticho Sandstone	Enti-12	X	X	R	X		X
8	Enticho Sandstone	Enti-13	X	X	R	X		X
9	Enticho Sandstone	S1	X	X	O			
10	Enticho Sandstone	S2	X	X	O			
11	Enticho Sandstone	S3	X	X	O			
12	Enticho Sandstone	S4	X	X	O			
13	Enticho Sandstone	Nib-1	X	X		X		X
14	Enticho Sandstone	Nib-2	X	X	R		X	
15	Enticho Sandstone	Nib-3	X	X		X		X
16	Enticho Sandstone	Nib-4	X	X	O			
17	Enticho Sandstone	Nord-1	X	X	O			
18	Enticho Sandstone	Nord-2	X	X	O			
19	Enticho Sandstone	Nord-3	X	X	O			
20	Edaga Arbi Glacials	Eda-1	X	X				
21	Edaga Arbi Glacials	Eda-2	X	X	R	X		
22	Edaga Arbi Glacials	Eda-3	X	X	R	X		
23	Enticho Sandstone*	Eda-4	X	X	O			
24	Edaga Arbi Glacials	Eda-5	X	X	R			
25	Edaga Arbi Glacials	Eda-6	X	X	O			
26	Edaga Arbi Glacials	Eda-8	X	X	O			
27	Edaga Arbi Glacials	Eda-9	X	X	R	X	X	X
28	Edaga Arbi Glacials	Eda-10	X	X	O			
29	Edaga Arbi Glacials	Eda-11	X	X	R	X	X	X
30	Edaga Arbi Glacials	Eda-12	X	X	R		X	X
31	Edaga Arbi Glacials	Hu-1	X	X	R		X	X
32	Edaga Arbi Glacials	Hu-2	X	X	R		X	X
33		Gr-3	X*	X				
34		Gr-4	X*	X				
35		Gr-5	X*	X				
36		Gr-6	X*	X				
37		Gr-7	X*	X				
38	Boulders in Edaga Arbi tillite	Gr-8	X*	X				
39		Gr-9	X*	X				
40		Gr-10	X*	X				
41		Bas-1	X*	X				
42		Bas-2	X*	X				
43		Gn-1	X*	X				
44	Basement	Gr-1	X*	X				
45	Basement	Gr-2	X*	X				
46	Basement	Neop-1	X*	X				
47	Basement	Neop-2	X*	X				
48	Basement	Neop-3	X*	X				
49	Basement	Neop-4	X*	X				
50	Basement	Neop-5	X*	X				

Appendix to Chapter 2

Table A 3: Results of petrographic point-counting analysis of thin sections. Values given in %. Qzm = monocrystalline quartz, Qzmu = monocrystalline quartz with undulose extinction, Qzp = polycrystalline quartz (subgrain formation), Qzmicr = microcrystalline quartz, Pl = plagioclase, Kfs = potassium feldspar, Lp = plutonic lithic fragment, Lv = volcanic lithic fragment (includes metavolcanic clasts, since oriented texture is rarely visible but metamorphic overprint is probable), Ls = sedimentary lithic fragments, Lms=metasedimentary lithic fragments, Lmi=metamorphic igneous lithic fragment, other=minor components such as accessories, unid.= unidentified, e.g., strongly altered. Mineral abbreviations of accessories after Kretz (1983) and Whitney and Evans (2010). Ap = apatite, Cal = calcite, Chl = chlorite, Grt = garnet, Ms = muscovite, Op = opaque, Px = pyroxene, Sil = sillimanite, St = staurolite, Tur = tourmaline, Zrn = zircon. Carbonate cement: 0 = not present, + = up to 5%, ++ = 20–25%. GS = grain size. Sorting: − − = very poor, − = poor, 0 = moderate, + = good, ++ = very good. Roundness: − − = angular, − = subangular, 0 = subrounded, + = rounded, ++=well rounded.

Sample	Formation	Qz$_m$ [%]	Qz$_{mu}$ [%]	Qz$_p$ [%]	Qz$_{micr}$ [%]	Pl [%]	Kfs [%]	Lp [%]	Lv [%]	Ls [%]	Lms [%]	Lmi [%]	Other [%]	Unid [%]	Cts
Enti-4	Enticho	69.3	5,7	9,3	1,0	5,0	5,7	2,3	0,0	1,0	0,0	0,0	0,7	0,0	300
Enti-5	Enticho	69.0	9,7	8,7	0,0	4,0	7,3	0,3	0,0	0,0	0,0	0,0	0,0	1,0	300
Enti-7	Enticho	63.7	14,3	5,7	0,7	5,3	10,0	0,0	0,0	0,0	0,0	0,0	0,0	0,3	300
Enti-9	Enticho	68.3	15,7	6,7	0,0	4,0	4,0	0,0	0,0	0,7	0,0	0,0	0,7	0,0	300
Enti-13	Enticho	62.3	14,7	18,3	0,7	0,3	1,3	0,7	0,0	1,0	0,0	0,0	0,3	0,3	300
S1	Enticho	48.3	31,0	12,3	0,0	1,3	5,3	1,7	0,0	0,0	0,0	0,0	0,0	0,0	300
S2	Enticho	68.7	15,3	6,3	0,0	3,3	4,3	0,0	0,0	0,0	0,0	0,0	0,7	1,3	300
Nib-1	Enticho	80.3	8,7	4,0	0,7	0,3	1,3	0,7	2,0	0,0	0,0	0,0	0,7	1,3	300
Nib-2	Enticho	73.3	9,0	5,7	0,0	4,3	7,0	0,3	0,0	0,0	0,0	0,0	0,0	0,3	300
North-1	Enticho	70.0	21,3	1,3	0,0	2,0	5,0	0,3	0,0	0,0	0,0	0,0	0,0	0,0	300
North-2	Enticho	73.3	15,7	6,7	0,0	0,0	0,0	0,0	0,0	4,3	0,0	0,0	0,0	0,0	300
Enti-6	Enticho	78.0	17,7	3,3	0,3	0,0	0,7	0,0	0,0	0,0	0,0	0,0	0,0	0,0	300
Enti-10	Enticho	85.0	9,3	2,3	0,0	0,3	0,0	0,0	0,0	0,0	0,0	0,0	3,0	0,0	300
Enti-12	Enticho	87.3	8,3	3,7	0,0	0,0	0,3	0,0	0,0	0,0	0,0	0,0	0,3	0,0	300
S3	Enticho	77.3	12,0	9,3	0,7	0,0	0,0	0,0	0,0	0,0	0,0	0,0	0,7	0,0	300
S4	Enticho	79.0	14,7	6,3	0,0	0,0	0,0	0,0	0,0	0,0	0,0	0,0	0,0	0,0	300
Nib-3	Enticho	84.7	7,7	5,3	0,0	0,3	0,0	1,7	0,0	0,0	0,0	0,0	0,3	0,0	300
Nib-4	Enticho	70.3	26,3	2,7	0,0	0,0	0,0	0,3	0,0	0,0	0,0	0,0	0,3	0,0	300
North-3	Enticho	81.7	18,0	0,3	0,0	0,0	0,0	0,0	0,0	0,0	0,0	0,0	0,0	0,0	300
Eda-2	Edaga A.	63.0	14,3	0,3	3,7	3,3	3,0	0,0	2,7	1,7	0,0	0,0	6,7	1,3	300
Eda-3	Edaga A.	76.3	10,7	0,3	0,0	3,3	8,3	0,7	0,0	0,0	0,3	0,0	0,0	0,0	300
Eda-4	Edaga A.	68.7	20,0	0,0	0,0	4,0	5,7	0,3	0,7	0,0	0,3	0,0	0,0	0,3	300
Eda-5	Edaga A.	84.3	10,3	0,7	0,0	0,0	4,0	0,0	0,0	0,0	0,0	0,0	0,3	0,3	300
Eda-6	Edaga A.	60.7	3,7	1,0	0,3	5,3	21,0	0,0	0,3	3,7	0,0	0,0	3,0	1,0	300
Eda-8	Edaga A.	76.0	10,0	0,0	1,3	5,0	3,3	0,0	0,0	1,3	0,0	0,0	0,0	3,0	300
Eda-10	Edaga A.	52.3	4,7	3,0	0,7	6,3	22,3	6,0	1,7	1,0	1,3	0,3	0,3	0,0	300
Eda-11	Edaga A.	70.7	2,3	2,7	5,3	6,3	6,3	0,0	1,0	1,3	0,0	0,0	1,3	2,7	300
Hu-1	Edaga A.	39.3	5,7	0,7	0,0	12,0	36,7	4,3	0,0	1,0	0,0	0,0	0,3	0,0	300
Eda-9	Edaga A.	67.7	14,7	2,0	2,0	1,7	3,7	0,0	0,0	0,0	0,0	0,0	7,7	0,7	300
Eda-12	Edaga A.	61.3	5,3	1,3	1,3	7,3	16,3	0,0	1,7	0,0	0,0	0,0	1,0	4,3	300
Hu-2	Edaga A.	46.0	7,3	0,0	0,0	9,0	37,0	0,0	0,0	0,0	0,0	0,0	0,7	0,0	300
Eda-1	Edaga A.	58.3	7,3	3,0	1,3	6,7	8,0	7,0	2,7	1,7	0,3	0,0	1,3	2,3	300

Sample	Formation	Accessories	Carbonate cement	Matrix [%]	GS (mm)	Sorting	Roundness
Enti-4	Enticho	Tur, Zrn	0	40	0.05-4	--	-
Enti-5	Enticho		0	40	0.05-4	--	-- to ++
Enti-7	Enticho		0	10	0.1-1	0	+
Enti-9	Enticho	Mica, Px (?)	0	35	0.05-2; 0.1-1 (layers)	-	- to +
Enti-13	Enticho	Zrn	0	5	0.1-1	0	- to +
S1	Enticho		0	< 5	0.1-5	--	+ to ++
S2	Enticho		0	< 5	0.1-1	-	- to ++
Nib-1	Enticho	Tur	0	< 5	0.1-1	0	- to +
Nib-2	Enticho	Zrn	0	25	0.05-1.2	-	- to ++
North-1	Enticho		0	5	0.1-0.5	+	- to +
North-2	Enticho		0	50	0.05-7	-	- to ++
Enti-6	Enticho		0	5	0.1-1	+	- to ++
Enti-10	Enticho	Op+, Px?, Chl, Ap	0	< 5	0.1	++	-
Enti-12	Enticho	Grt	0	10	0.1-1.2	+	+
S3	Enticho	Chl, Op	0	< 5	0.1-1	-	- to +
S4	Enticho		0	55	0.1-1	0	+
Nib-3	Enticho	Zrn	0	< 5	0.1-1	0	+
Nib-4	Enticho		0	< 5	0.1-0.8	+	+
North-3	Enticho		0	< 5	0.1-0.6	+	+ to ++
Eda-2	Edaga Arbi	Op+, Grt, Zrn+, Cal, Ms	+	25	0.05-0.2	+	+
Eda-3	Edaga Arbi		+	< 5	0.05-0.3	0	0 to +
Eda-4	Edaga Arbi	Grt	0	15	0.05-0.3	0	0 to +
Eda-5	Edaga Arbi	Zrn+	0	35	0.05-0.5	0	-- to +
Eda-6	Edaga Arbi	Zrn+, Grt, Sil, St	++	< 5	0.1-0.3	+	-
Eda-8	Edaga Arbi		++	25	0.05-0.1	+	+
Eda-10	Edaga Arbi		+	20	0.1-0.7	0	- to 0
Eda-11	Edaga Arbi	Op, Chl	++	40	0.05-0.5	0	-
Hu-1	Edaga Arbi	Op	+	5	0.1-3	--	- to 0
Eda-9	Edaga Arbi	Chl+, Ms	0	35	0.05-0.1	++	+
Eda-12	Edaga Arbi	Zrn, Grt, Cal	0	40	0.05-0.2	0	- to 0
Hu-2	Edaga Arbi	Tur, Grt	0	10	0.1-0.3	+	0 to +
Eda-1	Edaga Arbi	Op, Grt	++	< 5	0.1-0.3	0	+

Table A 4: The analytical data of bulk geochemistry (XRF and ICP-MS) can be found as Excel file in the supplementary material to this thesis and in the supplementary material of the article *Provenance of sandstones in northern Ethiopia during Late Ordovician and Carboniferous–Permian Gondwana glaciations: petrography and geochemistry of the Enticho Sandstone and the Edaga Arbi Glacials* (https://doi.org/10.1016/j.sedgeo.2017.10.006).

Appendix to Chapter 3

Table A 5: Laser Ablation ICP-MS operation parameters.

Laboratory	**Institut für Mineralogie, Westfälische Wilhelms-Universität Münster**
Laser ablation system	**Photon Machines, Analyte G2, Excimer laser**
Ablation cell	HelEx 2-volume cell
Wavelength	193 nm
Pulse width	4 ns
Fluence	3–4 J/cm²
Repetition rate	10 Hz
Ablation time	37 s
Spot size	25µm
Sampling mode	Static
Carrier gas	He in the cell, Ar sampling and cooling gas
Carrier gas flow	0.9 L/min for mass-flow controller 1; 0.4 L/min for mass-flow controller 2
ICP-MS instrument	**ThermoFisher Element 2, single-collector ICP-MS**
Radio frequency power	1250 W
Sample and cooling gas flow	1 L/min; 16 L/min
Detection system	SEM
Masses measured	202, 204, 206, 207, 238
Settling time	1 ms/amu
Sample time	40 ms (202, 204, 207), 10 ms (206), 4 ms (238)
Sweep time	160 ms (202, 204, 207), 40 ms (206), 10 ms (238)
Integration time	0.56 ms
Number of runs	91
Background time	12 s

Table A 6: The analytical data of zircon U–Pb geochronology can be found as Excel file in the supplementary material to this thesis and in the supplementary material to the article *Provenance of Ordovician–Silurian and Carboniferous–Permian glaciogenic successions in Ethiopia revealed by detrital zircon U–Pb geochronology* (https://doi.org/10.1144/jgs2019-027).

Appendix to Chapter 4

Table A 7: Heavy mineral counts in %. Samples marked with an asterisk (*) have been counted using Raman spectroscopy. Zrn – zircon, Rtl – rutile, Tur – tourmaline, Grt – garnet, Ap – apatite, Ep – epidote group, St – staurolite, Mon – monazite, Tit – titanite, n – number of grains counted.

Sample	Zrn	Rtl	Tur	Grt	Ap	Ep	St	Mon	Tit	Others	Sum	n
Enti-4*	12.6	4.2	5.6	68.5	9.1	0.0	0.0	0.0	0.0	0.0	100.0	143
Enti-5*	34.4	8.2	6.8	44.4	0.0	0.2	2.2	3.7	0.0	0.0	100.0	511
Enti-6*	55.0	16.4	14.9	0.0	0.0	0.7	4.5	7.8	0.0	0.7	100.0	269
Enti-7	57.0	14.5	11.0	11.0	1.0	0.0	3.5	1.0	1.0	0.0	100.0	200
Enti-9*	28.7	24.1	17.2	27.6	0.0	0.0	2.3	0.0	0.0	0.0	100.0	87
Enti-10	50.0	23.0	17.5	0.0	1.0	0.0	0.5	7.5	0.5	0.0	100.0	200
Enti-12*	77.8	9.4	12.7	0.1	0.0	0.0	0.0	0.0	0.0	0.0	100.0	937
Enti-13*	78.3	8.8	7.8	0.2	0.0	0.2	0.0	4.7	0.0	0.0	100.0	591
S1	39.6	6.6	21.7	2.8	9.4	2.8	9.4	7.5	0.0	0.0	100.0	106
S2	58.0	12.6	8.4	1.7	12.6	0.0	0.8	5.9	0.0	0.0	100.0	119
S3	56.0	14.2	14.9	2.1	2.1	0.0	4.3	5.0	1.4	0.0	100.0	141
S4	52.0	7.5	26.5	0.5	0.0	0.0	8.0	5.0	0.5	0.0	100.0	200
Nib-2*	51.9	21.4	14.3	10.0	0.0	0.0	0.0	2.4	0.0	0.0	100.0	210
Nib-4	49.7	27.2	14.3	0.0	0.7	0.0	0.7	7.5	0.0	0.0	100.0	147
Nord-1	70.5	10.0	4.5	10.5	0.0	0.5	0.5	3.5	0.0	0.0	100.0	200
Nord-2	54.0	10.5	10.5	19.0	0.0	1.5	0.0	4.5	0.5	0.0	100.0	200
Nord-3	60.5	17.5	8.5	2.0	0.0	1.0	1.5	6.5	2.5	0.0	100.0	200
Eda-2*	7.9	4.0	9.9	0.3	77.1	0.7	0.2	0.0	0.0	0.0	100.0	607
Eda-3*	10.4	7.1	14.9	0.0	66.9	0.0	0.0	0.6	0.0	0.0	100.0	154
Eda-4	7.0	2.5	13.5	8.5	68.5	0.0	0.0	0.0	0.0	0.0	100.0	200
Eda-5*	73.6	10.7	11.8	0.0	3.1	0.0	0.5	0.0	0.2	0.0	100.0	549
Eda-6	1.5	1.5	1.0	42.0	7.0	45.0	0.0	1.5	0.5	0.0	100.0	200
Eda-8	2.5	1.5	2.0	28.5	64.0	0.0	0.0	0.0	1.5	0.0	100.0	200
Eda-9*	5.6	10.2	15.3	15.1	52.8	0.0	0.4	0.5	0.0	0.0	100.0	549
Eda-10	5.0	1.5	0.0	86.0	7.5	0.0	0.0	0.0	0.0	0.0	100.0	200
Eda-11*	5.0	4.5	1.3	69.8	19.3	0.0	0.0	0.3	0.0	0.0	100.0	400
Eda-12*	0.4	4.6	0.1	20.8	17.6	50.6	0.0	0.0	5.9	0.0	100.0	790
Hu-1*	2.9	0.6	0.8	67.0	27.9	0.1	0.0	0.1	0.3	0.3	100.0	724
Hu-2*	2.0	0.0	0.4	40.5	57.0	0.0	0.0	0.0	0.0	0.0	100.0	901

Table A 7 continued. TiO2 minerals: Rtl – rutile, An – anatase, Bro – brookite, An-bro – anatase-brookite intergrowth, An-rtl – anatase-rutile intergrowth.

Sample	opaque	translucent	n	HM yield [wt%]	TiO$_2$ minerals identified during Raman spectroscopy (%)				
					Rtl	An	Bro	An-bro	An-rtl
Enti-4*	58	42	100	0.993	83.3	0.0	0.0	16.7	0.0
Enti-5*	10	90	100	0.467	82.9	0.0	0.0	14.6	2.4
Enti-6*	51	49	100	0.365	81.4	7.0	9.3	2.3	0.0
Enti-7	62	38	100	0.977					
Enti-9*	29	71	100	0.426	76.2	4.8	0.0	4.8	14.3
Enti-10	23	77	100	0.566					
Enti-12*	31	69	100	2.496	89.7	0.0	0.0	6.9	3.4
Enti-13*	38	62	100	0.915	92.3	3.8	0.0	3.8	0.0
S1	76	24	100	0.948					
S2	79	21	100	0.754					
S3	71	29	100	0.044					
S4	58	42	100	0.016					
Nib-2*	62	38	100	1.244	100.0	0.0	0.0	0.0	0.0
Nib-4	70	30	100	3.941					
Nord-1	18	82	100	0.367					
Nord-2	18	82	100	0.030					
Nord-3	21	79	100	1.560					
Eda-2*	30	70	100	0.035	83.3	4.2	0.0	12.5	0.0
Eda-3*	51	49	100	0.430	63.6	0.0	0.0	36.4	0.0
Eda-4	27	73	100	1.007					
Eda-5*	40	60	100	0.584	84.7	5.1	0.0	10.2	0.0
Eda-6	25	75	100	2.043					
Eda-8	76	24	100	0.460					
Eda-9*	12	88	100	0.097	33.9	14.3	10.7	35.7	5.4
Eda-10	16	84	100	3.117					
Eda-11*	67	33	100	2.123	55.6	5.6	0.0	38.9	0.0
Eda-12*	17	83	100	0.370	35.3	5.9	8.8	26.5	23.5
Hu-1*	53	47	100	0.905	50.0	0.0	0.0	50.0	0.0
Hu-2*	25	75	100	0.876					

Table A 8: Heavy mineral counts for four samples of which different grain size fractions have been analysed in %. Note that the fraction 63–125 µm has been counted by both optical analysis and Raman spectroscopy. Zrn – zircon, Rtl – rutile, Tur – tourmaline, Grt – garnet, Ap – apatite, Ep – epidote group, St – staurolite, Mon – monazite, Tit – titanite.

		Method	Zrn	Rtl	Tur	Grt	Ap	Ep	St	Mon	Tit	Others	Sum
Enti-4	40-63 µm	Optical	23.0	9.0	5.5	51.0	8.0	2.0	0.0	1.5	0.0	0.0	100
	63-125 µm	Optical	22.0	4.0	12.0	54.0	8.0	0.0	0.0	0.0	0.0	0.0	100
	63-125 µm*	Raman	12.6	4.2	5.6	68.5	9.1	0.0	0.0	0.0	0.0	0.0	100
	125-500 µm	Optical	10.0	6.7	13.3	53.3	3.3	0.0	6.7	6.7	0.0	0.0	100
Enti-12	40-63 µm	Optical	69.5	11.0	16.0	0.0	0.0	0.0	0.0	1.5	2.0	0.0	100
	63-125 µm	Optical	58.0	5.5	24.5	0.0	0.0	9.0	1.0	1.0	0.0	1.0	100
	63-125 µm*	Raman	77.8	9.4	12.7	0.1	0.0	0.0	0.0	0.0	0.0	0.0	100
	125-500 µm	Optical	45.1	6.3	46.5	1.4	0.0	0.0	0.0	0.7	0.0	0.0	100
Eda-2	40-63 µm	Optical	25.5	3.5	8.5	0.0	60.5	1.5	0.5	0.0	0.0	0.0	100
	63-125 µm	Optical	8.5	4.5	16.0	0.5	66.5	4.0	0.0	0.0	0.0	0.0	100
	63-125 µm*	Raman	7.9	4.0	9.9	0.3	77.1	0.7	0.2	0.0	0.0	0.0	100
	125-500 µm	Optical	28.0	12.0	8.0	2.0	46.0	2.0	0.0	0.0	2.0	0.0	100
Hu-1	40-63 µm	Optical	6.0	0.0	3.0	46.5	44.5	0.0	0.0	0.0	0.0	0.0	100
	63-125 µm	Optical	1.5	0.5	1.0	55.5	39.0	2.5	0.0	0.0	0.0	0.0	100
	63-125 µm*	Raman	2.9	0.6	0.8	67.0	27.9	0.1	0.0	0.1	0.3	0.3	100
	125-500 µm	Optical	1.5	0.5	1.5	77.5	19.0	0.0	0.0	0.0	0.0	0.0	100

Table A 9: The analytical data from rutile and garnet chemical analyses can be found as Excel file in the supplementary material to this thesis and in the supplementary material to the article *Heavy minerals as provenance indicator in glaciogenic successions: An example from the Palaeozoic of Ethiopia* (https://doi.org/10.1016/j.jafrearsci.2020.103813).
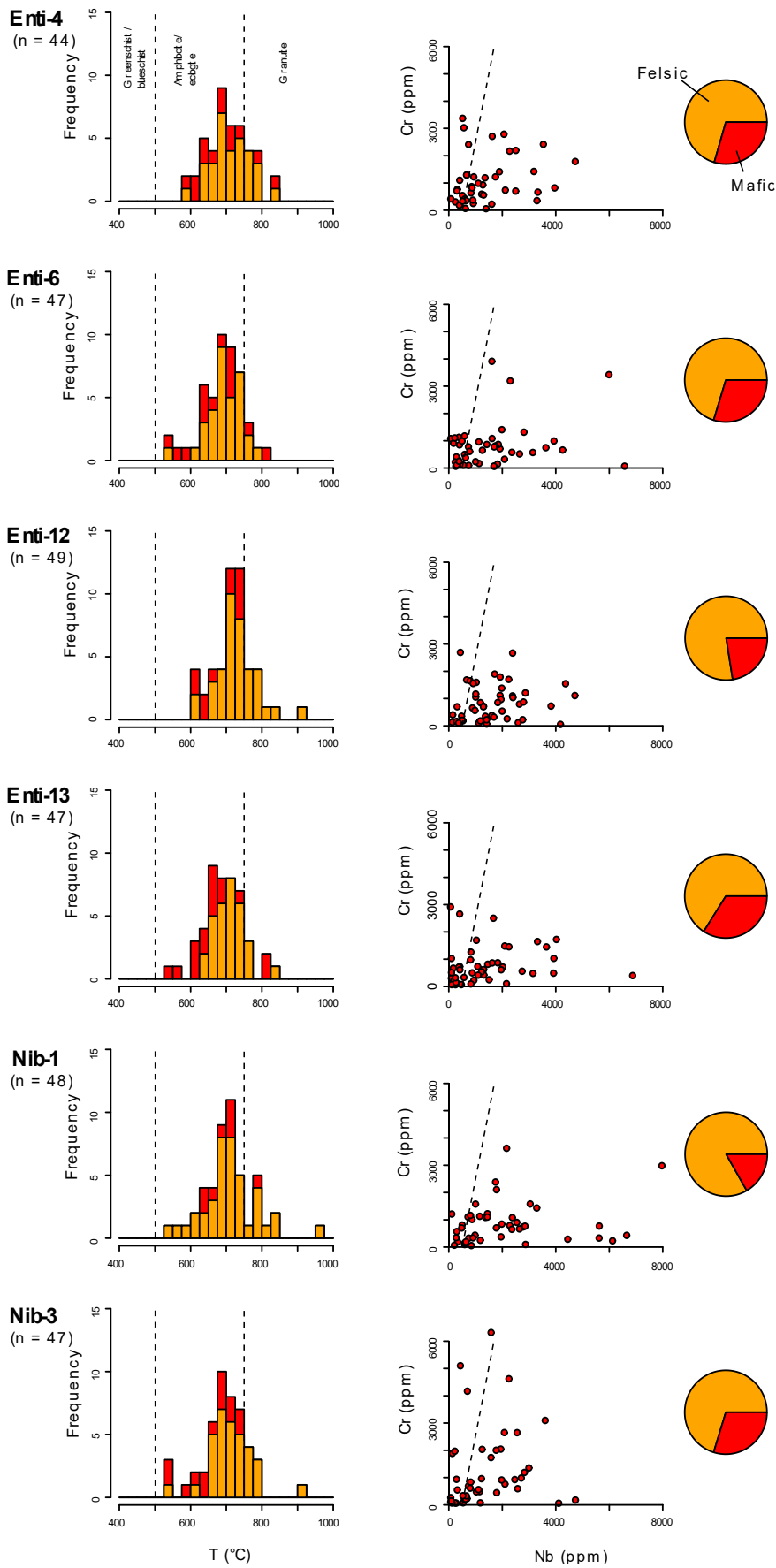
Figure A 1: Results of rutile chemical analyses displayed for the single samples of the Enticho Sandstone. Left: histograms of the calculated formation temperatures from Zr-in-rutile thermometry; Right: Cr-Nb crossplot and pie charts for classification of rutiles derived from metamafic and metafelsic source rocks after Triebold et al. (2012).
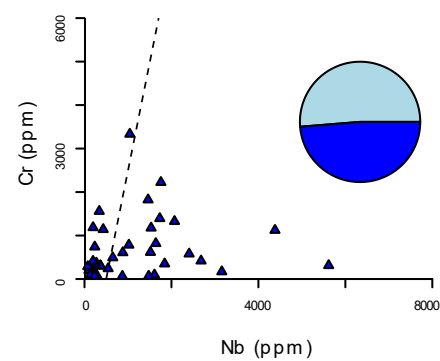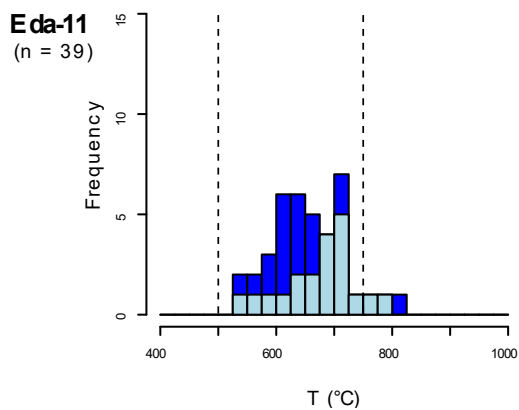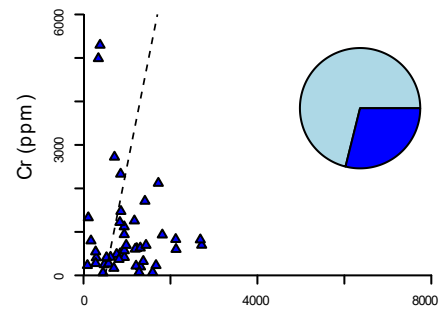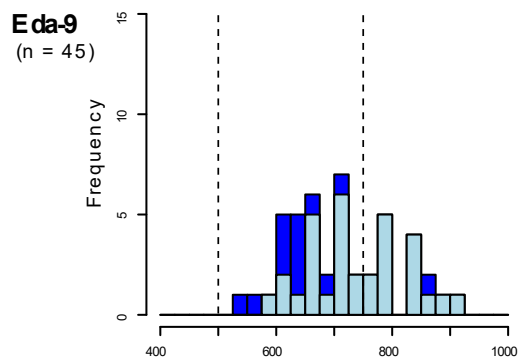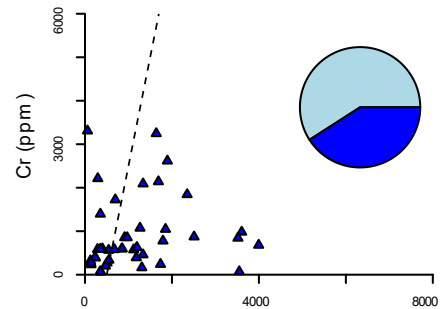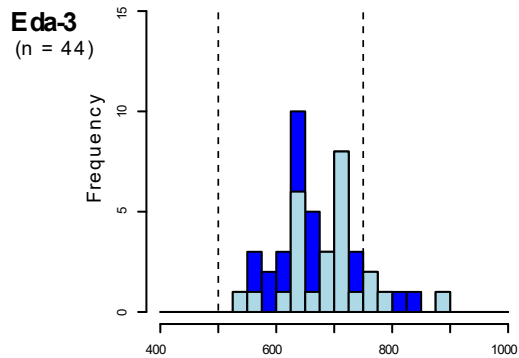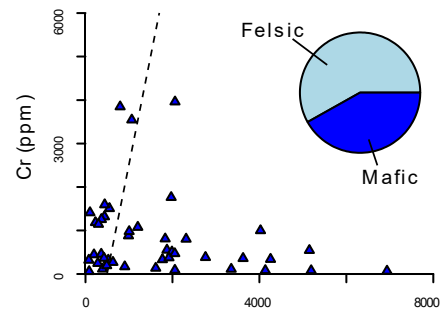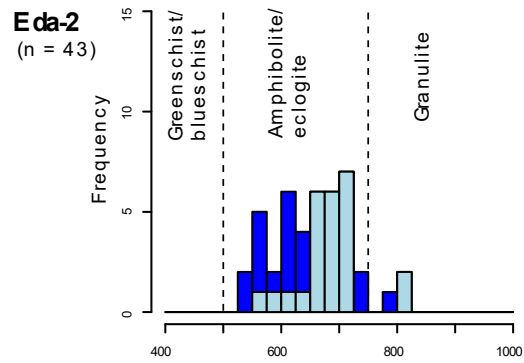
Figure A 2: Results of rutile chemical analyses displayed for the single samples of the Edaga Arbi Glacials. Left: histograms of the calculated formation temperatures from Zr-in-rutile thermometry; Right: Cr-Nb crossplot and pie charts for classification of rutiles derived from metamafic and metafelsic source rocks after Triebold et al. (2012).
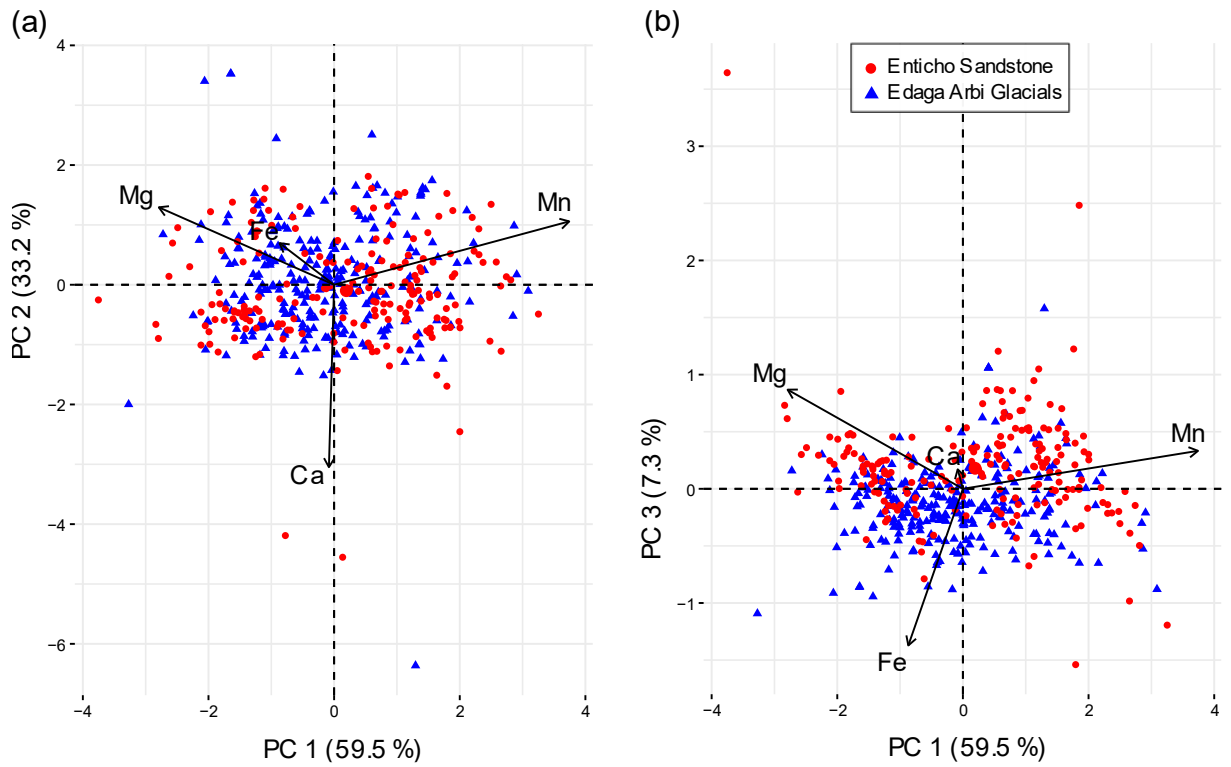
Figure A 3: PCA biplot based on the centred log-ratio (clr) transformed concentrations of the endmember-sensitive elements in garnet from the Enticho Sandstone and the Edaga Arbi Glacials. (a) First and second principal component. (b) First and third principal component.